UNIVERSITY OF
BIRMINGHAM

DEVELOPMENT OF AN MOF BASED ADSORPTION AIR CONDITIONING SYSTEM FOR AUTOMOTIVE APPLICATION

By

Baosheng Shi

A thesis submitted to the
University of Birmingham for the

Degree of Doctor of Philosophy

School of Mechanical Engineering
College of Engineering and Physical Sciences
The University of Birmingham
June - 2015

ABSTRACT

Heat powered adsorption systems offer advantages for air conditioning of automotive vehicles in terms of reducing fuel consumption and CO_2 emissions. However, published literature shows that developed adsorption systems are bulky and expensive, hence there is no commercial implementation of such systems. Metal organic framework (MOF) material is a new class of adsorbent material that has high surface area, high pore volume, highly tunable structural properties and uniform pore size. This PhD research project set out to investigate the feasibility of an MOF based adsorption air conditioning system for automotive application. To achieve this, utilising a working pair with high refrigerant adsorption capacity and adsorber bed design with good heat and mass transfer performance was investigated. Therefore, the adsorption characteristics of three water based adsorbents: silica gel RD-2060, SAPO-34 and CPO-27Ni were experimentally tested using a DVS analyser. Their adsorption characteristics were compared for relative pressure values ranging from 0 to 0.4 applicable in air conditioning systems, the water uptake of CPO-27Ni MOF is higher than that of SAPO-34 and silica gel RD-2060, indicating that the CPO-27Ni is the most promising adsorbent among these three materials. In addition, a finite element model was developed to evaluate and compare the adsorption performance of three different adsorption bed designs: a rectangular finned tube adsorption bed, a honeycomb finned rectangular channel adsorption bed and a helix finned tube adsorption bed. The rectangular finned tube adsorption bed was found to outperform the other designs, in terms of its water uptake and HCR.

A lab-scale test facility, based on a single bed refrigeration cycle containing one adsorber bed and one heat exchanger, used as both the evaporator and condenser, was constructed. The effects of various operating conditions on the system's performance including dry adsorbent desorption time, cooling water flow rate, adsorption time, desorption time and temperatures of evaporation and condensation was experimentally investigated using this test facility.

A lumped-parameter mathematical simulation technique was developed to simulate the working process of the automotive adsorption air conditioning system based on a two-bed system capable of continuous cooling. The performance of the adsorption cooling system was investigated at varying cycle times, varying heating fluid temperatures and flow rates and with different adsorption bed fin number and fin height using this mathematical model. The results show that this adsorption air conditioning system can produce the required cooling capacity of 2.39kW, with specific cooling power (SCP) of 440W/kg and coefficient of performance (COP) of 0.456, when a desorption temperature of 130 ℃ is obtained by hot oil heated by the engine's exhaust gas.

ACKNOWLEDGEMENTS

My highest appreciation is directed to Dr. Raya Al-Dadah, for her patience and kindness, as well as her academic experience, which are all invaluable to me. I am deeply indebted to her for her help in applying for the project, her continuous supervision, scientific discussion, original ideas and guidance and reviewing both the thesis and scientific papers. I would like to express my deep and special appreciation to the University of Birmingham and the Chinese Scholarship Council for supporting me financially during my study.

I wish to express my deep gratitude to Dr. Saad Mahmoud for his various invaluable suggestions and help. My warm thanks also go to Dr. Ahmed Elsayed for his academic advice and help. I would like to thank Mr Simon Rowan for helping me construct my test facility. I wish to thank Mr James Bowen for the help during the DVS measurement. Many thanks also to Janet's Proofreading Service for copy editing this thesis for conventions of language, spelling and grammar. I would like also to express my appreciation to all staff members of the School of Mechanical Engineering, University of Birmingham who have supported me.

I would like to submit my sincere appreciation to my parents, who are a constant source of emotional and moral support during my postgraduate years. Finally, the informal support and encouragement of my many friends are indispensable, especially the continuous support from Miss Siqiao Feng.

CONTENTS

LIST OF FIGURES

LIST OF TABLES

ABBREVIATIONS

ABS-PD	Absolute percent deviation
AIPO	Alumino-phosphate
APD	Average percent deviation
CFC	Chlorofluorocarbon
COP	Coefficient of performance
DVS	Dynamic vapour sorption
FE	Finite element
HCFC	Hydrochlorofluorocarbon
HCR	Heat capacity ratio
HD	High density
HFC	Hydrofluorocarbon
LD	Low density
LDF	Linear driving force
MOF	Metal organic frameworks
PID	Proportional-integral-derivative
RD	Regular density
RH	Relative humidity
RTD	Resistance temperature detector
SAPO	Silica-alumino-phosphate
SCP	Specific cooling power

NOMENCLATURE

Symbols	Description	Unit
$a, a_0 - a_3$	Constant coefficient	(-)
A, A_0	Constant coefficient	kg/kg
A_1	Constant coefficient	kg/(kg K)
A_2	Constant coefficient	kg/(kg K^2)
A_3	Constant coefficient	kg/(kg K^3)
$b, b_0 - b_3$	Constant coefficient	(-)
B, B_0	Constant coefficient	(-)
B_1	Constant coefficient	K^{-1}
B_2	Constant coefficient	K^{-2}
B_3	Constant coefficient	K^{-3}
C	Water vapour concentration	mol/m^3
Cp	Specific heat capacity	J/(kg K)
d	Diameter	m
D_{eff}	Diffusion coefficient	m^2/s
D_S	Surface diffusivity	m^2/s
D_{SO}	Pro-exponential factor	m^2/s
E	Characteristic adsorption work	J/mol
E_a	Activation energy	J/mol

f_c	Friction factor	(-)
h	Enthalpy	J/(kg K)
ΔH	Isosteric enthalphy	J/kg
h_{fg}	Water latent heat of evaporation	J/kg
$\vec{I}$	Unit matrix	(-)
k	Thermal conductivity	W/(m K)
K	Overall heat transfer coeffficient	W/(m K)
k_{kur}	Turbulent kinetic energy	m^2/s^2
K_0	Pre-exponential constant in equation 3-1	Pa^{-1}
$\dot{m}$	Flow rate	L/min
M	Molar mass of water	kg/mol
n	Exponential coefficient in equation 3-14	(-)
N_{data}	Data number	(-)
Nu	Nuslet number	(-)
P	Pressure	Pa
Pt	Prandtl number	(-)
Q_{heat}	Heat power input	W
R	Ideal gas constant	J/(mol K)
R_{cont}	Thermal contact resistance	K/kW
R_p	Radius of adsorbent granules	K/kW
Re	Reynolds number	(-)
S	Surface area	m^2
t	Time	s
T	Temperature	K
t_1	Tóth constant	(-)

$\vec{u}$	Velocity field	m/s
U	Uncertainty	(-)
UA	Overall conductance	W/K
w	Water vapour uptake	kg/kg
w_0	Maximum adsorption capacity	kg/kg
w_m	Monolayer capacity in equation 3-1	kg/kg
$w_{\max}$	Equilibrium water vapour uptake	kg/kg

Greek symbols	**Description**	**Unit**
ρ	Density	kg/m^3
ε	Porosity	(-)
κ	Permeability	m^2
ε_0	Tube internal wall roughness	m
δ_p	Half of distance between two fins	m

Subscripts	**Description**
ads	Adsorbent
Al	Aluminium
bed	Adsorption bed
bed,in	Inlet of adsorption bed
bed,out	Outlet of adsorption bed
c	Heating/cooling fluid
chw	Chilled water

chw,in	Chilled water at inlet of evaporator
chw,out	Chilled water at outlet of evaporator
$cond$	Condenser
$condw$	Cooling fluid in the condenser
$condw,in$	Cooling fluid at the inlet of the condenser
$condw,out$	Cooling fluid at the outlet of the condenser
Cu	Copper
$Cubed$	Copper in the adsorption bed
$Cucond$	Copper in the condenser
$Cuevap$	Copper in the evaporator
$cycle$	Refrigeration cycle
des	Desorption
dry	Dry adsorbent
eq	Equality
$evap$	Evaporator
fin	Fin
$fin,side$	Side of fins
i	Inside
$metal$	Metal
o	Outside
ref	Refrigerant
$refevap$	Refrigerant in the evaporator
sat	Saturate
t	Tube
w	Water

LIST OF PUBLICATIONS

1) Shi, B., Elsayed, A., AL-Dadah, R., Mahmoud, S. CFD simulation of honeycomb adsorption bed for automotive cooling system. *International Conference on Heat Transfer and Fluid Flow 2014: Czech.*
2) Shi, B., AL-Dadah, R., Mahmoud, S., Elsayed, A., Rezk, A. Mathematical and CFD modelling for a rectangular finned tube adsorption bed for automotive cooling system. *International Conference on Applied Energy 2013: South Africa.*
3) Elsayed, A., AL-Dadah, R., Mahmoud, S., Shi, B., Rezk, A., Rahbar, K. Adsorption low temperature cooling using activated carbon/ethanol working pairs. *International Conference on Applied Energy 2013: South Africa.*
4) Rezk, A., AL-Dadah, R., Mahmoud, S., Elsayed, A., Shi, B. Ethanal adsorption characteristics on metal organic frameworks for low temperature cooling applications. *International Conference on Applied Energy 2012: Suzhou, China.*
5) Mahmoud, S., Tang, A., Toh, C., AL-Dadah, R., Shi, B., Soo, L. Experimental investigation of the effect of fin configuration on the thermal performance of various PCM based heat sinks. *International Conference on Applied Energy 2012: Suzhou, China.*
6) Rezk, A., AL-Dadah, R., Mahmoud, S., Shi, B., Elsayed, A. Experimental investigation of silica gel granular packed rectangular finned tube adsorbent-bed. *Heat Powered Cycles Conference 2012: Germany.*

CHAPTER 1 GENERAL INTRODUCTION

1.1 Introduction and background

Refrigeration systems are widely used in many applications such as air conditioning, food industries, vaccine protection, cold storage, supermarket display and retail [1, 2]. Approximately 30% of worldwide energy is consumed by refrigeration and air-conditioning systems [3]. In terms of automotive application, the air conditioner aims at providing comfort for drivers and passengers. At present nearly all automotive air conditioners use traditional mechanical vapour compression refrigeration systems driven by the main car engine. Therefore, it reduces the automotive driving performance and increases the fuel consumption and exhaust gas pollutants' emissions. For a 1200kg car running at 56km/h, the mechanical vapour compression refrigeration air-conditioner can add up to 5-6kW peak power draw on the engine [2]. Moreover, the air conditioning system can increase the fuel consumption by up to 70% for a B class car on an urban cycle under severe ambient conditions (35℃ and 60%RH) [4]. Overall, the efficiency of a diesel engine is about 35%-40% and the rest of the energy is lost mainly to the engine coolant loop and the engine exhaust gases [5, 6]. Methods of utilising the waste energy from the automotive engine to drive the car air conditioning system are worthy of investigation. Moreover, it has been agreed by the Montreal Protocol, the Kyoto Protocol and the Vienna Convention that HCFCs and CFCs are phased out. HFCs are also one of the main greenhouse gases which are currently used in most automotive air conditioners. At present, researchers are looking

for techniques to reduce energy consumption and meet the greenhouse gas emission targets.

An adsorption refrigeration system is an alternative technique for the mechanical vapour compression refrigeration system. It can be driven by low-grade heat (80-150 ℃) like solar energy, or waste heat from industrial processes, or automotive engines [7]. However, there is still no working prototype available commercially for automobiles at present, because of its low efficiency, large weight and volume [8]. The working principle of the adsorption refrigeration system is based on the adsorption process of a refrigerant on a porous solid adsorbent material. Figure 1-1 shows a basic adsorption refrigeration system consisting of three main parts: adsorber, condenser and evaporator. The refrigerant vapour is desorbed by heating the adsorbent material and condensed in the condenser. In the adsorption process, the adsorbent material adsorbs the refrigerant vapour generated in the evaporator. As the refrigerant liquid evaporates in the evaporator to produce vapour, it absorbs heat from the surrounding producing cooling effect. The cooling effect can be used for various cooling applications like automotive air conditioning.

Different working pairs, including adsorbent and refrigerant, influence the performance of an adsorption refrigeration system. Based on published research on adsorption air-conditioning systems the most commonly used working pairs are activated carbon/ammonia, activated carbon/methanol, activated carbon/ethanol, silica gel/water and zeolite/water [9-11]. However, recently advanced adsorbent materials have been developed with superior adsorption characteristics like metal organic framework (MOF) material. MOFs have a larger refrigerant uptake capacity

compared with other adsorbents; which can increase the performance of an adsorption refrigeration system dramatically [12-14].

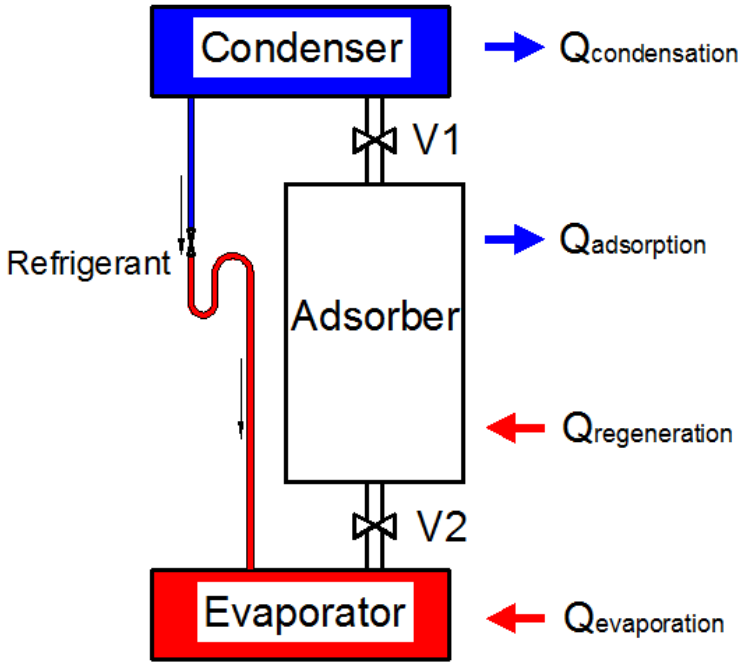

Figure 1-1 Basic adsorption refrigeration system

1.2 Aims and objectives

The main aim of this PhD project is to develop an MOF based adsorption air conditioning system for automotive application; to produce the required 2kW cooling load with high specific cooling power (SCP) for the normal cooling requirements of a car's cabin and high energy utilisation efficiency with a high coefficient of performance (COP). To achieve this research aim, the detailed project objectives are set out below:

a) Review of various advanced adsorbent materials and adsorption bed structures to identify their advantages and disadvantages. In particular, research work on metal organic frameworks and their adsorption characteristics will be reviewed.

b) Review of research on adsorption air conditioning systems for automotive application and determine the parameters that can improve the system cooling performance.

c) Investigate the adsorption characteristics of various advanced adsorbent materials and select the adsorbent with the best performance in terms of SCP and COP, to be utilised in adsorption air conditioning systems for automotive application.

d) Develop a finite element model to simulate the adsorption process of various adsorption bed designs. The adsorption bed design with the best adsorption performance will be constructed and tested.

e) Design and construct a test facility to validate the simulation model and help understand the effect of operating conditions on the MOF based adsorption cooling system's performance in terms of SCP and COP.

f) Develop a lumped-parameter mathematical model to simulate the working process of the whole adsorption refrigeration system for automotive application. Use this model to select the optimum operating conditions and physical parameters which can produce the best system performance.

1.3 Thesis outline

This thesis consists of eight chapters. Chapter 1 introduces the main research work covered in this thesis. It includes project aims, objectives and the thesis outline.

Chapter 2 reviews research work on adsorption cooling techniques including: adsorption refrigeration cycles, adsorbents/refrigerant working pair and adsorption bed structure. A review of research work regarding the development of adsorption cooling systems for automotive application and the comparison of their performance is presented.

Chapter 3 presents an investigation on adsorbent materials using water as refrigerant, including silica gel RD-2060, SAPO-34 an advanced zeolite material and CPO-27Ni MOF material produced by Johnson Matthey PLC. The water uptake characteristics of these three adsorbents are experimentally tested and their adsorption characteristics are compared. Fitting equations of water adsorption isotherms and kinetics for both CPO-27Ni and SAPO-34 are developed based on the experimental results and presented in this chapter.

Chapter 4 presents the development of finite element modelling to simulate the adsorption process for three adsorption bed designs packed with CPO-27Ni MOF adsorbent material, including a rectangular finned adsorption bed, a honeycomb finned adsorption bed and a helix finned adsorption bed. The performances of three adsorption bed designs are compared based on the simulation results.

Chapter 5 introduces the design and construction of the test facility which will be used to study the effect of operating conditions on MOF adsorption bed performance. Details of all the instruments will be described and the commissioning and repeatability testing will also be presented. The finite element model with all governing equations described in Chapter 4 is validated using the experimental results.

Chapter 6 presents an experimental investigation on the effect of operating conditions on the performance of an adsorption cooling system packed with CPO-27Ni MOF granules, including dry adsorbent desorption time, cooling water flow rate, adsorption time, desorption time and temperatures of evaporation and condensation.

Chapter 7 presents the development of a lumped-parameter mathematical model to simulate the working process of two-bed adsorption refrigeration system for automotive application, using CPO-27Ni adsorbent material. The mathematical model is validated with experimental results described in Chapter 6 and an investigation of the performance of the two-bed adsorption cooling system is carried out using this model. The optimum operating conditions and physical parameters are determined to achieve the best working performance.

The investigation of this MOF based adsorption air conditioning system for automotive application will be concluded in Chapter 8. The major findings from this research are summarized and possible future research work are suggested.

CHAPTER 2 LITERATURE REVIEW

2.1 Introduction

Adsorption cooling technology can be driven by low-grade heat sources (80-150 ℃) like solar and geothermal energy, or waste heat from industrial processes, or an automotive engine [7]. Therefore, it becomes an alternative technology for the traditional vapour compression refrigeration system. However, there is still no working prototype available commercially for automobiles at present because of its low efficiency, large weight and volume and high cost [8]. This chapter presents a comprehensive review of various adsorption refrigeration systems. The review includes research work regarding adsorption refrigeration cycles; adsorption working pairs including adsorbents and refrigerants; as well as adsorption bed structures. Progress on an adsorption air conditioning system for automotive application is also reviewed.

2.2 Adsorption process

Adsorption is a surface phenomenon that occurs at the interface of two phases; where cohesive forces including Van der Waals forces and hydrogen bonding, act between the molecules of all substances irrespective of their state of aggregation [15, 16]. Molecules of one substance have a mutual attraction with each other, which causes unbalanced forces of molecules at the surface. This force field can adsorb molecules

of another substance at the interface. The adsorbing phase is named the adsorbent, which is usually a solid phase. The material adsorbed is called the refrigerant which is usually a fluid or gas phase.

The adsorption process is accompanied by the evolution of heat [17]. The amount of heat released depends on the magnitude of the cohesive forces and the latent heat of the refrigerant condensation. Usually the adsorption heat is about 30-100% higher than the heat of condensation of the refrigerant [16]. Therefore, when a dry adsorbent and refrigerant in a liquid phase coexist separately in a closed vessel, the refrigerant molecules will be adsorbed onto the surface of the adsorbent molecules in the form of vapour instead of a liquid phase. The evaporation process will consume the heat from the liquid refrigerant and the adsorption heat will produced in the adsorption process. In this way, the temperature of the liquid refrigerant will decrease while the adsorbent's temperature will rise. An adsorption air conditioning system can utilise this process to obtain a cooling effect.

There are two kinds of adsorption processes: physical adsorption and chemical adsorption; depending on the type of cohesive force formed between adsorbents and refrigerants. The physical adsorption process binds molecules of the refrigerant and adsorbents caused by Van der Waals forces, which mainly includes dispersion, Debye and orientation forces [18]. It is a physical binding process that means molecules of both the adsorbent and refrigerant keep their original composition after the adsorption process. The refrigerant molecules can be adsorbed on the outside surface and also can be stored in the volume of micropores in the adsorbents. A chemical adsorption process is caused by valency forces formed during the reaction between refrigerant

molecules and surface molecules of adsorbents. The molecules after adsorption do not keep their original composition because of the chemical reaction. Besides, the requirement of heat and mass transfer is more critical for a chemical adsorption process to overcome the phenomena of salt swelling and agglomeration [18].

The heat of adsorption in the physical adsorption process is usually much smaller than that in the chemical adsorption process. Thus, the physical adsorbents can be restored to their original conditions by a desorption process. A desorption process happens when heat is applied to adsorbents. Thus, the physical adsorption process and desorption process are reversible [16]. However, the bonding forces of chemical adsorption are much larger than in the physical process. Therefore, more heat is liberated leading to chemical changes in some types of chemically adsorbed compounds and this process is irreversible [16]. For this reason, most adsorption refrigeration systems utilise physical adsorption processes instead of the chemical adsorption process. In this research, only adsorption air conditioning systems using a physical adsorption cycle are presented and investigated.

2.3 Adsorption refrigeration system - operating principle

A basic adsorption refrigeration system consists of three main parts: an adsorber, condenser and evaporator, as shown in Figure 2-1. Figure 2-2 shows the P-T diagram for the working process of an adsorption refrigeration system. The adsorption refrigeration cycle contains four steps: preheating, desorption, precooling and adsorption. The sequence of the various processes are shown in Figure 2-3 and

explained in detail as follows. The valve operation during the cycle is shown in Table 2-1.

Preheating: In the preheating process, the adsorber bed is heated which makes adsorbent material desorb the refrigerant bonded on its surface. Since all the valves are closed, the adsorber pressure increases from the evaporation pressure to the condensation pressure based on the set temperature of the evaporator and condenser. This is the process of a-b in Figure 2-2 and shown schematically in Figure 2-3(a).

Desorption: After the preheating process and raising the pressure, valve 1 connecting the adsorber and condenser is opened. The refrigerant vapour enters the condenser and is condensed to a liquid phase. This condensation process releases heat to the surroundings which is the process of b-e on the P-T diagram. The liquid refrigerant flows from the condenser to the evaporator shown as e-f. At the same time, the pressure of the adsorber bed remains the same, but the adsorber's temperature continuously increases since the heat is supplied. This is the process of b-c shown in Figure 2-2 and schematically shown in Figure 2-3(b).

Precooling: After the adsorbents' material desorbs the refrigerant, valve 1 is closed. The heating process stops and the adsorption bed is cooled by the ambience or other cold medium as shown in Figure 2-3(c). The adsorbents begin adsorbing the refrigerant which is still in the adsorber, causing a pressure drop from the condensing pressure to the evaporator pressure, as shown in process c-d on the P-T diagram.

Adsorption: In the adsorption process, valve 2, which connects the adsorber to the evaporator, is opened. The temperature of the adsorber remains low and the adsorbent continues adsorbing refrigerant vapour, which is stage d-a, shown in Figure 2-3(d). On the other hand, liquid refrigerant in the evaporator is in the evaporation process and extracts heat from its surroundings; the process of f-a, which creates the cooling effect. After this stage, all the processes are repeated to make the adsorption refrigeration system work continuously.

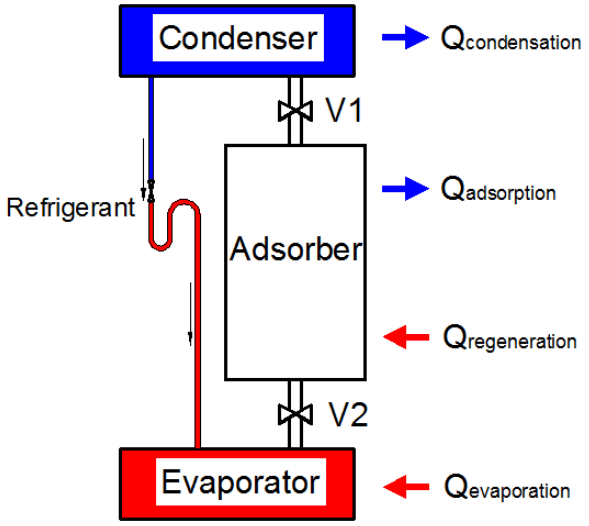

Figure 2-1 Basic adsorption refrigeration system

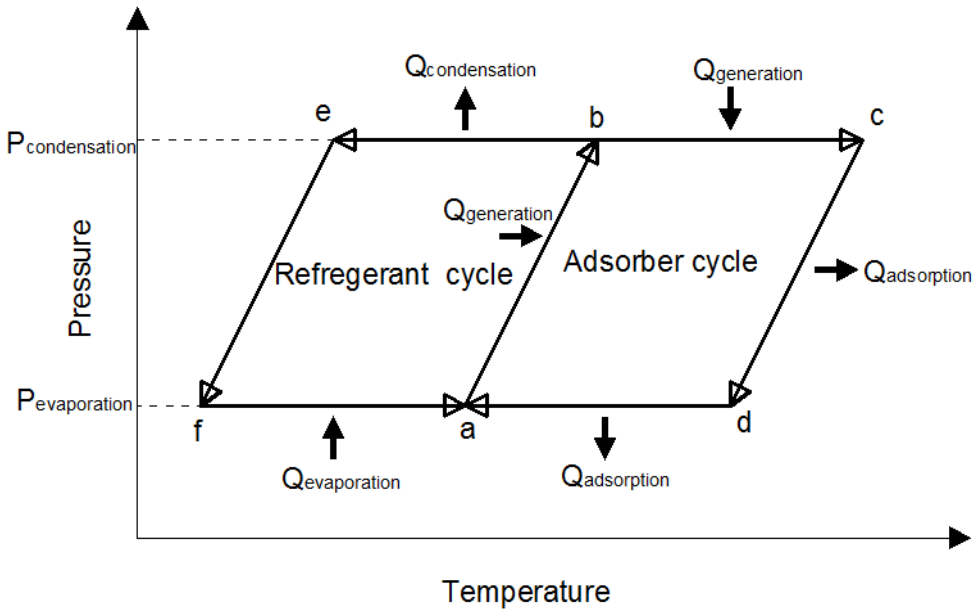

Figure 2-2 Adsorption cycle P-T diagram

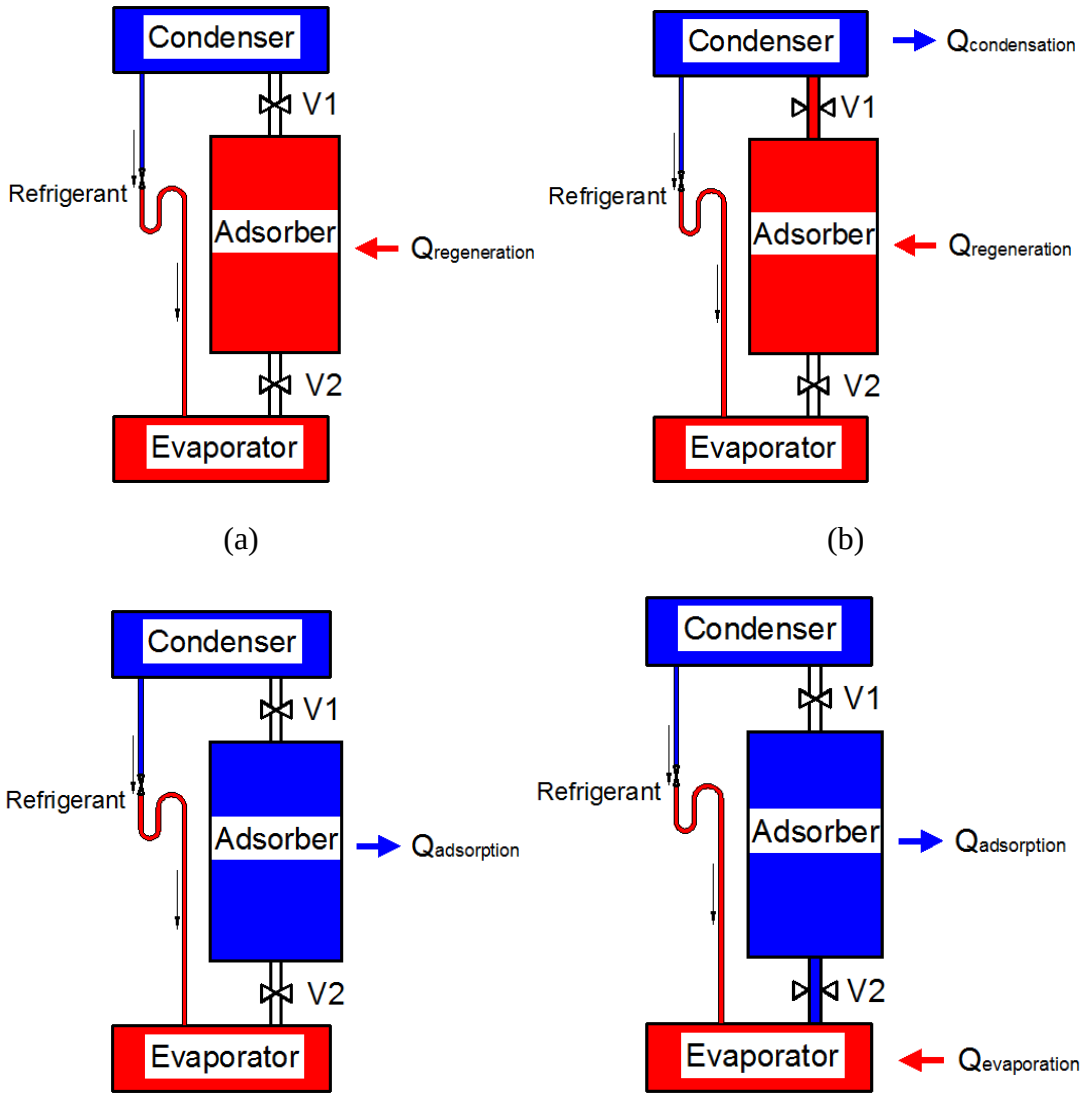

Figure 2-3 Adsorption refrigeration system operation principle: (a) preheating; (b) desorption; (c) precooling; (d) adsorption.

Table 2-1 Adsorber and valve operation

Mode	Adsorber	V1	V2
Preheating	Heating	Closed	Closed
Desorption	Heating	Open	Closed
Precooling	Cooling	Closed	Closed
Adsorption	Cooling	Closed	Open

2.4 Adsorption refrigeration system - historical background

The application of the adsorption phenomenon has a long history. In 3750 BC, Egyptians and Sumerians started utilising adsorption phenomenon to reduce copper, zinc and tin ores in the manufacturing process of bronze [19]. In ancient times, charcoal was the dominant adsorbent. Scheele 1773 and Fontana 1777 first experimentally measured the uptake of some gases by charcoal and clays. The adsorption phenomenon was firstly observed by Michael Faraday in 1848 by an experimental set-up using silver chloride and ammonia as a working pair [20]. Kayser introduced the terms 'adsorption' and 'isotherm' in 1881.

The application of the adsorption process for refrigeration began in the early 1900s. In 1929, Hulse and Miller demonstrated an adsorption air conditioning system for a railway carriage using silica gel and sulphur dioxide as a working pair [21].

However, the research on an adsorption refrigeration system was stopped due to the development of compressors and electrical motors; the improvement in power station efficiency; and the introduction of CFCs in the 1930s. In the last three decades, the research and development of an adsorption cooling system has increased. It is considered as one kind of environmentally-friendly technology that can replace the traditional vapour compression refrigeration system.

2.5 Environmental regulation

The ozone layer is a region of the earth's stratosphere which can absorb 98% of ultraviolet radiation from the sun. The holes of the ozone layer over the two poles have been confirmed by NASA's investigation [22, 23]. This was associated with the release of chlorine; a major component of the CFC refrigerant used in mechanical vapour compression systems. To prevent ozone depletion, the Vienna Convention for the Protection of the Ozone Layer had been agreed upon in 1985 and came into force in 1989; it was to be the foundation of the 1987 Montreal Protocol which phased out CFCs in 1995 and HCFCs by 2030.

Global warming is the phenomenon of increasing the earth's average temperature due to the heat preservation of greenhouse gases. The high temperature breaks the ecological balance, causing drought and melting of the ice at the two poles, which leads to floods and the submergence of coastal cities. The Kyoto Protocol was agreed to reduce greenhouse gases' emissions including carbon dioxide (CO_2), methane (CH_4), nitrous oxide (N_2O), hydrofluorocarbons (HFC), perfluorocarbons (C_xF_y) and sulphur hexafluoride (SF_6).

The vapour compression refrigeration system utilises CFCs and HCFCs which have a high global warming impact. Moreover, the vapour compression refrigeration system is driven by electrical power which is mainly produced by combustion of fossil fuels, contributing to the release of CO_2 to the atmosphere.

The adsorption refrigeration system can be driven by solar energy and waste heat from industrial processes and automotive engines. Besides, the refrigerants used in the

adsorption refrigeration systems are environmentally friendly, including water, ammonia, methanol and ethanol. Therefore, no ozone depletion or global warming is produced in the working process of adsorption refrigeration systems. Based on the above environmental regulations, the adsorption refrigeration technique is a promising technology to replace the traditional vapour compression refrigeration system and meet the requirements for protecting the environment.

2.6 Adsorption refrigeration cycles

Many configurations of adsorption refrigeration cycles were investigated by researchers, including a single bed cycle, two-bed cycle and multi-bed cycle. Each cycle is explained in detail in the following sections.

The adsorption system performance is described using the cooling capacity, specific cooling power (SCP) and coefficient of performance (COP). The specific cooling power is defined as the ratio of cooling capacity to the mass of adsorbent material used. The coefficient of performance is defined as the ratio of cooling capacity to the amount of heat required to desorb the refrigerant.

2.6.1 Single bed cycle

The basic adsorption refrigeration cycle is a single bed cycle consisting of one adsorption bed, evaporator and condenser. The operation principle is explained in detail in section 2.3. It has the advantage of being of small volume and low weight, as

well as having a simple structure with fewer valves. However, the adsorption cycle with a single bed cannot provide continuous cooling capacity, because the adsorber bed can either be connected to the evaporator or the condenser at any one time. Only the evaporation process can produce a cooling effect. For this reason, the specific cooling power (SCP) and coefficient of performance (COP) of an adsorption cooling system utilising the single bed cycle are relatively low. Based on the literature review, the COP and SCP of a single bed refrigeration cycle are usually below 0.3 and 50W/kg respectively [2, 24-30]. To obtain a continuous cooling capacity, a refrigeration cycle with two or more adsorption beds is needed.

2.6.2 Two-bed cycle

Most adsorption refrigeration systems use a two-bed cycle as shown in Figure 2-4. Its thermodynamic cycle is shown in Figure 2-5 and the modes of operation of the adsorbers and valves are described in Table 2-2. The operating principle of each adsorber bed is the same as was explained in section 2.3. A two-bed cycle system contains two adsorber beds which work in opposite modes. Specifically, in the switching period, one adsorber is in a preheating process while the other adsorber is in a precooling process. In the adsorption/desorption process, one adsorber is in desorption mode, while the other adsorber is in adsorption mode. The condenser and evaporator will be connected to each adsorber in turn depending on the operation mode. In this way, the evaporator can work continuously providing cooling all the time. Compared with the single bed refrigeration cycle, two-bed refrigeration cycle usually can obtain better operating conditions including high evaporation temperature and low condensation temperature. It can increase the adsorption systems'

performance in terms of SCP and COP. Besides, the mass recovery and heat recovery processes can be applied during the work process of the two-bed refrigeration cycle. Therefore, the SCP and COP can be improved dramatically compared with that of single bed refrigeration cycle. Based on the published literature, the COP and SCP of an adsorption cooling system with a two-bed cycle are higher than 0.3 and 100 W/kg, respectively [4, 31-37].

Moreover, mass and heat recovery can be applied to the two-bed adsorption refrigeration cycle during the switching period, to improve the performance of the whole refrigeration cycle [38]. In the mass recovery process, the two adsorbers are connected to increase the pressure change rate because of the pressure difference between the two adsorbers [39]. As for the heat recovery process, the cooling water first flows through the adsorber and then through the desorber to reduce the energy required for desorption; thus increasing the cycle's COP.

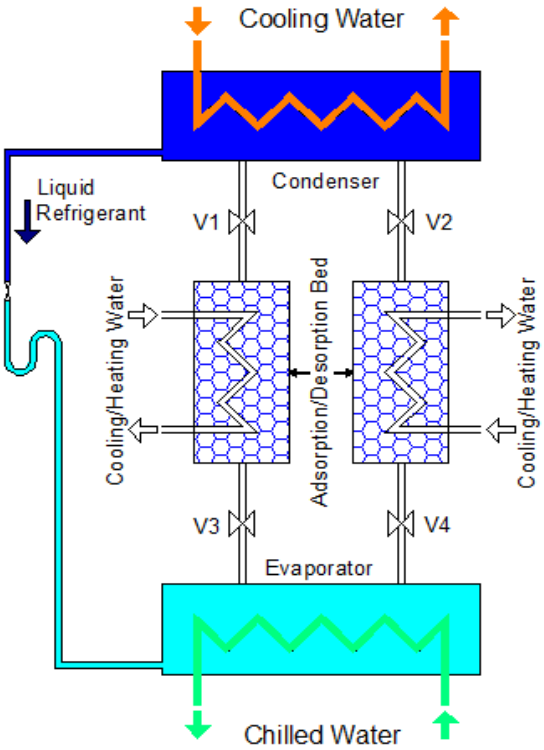

Figure 2-4 Two-bed adsorption refrigeration system

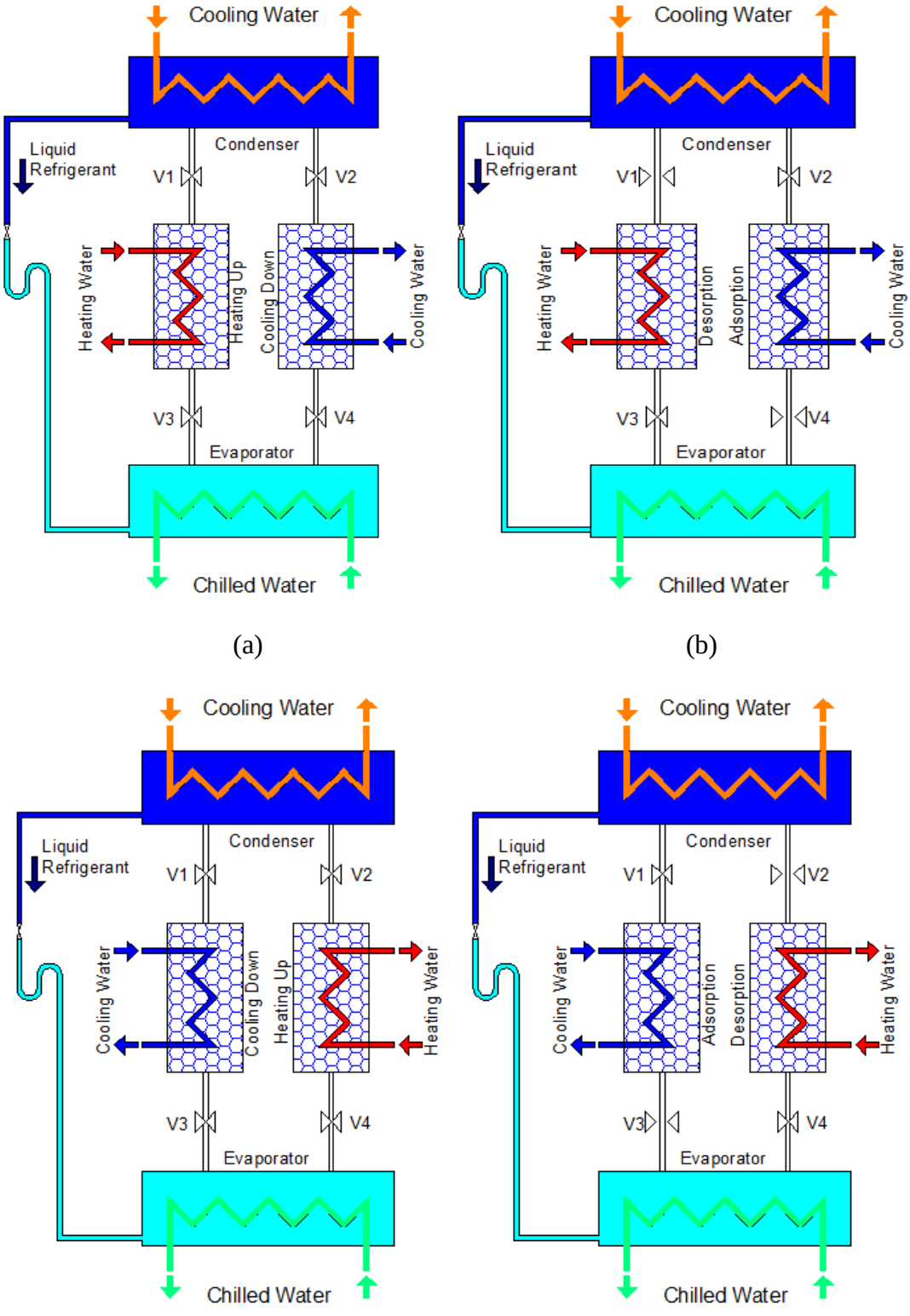

Figure 2-5 Two-bed adsorption refrigeration system operating principle: (a) switching period; (b) adsorption/desorption; (c) switching period; (d) desorption/adsorption

Table 2-2 Adsorber and valve operation for a two-bed cycle

Mode	Adsorber 1	Adsorber 2	V1	V2	V3	V4
Switching period	Preheating	Precooling	Closed	Closed	Closed	Closed
Ads/desorption	Desorption	Adsorption	Open	Closed	Closed	Open
Switching period	Precooling	Preheating	Closed	Closed	Closed	Closed
Ads/desorption	Adsorption	Desorption	Closed	Open	Open	Closed

2.6.3 Multi-bed cycle

Though the two-bed refrigeration cycle can produce continuous cooling, there is still a degree of discontinuity because of the switching period. For this reason, a multi-bed cycle including three-bed, four-bed and six-bed cycles are introduced by many researchers to provide continuous cooling and enhance the SCP.

The three-bed cycle contains three adsorption beds, an evaporator and a condenser as shown in Figure 2-6 [40, 41]. Each adsorption bed goes through four modes of operation; which are preheating, desorption, precooling and adsorption. Therefore, there are 12 modes of operation for the whole system during the cycle as shown in Table 2-3. The valve connecting the adsorber and condenser opens only during the desorption period of the adsorber, while the valve connecting the adsorber and evaporator opens only during the adsorption period. During the precooling and preheating mode, all valves are closed to make a change of pressure and temperature inside the adsorbers.

Usually the desorption process is quicker than adsorption process during the working cycle which means that the time needed for desorption process is shorter than that of adsorption process [42]. Therefore, the advantage of three-bed cycle is that the system

can manage adsorption kinetics and works with one adsorption bed and two desorption beds at the same time. It can reduce the cycle time and thus increase cooling load, SCP and COP.

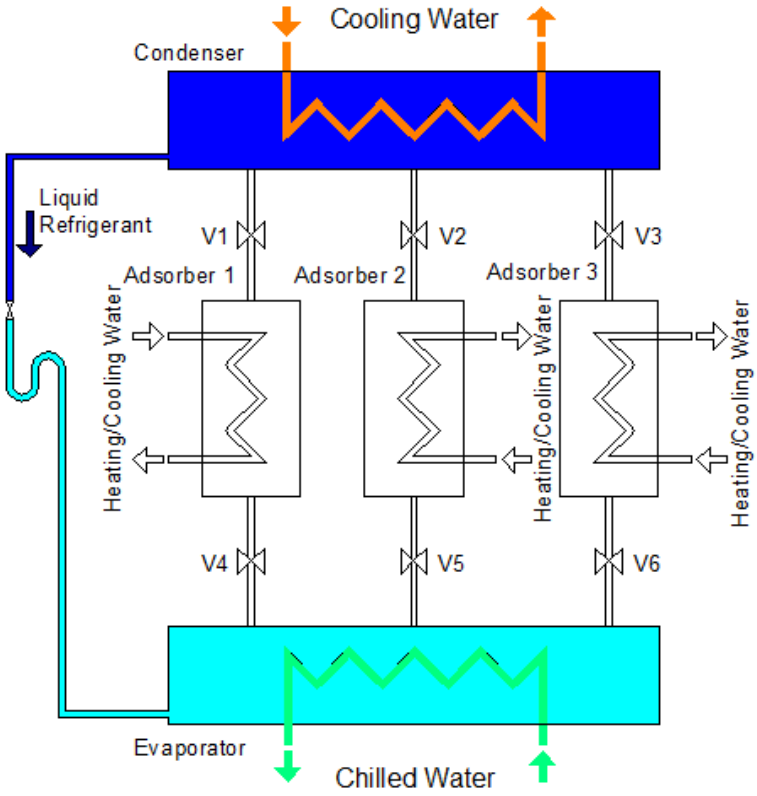

Figure 2-6 Three-bed adsorption refrigeration system

Table 2-3 Adsorber modes and valve operation for a three-bed cycle

Mode	1	2	3	4	5	6	7	8	9	10	11	12
V1	O	O	O	O	O	X	X	X	X	X	X	X
V2	X	X	X	X	O	O	O	O	O	X	X	X
V3	O	X	X	X	X	X	X		O	O	O	O
V4	X	X	X	X	X	X	O	O	O	O	O	X
V5	O	O	O	X	X	X	X	X	X	X	O	O
V6	X	X	O	O	O	O	O	X	X	X	X	X
Adsorber 1												
Adsorber 2												
Adsorber 3												

Adsorption Preheating Desorption Precooling

The four-bed cycle and six-bed cycle systems contain four adsorption beds and six adsorption beds respectively, as presented in Figure 2-7 [43-49] and Figure 2-8 [50-53]. The adsorbers' operating modes are described in Table 2-4 and Table 2-5. In the cycle half of the adsorption beds are heated in parallel and the other half are cooled. Between the adsorption and desorption process, precooling and preheating are applied. Furthermore, mass recovery can be applied to improve the adsorption refrigeration performance.

In addition to providing more continuous cooling, the multi-bed cycle provides the advantage of utilising low temperature heat sources of around 45-80 ℃ [40, 41, 43-53]. This kind of heat source cannot be applied to a two-bed cycle. Table 2-6 shows a comparison between the single bed cycle, two-bed cycle and multi-bed cycle.

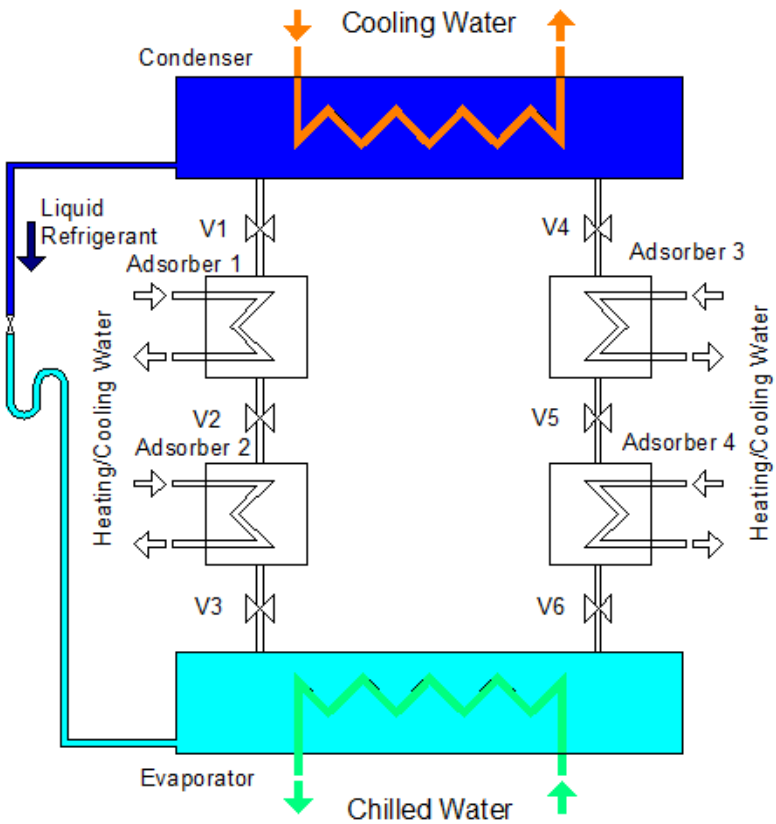

Figure 2-7 Four-bed adsorption refrigeration system

Table 2-4 Adsorber modes and valve operation for a four-bed cycle

Mode	1	2	3	4
Adsorber 1	Precooling	Mass recovery	Preheating	Desorption
Adsorber 2	Preheating	Mass recovery	Precooling	Adsorption
Adsorber 3	Preheating	Desorption	Precooling	Mass recovery
Adsorber 4	Precooling	Adsorption	Preheating	Mass recovery
V1	Closed	Closed	Closed	Open
V2	Closed	Open	Closed	Closed
V3	Closed	Closed	Closed	Open
V4	Closed	Open	Closed	Closed
V5	Closed	Closed	Closed	Open
V6	Closed	Open	Closed	Closed

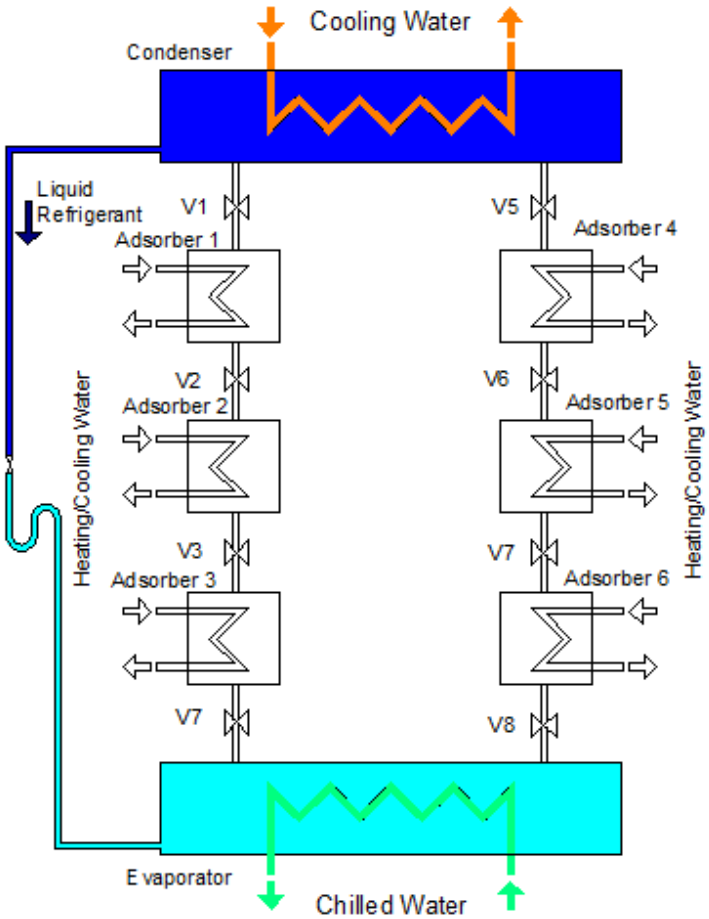

Figure 2-8 Six-bed adsorption refrigeration system

Table 2-5 Adsorber modes and valve operation for a six-bed cycle

Mode	1	2	3	4
Adsorber 1	Precooling	Mass recovery	Preheating	Desorption
Adsorber 2	Preheating	Mass recovery	Precooling	Mass recovery
Adsorber 3	Precooling	Adsorption	Preheating	Mass recovery
Adsorber 4	Preheating	Desorption	Precooling	Mass recovery
Adsorber 5	Precooling	Mass recovery	Preheating	Mass recovery
Adsorber 6	Preheating	Mass recovery	Precooling	Adsorption
V1	Closed	Closed	Closed	Open
V2	Closed	Open	Closed	Closed
V3	Closed	Closed	Closed	Open
V4	Closed	Open	Closed	Closed
V5	Closed	Open	Closed	Closed
V6	Closed	Closed	Closed	Open
V7	Closed	Open	Closed	Closed
V8	Closed	Closed	Closed	Open

Table 2-6 Comparison between three types of cycles

Cycle		Modes	Amount of valves	COP	SCP	Remarks
Single bed		4	2	0.11-0.38	23.5-33 W/kg	Compact and simple Discontinuous cooling
Two-bed		4	4	0.08-0.5	7.6-152 W/kg	Compact Commonly applied in commercial use
Multi-bed	Three-bed	12	6	0.25-0.73	100-300 W/kg	Can utilise low temperature heat source More continuity in cooling provided compared to two- bed cycle
	Four-bed	4	6			
	Six-bed	4	8			

2.7 Physical adsorbents

Adsorption processes include a physical adsorption process and a chemical adsorption process, as explained in section 2.2. This project focuses only on the physical adsorption process. Adsorbents used in the physical adsorption process are named physical adsorbents. Physical adsorbents usually have high porosity with different pore sizes to provide large surface and adsorption capacity. They can adsorb refrigerant molecules by Van der Waals force. There are several requirements for physical adsorbents to be applied in the adsorption refrigeration system as follows [16, 22, 23, 54]:

(a) A large adsorption uptake in an equilibrium state, with temperature variation to attain a high cooling capacity.

(b) Good thermal conductivity and low specific heat to achieve high heat transfer performance and large efficiency.

(c) Compatible with the refrigerant.

(d) Low cost and widely available.

(e) Non-toxic, non-corrosive and chemically stable in the working temperature range.

Based on these requirements, there are primarily five types of adsorbents as reported in publications. They are activated carbon, silica gel, zeolite, metal-alumino-phosphates and metal organic frameworks. This section introduces each type of these physical adsorbents.

2.7.1 Activated carbon

Activated carbon can be produced using high temperature heating to pyrolyse and carbonise materials like wood, peat, coal, fossil oil, chark, bone, coconut shell and nut stone and then activate the carbon with gases [8, 15, 18]. Due to the activation process, the carbon attains a very high degree of porosity and an extensive surface of 500-1500m^2/g [18]. Refrigerants adsorbed by activated carbon are ammonia, methanol, ethanol and R134a [8, 15, 18, 22, 23, 55-57]. The refrigerant uptake rate of activated carbon is relatively high due to its large porosity. The adsorption heat of activated carbon pairs is relatively low, 1800-2000kJ/kg for an activated carbon/methanol pair; while its thermal conductivity of 0.4W/(m·K) is poor [22, 23, 57, 58]. The activated carbons used for a refrigeration system are usually in the forms of powders, micro-porous, granulated, molecular sieves and carbon fibres [15]. The activated carbon fibres have a better mass and heat transfer performance as reported recently by [23].

2.7.2 Silica gel

Silica gel ($SiO_2.xH_2O$) is a form of synthetic silica. It is a rigid and continuous trap of colloidal silica connected to tiny grains of hydrated SiO_4 [1, 18, 23]. The existence of polar hydroxyl in the structure means that hydrogen bonds may be formed with polar oxides, like water or alcohol. For this reason silica gel is frequently used as a desiccant to adsorb water and produce dehumidification [18, 23]. There are three types of silica gel depending on pore size. They are low density (LD), regular density (RD) and high density (HD), with pore sizes of 1-2nm, 2-3nm and 15-20nm respectively. Granules of silica gel with these pore sizes can provide a surface area

ranging from 100 to 1000m^2/g. [1, 18, 23]. The working refrigerant normally used with silica gel is water with a high latent heat of evaporation. The silica gel can be generated by low temperature heat sources in the range 50-120℃ and has a large adsorption capacity [23]. However, low mass transfer resulting from the required low pressure working conditions and the large adsorption heat of 2500-2800kJ/kg, are disadvantages of silica gel for application in an adsorption cooling system [15, 23].

2.7.3 Zeolite

Zeolite is the alumina-silicate crystal formed with alumina-silicate and alkali or alkali soil [18, 23]. The molecular formula of zeolite is:

$M_{y/n}((AlO_2)_y(SiO_4)_m)zH_2O$

Where M is the general metal, y and m are both integers and y/m is larger than or equal to 1; n is the valency number of M; z is the number of water molecules inside a crystal cell. Figure 2-9 shows a crystal cell unit of zeolite [18]. The positive ion has its electric charge balance with the electric charge of aluminium atom. The alumina-silicate skeletal has a cage format with the porosity of between 0.2 and 0.5. It is usually connected by six casement sections, which can adsorb a large amount of extra molecules [18]. The zeolite can be formed naturally (40 types) or artificially (around 150 types). The zeolite used in adsorption cooling systems is made artificially and classified in groups such as A, B, X and ZSM; which tend to be more expensive compared to other adsorbents. The refrigerant typically used with zeolite is water. The adsorption heat of zeolite/water is high, 3000-4500kJ/kg; and its heat transfer performance is poor, with the thermal conductivity of 0.2W/(m·K) [59, 60]. Zeolites

have a high generation temperature of around 200-300℃; thus they require high temperature heat sources and usually need a long time to be heated to such a high temperature. Due to this reason, adsorption refrigeration systems using zeolite as adsorbents usually need a long cycle time. Besides, the required low pressure operating condition decreases the mass transfer performance of the zeolite/water working pair and thus decreases adsorption capacity.

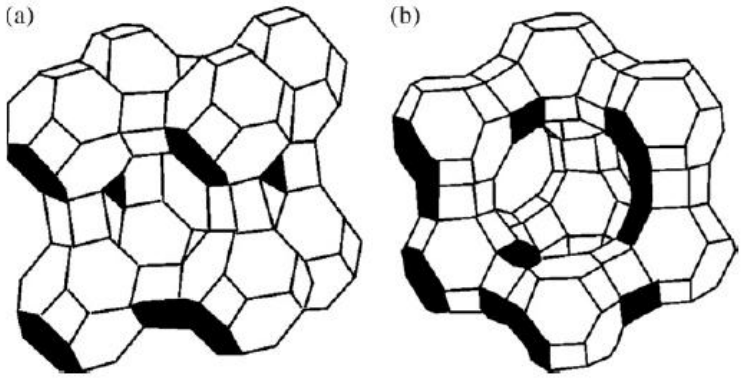

Figure 2-9 Crystal cell unit of zeolite: (a) A zeolite; (b) X, Y zeolite or faujasite [18]

2.7.4 Metal-alumino-phosphates

There are two kinds of metal-alumino-phosphates used as adsorbents in an adsorption cooling system: alumino-phosphates (AIPOs) and silica-alumino-phosphates (SAPOs) [61]. They have a similar pore system and structure to zeolite. However, AIPOs and SAPOs have a lower driving temperature and faster adsorption kinetics than zeolite [62-65]. For this reason, they have attracted increasing research interest during recent years. It has been reported that AIPOs and SAPOs can be regenerated at a regeneration temperature of 90℃ [61, 66]. Also, the thermal stability of many types

of metal-alumino-phosphates is high because they can stand a high temperature of 400-600 ℃ during synthesis [61]. Among the metal-alumino-phosphates, SAPOs have a larger water adsorption capacity than that of AIPOs, because of the existence of extra-hydrophilic sites (SiO_4^{4-}) in the framework [67]. However, the price of metal-alumino-phosphates is higher than other adsorbents due to its synthesis process [68].

2.7.5 Metal organic frameworks

Metal organic frameworks (MOFs) contain two main parts: the metal clusters considered as an inorganic secondary building unit which act as joints of the MOFs; and the polyfunctional organic linkers known as a organic secondary building unit; they act as struts that bridge the metal clusters [9, 12, 69]. The two main components are connected to each other by coordination bonds, together with other intermolecular interactions to form a net work with defined topology, yielding porous three-dimensional networks with large pore volume and high surface areas [9, 12]. Therefore, the MOFs' molecular structure containing unsaturated metal centres or open-metal sites, has been used to develop materials with improved adsorption capacity [10]. During the last decade, MOFs attracted significant research for application in energy storage, separation, sensors and catalysis [69]. MOFs have many advantages, including a high specific surface area (up to 5500m^2/g); high pore volume; highly tunable structural properties and uniform pore size [9-11]. They have a larger water uptake capacity compared with other adsorbents; thus they can increase the performance of an adsorption refrigeration system dramatically. However, some of the MOFs are unstable in the presence of a large amount of water, which restricts their application in an adsorption cooling system [70, 71].

The first idea to apply MOFs for adsorption heat transformation cycles was suggested by Aristov in 2007 [72]. Based on the literature review, many types of MOFs have been investigated regarding their adsorption properties. Among them, three types of MOFs are commonly investigated, including Cu-BTC, MIL-101Cr and CPO-27; these will be described as follows:

Cu-BTC (also named HKUST-1) has the molecular formula of $Cu_3(BTC)_2$, where BTC is benzene-1,3,5-tricarboxylate [73, 74]. The water adsorption process in Cu-BTC was investigated in a molecular scale by [73-75] and the water uptake amount of Cu-BTC was tested by [13, 66, 76]. Among these studies, Wang et al. [76] measured the water uptake of Cu-BTC at 22 ℃ and 2.7mbar and achieved up to 6wt%. The different colour of Cu-BTC at dry and wet conditions indicates its application as a highly sensitive moisture sensor. Rezk et al. [13] investigated the water uptake characteristics of many types of MOFs including Cu-BTC, Fe-BTC, MIL-53Cr, MIL-53Fe, BIRM-1, BIRM-1-K and BIRM-1-Li. They concluded that Cu-BTC and Fe-BTC have the highest water adsorption characteristics due to their large porosity and surface area. Also, Henninger et al. [66] reported that the highest water vapour uptake of Cu-BTC is about $0.324 kg_{ref}/kg_{ads}$, with a desorption temperature of 140 ℃ and adsorption temperature of 30 ℃. However, the water uptake decreased within 30 cycles by about 37%, which means that it is not stable in adsorption cycles with water vapour. This conclusion was also confirmed by the research of Gul-E-Noor et al. [74] who showed that the presence of water in the Cu-BTC network leads to the decomposition of the structure.

MIL-101Cr (MIL for Material Institute Lavoisier) was investigated by many researchers in terms of the adsorption characteristics of water [9, 14, 61] and ethanol [12]. Kusgens et al. [9] tested and compared five types of MOFs including Cu-BTC, ZIF-8, MIL-101Cr, MIL-100Fe and DUT-4. They concluded that although Cu-BTC is the most hydrophilic MOF, it is unstable towards water. Regarding MIL materials, they concluded that MIL-101Cr and MIL-100Fe are the most promising as hydrophilic mesoporous compounds. The work carried out by Ehrenmann et al. [14] indicated a high water vapour uptake of 1.01kg_{ref}/kg_{ads} by MIL-101Cr and a slight decrease to 0.968kg_{ref}/kg_{ads} after 40 cycles. Results showed that the highest change in the amount of water is within the relative pressure (P/P_0) of 0.3 and 0.6. Aristov [61] measured the water vapour uptake of MIL-101Cr at 35 ℃ and found it to be 0.3kg_{ref}/kg_{ads} within P/P_0=0.34-0.38; and a larger uptake lift of 0.4kg_{ref}/kg_{ads} was achieved by modified MIL-101Cr. Rezk et al. [12] investigated the adsorption characteristics of ethanol with 6 types of MOFs, including MIL-101Cr, MIL-100Cr, MIL-53Cr, CPO-27Ni, Cu-BTC and Fe-BTC. They showed that the adsorption uptake of ethanol by MIL-101Cr is superior to other MOFs with a value of up to 1.2kg_{ref}/kg_{ads} and is stable after 20 cycles at 25 ℃.

CPO-27 (also named MOF-74) is one type of MOF that attracts increasing research. There are four types of CPO-27 including CPO-27Zn [77], CPO-27Co [78], CPO-27Ni [79] and CPO-27Mg [80]. Glover et al. [80] investigated all these four types on the adsorption characteristics of toxic gases such as ammonia, cyanogen chloride, octane and sulphur dioxide. The authors stated that the competitive adsorption of water was seen on all of the adsorbents examined with the water uptake of 0.1-0.5 kg_{ref}/kg_{ads}, which indicated that CPO-27 can be used for water adsorption application.

The research regarding the water adsorption of CPO-27 is not much until now. Table 2-7 shows the summary of characteristics of the three main MOFs.

Table 2-7 Summary of characteristics of the three main MOFs' materials

MOFs	Refrigerant uptake	Remarks
Cu-BTC	Water-6wt% [76] Water-0.324kg_{ref}/kg_{ads} [66]	Not stable with water vapour
MIL-101Cr	Water-1.01kg_{ref}/kg_{ads} [14] Water-0.3 kg_{ref}/kg_{ads} [61] Ethanol-1.2 kg_{ref}/kg_{ads} [12]	Stable with water vapour
CPO-27	Water-0.1-0.5 kg_{ref}/kg_{ads} [80]	Research regarding water adsorption application is not much. Only [80] investigated the water adsorption of CPO-27

Moreover, some other types of MOFs have been investigated for adsorption application. Henninger et al. [81] suggested ISE-1 as the adsorbent for low temperature heating and cooling application. The water vapour uptake of 0.21kg_{ref}/kg_{ads} by ISE-1 was achieved with the desorption temperature of 140 ℃, adsorption temperature of 30 ℃, evaporation temperature of 10 ℃ and condensation temperature of 35 ℃. The research by Karra et al. [10] proved that MOF-14 is a promising porous material for CO_2 adsorption, but the water uptake is less than one-tenth of that of Cu-BTC and CPO-27Mg. Kondo et al. [70] investigated and compared three types of 3-D pillared-layer MOFs and the maximum water vapour uptake was 0.27kg_{ref}/kg_{ads}. Saha and Deng [82] studied the ammonia adsorption and its effects on framework stability of MOF-5 and MOF-177. They found that ammonia will destroy MOF-5 and MOF-177; thus they are not suitable for ammonia adsorption. Lincke et al. [11] investigated the adsorption capacity of nitrogen, argon, carbon dioxide, methanol and methane by a new copper-based MOF material and found unusual adsorption-

desorption isotherms with one or two hysteresis loops. Furukawa et al. [83] measured the water adsorption capacity of some types of MOFs. The results showed that MOF-801 takes up 22.5wt% at P/P_0=0.1 and MOF-841 takes up 44wt% at P/P_0=0.3. The authors suggested MOF-801 can be used in advanced thermal batteries while MOF-841 can be used in the capture and release of atmospheric water in remote deserts.

2.8 Refrigerant

The refrigerant selected for application in adsorption cooling systems should have the following properties [16, 18, 54]:

(a) High latent heat of vaporization to attain large cooling capacity during the evaporation process.

(b) Small molecule size to be easily adsorbed by adsorbents.

(c) Good thermal and chemical stability with the adsorbent over the operating temperature range.

(d) Should be non-toxic, non-corrosive, non-flammable and environment-friendly.

Based on these requirements, at present, refrigerants frequently used are water, ammonia, methanol and ethanol [1, 18].

Water is one of the most ideal refrigerants because it is non-toxic, non-flammable and friendly to the environment. Many researchers have used it as a refrigerant in adsorption refrigeration systems because it has a large latent heat of vaporization to increase cooling capacity per unit refrigerant flow rate [18]. Water can be used with silica gel, zeolite, SAPOs and MOFs. However, since the boiling point of water is

100 ℃ at atmosphere pressure, an adsorption system utilising water as a refrigerant requires a vacuum operating condition, which increases the system's complexity and cost. Another disadvantage of water as a refrigerant is the large adsorption heat which can decrease the adsorption system’s performance. Finally, the temperature of the cooling effect cannot be lower than 0 ℃ because of the solidification of water at this temperature.

Ammonia can work at positive pressure as its boiling temperature is below 0 ℃ at 1atm. It also has a relatively high latent heat of vaporization. Usually ammonia is employed with activated carbon. On the other hand, ammonia as a refrigerant has the disadvantages of large adsorption heat, toxicity and flammability; which restricts its applications for adsorption refrigeration systems.

Methanol and ethanol are used with activated carbon, but their latent heat of evaporation is lower than that of water and ammonia. However, they both work in vacuum conditions. They are also toxic and flammable. Furthermore, methanol will be boiling at 65 ℃ and is harmful to the environment [84].

2.9 Adsorption working pairs

For air-conditioning applications, there are five commonly used working pairs including: activated carbon/ammonia, activated carbon/methanol, activated carbon/ethanol, silica gel/water and zeolite/water. In addition to these most used pairs, there are some new adsorption working pairs attracting researchers' attention, such as: SAPO/water and MOF/water because of their large adsorption capacity and low

generation temperature, which means that they can utilise low-grade heat sources to provide a large cooling effect. The characteristics of these pairs are shown in Table 2-8.

2.10 Adsorption cooling system for automotive application

The application of adsorption cooling systems for automotive air conditioning has attracted significant research work, as the systems can be driven by waste heat either from the engine coolant water or from the engine exhaust gases. In this way, it reduces fuel consumption and exhaust gas emissions. At present, vapour compression systems are widely used for cooling in automotive applications, but they are powered by the main engine and lead to more fuel consumption as well as carbon dioxide emissions. A vapour compression refrigeration cycle compressor can add up to 5-6kW peak power load to the car's engine. Overall, the efficiency of a diesel engine is about 35%-40% and the rest of the energy is lost mainly to the engine coolant loop and the engine exhaust gases [5, 6]. Generally, the temperature of the engine coolant water is 90-95 ℃ for cars and 80-90 ℃ for trucks [85]; while the temperature of exhaust gas discharged from the tailpipe comes within 150-450 ℃ [86]. Such conditions are sufficient for an adsorption cooling system to provide enough cooling power for a car cabin [35]. Besides, the adsorption system has the advantages of fewer moving parts, low maintenance cost, simplicity in structure and flexibility in operation, compared with vapour compression refrigeration systems for automotive application [87, 88].

Table 2-8 Characteristics of most used adsorption working pairs

Working pair / Characteristics	AC/ammonia	AC/methanol	AC/ethanol	Silica gel/ water	Zeolite/water	SAPO-34/ water	MIL-101(Cr) /water
Operation pressure	Positive pressure	Vacuum	Vacuum	Vacuum	Vacuum	Vacuum	Vacuum
Generating temperature (℃)	80-200	80-100	80-120	50-120	200-300	80-90	90-140
Adsorption heat (kJ/kg)	2000-2700	1800-2000	1200-1400	2500-2800	3000-4500	3240-3600	3170
Adsorption capacity (kg_{ref}/kg_{ads})	0.29	0.45	0.19	0.3	0.17	0.29	1
Refrigerant latent heat of vaporization at 15℃ (kJ/kg)	1206	1102	842	2466	2466	2466	2466
Refrigerant boiling point (℃)	-34	65	79	100	100	100	100
Refrigerant solidification point (℃)	-77	-98	-40	0	0	0	0
Refrigerant thermal stability	Yes	No	Yes	Yes	Yes	Yes	Yes
Refrigerant toxicity	Yes	Yes	Yes	No	No	No	No
Refrigerant flammability	Yes	Yes	Yes	No	No	No	No

In 1993, Suzuki [89] made a preliminary study to explain the technological limits in the application of an adsorption system to passenger cars' air conditioning. He concluded that the adsorbent material and the adsorber bed design to improve heat transfer characteristics are the most important issues for the application of adsorption cooling systems in automobiles. In 2006 Lambert and Jones [87, 88] proposed conceptual and detailed design options for an automotive adsorption air conditioner powered by exhaust heat. They explained that for automotive application, the adsorption cooling system can reduce fuel consumption while increasing the whole mass, compared with a mechanical air conditioner. Inoue et al. [90] conducted a study on adsorption refrigerators for automobiles utilizing heat from engine coolant water. The study was focused on the effect of relative humidity on the adsorption isotherm to determine the required properties of adsorbent material for automotive air conditioning in high ambient temperature conditions.

A number of researchers have investigated the adsorption cooling system for automotive application and prototypes have been constructed and tested with silica gel/water [35, 36, 91], zeolite/water [5, 6, 86, 92-96] and activated carbon/ammonia [4, 34] as adsorbent/refrigerant working pairs. Most investigations are focused on an adsorption cooling system using a two-bed structure [7], without mass and heat recovery in the working cycle to simplify the system structure and decrease the weight. Several bed configurations have been utilized including plate heat exchangers, finned tube heat exchangers, annulus tube heat exchangers and modular assembled adsorber heat exchangers.

2.10.1 Adsorption bed structure

Adsorption beds are important parts of the adsorption refrigeration system and their structures affect the heat and mass transfer in the adsorption process; thus they have an effect on the overall performance of the adsorption cooling system. Based on published research, four types of adsorption bed structures have been investigated for adsorption cooling systems in automotive applications; they are described in the following sections.

2.10.1.1 Plate heat exchanger

Critoph, Tamainot-Telto and Metcalf [4, 34] at the University of Warwick UK developed a car adsorption air conditioning system using an activated carbon-ammonia working pair. The adsorber bed has a structure of a plate heat exchanger with the cooling/heating fluid passing through small channels, as shown in Figure 2-10. Activated carbon weighing 2kg is packed between thermal fluid channels and ammonia gas is adsorbed/desorbed from the adsorbent and flows from the centre of the upper/lower face. The system contains two adsorber beds to ensure continuous cooling output and both are driven by engine coolant loop water with a temperature of about 90℃. Such a system produced a cooling power of 1.6kW and a COP of 0.22. The most noteworthy characteristic for this research is that the operating cycle time is only 1min with mass recovery; thus achieving a large SCP of 800W/kg. The performance could also be improved by using both mass and heat recovery and optimised cycle time.

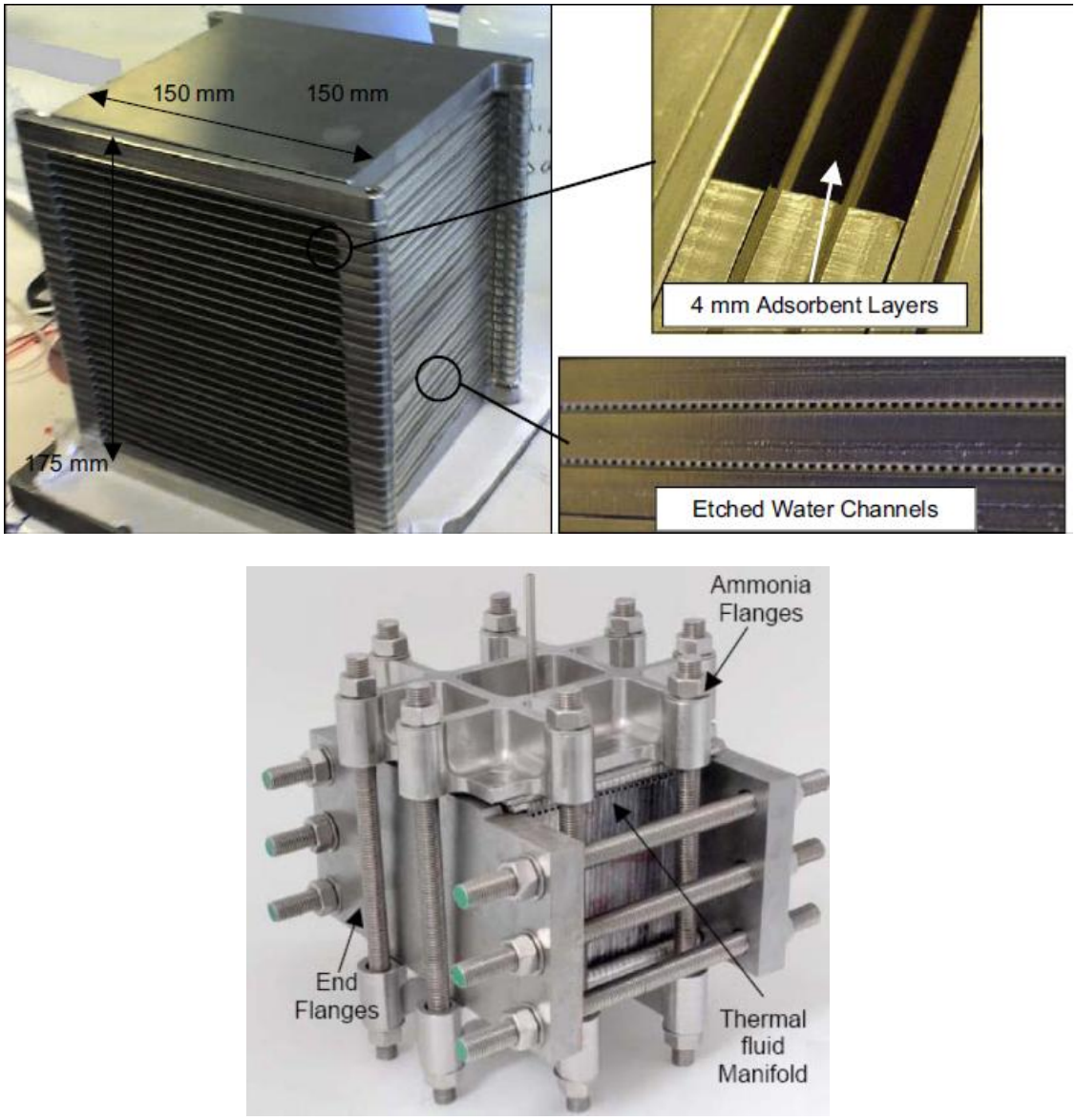

Figure 2-10 Adsorption generator by Critoph et al. [4, 34]

2.10.1.2 Finned tube heat exchanger

de Boer et al. [35, 36] designed and tested a silica gel-water adsorption cooling system for mobile air conditioning. This system consists of two adsorber beds; each has three tube-fin heat exchangers connected in parallel as shown in Figure 2-11(a). The beds are packed with 6kg of silica gel grains and produced a 2kW cooling load when tested in the lab without mass

or heat recovery. Driven by a 90℃ engine coolant loop which is also heated by exhaust gas, the system achieved a COP of 0.4. An on-board test was carried out in a Fiat Grande Punto shown in Figure 2-11(b); where a cooling load of 0.8kW was only achieved due to the poor heat transfer performance between the condenser and the ambient air. Besides, the system has a weight of 86kg, which is very heavy and can reduce a car's dynamic performance.

Verde et al. [85] set up a lumped parameter model and constructed a lab-scale prototype for a two-bed adsorption air conditioning system driven by an engine coolant loop for a truck's cabin. The adsorbent used was SAPO-34 with 5.76kg adsorbent granules packed into the finned flat-tube heat exchanger, as shown in Figure 2-12. The results showed that this system was able to produce a cooling power of 2 to 3kW and a COP of 0.6 without heat or a mass recovery process. The large COP means this design can use waste heat efficiently and this kind of adsorbent shows promising potential for automotive adsorption cooling system application. Further research is needed to investigate the performance of the cycle with heat and mass recovery and optimized operating parameters.

Vasta et al. [37] developed and tested an automotive adsorption air conditioning system using SAPO-34/water as a working pair. This system was driven by an engine coolant loop with a temperature of 90℃. A double-bed configuration with a finned flat tube heat exchanger packed with 4.6kg of adsorbent, as shown in Figure 2-13, was used and operated without heat or mass recovery. Such a system has an overall volume of 170dm^3 and a weight of 60kg. The experimental results showed that the system delivered an average cooling load of 1-2.3kW with a SCP of 300-600W/kg and a COP of 0.25-0.45 for normal climate conditions with a short cycle time of 420s-620s. The authors also conducted an experiment to test the performance of the cooling system in a real truck cabin and the results showed that this

system successfully obtained a cooling load of 2kW and delivered continuously cold air at 9℃. Further work is needed to reduce the system's overall volume and weight; such as incorporating mass or heat recovery techniques.

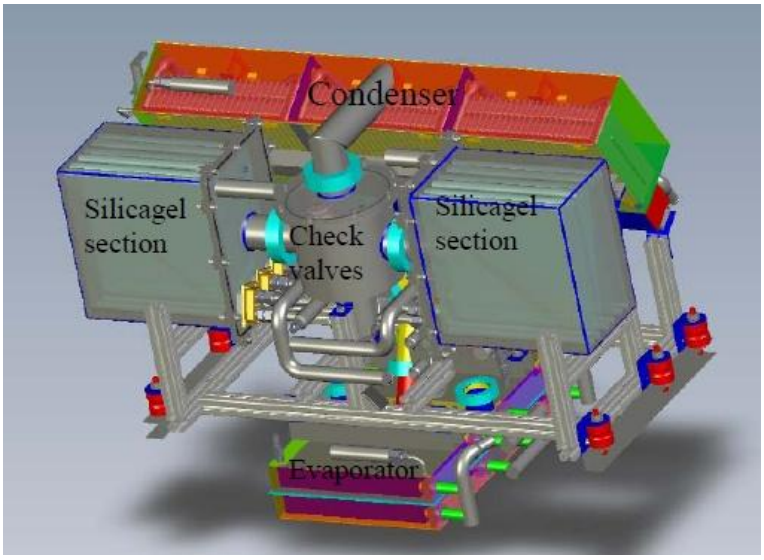

(a)

(b)

Figure 2-11 Automobile adsorption cooling system by Boer: (a) design drawing (b) on-board test [35, 36]

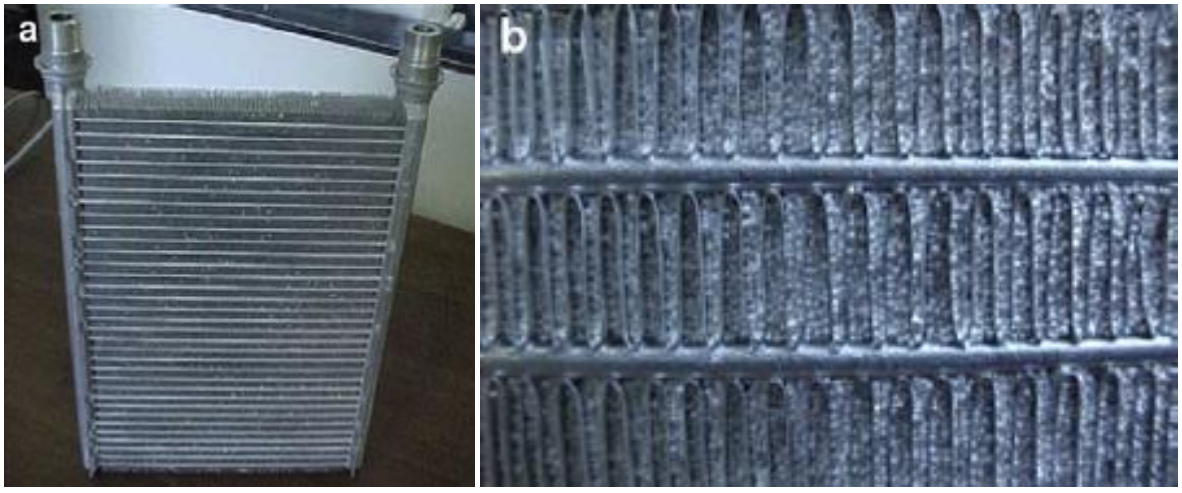

(a) (b)

Figure 2-12 Adsorber heat exchanger by Verde et al.: (a) general (b) detailed view [85]

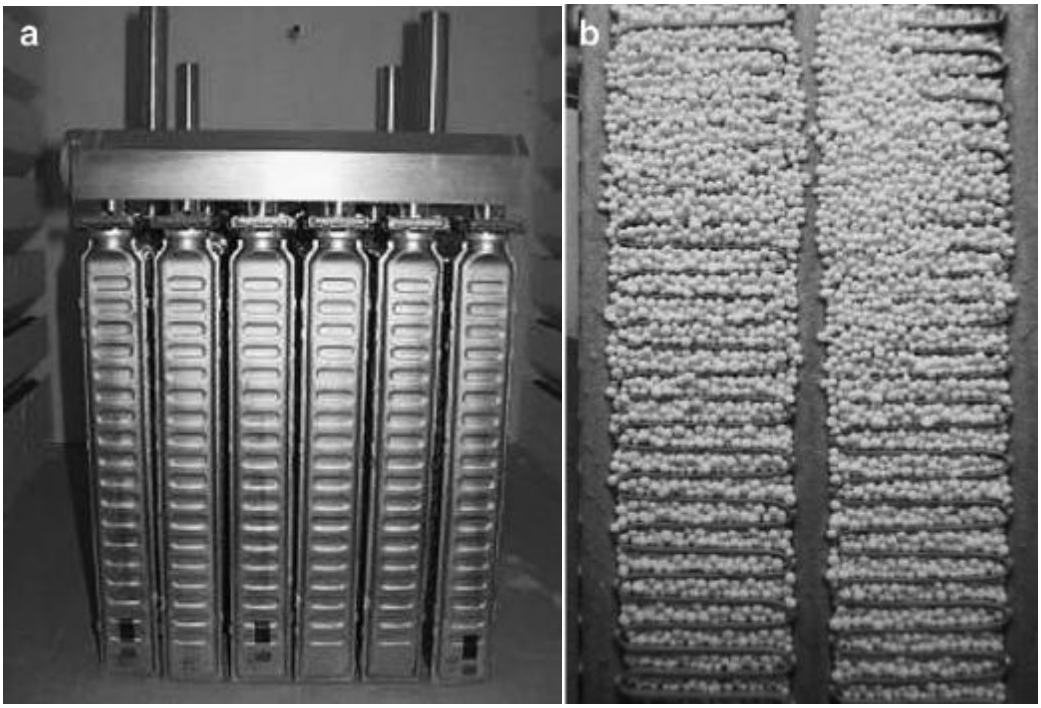

(a) (b)

Figure 2-13 Adsorber reactor by Vasta et al.: (a) overall view (b) detailed view [37]

Sharafian and Bahrami [2] recommended a finned tube adsorber bed design in one of their review papers over various adsorber bed designs; stating that it performed better than other

designs. Further optimization of fin spacing and fin height in finned tube adsorber beds and increasing thermal conductivity of adsorbent materials, are proposed methods to improve the adsorption performance.

2.10.1.3 Annulus tube heat exchanger

Zhang [5] designed and tested an automobile adsorption cooling system using zeolite/water as a working pair, driven by exhaust gas from a diesel engine. The adsorber had a simple structure of tube and radial fins fitted in a circular shell, as shown in Figure 2-14. The results showed that this adsorber was able to be driven by exhaust gases up to 200℃ which is available after being processed by the catalytic converter [86]; giving a SCP of 25.7W/kg and COP of 0.38 without heat or mass recovery. The main reasons for such low SCP is the long cycle time of 131.5min, the use of a single bed system with a large weight of 31kg and operating intermittently. Performance may be enhanced by using two or more adsorber beds in the system with optimum operating parameters.

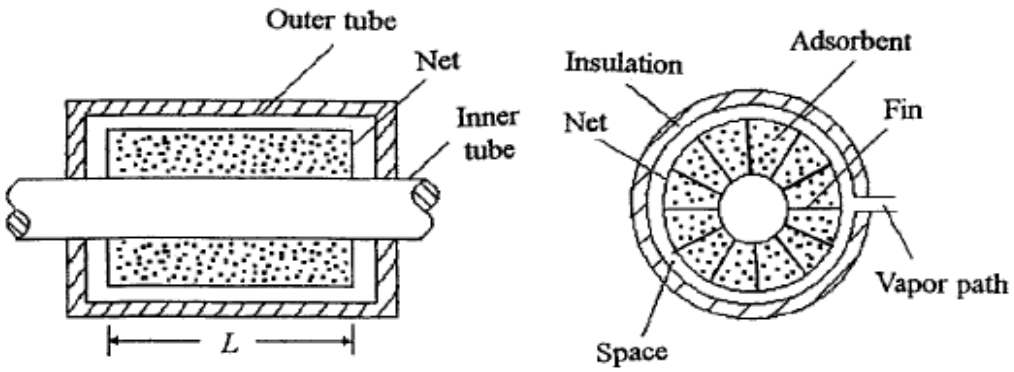

Figure 2-14 Schematic of the adsorber by Zhang [5]

2.10.1.4 Modular assembled adsorber heat exchanger

Zhong et al. [86] developed a lumped parameter model to study the performance of an adsorption air conditioning system for heavy-duty vehicles using zeolite/water as a working pair. The system design involved a modular assembly containing an adsorber, a heat-pipe type heat exchanger and an adiabatic section in between, as shown in Figure 2-15(a). The module was a sealed vessel that was maintained under vacuum pressure to ensure effective operation of the zeolite/water pair. The adsorption cooling system was powered by exhaust gases which reached about 250℃ and simulation results showed that this system could produce a SCP of 70.6W/kg and a COP of 0.436 when packed with 4kg of adsorbents. The low SCP could be due to the long cycle time of 30min. More research has been conducted by Zhong [6] on this air conditioning structure, which showed that it needs about 8 modules to produce 3.5kW cooling output using advanced designs, such as consolidated zeolite and adding fins or metal foams.

Wu et al. [92] studied an adsorption cooling module driven by exhaust waste heat with a similar structure, as shown in Figure 2-16. In the experimental tests, each module could deliver 2-10.5W cooling output, depending on the evaporating temperature. The authors proposed a multiple module adsorption air conditioning system for a truck cabin using this design of cooling modules.

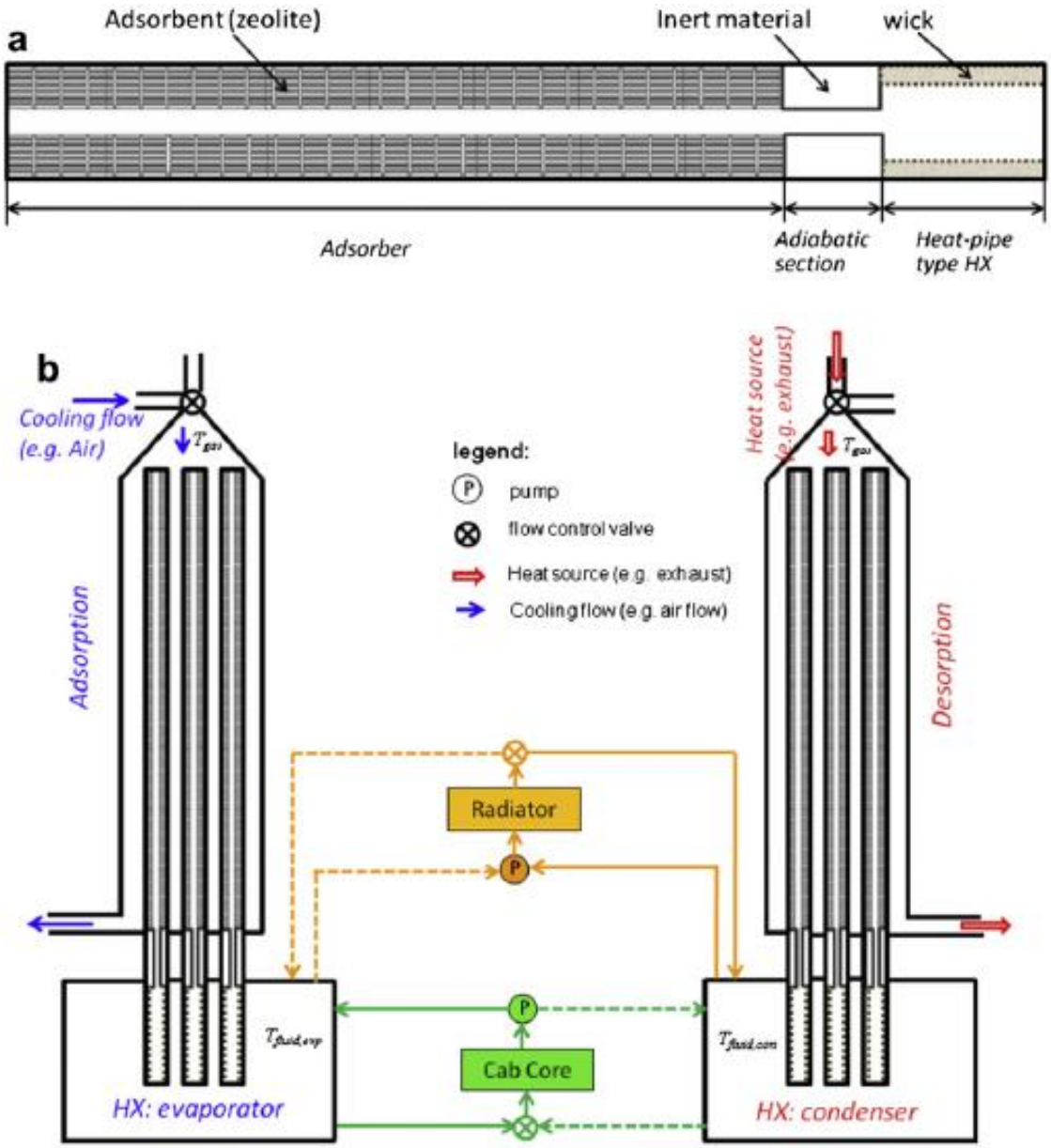

Figure 2-15 Schematics of (a) an individual module and (b) the system integration by Zhong et al. [86]

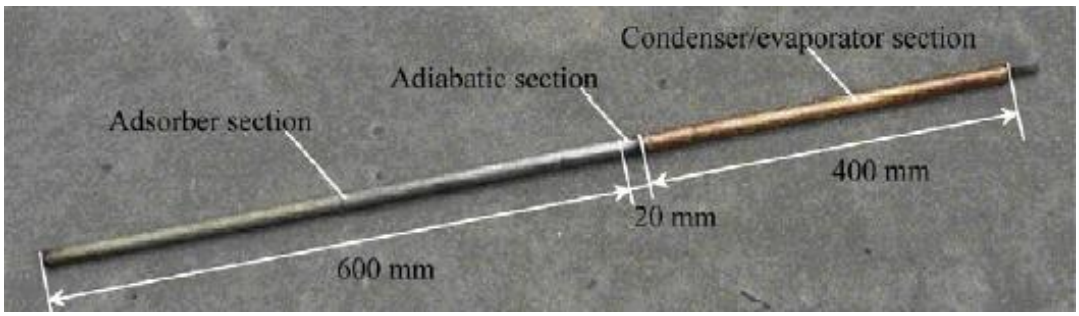

Figure 2-16 Adsorption cooling module by Wu et al. [92]

Table 2-9 compares all the systems described above in terms of adsorption bed structure, operating parameters and performance. Based on the values given in the table, the following conclusions can be made:

1. Many adsorption working pairs have been investigated in an adsorption cooling system for automotive application, including: activated carbon/ammonia, activated carbon/methanol, SAPO-34/water, silica gel/water and zeolite/water. Among these adsorption working pairs, SAPO-34/water, silica gel/water and activated carbon/ammonia were used with a regeneration temperature of around 90℃ using the engine coolant loop; while zeolite/water and activated carbon/methanol were applied with a regeneration temperature of above 200℃ using the exhaust gases.

2. The evaporation temperature investigated is normally below 15℃ except for the research by Tamainot-Telto and Critoph; while the condensation temperature used is normally above 32℃.

3. The adsorption cooling system for automotive application is not compact enough; leading to a heavy weight (35kg by Critoph, 60kg by Vasta, 86kg by Boer) and large volume (19.9dm^3 by Critoph, 170dm^3 by Vasta).

4. The system employed with the activated carbon/ammonia working pair can achieve the largest SCP of 800W/kg; however, ammonia used as the refrigerant is toxic. The adsorption cooling system using water, which is environmentally friendly and nontoxic, achieved an SCP of up to 334W/kg.

5. The COP of nearly all the adsorption cooling systems investigated for automotive application was below 0.5, except for the work by Verde. Therefore more research is needed to investigate a means of enhancing the performance of the adsorption system to utilise efficiently the waste heat from automotive engines and to provide for the required air conditioning without increasing the size of the engine.

Table 2-9 Published work on adsorption cooling system for automotive application

Author	Adsorber heat exchanger configuration	Mass of adsorbent (kg)	Heat source	T_{evap} (°C)	T_{cond} (°C)	SCP (W/kg)	Cooling load (kW)	T_{gen} (°C)	COP	Cycle time (min)	Weight (kg)	Volume (dm^3)	Mass recovery
Tamainot-Telto et al. (2009) [34]	Plate heat exchanger (AC/ammonia)	2	Engine coolant loop	20	32	800	1.6	90	0.22	1	9 for each reactor	-----	Yes
Critoph et al. (2010) [4]	Plate heat exchanger (AC/ammonia)	2	Engine coolant loop	21	32	800	1.6	92	0.22	2.5	35	19.9	Yes
Boer et al. (2008, 2009) [35, 36]	Finned flat tube heat exchanger (silica gel/water)	6	Engine coolant loop & exhaust gas	15	33	334	2 (lab); 0.8 (on-board)	90	0.4 (lab); 0.5—0.6 (on-board)	3	86	-----	No
Zhong et al. (2011) [86]	Modular assembled adsorber and heat exchanger (zeolite/water)	4	Exhaust gas	7	38	70.6	0.28	250	0.436	30	-----	-----	No
Verde et al. (2010) [85]	Finned flat tube heat exchanger (SAPO-34/water)	5.76	Engine coolant loop	10	35	300	2—3	90	0.6	10	-----	13.2 for adsorber	No
Zhang (2000) [5]	Annulus tube heat exchanger (zeolite/water)	6.2	Exhaust gas	10	45	25.7	0.16	200	0.38	131.5	31 for adsorber	-----	No
Ramji et al. (2014) [97]	Annulus tube heat exchanger (AC/methanol)		Exhaust gas				0.65	200	0.25	20			
Vasta et al. (2011) [37]	Finned flat tube heat exchanger (AQSOA-FAM-Z02/water)	4.6	Engine coolant loop	12	35	276	1.2 (lab); 2 (in truck test)	90	0.303	620s	60	170	No
Wu et al. (2011) [92]	Modular assembled adsorber and heat exchanger (zeolite/water)	45g per module	Exhaust gas	16.2	18	233	0.0105	325					No

2.10.2 Simulation of adsorption systems

Simulation methods are powerful tools in investigating the performance of an adsorption air-conditioning system and investigating means of improving the design of adsorption beds and overall system performance. In modelling, the performance of the adsorption refrigeration system can be evaluated based on several differential governing equations that determine the various operating parameters, such as temperature, pressure and refrigerant uptake.

There are primarily two simulation methods for solving the equations that describe the performance of the adsorption system. The first is mathematical modelling based on solving governing equations mathematically by a differential equation solver [53, 60, 98-135]. The second is finite element modelling using computational finite element technique completed by commercially available software [136, 137].

2.10.2.1 Mathematical modelling

At present, mathematical modelling is the most commonly used technique to predict the performance of an adsorption refrigeration system. Various adsorption cycles and adsorption bed designs using different working pairs, including activated carbon/ammonia, zeolite/water and silica gel/water, were modelled [53, 60, 98-126]. Mathematical modelling solves a set of differential equations to simulate the heat and mass transfer of an adsorption cooling system with an adsorber, evaporator and condenser. There are several mathematical modelling methods including the lumped-

parameter simulation technique, distributed-parameter simulation technique and dynamic simulation technique.

The lumped-parameter simulation technique is the simplest method due to several assumptions used to simplify the governing equations. The most important assumption is that each component of the adsorption bed (tube, fins and adsorbent material) are assumed to have the same properties in every position and status during the same period of time [53, 104-118, 127, 128]. Therefore, the governing equations of a lumped-parameter simulation are reduced to differential equations of time, including adsorption isotherms and kinetic equations, heat transfer and mass balance equations.

The distributed-parameter simulation technique takes into account the variation in properties and status at different positions of all the parts [119-124, 129]. In this way, governing equations of distributed-parameter simulation are differential equations of time and position.

The dynamic simulation technique improves the distributed-parameter simulation method, by taking into account the diffusion of refrigerant vapour in the adsorbent granules [60, 125, 126, 130, 131]. Therefore the dynamic simulation technique contains the diffusion equation. Classes of governing equation of these three methods are summarised in Table 2-10.

Table 2-10 Classes of governing equation of three mathematical modelling methods

Lumped-parameter simulation technique	Distributed-parameter simulation technique	Dynamic simulation technique
• Adsorption isotherms and kinetic equation • Heat transfer equations • Mass balance equation	• Adsorption isotherms and kinetic equation • Heat transfer equations • Mass balance equation	• Adsorption isotherms and kinetic equation • Heat transfer equations • Mass balance equation • Diffusion equation

2.10.2.2 Finite element modelling

Finite element modelling utilises three-dimensional detailed geometry to simulate the adsorption beds. The Navier-Stokes equations are the principal equations which are considered to describe the transfer of mass and energy [138, 139]. These coupled differential equations can be solved by a computational finite element (FE) technique [136]. In this way, the whole geometry is meshed to discrete finite control volumes; governing equations are applied to each domain and solved by computational techniques.

Finite element modelling can accurately simulate the diffusion, heat and mass transfer of the actual processes occurring in the adsorption cooling system [140]. With the development of advanced, fast, high powered computers, the finite element modelling technique is becoming a practical tool for investigating performance of adsorption cooling systems [139-141]. There is a great deal of finite element software like SolidWorks Flow Simulation, COMSOL Multiphysics, ANASYS CFX and Fluent. However, there is limited published work involving the use of finite element to simulate the adsorption cooling system, compared to the use of mathematical modelling [136, 137].

2.10.2.3 Simulation work on an automotive adsorption air conditioner

Some researchers used simulation techniques to investigate the performance of an adsorption cooling system for automotive application. Zhang and Wang [142] set up a lumped parameter model and concluded that improving overall heat transfer coefficient and mass transfer coefficient is essential to increase SCP, which is the most important parameter for application in automobile adsorption coolers. Hu et al. [143] successfully built up a mathematical model using LDF (linear driving force) to study the effect of cycle time, adsorbent thickness, heating fluid temperature and mass recovery on the performance of a composite zeolite with aluminium foam-water adsorption refrigeration system driven by engine exhaust heat. The authors concluded that the composite zeolite with aluminium foam and the mass recovery cycle can improve the value of COP and SCP at a short cycle time. However, in this model the thermal resistance between the metal tube and adsorbent bed was neglected, which needs to be further improved. Jribi et al. [144] developed a mathematical model of an activated carbon/HFO-1234ze(E) adsorption cooling cycle for automobile air conditioning applications using waste heat. A four-bed adsorption cooling system packed with 8kg of adsorbents was simulated and the results showed that the system was able to produce 2kW of cooling load.

Ramji et al. [97] set up a finite element model and tested an automobile adsorption air conditioning system with annulus tube heat exchanger shown in Figure 2-17 and activated carbon/methanol as the working pair. The adsorption system is driven by engine exhaust gas of 200℃. The results of the model were validated with the experimental results and showed that the adsorption cooling system was able to

produce a cooling power of 0.65kW and COP about 0.25 with cycle time of 1200s. The authors also concluded that wall thickness of the adsorber is one of the most important parameters to improve the heat transfer performance. Further research is needed to increase the COP and SCP, with the suggested cycle time of less than 10-15min for an automobile adsorption cooling system.

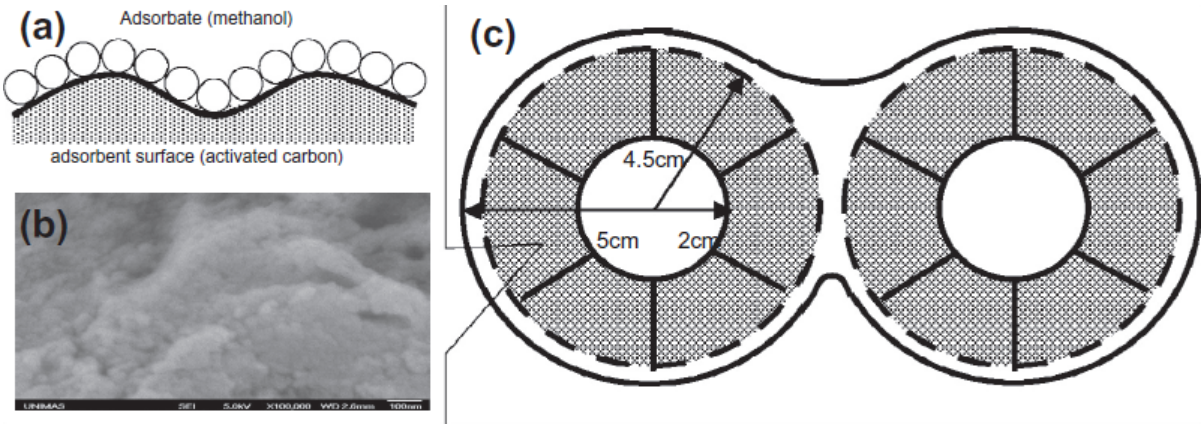

Figure 2-17 Schematic of adsorber by Ramji et al. [97]

2.10.3 Adsorption cooling system for a locomotive driver's cabin

Jiangzhou et al. [93-96] designed and tested an adsorption air-conditioner to be used in a locomotive driver's cabin which was driven by waste heat from internal combustion engine exhaust gas, using zeolite/water as the working pair. Experimental test results showed that this system could produce more than 4kW for 1.5h as well as a COP of 0.25 with 140kg adsorbent material. In the prototype testing, 3-4.2kW cooling capacity was achieved under typical conditions. The authors concluded that the cooling power output was strongly influenced by the operating conditions of the train. Further investigation for improvement of the system is needed to meet the

requirements for cooling of a locomotive driver's cabin space and realize commercial applications.

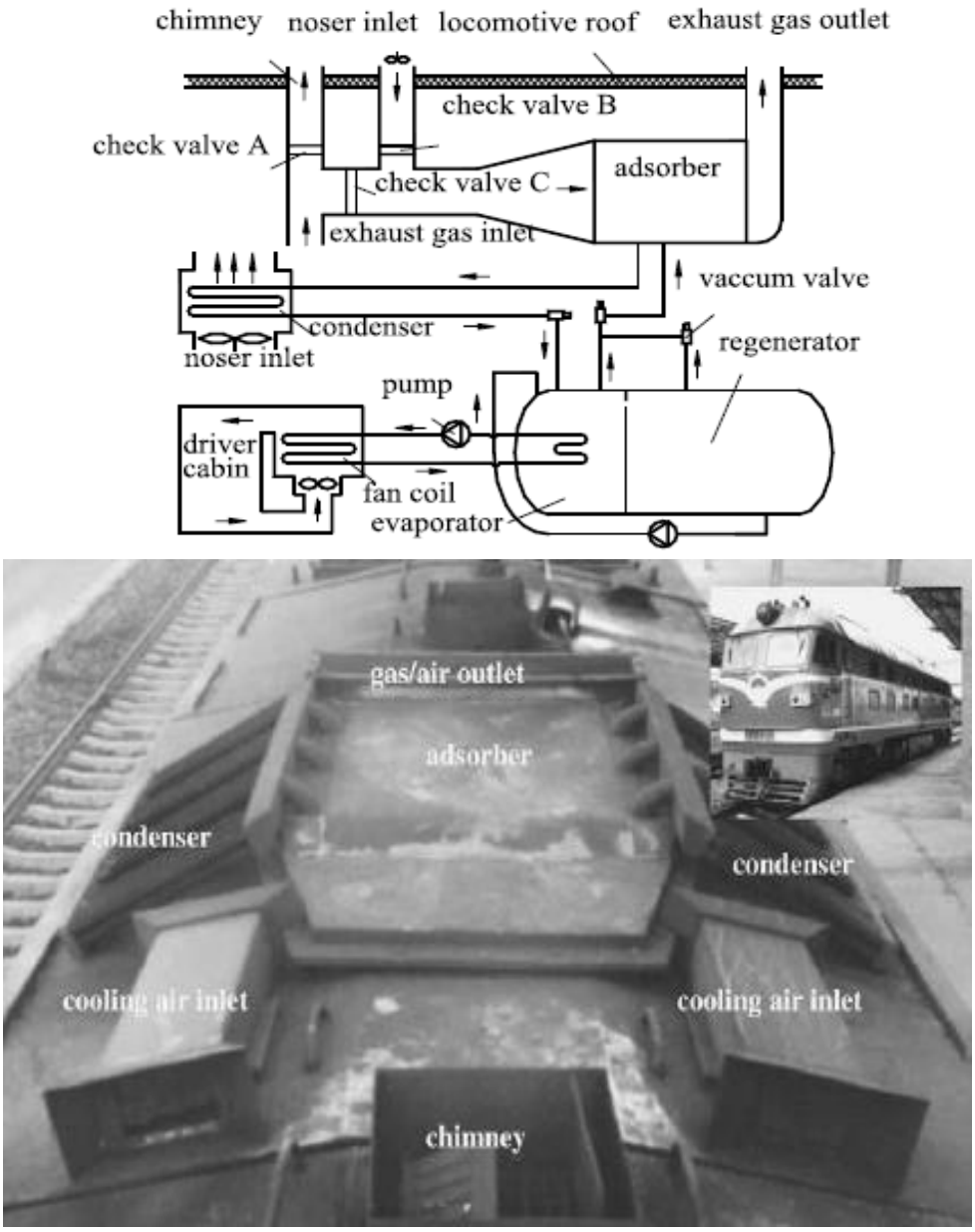

Figure 2-18 Adsorption cooling system for locomotive driver-cabin by Jiangzhou et al. [93-96]

2.11 Summary and conclusions

Nowadays, almost all the automotive air-conditioners utilise a traditional mechanical vapour compression cycle. They are driven by the car engine and result in increasing fuel consumption and pollutant emissions. Also the refrigerant used has high global warming potential. Therefore, new energy efficient and environmentally friendly cooling technology is needed. Adsorption cooling technology is a good alternative solution that can use low-grade waste heat from the automotive engine. Since it does not need fuel to drive, there is no pollution produced in the operation process of an adsorption automotive air conditioner.

It is clear from the literature review that significant research on adsorption cooling techniques for automotive application has been carried out. These investigations proved that the adsorption cooling system is able to produce the cooling load required for vehicles using waste heat from the engine coolant loop and/or engine exhaust gases; which shows a promising potential for reducing fuel consumption and exhaust gas emission. However, there is still no commercial use of the adsorption system in automotive applications. This is mainly due to two reasons:

1. The adsorption cooling system is not compact enough, leading to heavy weight and large volume. The heavy weight increases the engine load and affects the dynamic performance of the engine and the large volume also reduces the feasibility to fit the adsorption refrigeration system into the required space in cars.
2. The adsorption cooling system has a low COP, mostly below 0.5, which shows that the system is not efficient enough to use waste energy to produce cooling.

Therefore, further research is needed to make the adsorption cooling system more compact and efficient for automotive application. Overall, to develop a compact automotive adsorption cooling system a target of more than 400 W/kg for SCP and more than 0.5 for COP should be achieved [8]. Generally, the system should have a weight of less than 30kg and a volume of less than 16dm^3.

Based on the comprehensive literature review of adsorption refrigeration techniques described above, the following conclusions can be made:

1. There are many types of adsorption refrigeration cycles and each of them has advantages and disadvantages. Generally, the two-bed cycle is most commonly applied in commercial use and attracts most researchers' attention. It is the simplest cycle which can provide a continuous cooling effect.

2. The working pair is one of the most important issues affecting the performance of the adsorption refrigeration system. Advanced metal organic framework adsorbent materials have shown high water adsorption characteristics that can be used in the development of a compact and efficient cooling system for automotive application. Using a working pair with high refrigerant adsorption capacity will improve the cooling capacity and efficiency.

3. The adsorption bed design has a significant effect on the heat and mass transfer performance. An adsorption bed design which has good heat and mass transfer performance will enhance the performance of the adsorption air conditioning system, including its cooling capacity and efficiency.

Therefore, this research aims to investigate the use of MOF adsorbent materials and adsorption bed design to develop an adsorption air conditioning system for automotive application.

CHAPTER 3 ADSORBENT MATERIALS CHARACTERISATION

3.1 Introduction

The working pair is one of the most important issues affecting the performance of the adsorption refrigeration system, as concluded in section 2.11. Therefore, utilising an adsorption working pair with high refrigerant uptake is an efficient method to improve performance; such as the cooling capacity and efficiency of the adsorption air conditioning system. Increasing the refrigerant uptake per unit mass of adsorbent materials results in decreasing the mass of the adsorbent; and hence reduces the adsorber bed's mass and volume, leading to reducing the overall system size.

In this research, water is chosen as the refrigerant because it has a large latent heat of vaporization and it is environmentally friendly. Adsorbents used with water are zeolite, silica gel, SAPOs and MOFs. Among these adsorbent materials, zeolite needs the highest generation temperature, higher than 200 ℃, which is difficult to achieve in an automotive application. Therefore, investigation of zeolite adsorbent is not included in this research.

Based on the literature review in section 2.7.5, there are many types of MOFs which have been investigated regarding their water adsorption properties. The group led by Dr. Raya AL-Dadah at the University of Birmingham tested the water uptake

characteristics of several MOFs' adsorbent materials, including MIL-101Cr, MIL-100Cr, Fe-BTC, Cu-BTC and CPO-27Ni. The results are shown in Figure 3-1. The horizontal axis is the relative pressure which presents the ratio of water vapour pressure to the pressure of the adsorption bed. The working relative pressure of the adsorption air conditioning system is normally between 0 and 0.4. For example, at the operating conditions normally used in the research of automotive adsorption air conditioning systems, with the desorption temperature of 90 ℃ and condensation temperature of 20 ℃ in the desorption process, the relative pressure value is 0.03 and with the adsorption temperature of 30 ℃ and evaporation of 15 ℃ in the adsorption process, the relative pressure value is 0.4. It is clear from Figure 3-1 that MIL-101Cr and MIL-100Cr has large water uptake, but the highest increase in the water uptake occurs when the relative pressure is larger than 0.4 which is not in the working relative pressure range. In the working relative pressure range the water adsorption isotherms of Cu-BTC and CPO-27Ni are higher than those of MIL-101Cr, MIL-100Cr and Fe-BTC. However, Cu-BTC is not stable in adsorption cycles with water vapour, as explained in section 2.7.5. On the contrary, the water adsorption process of CPO-27Ni shows a stable operation after 40 cycles. Therefore, CPO-27Ni is chosen in this research as a promising MOF adsorbent material to improve the performance of an adsorption air conditioning system for automotive application.

This chapter investigates the water vapour uptake of three adsorbent materials, including silica gel RD-2060, SAPO-34 and CPO-27Ni with water as the refrigerant. The water uptake characteristics of CPO-27Ni and SAPO-34 were tested using the dynamic vapour sorption (DVS) analyser and the results were compared to silica gel

RD-2060. Based on the experimental results, equations of water adsorption isotherms and kinetics for both CPO-27Ni and SAPO-34 are developed.

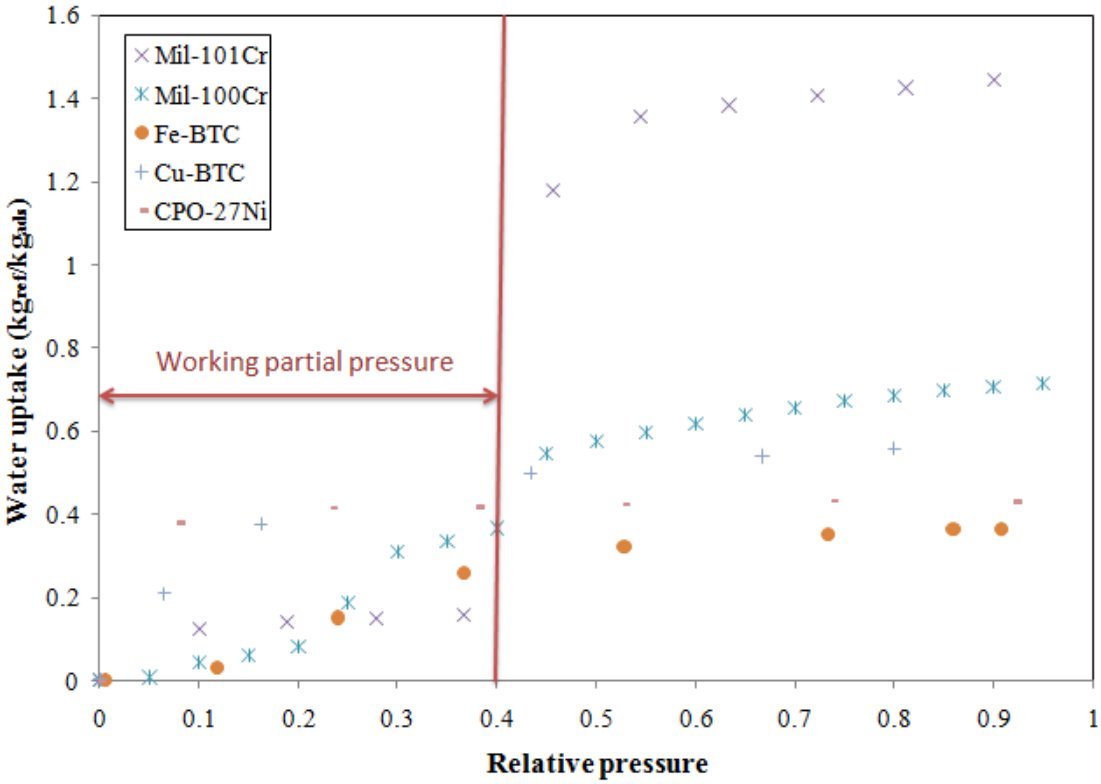

Figure 3-1 Adsorption characteristics of MOFs' adsorbent materials (T=25 ℃)

3.2 DVS test work

A dynamic vapour sorption (DVS) gravimetric analyser has been used to investigate the water adsorption isotherms and kinetics of SAPO-34 and CPO-27Ni under different relative pressures, as shown in Figure 3-2. The DVS analyser can directly measure the adsorbent's mass and prevent refrigerant vapour condensation on the moving balance parts [1]. The ultra-sensitive recording microbalance is used to measure the adsorbent's mass with the accuracy of one part in ten million of the sample mass, which has the advantage of high long-term stability in the microgram

level [145]. Before loading the sample, dry nitrogen flow is used to purge the balance head and reaction chamber to remove any vapour left from the previous experiments. After that the nitrogen flow stops and only the refrigerant vapour flows through the adsorbent material in the following steps. The purge flow is controlled automatically to prevent vapour condensation in the balance head. Therefore accurate refrigerant uptake measurements can be achieved. The refrigerant vapour pressure is controlled by the mass flow controller in mixing dry and saturated refrigerant vapour. The pressure and temperature are monitored by the optical vapour pressure sensor and RTD thermocouple; which are very close to the sample pan during the test. The DVS analyser is controlled by a PC microcomputer which is interfaced with the microbalance.

During the test, a 10mg adsorbent sample is placed in the reaction chamber and dried at a temperature of 150 ℃ until there is no change in the adsorbent's mass. Then the adsorbent begins to adsorb the refrigerant vapour at a fixed temperature of 25 ℃. The adsorption isotherm is calculated by measuring the adsorbent uptake at each value of vapour pressure at the point of no change in the adsorbent's mass as shown in Figures 3-3 and 3-4.

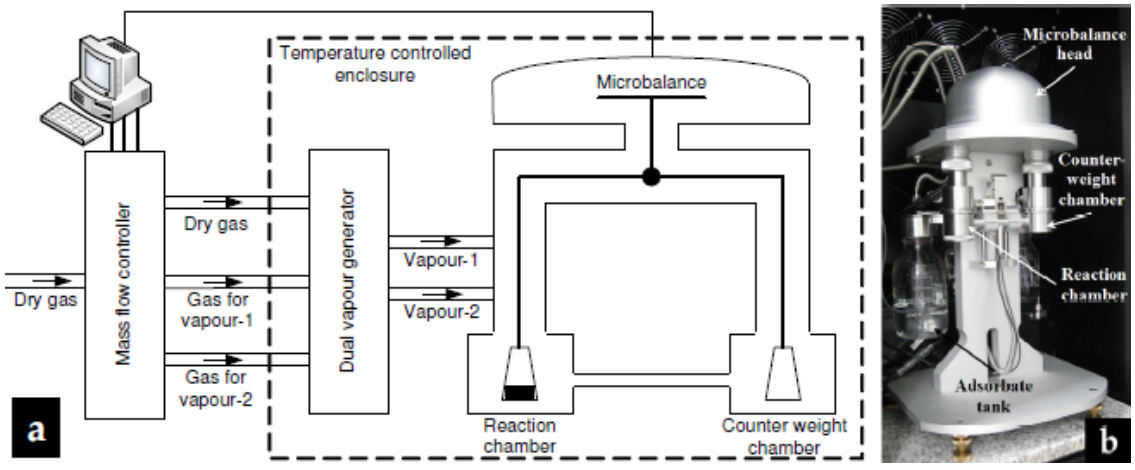

Figure 3-2 Schematic and pictorial diagram for the DVS analyser [1]

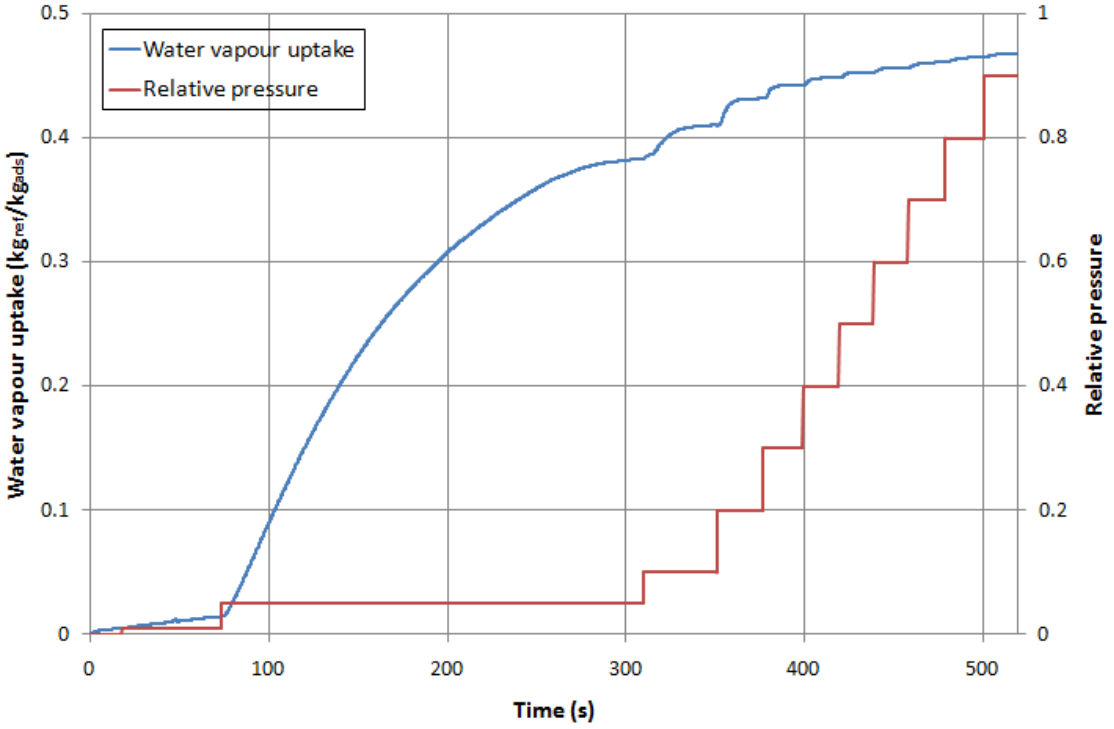

Figure 3-3 Temporal evaluation of the relative pressure and water vapour uptake for CPO-27Ni (T=25 ℃)

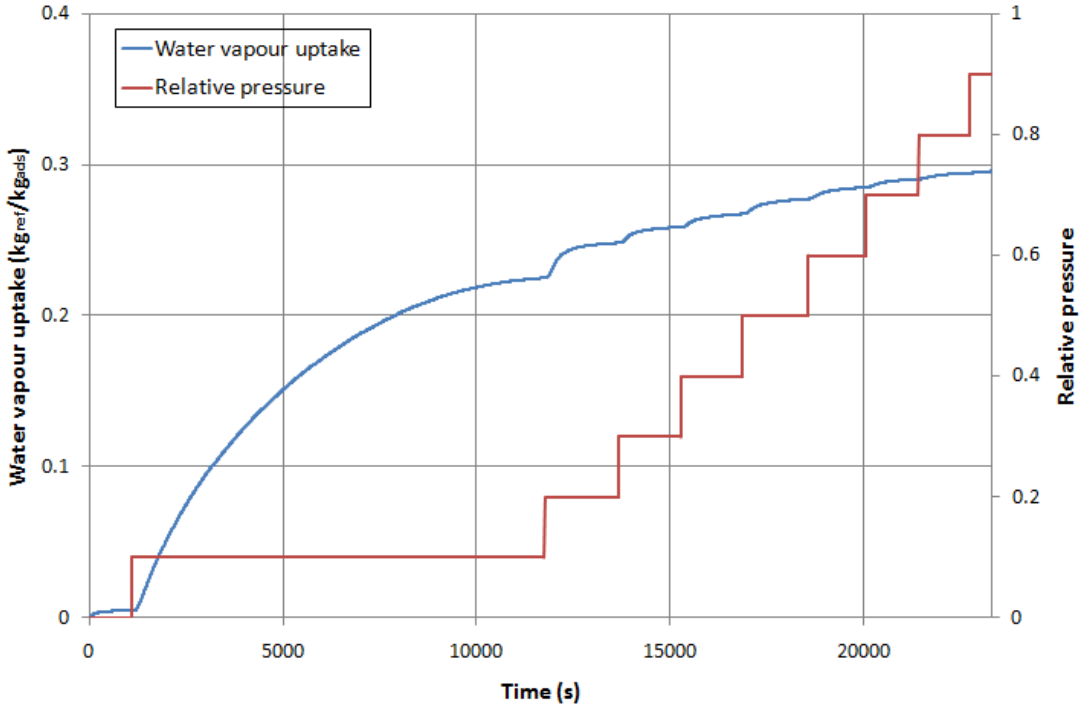

Figure 3-4 Temporal evaluation of the relative pressure and water vapour uptake for SAPO-34 (T=25 ℃)

3.3 Adsorption performance comparison

Figure 3-5 compares the equilibrium water vapour uptakes of silica gel RD-2060, SAPO-34 and CPO-27Ni based on the test results obtained using the DVS analyser. It is clear that during the working relative pressure between 0 and 0.4, the water vapour uptake of CPO-27Ni is much higher than those of SAPO-34 and silica gel RD-2060. At the relative pressure of 0.4, the water vapour uptake of CPO-27Ni is 0.451, which is 61.8% and 104.1% higher than those of SAPO-34 and silica gel RD-2060 respectively. Besides, the increase of water vapour uptake for CPO-27Ni is the highest among the three adsorbent materials with the increase of relative pressure from 0 to 0.1. Therefore, based on the outstanding water adsorption performance, it can be concluded that the CPO-27Ni is a promising adsorbent material to improve the performance of an adsorption air conditioning system for automotive application.

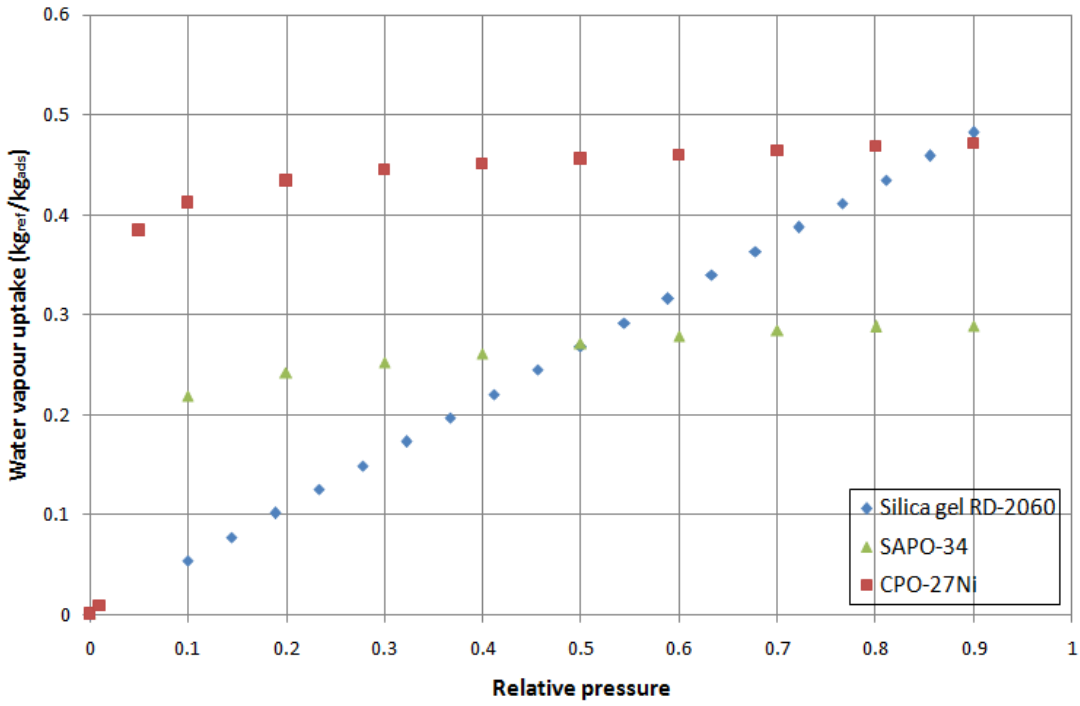

Figure 3-5 Comparison of water vapour uptake for silica gel RD-2060, SAPO-34 and CPO-27Ni

3.4 Adsorption isotherms and kinetics equations for SAPO-34/water and CPO-27Ni/water

3.4.1 Literature review of adsorption isotherms

Nearly all published research utilises the linear driving force equation (LDF) to describe the adsorption kinetics of an adsorption working pair. However, various adsorption isotherm equations have been developed. Therefore this section presents the literature review of adsorption isotherms.

Adsorption isotherms describe the maximum amount of refrigerant contained in the adsorbent at a certain temperature and pressure. Numerically, it equals to the ratio of the maximum mass of the refrigerant to the mass of the adsorbent. There are six types of equations used to model the isotherms of adsorption working pairs. They are described in the following paragraphs.

The Tóth equation 3-1 has been used to estimate the equilibrium water uptake for silica gel by Chua et al. [120], Voyiatzis et al. [121] and Saha et al. [124].

$$w_{\max} = \frac{w_m K_0 \exp\left[\Delta H_{ads} / (RT_{ads})\right] P_{\text{ads}}}{\left\{1 + \left\{K_0 \exp\left[\Delta H_{ads} / (RT_{ads})\right] P_{\text{ads}}\right\}^{t_1}\right\}^{1/t_1}} \tag{3-1}$$

Where, w_m denotes the monolayer capacity; K_0 is the pre-exponential constant; ΔH_{ads} is the isosteric enthalpy of adsorption and t_1 is the dimensionless Tóth constant. T_{ads} and P_{ads} are the temperature and pressure of the adsorbent respectively.

Khan et al. [112] and Miyazaki and Akisawa [113] also presented the adsorption isotherm of silica gel/water using the following equation:

$$w_{\max} = \frac{0.8 \times [P_{sat}(T_{ref}) / P_{sat}(T_{ads})]}{1 + 0.5 \times [P_{sat}(T_{ref}) / P_{sat}(T_{ads})]} \tag{3-2}$$

Where T_{ref} represents the temperature of the refrigerant vapour.

Freundlich's equation 3-3 was also developed to describe the adsorption isotherm of silica gel/water [109, 110]:

$$w_{\max} = 0.346 \left[\frac{P_{sat}(T_{ref})}{P_{sat}(T_{ads})} \right]^{1/1.6} \tag{3-3}$$

Equations 3-2 and 3-3 are more accurate than equation 3-1 because they take the pressure and temperature of both the refrigerant vapour and the adsorbent into consideration. A modified Freundlich's equation 3-4 was developed [53, 105, 108, 115-118, 135] to estimate the equilibrium water vapour uptake by silica gel more accurately.

$$w_{\max} = A(T_{ads}) \left[\frac{P_{sat}(T_{ref})}{P_{sat}(T_{ads})} \right]^{B(T_{ads})} \tag{3-4}$$

Where $A(T_{ads})$ and $B(T_{ads})$ are determined by equations 3-5 and 3-6; where A_{0-3} and B_{0-3} are all empirical constants shown in Table 3-1.

$$A(T_{ads}) = A_0 + A_1 T_{ads} + A_2 T_{ads}^2 + A_3 T_{ads}^3 \tag{3-5}$$

$$B(T_{ads}) = B_0 + B_1 T_{ads} + B_2 T_{ads}^2 + B_3 T_{ads}^3 \tag{3-6}$$

Table 3-1 Constants in equations 3-5 and 3-6

Constant	Value	Unit
A_0	-6.5314	$kg_{water}/kg_{silicagel}$
A_1	7.2452×10-2	kg_{water} /($kg_{silicagel}$ K)
A_2	-2.3951×10-4	kg_{water} /($kg_{silicagel}$ K^2)
A_3	2.5493×10-7	kg_{water} /($kg_{silicagel}$ K^3)
B_0	-15.587	1
B_1	0.15915	K^{-1}
B_2	-5.0612×10-4	K^{-2}
B_3	5.3290×10-7	K^{-3}

Apart from the equations introduced above, equations 3-7 to 3-9 are also used to estimate isotherms of zeolite/water [60, 122, 123, 125, 126], silica gel/water [136] and activated carbon/methanol [122]; where $a_{0\text{-}3}$ and b_{0-3} are all empirical constants.

$$\ln(P_{ads}) = a(w_{\max}) + \left[b(w_{\max}) / T_{ads}\right] \tag{3-7}$$

$$a\left(w_{\max}\right) = a_0 + a_1 w_{\max} + a_2 w_{\max}^2 + a_3 w_{\max}^3 \tag{3-8}$$

$$b\left(w_{\max}\right) = b_0 + b_1 w_{\max} + b_2 w_{\max}^2 + b_3 w_{\max}^3 \tag{3-9}$$

Finally, equation 3-10 was also used to present the isotherm of silica gel/water, activated carbon/ammonia, activated carbon/methanol and activated carbon/ethanol: where w_0 is the maximum adsorption capacity and $F(P,T)$ is a function of pressure and temperature as shown in Table 3-2.

$$w_{\max} = w_0 \exp\left[F(P,T)\right] \tag{3-10}$$

The following sections describe the adsorption isotherms and kinetics of SAPO-34/water and CPO-27Ni/water respectively.

Table 3-2 Detailed equations for equation 3-10

Reference	Equations	Adsorption working pair	Equation's name
[106, 111]	$w_{\max} = w_0 \exp\left[18\Delta H_{ads} / RT_{ads}\right] P$ (3-11)	Silica gel/water	Henry's law equation
[102, 107]	$w_{\max} = w_0 \exp\left[-K(T_{ads} / T_{sat} - 1)^n\right]$ (3-12)	Activated carbon/ ammonia	Dubinin-Radushkevich equation
[130, 131]	$w_{\max} = w_0 \exp\left\{-D\left[T_{ads} \ln\left(P_{sat} / P_{ads}\right)\right]^n\right\}$ (3-13)	Activated carbon/ methanol	Dubinin-Astakhov equation
[134]	$w_{\max} = w_0 \exp\left\{-\left[\frac{-RT_{ads} \ln\left(P_{sat} / P_{ads}\right)}{E}\right]^n\right\}$ (3-14)	Activated carbon/ ethanol	Dubinin-Astakhov equation
[127]	$w_{\max} = w_0 \exp\left\{-D\left[T_{ads} \ln\left(P_{sat} / P_{ads}\right)\right]^2\right\}$ (3-15)	Activated carbon/ ethanol	Dubinin-Radushkevich equation

3.4.2 Adsorption isotherm equations

In this section, the equilibrium of water uptake for SAPO-34 and CPO-27Ni are measured and equations for the adsorption isotherm of SAPO-34/water and CPO-27Ni working pairs are developed.

Based on the experimental results described in section 3.3, equilibrium water uptake is determined using the same equation as equation 3-14 for both SAPO-34 and CPO-27Ni. The data are fitted and the parameters of w_0, n and E are determined using Engineering Equation Solver software, with values shown in Table 3-3. The fitting of the experimental results of SAPO-34/water and CPO-27Ni to the equations are shown in Figures 3-6 and 3-7 respectively. The deviation between the predicted and experimental adsorption isotherm for SAPO-34 and CPO-27Ni are 6.5% and 5.1%

respectively, indicating the good agreement between the adsorption isotherm equations and the experimental results.

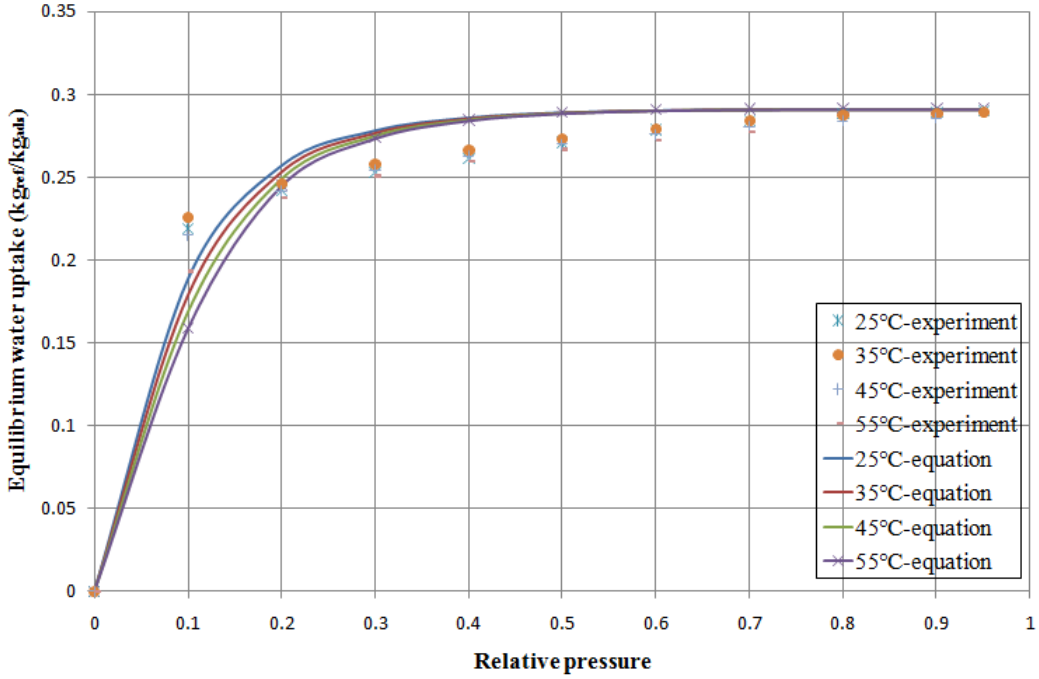

Figure 3-6 Fitting of adsorption isotherm equation to experimental results of SAPO-34/water

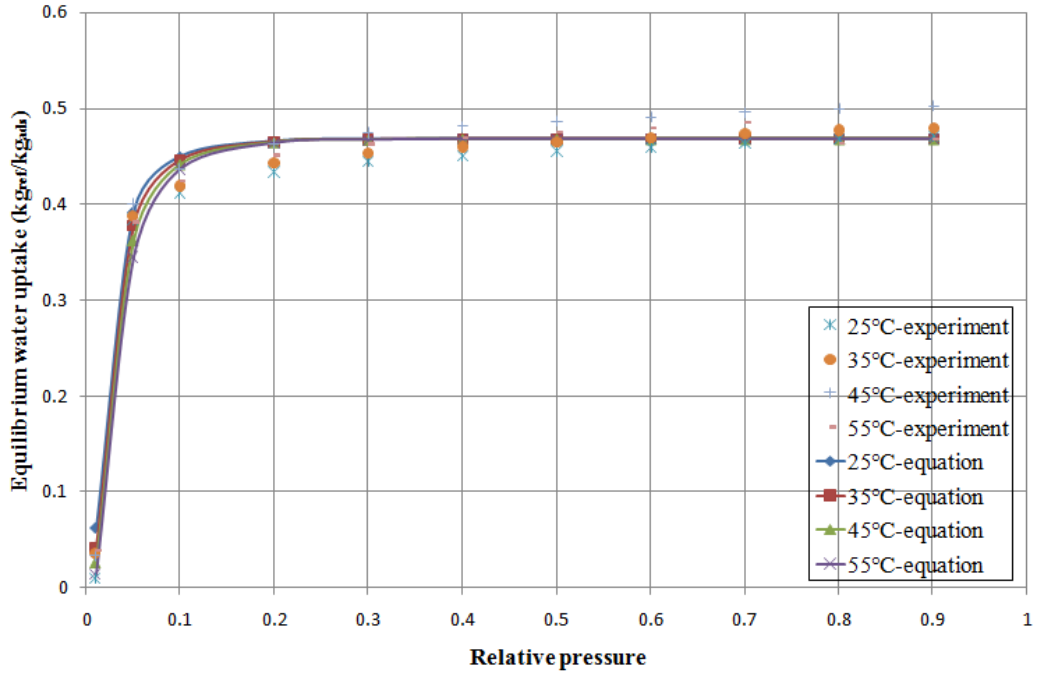

Figure 3-7 Fitting of equation to experimental results for adsorption isotherm of CPO-27Ni/water

Table 3-3 Parameters of equation 3-14

Parameter	SAPO-34/water	CPO-27Ni/water
w_0	0.291211	0.46826
n	3.5	5.6476
E	7239.17J/mol	10088.7J/mol

3.4.3 Adsorption kinetics equations

Adsorption kinetics describes the speed of the adsorption process which is influenced by the heat and mass transfer performance of the adsorption beds. A higher adsorption rate can be achieved with better heat transfer performance for the same adsorbent materials. In the modelling, the conventional linear driving force equation (LDF) [105] can be used to model the adsorption kinetics; equation 3-16.

$$\frac{dw}{dt} = K\left(w_{\max} - w\right) \tag{3-16}$$

Where, w is the water vapour uptake per unit mass of dry adsorbent determined as the ratio of the mass of water vapour adsorbed to the mass of dry adsorbent granules. K is the overall heat transfer coefficient, which is calculated by equation 3-17 and $w_{\max}$ is determined using adsorption isotherms.

$$K = \frac{15D_S}{R_p^2} \tag{3-17}$$

Where D_S is the surface diffusivity calculated by equation 3-18 [113] and R_p is the radius of the adsorbent granules.

$$D_S = D_{SO}\exp(\frac{E_a}{RT_{bed}}) \tag{3-18}$$

Where, D_{SO} is the pre-exponential factor of the effective water diffusivity in the adsorbent granules; E_a is activation energy; R is the ideal gas constant and T_{bed} is the bed temperature.

3.4.3.1 Radius of adsorbent granules

To measure the size of SAPO-34's granules a laser diffraction particle measuring technique is utilised. The laser diffraction technique is the most frequently used technique for measuring particle size. It is a quick and easy-to-apply method to determine the distribution of the particle size based on the analysis of a huge number of particles [146]. Its optical set-up is shown in Figure 3-8. The laser diffraction analyzers pass a laser beam through a sample. The light scattered from all particles in the sample's volume is collected using a Fourier transform lens and focused onto a detector. Therefore, the sample particle size distribution can be determined from the angular distribution of scattered light across the detectors using Fraunhofer's diffraction theory [147]. The standard deviation of the laser diffraction particle measuring technique is less than ±1.2% [148].

The results of the laser diffraction particle sizing of SAPO-34's granules are shown in Figure 3-9 and Table 3-4. The volume average granule diameter is determined to be 0.2955mm.

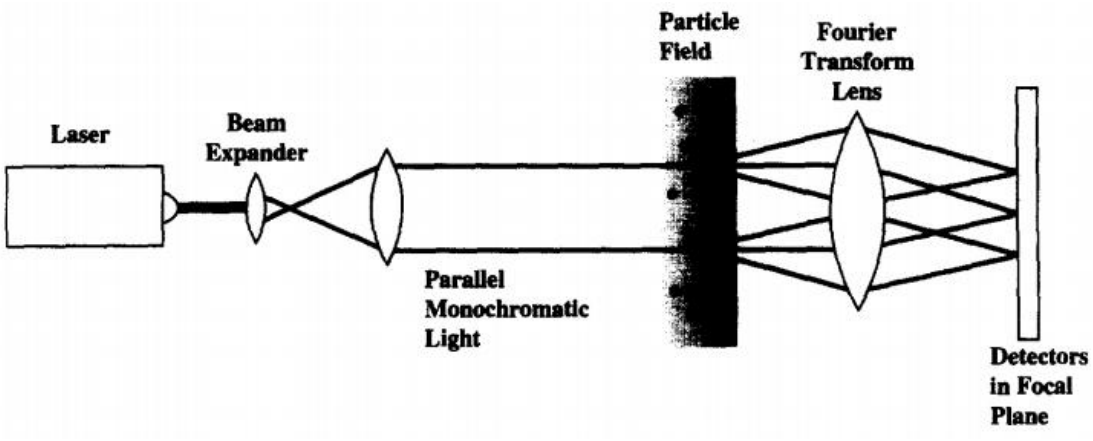

Figure 3-8 Optical set-up for laser diffraction particle sizing [147]

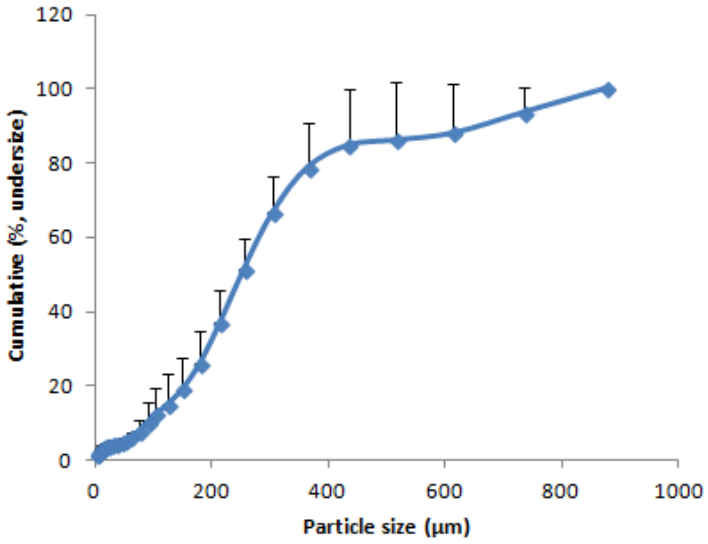

Figure 3-9 SAPO-34 granules' diameter measurement result

Table 3-4 SAPO-34 granules' diameter measurement result

Granule diameter (µm)	Cumulative
<104.5 ±24.3	10%
<138.5 ±32.4	16%
<253.3 ±30.3	50%
<489.3 ±175.3	84%
<563.9 ±200.6	90%
<722.8 ±198.5	99%
Volume average granule diameter (µm)	295.5 ±74.4

The CPO-27Ni adsorbent material was manufactured by Johnson Matthey PLC who supplied a total of 5kg of this MOF's material. The particle size of this 5kg ranged from 20 microns to 2000 microns. Therefore a sieving technique was used to separate the particles into different size ranges. Past research work has shown that utilising small size particles results in enhancing the adsorption process [1]. However, small size particles are difficult to contain within the adsorber bed. The sieving device separated the CPO-27Ni into the following size ranges: (1) 20-45 microns; (2) 45-90 microns; (3) 90-125 microns; (4) 125-355 microns; (5) 355-850 microns; (6) 850-2000 microns. To use particle size close to that of SAPO-34, the CPO-27Ni particle size ranging from 0.125mm to 0.355mm were used. The average value of the granule diameter was 0.24mm.

3.4.3.2 Pre-exponential factor and activation energy

The adsorption kinetics of SAPO-34/water can be determined using the experimental result. It was found that the adsorption kinetics of SAPO-34/water had a large increase step when the relative pressure increased to 0.2 from the DVS measurement results. Therefore, the fitting of the adsorption kinetics equation was carried out by dividing the measured data into two parts: (1) relative pressure value below 0.2 and (2) relative pressure value higher than 0.2, as shown in Figure 3-10. Values of D_{SO} and E_a required for equation 3-18 at both relative pressure ranges can be calculated using Engineering Equation Solver software, with values listed in Table 3-5 with the deviation of 3.5% for relative pressure value below 0.2 and 3.1% for relative pressure value higher than 0.2. The fitting of adsorption kinetics equation to experimental results of SAPO-34/water is shown in Figure 3-10.

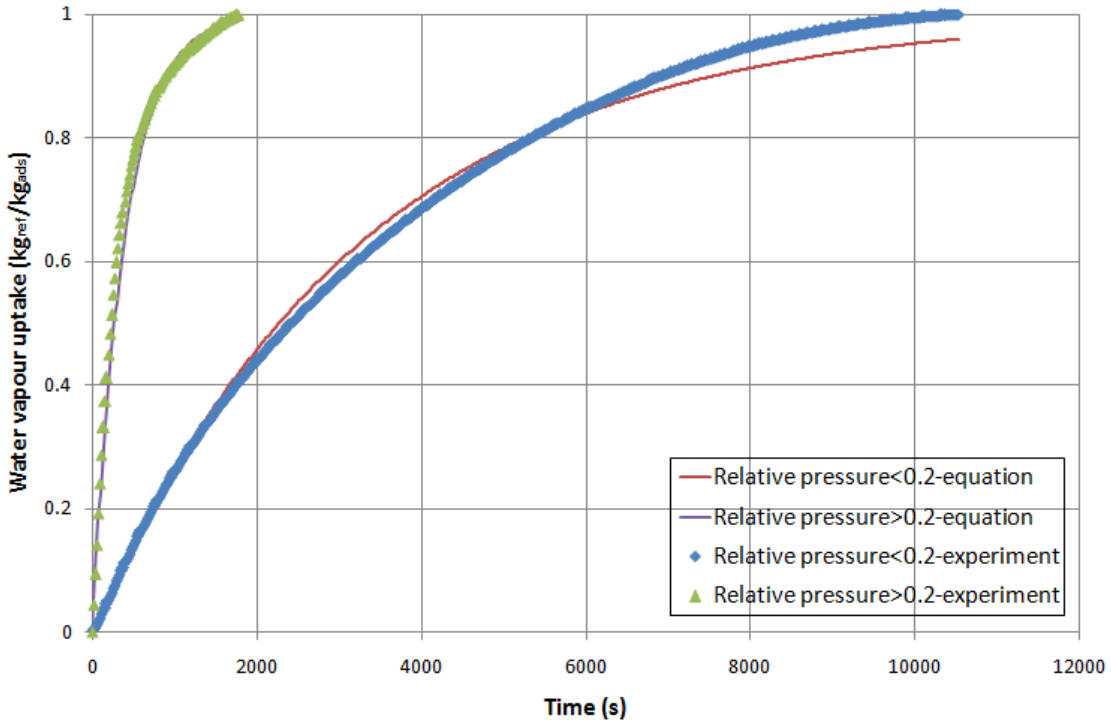

Figure 3-10 Fitting of adsorption kinetic equation to experimental results of SAPO-34/water

Table 3-5 Values of D_{SO} and E_a for adsorption kinetics of SAPO-34/water

Relative pressure<0.2	Relative pressure>0.2
$D_{SO}=2.7743\times10^{-5}m^2/s$	$D_{SO}=4.8516\times10^{-9}m^2/s$
$E_a=4.4423\times10^4 J/mol$	$E_a=1.7710\times10^4 J/mol$

It was also found that the adsorption kinetics of CPO-27Ni/water had a large increase step when the relative pressure increased to 0.2 from the DVS measurement results. Therefore, the adsorption kinetics were also determined by dividing the experimental results into two similar relative pressure ranges which are: (1) relative pressure below 0.2 and (2) relative pressure higher than 0.2, as shown in Figure 3-11 with the deviation of 7.6% for relative pressure value below 0.2 and 9.4% for relative pressure value higher than 0.2. Values of D_{SO} and E_a for the two relative pressure ranges are determined using Engineering Equation Solver software and listed in Table 3-6. The

fitting of equation to experimental results for adsorption kinetics of CPO-27Ni is shown in Figure 3-11.

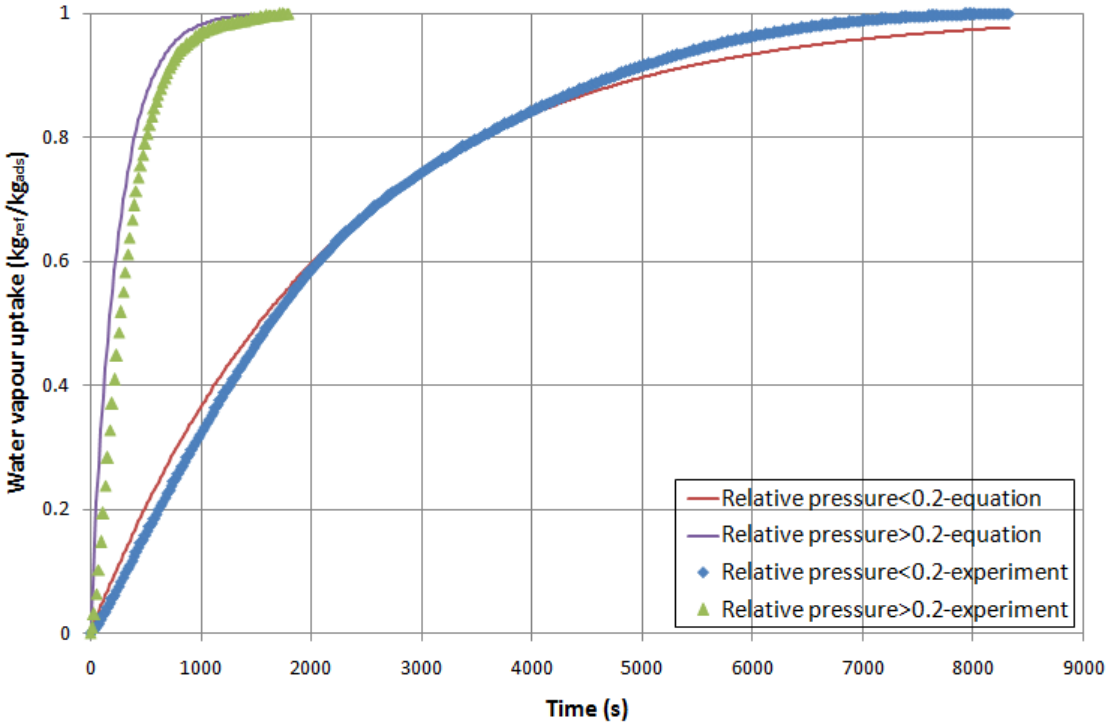

Figure 3-11 Fitting of equation to experimental results for adsorption kinetics of CPO-27Ni/water

Table 3-6 Values of D_{SO} and E_a for adsorption kinetics of CPO-27Ni/water

Relative pressure<0.2	Relative pressure>0.2
$D_{SO}=7.8299\times10^{-8}m^2/s$	$D_{SO}=7.4677\times10^{-10}m^2/s$
$E_a=3.2006\times10^4 J/mol$	$E_a=1.4806\times10^4 J/mol$

3.5 Summary

In this research, water was chosen as the refrigerant because it has a large amount of latent heat of vaporization and it is environmentally friendly. Based on the test results of AL-Dadah and her coworkers, CPO-27Ni has the best water adsorption

characteristics among several MOFs' adsorbent materials tested; therefore it is chosen as the adsorbent material to be investigated in this research. This chapter investigated the performance of CPO-27Ni compared to silica gel RD-2060, a commercially used adsorbent and SAPO-34, an advanced zeolite adsorbent. The water uptake characteristics of all three adsorbents were tested using the dynamic vapour sorption (DVS) analyser. It is concluded that the CPO-27Ni is the most promising among the three adsorbent materials thus it can be used to improve the performance of an adsorption air conditioning system for automotive application. Finally, fitting equations of adsorption isotherms and kinetics for CPO-27Ni/water and SAPO-34/water were developed based on the experimental results.

CHAPTER 4 FINITE ELEMENT MODELLING FOR THREE ADSORPTION BED DESIGNS

4.1 Introduction

The adsorption working pair and adsorption bed design are two of the most important issues affecting the performance of the adsorption air conditioning system, as explained in section 2.11. Chapter 3 investigated several adsorbent materials based on water as a refrigerant and it is concluded that CPO-27Ni/water is a promising working pair to improve the performance of an adsorption air conditioning system for automotive application. Apart from the adsorption working pair, investigation of the adsorption bed design is also important to achieve better heat and mass transfer performance and thus improve the cooling capacity and efficiency of the adsorption air conditioning system.

Modelling techniques are powerful tools in investigating the performance and improving the design of adsorption beds. This chapter investigates three adsorption bed designs, including a rectangular finned tube adsorption bed, honeycomb finned rectangular channel adsorption bed and helix finned tube adsorption bed. A finite element modelling method was utilised in this research because of its advantages of high accuracy, as explained in section 2.10.2.2. Finite element models using COMSOL Multiphysics software were developed for these three adsorption bed

designs and were applied using CPO-27Ni/water. The performances of the three adsorption bed designs were then compared.

4.2 Governing equations

This section describes the governing equations of the finite element simulation process. The governing equations are principally divided into four groups; which are equations of adsorption isotherms and kinetics, diffusion, heat transfer and flow of heating/cooling fluid.

4.2.1 Adsorption isotherms and kinetics equations

Adsorption isotherms and kinetics equations of the CPO-27Ni/water working pair have been presented in detail in section 3.4; they are equations 3-14, 3-16 to 3-18.

4.2.2 Diffusion equations

There are two methods used to describe the diffusion process of refrigerant in the adsorbent material in the finite element modelling. The first method is based on modelling adsorbent material as physical particles using equation 4-1 [149]. The second method considers adsorbent material as a solid volume with certain porosity using Darcy equation 4-2 [150].

$$\frac{\partial C}{\partial t} - \nabla \cdot \left(D_{eff} \nabla C \right) = - \frac{\rho_{dry}}{M \varepsilon_{ads}} \frac{\partial x}{\partial t} \tag{4-1}$$

$$\frac{\partial}{\partial t}\left(\rho_w \varepsilon_{ads}\right)+\nabla\left[\rho_w\left(-\frac{\kappa}{\mu}\nabla P_{ads}\right)\right]=\frac{\partial}{\partial t}\left(\rho_{ads} w\right) \tag{4-2}$$

Where C is the water vapour concentration; D_{eff} is the diffusion coefficient; ρ_{dry} is the density of the dry adsorbent; M is the molar mass of water; ε_{ads} is the porosity of the adsorbent bed; μ is the dynamic viscosity of the water vapour; ρ_w and ρ_{ads} are the density of the water vapour and adsorbent granules respectively. κ is the permeability of the adsorbent granules which can be determined by the Kozeny-Carman relationship as a function of the adsorbent porosity and radius of the adsorbent granules: equation 4-3 [60, 150].

$$\kappa=\frac{4\varepsilon_{ads}^2 R_p^2}{150\left(1-\varepsilon_{ads}\right)^2} \tag{4-3}$$

To simulate the cycling process of the whole adsorption cooling system including adsorbers, evaporator and condenser, the first method is preferred because it takes the movement of refrigerant particles into account. However, based on the published research this method is only used to simulate the diffusion process inside the thin layer of adsorbent material because its computational time is large [136, 149]. On the other hand, although porous model has some limitations, the results of finite element simulation calculated by all governing equations during our research work will be validated by experimental results with the acceptable average deviation to prove the equations' feasibility. Therefore the second method is chosen in our investigation process. Besides, since only the adsorber bed is simulated in this research using finite element modelling technique, the second method is used to save computational time. Therefore, the Darcy equation 4-2 is used in the finite element modelling to take into account the diffusion of water vapour in the adsorbent granules.

4.2.3 Energy equations

Energy equations are used to describe the heat transfer in the adsorption bed. Equations 4-4 to 4-7 describe energy conservation in the adsorbent granules, heating/cooling water, copper tubes and aluminium fins respectively.

$$\rho_{eq} Cp_{eq} \frac{\partial T_{ads}}{\partial t} + Cp_{ref} \nabla \left[T_{ads} \rho_{ref} \left(-\frac{\kappa}{\mu} \nabla P_{ads} \right) \right] = \nabla \left(k_{eq} \nabla T_{ads} \right) + \rho_{ads} \Delta H_{ads} \frac{\partial w}{\partial t} \tag{4-4}$$

$$\rho_w Cp_w \frac{\partial T_w}{\partial t} + Cp_w \vec{u} \nabla T_w = \nabla \left(k_w \nabla T_w \right) \tag{4-5}$$

$$\rho_{Cu} Cp_{Cu} \frac{\partial T_{Cu}}{\partial t} = \nabla \left(k_{Cu} \nabla T_{Cu} \right) \tag{4-6}$$

$$\rho_{Al} Cp_{Al} \frac{\partial T_{Al}}{\partial t} = \nabla \left(k_{Al} \nabla T_{Al} \right) \tag{4-7}$$

Where Cp, k, ρ, T are heat capacity, heat conductivity, density and temperature respectively. The subscripts of ads, ref, w, Cu, Al represent adsorbents, refrigerant water vapour, heating/cooling water, copper tubes and aluminium fins respectively. Term u is the velocity field of heating/cooling water. Cp_{eq} and k_{eq} are the thermal capacity and thermal conductivity of the adsorbent materials as calculated by equations 4-8 and 4-9 respectively.

$$\rho_{eq} Cp_{eq} = \left(\varepsilon_{ads} \rho_{ref} + \rho_{ads} w \right) Cp_{ref} + \rho_{ads} Cp_{ads} \tag{4-8}$$

$$k_{eq} = \left(1 - \varepsilon_{ads} \right) k_{ads} + \varepsilon_{ads} k_{ref} \tag{4-9}$$

The thermal contact resistance between the adsorbent granules and the heat exchanger's metal surface are determined by equations 4-10 and 4-11, developed by [1]. These equations are polynomial expressions for the thermal contact resistance for

three different granule sizes 50 and 100 mesh corresponding to granule diameters of 0.297mm, 0.149mm respectively.

$$R_{cont,50} = 0.0013T^2 - 0.1773T + 8.6221 \quad (4\text{-}10)$$

$$R_{cont,100} = 0.0012T^2 - 0.1624T + 7.6785 \quad (4\text{-}11)$$

Since the diameter of CPO-27Ni particles used in this research is 0.24mm as described in the section 3.4.3.1, the contact resistance is calculated using the following equation 4-12. The unit of all $R_{cont,50}$, $R_{cont,100}$ and R_{cont} is $m^2 \cdot K/kW$.

$$R_{cont} = R_{cont,50} - \frac{0.297mm - 0.24mm}{0.297mm - 0.149mm}\left(R_{cont,50} - R_{cont,\ 100}\right) \quad (4\text{-}12)$$

4.2.4 Flow of water equations

As for the equations that govern the flow of heating/cooling water, two conditions are considered in the modelling of laminar and turbulent flows. Equation 4-13 is used in the case of laminar flow with the Reynolds number less than 2300; while equation 4-14 is used for the turbulent flow condition when the Reynolds number is larger than 2300.

$$\rho_w \frac{\partial \vec{u}}{\partial t} + \rho_w (\vec{u}\nabla)\vec{u} = \nabla\left\{-P_w\vec{I} + \mu\left[\nabla\vec{u} + (\nabla\vec{u})^T\right]\right\} \quad (4\text{-}13)$$

$$\rho_w \frac{\partial \vec{u}}{\partial t} + \rho_w (\vec{u}\nabla)\vec{u} = \nabla\left\{-P_w\vec{I} + (\mu + \mu_T)\left[\nabla\vec{u} + (\nabla\vec{u})^T\right] - \frac{2}{3}\rho_w k_{kur}\vec{I}\right\} \quad (4\text{-}14)$$

Where P_w is the pressure; $\vec{I}$ is the unit matrix and k_{kur} is the turbulent kinetic energy.

4.3 Finite element modelling and results

Finite element modelling is used to simulate the adsorption bed and study the performance of different bed designs. In this research COMSOL Multiphysics software has been used to simulate the adsorption process occurring in the adsorption beds. The geometry of all adsorption bed designs are described in detail in the following sections.

4.3.1 Rectangular finned tube adsorption bed

A rectangular finned tube adsorption bed is a commercially available type of heat exchanger that contains tubes and rectangular fins as shown in Figure 4-1. This bed design is used by Weatherite manufacturing ltd in their silica gel/water adsorption chiller. The fins are uniformly distributed through the length of the tubes. To reduce the mass of the adsorption bed, aluminium was chosen as the material for the fins. The dimensions of each fin were 115×30×0.105mm. Four tubes were also distributed uniformly along the width of the adsorption bed, with an outside diameter of 15.875mm (3/4 inch) and a wall thickness of 0.8mm. Copper tubes were used as they have large thermal conductivity. Adsorbent granules were packed between the fins. In the adsorption process, the cooling water flows through tubes to cool down the adsorption bed; since the bed is hot after the desorption process. All parameters are shown in Table 4-1.

Since the adsorption bed is symmetrical around its longitudinal and lateral axes and in order to reduce computational time, only one quarter of the bed of full length and

whole fin number has been modelled, as seen in the zone shown in red lines in Figure 4-1. Figure 4-2 shows the overall geometry of the modelled adsorption bed and Figure 4-3 is a zoom out section.

The boundary conditions contain fixing the evaporation pressure on the surfaces between adsorbent material and refrigerant, and the symmetry around the surfaces on one side and the underside surfaces.

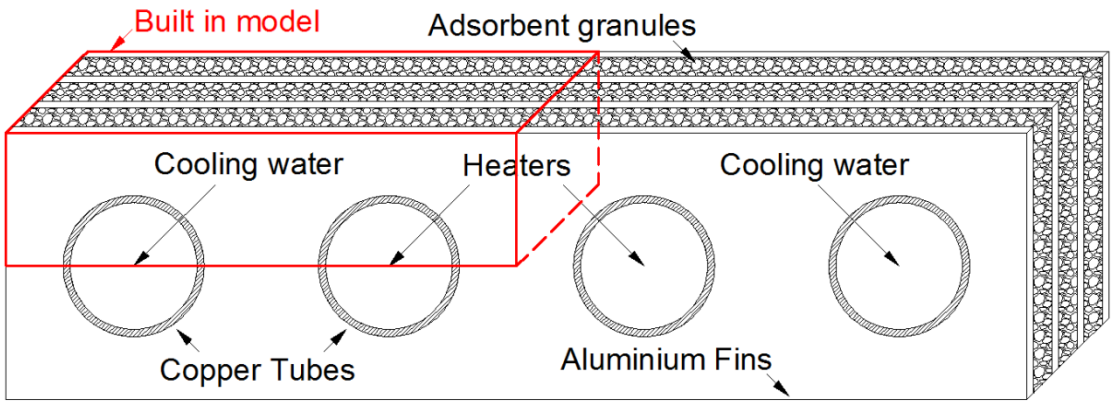

Figure 4-1 Part of adsorption bed modelled

Table 4-1 Adsorption bed parameters

Parameters	Value
Bed length	550mm
Fin width	115mm
Fin height	30mm
Fin pitch	1.016mm
Fin thickness	0.105mm
Tube outer diameter	15.875mm
Tube thickness	0.8mm
Fin number	540

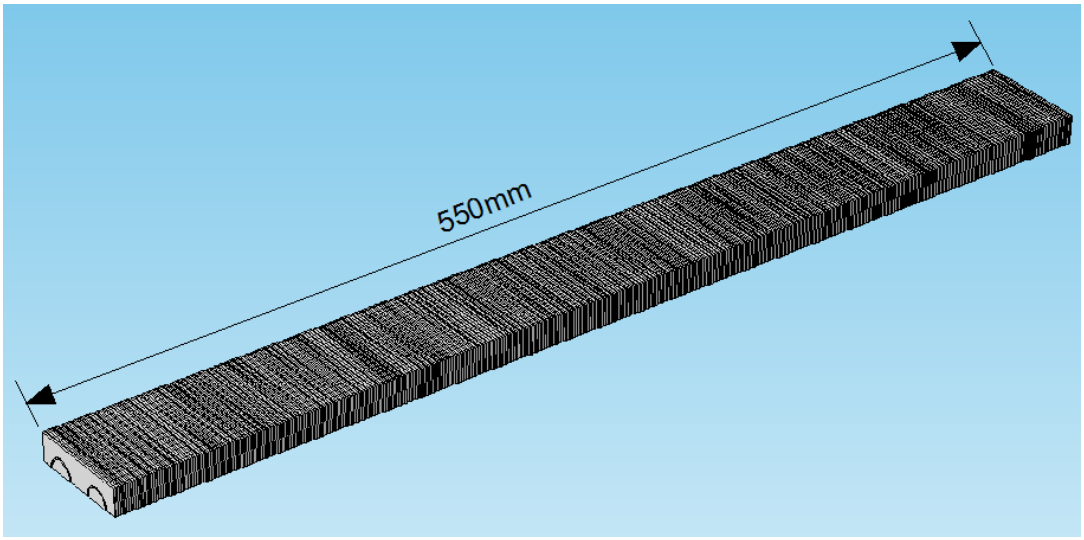

Figure 4-2 Overall geometry of the modelled adsorption bed

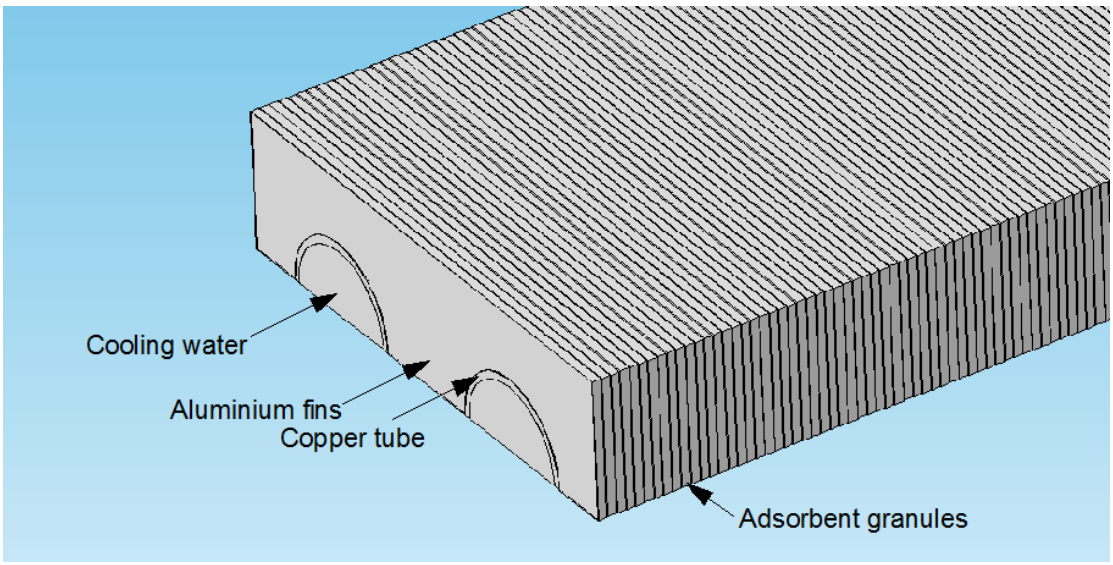

Figure 4-3 Zoom out section of adsorption bed

4.3.2 Honeycomb finned rectangular channel adsorption bed

The honeycomb adsorption bed contained six rectangular aluminium tubes and two layers of aluminium honeycomb structure. The cooling water flows through the tubes to cool down the adsorption bed during the adsorption process. Honeycomb fins were

attached on both upper and lower surfaces of the rectangular tubes, as shown in Figure 4-4. Adsorbent granules were packed inside the honeycomb cells, with all the design parameters shown in Table 4-2.

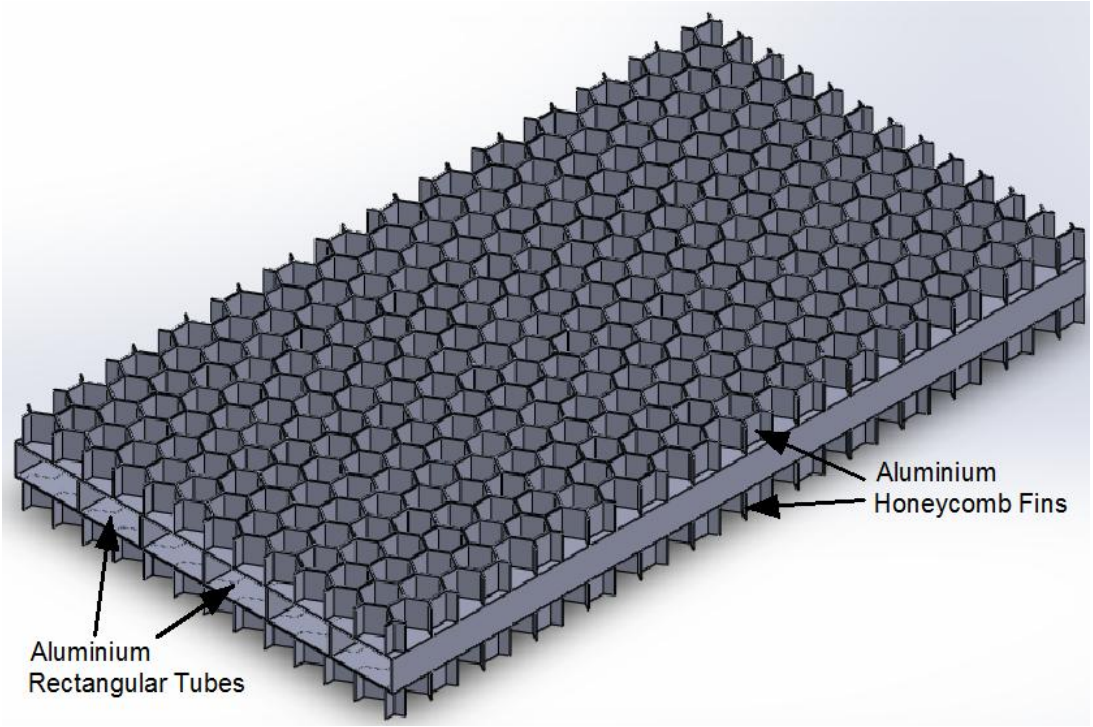

Figure 4-4 Diagram of adsorption bed with rectangular tubes and honeycomb fins

Table 4-2 Honeycomb finned adsorption bed design parameters

Parameters	Value
Bed length	275mm
Tube height	12mm
Tube width	25mm
Tube thickness	0.5mm
Honeycomb fin metal thickness	0.8mm
Honeycomb fin height	10mm
Honeycomb fin cell size	6.4mm

Due to the symmetry around its longitudinal and lateral axes and to reduce the computational time, one quarter of the adsorption bed with full bed length was simulated. Figure 4-5 shows a section of the adsorption bed with the honeycomb fins simulated.

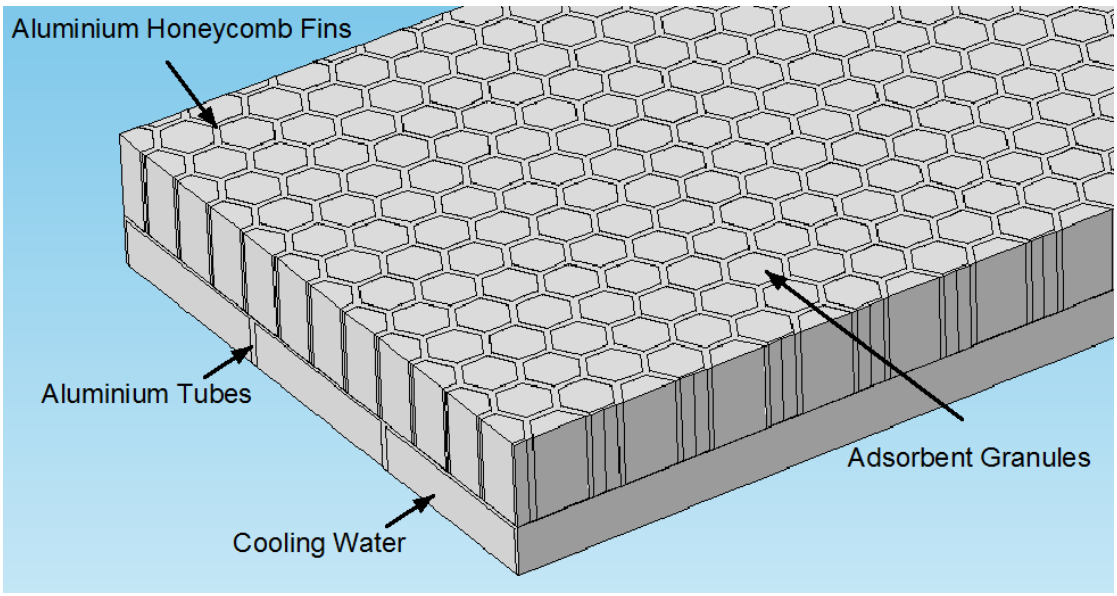

Figure 4-5 Diagram of one quarter of the adsorption bed simulated

The boundary conditions contain fixing the evaporation pressure on the surfaces between adsorbent material and refrigerant, and the symmetry around the surfaces on one side and the underside surfaces.

4.3.3 Helix finned tube adsorption bed

Figure 4-6 shows a schematic diagram of the helix finned tube used in the adsorption bed. It contained copper tube and small copper rectangular ring fins as shown in Figure 4-6(a). The ring fins were welded onto the tube's outside surface and they

were distributed on a helix line. In the adsorption process the cooling water flows through the tube to cool down the adsorption bed; since the bed is relatively hot after the desorption process. Adsorbent granules were packed in the space between the fins as shown in Figure 4-7(b); with the design parameters shown in Table 4-3. The boundary condition is fixing the evaporation pressure on the surfaces between adsorbent material and refrigerant.

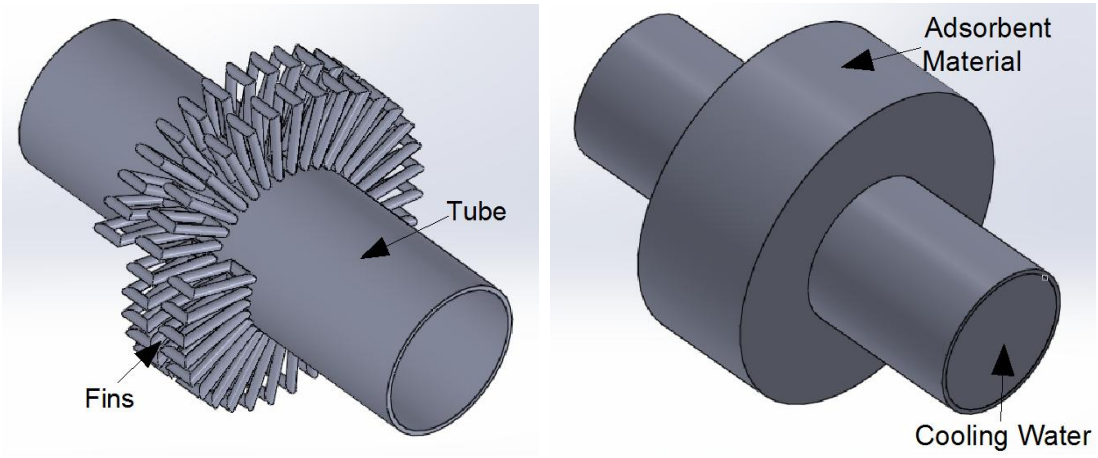

(a) (b)

Figure 4-6 Schematic diagram of helix finned adsorption bed: (a) tube and fins; (b) packed with adsorbent material

Table 4-3 Bed design parameters

Parameter	Value
Rectangular ring fin height	7.5mm
Rectangular ring fin width	2.5mm
Rectangular ring fin wire diameter	1mm
Rectangular ring fin number	100
Helix pitch	5mm
Tube length	50mm
Tube outside diameter	16mm
Tube thickness	0.5mm

4.4 Finite element modelling results and discussion

Adsorption process simulations for the three adsorption bed designs described in section 4.3 were carried out using the finite element simulation method outlined in section 4.2; with operating conditions which are normally used in research of automotive adsorption air conditioning systems, as shown in Table 4-4.

Table 4-4 Simulation operating conditions

Condition	Value
Initial bed temperature	90 ℃
Evaporator temperature	15 ℃
Cooling water inlet temperature	30 ℃
Cooling water flow rate	15L/min
Adsorption time	30min
Initial uptake rate	0.05 kg_{water}/kg_{ads}

Figure 4-7 shows the predicted temperature distribution at the last fin of the rectangular finned tube adsorption bed at time intervals of 100, 300, 600, 900, 1200, 1500 and 1800 seconds. It is clear from the figure that as the time increases, the temperature of the last fin approaches the coolant temperature.

The horizontal cut plane which has a distance of 8mm from the horizontal centre plane of the fin height was used to investigate the refrigerant flow velocity, as shown in Figure 4-8. Figure 4-9 shows the predicted refrigerant flow velocity magnitude distribution of the plane investigated at time intervals of 100, 600, 1200 and 1800 seconds. It is clear from the figure that the refrigerant flow velocity magnitude becomes smaller with the increase of time. This is because that the adsorption process is quickly at the beginning and becomes slower as the time increases.

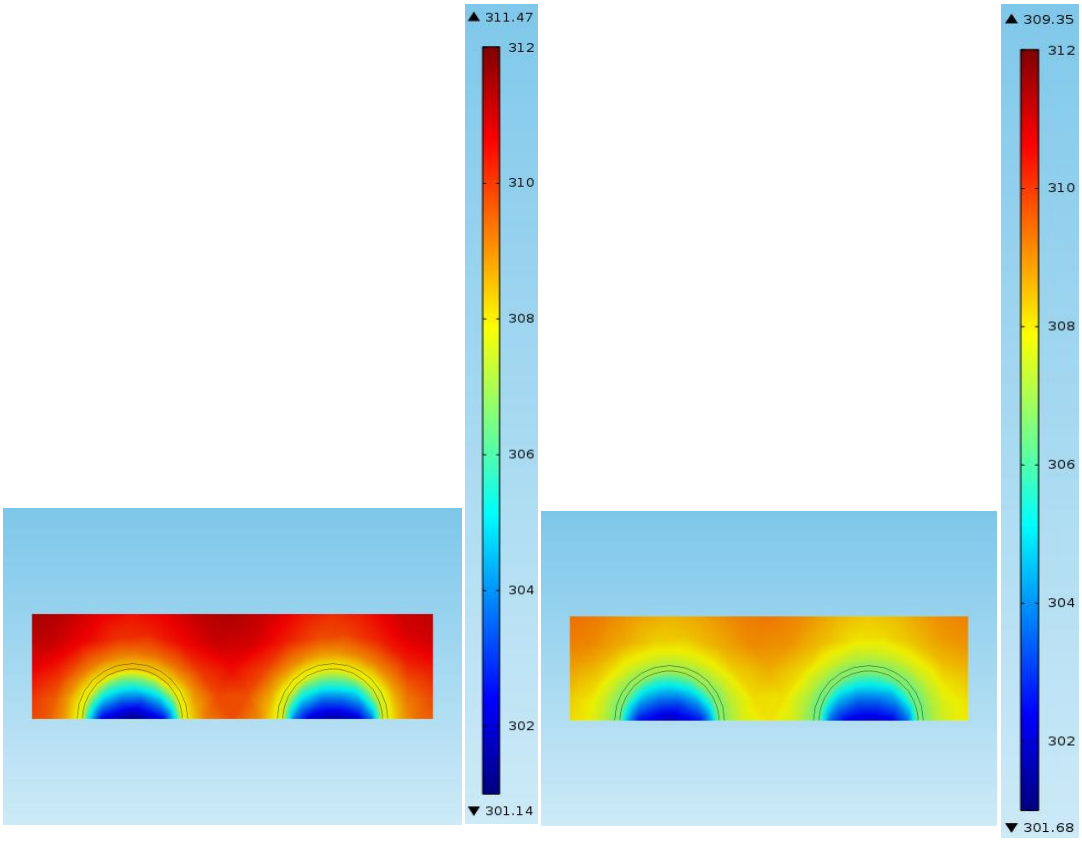
▲ 311.47
312
310
308
306
304
302
▼ 301.14
▲ 309.35
312
310
308
306
304
302
▼ 301.68

(a) (b)

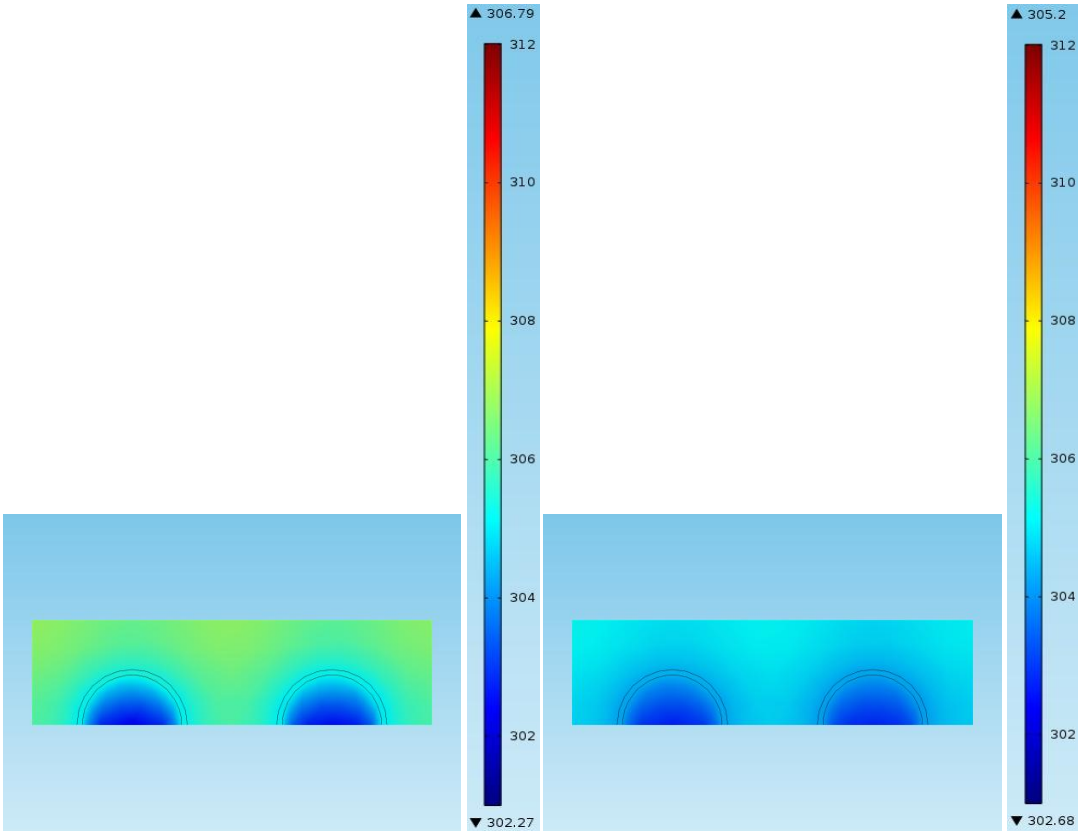
▲ 306.79
312
310
308
306
304
302
▼ 302.27
▲ 305.2
312
310
308
306
304
302
▼ 302.68

(c) (d)

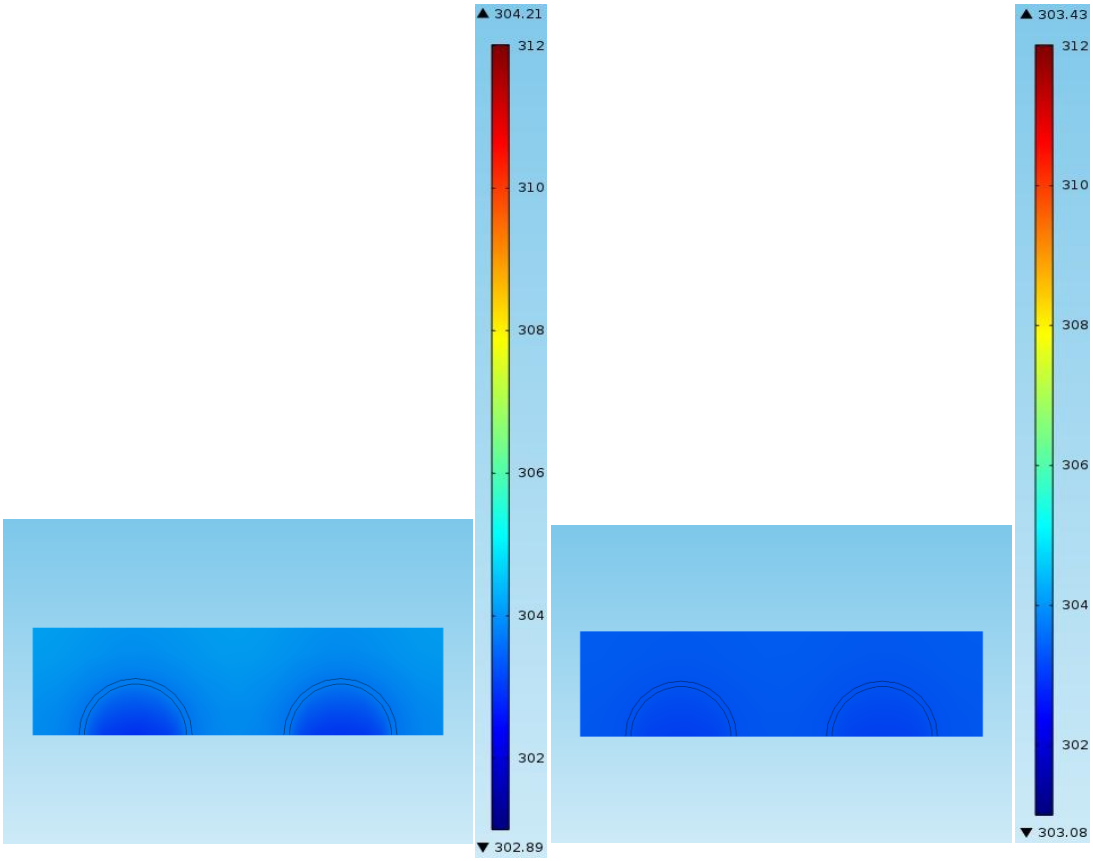

(e) (f)

Figure 4-7 Temperature distribution of the last fin of rectangular finned tube adsorption bed at (a) 100s; (b) 300s; (c) 600s; (d) 900s; (e) 1200s; (f) 1800s (The unit of the label is K)

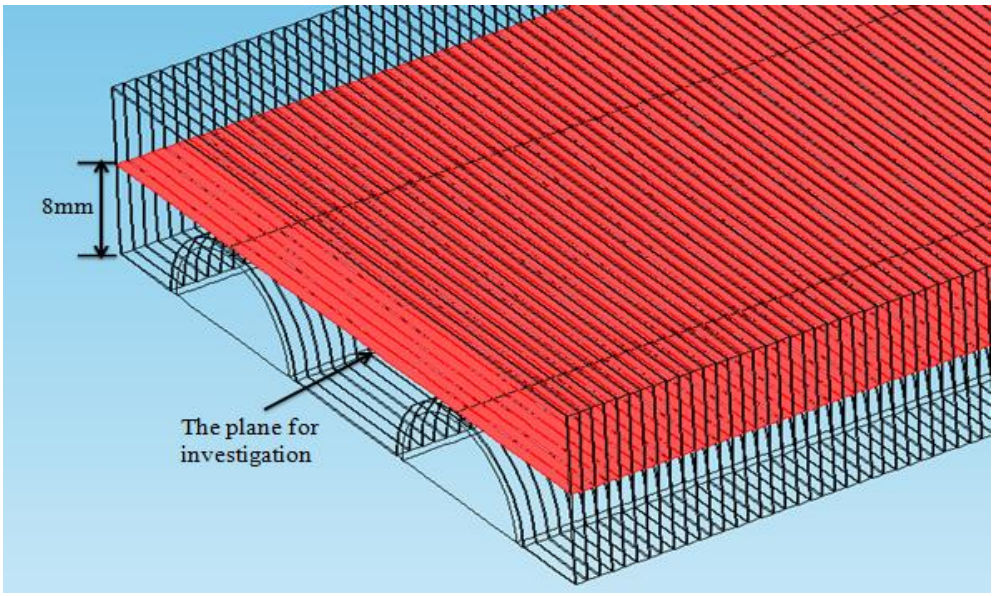

Figure 4-8 The horizontal cut plane to investigate the refrigerant flow velocity

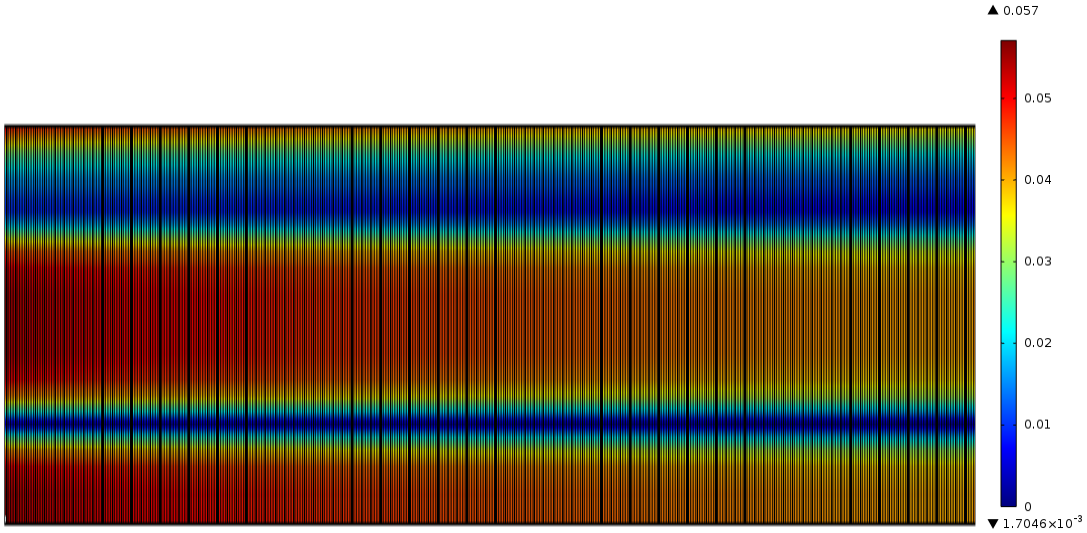
▲ 0.057
0.05
0.04
0.03
0.02
0.01
0
▼ 1.7046×10^-3

(a)

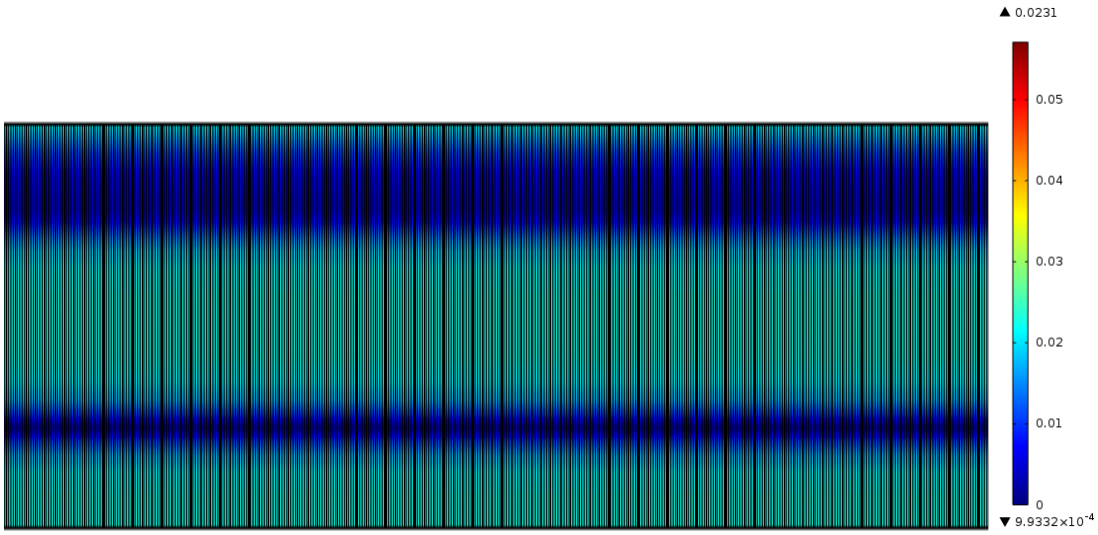
▲ 0.0231
0.05
0.04
0.03
0.02
0.01
0
▼ 9.9332×10^-4

(b)

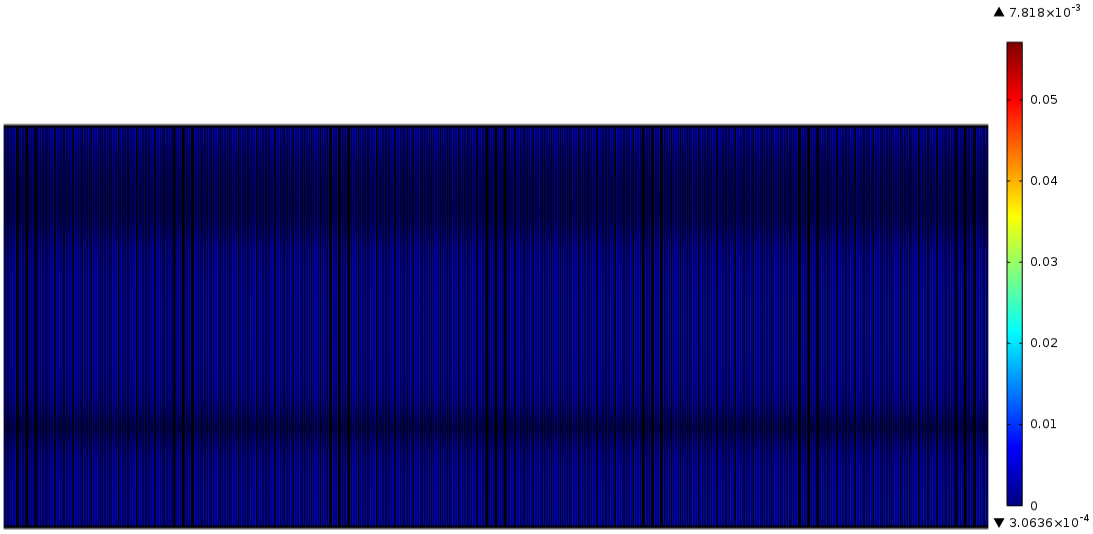

(c)

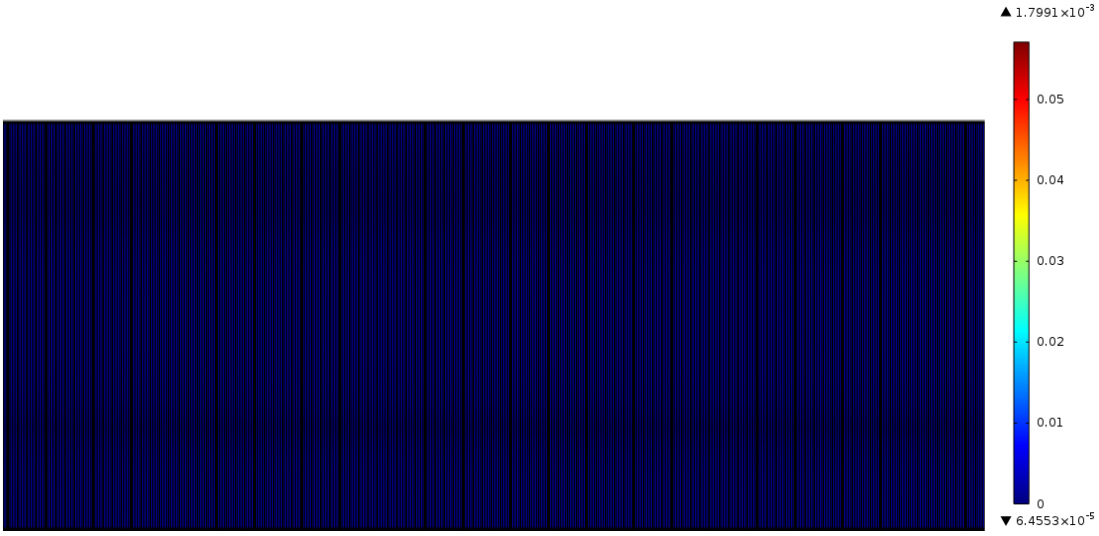

(d)

Figure 4-9 Refrigerant flow velocity magnitude distribution of the plane investigated at (a) 100s; (b) 600s; (c) 1200s; (d) 1800s

(The unit of the label is m/s)

Figure 4-10 shows the predicted temperature distribution at the horizontal centre plane of the fin height at time intervals of 100, 600, 1200 and 1800 seconds. The distribution of the adsorbent material is not continuous in y-axis because this cut

plane also contains areas of cooling water and copper tubes. It is clear from the figure that as the time increases, the temperature of the adsorbent material approaches the coolant temperature.

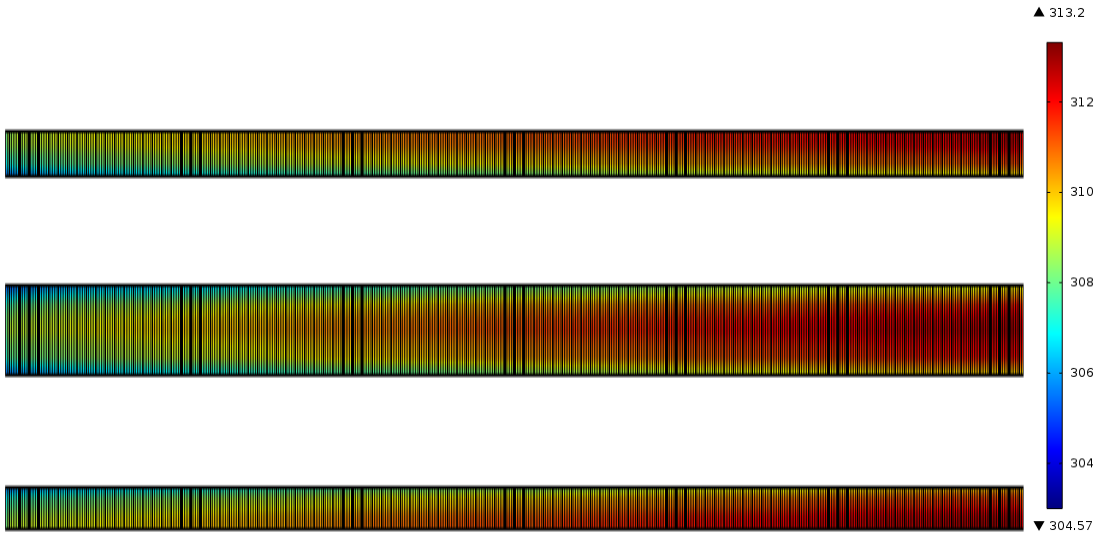

(a)

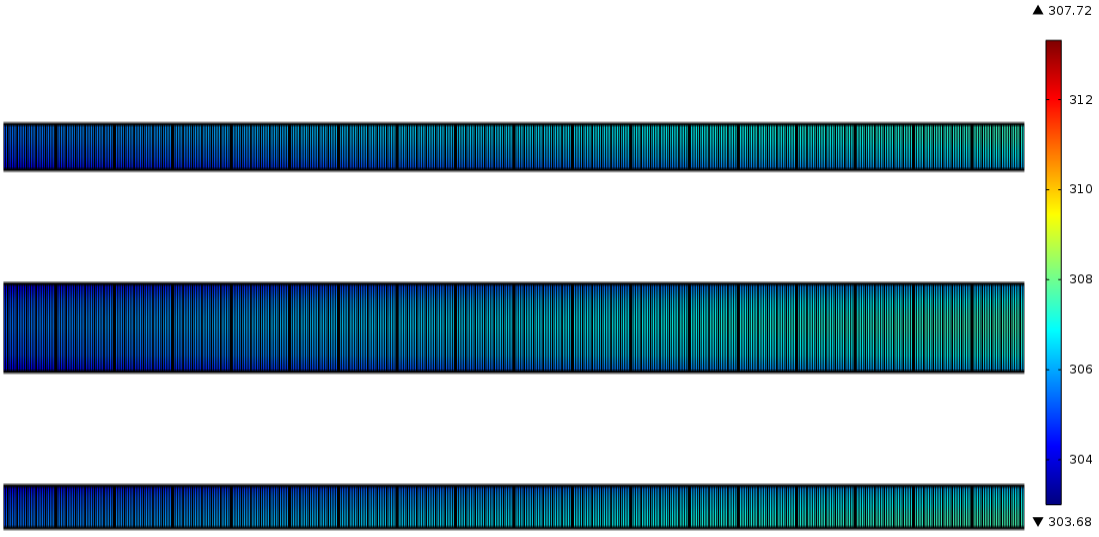

(b)

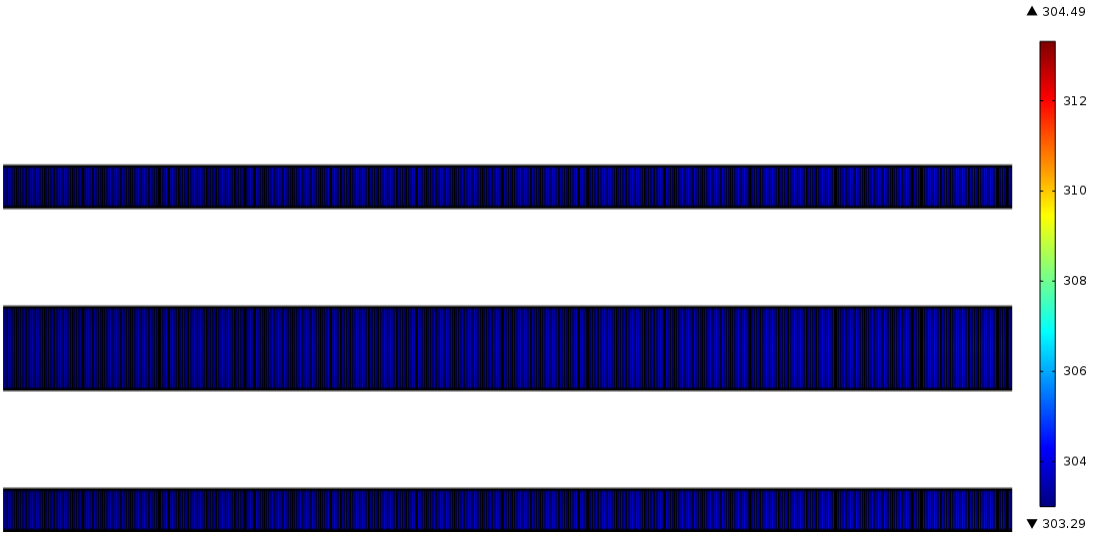

(c)

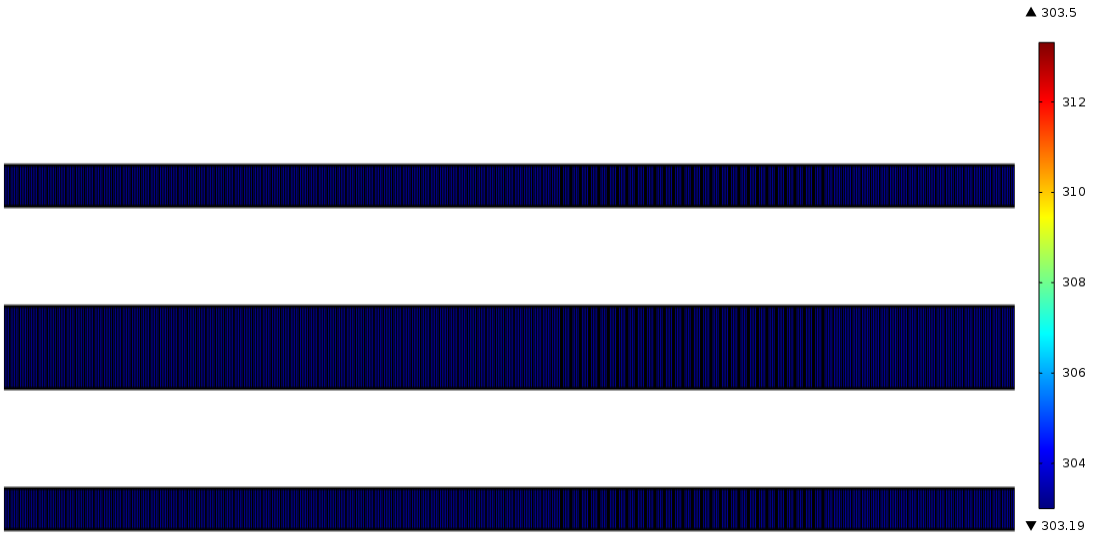

(d)

Figure 4-10 Adsorbent temperature distribution at the horizontal centre plane of the fin height at (a)100s; (b)600s; (c)1200s; (d)1800s

(The unit in the label is K)

Figure 4-11 shows the variation of water vapour uptake with time for the three adsorption bed designs. It is clear that the rate of water uptake increases with time and nearly reaches the equilibrium condition at the end of the simulation period. From the figure it can be found that the water vapour uptake of the rectangular finned

adsorption bed is higher than that of the honeycomb finned bed and helix finned bed, by 5.9% and 7% respectively at 600s of the adsorption process which is normally used as adsorption time in the research of adsorption cooling systems. This is due to the effective mass and heat transfer performance of the rectangular finned adsorption bed design. Therefore, the rectangular finned adsorption bed design has the largest water vapour uptake and thus can achieve the highest SCP.

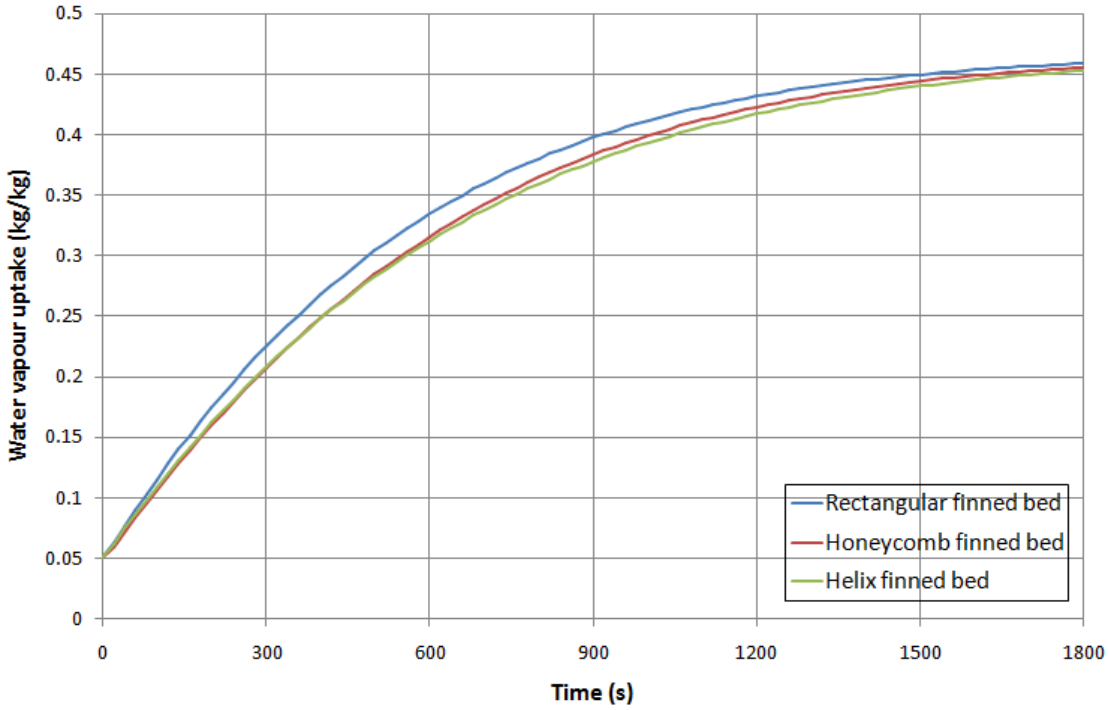

Figure 4-11 Comparison of water vapour uptake for three adsorption bed designs

Figure 4-12 shows the temperature distribution of three adsorption bed designs at 600s of the adsorption process and Figure 4-13 compares the average bed temperature with time of the three adsorption bed designs. The results show that during the adsorption process the rectangular finned adsorption bed has the lowest average adsorption bed temperature. This illustrates the better heat transfer performance of the

rectangular finned adsorption bed compared to both the honeycomb finned bed and the helix finned bed.

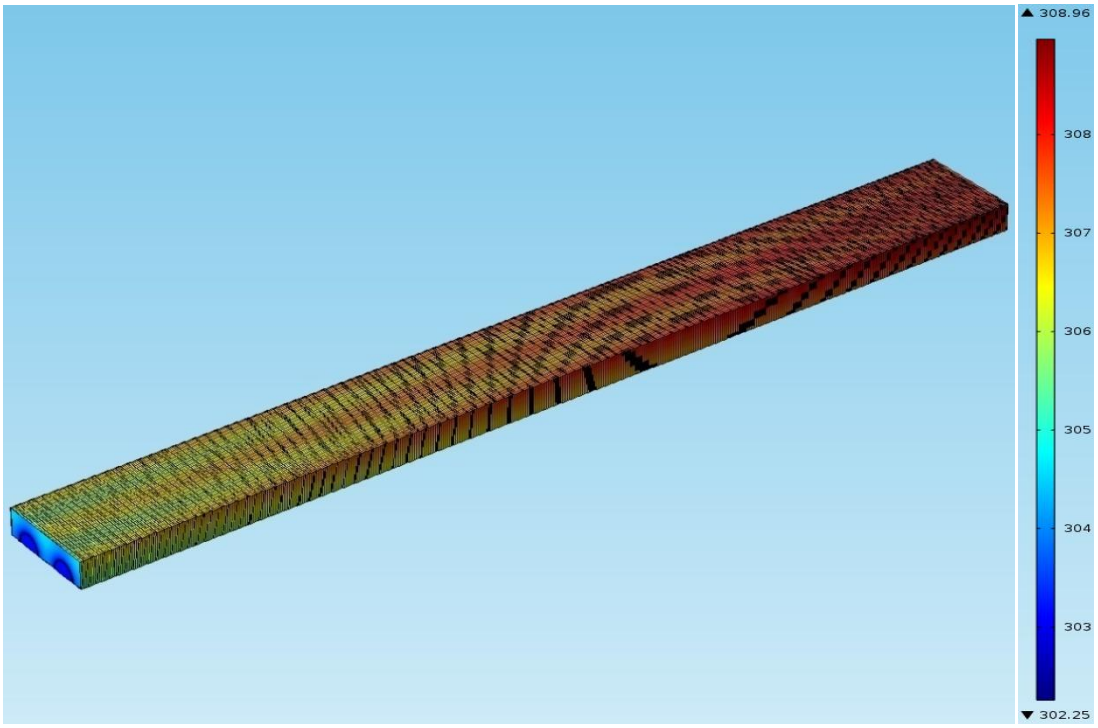

(a)

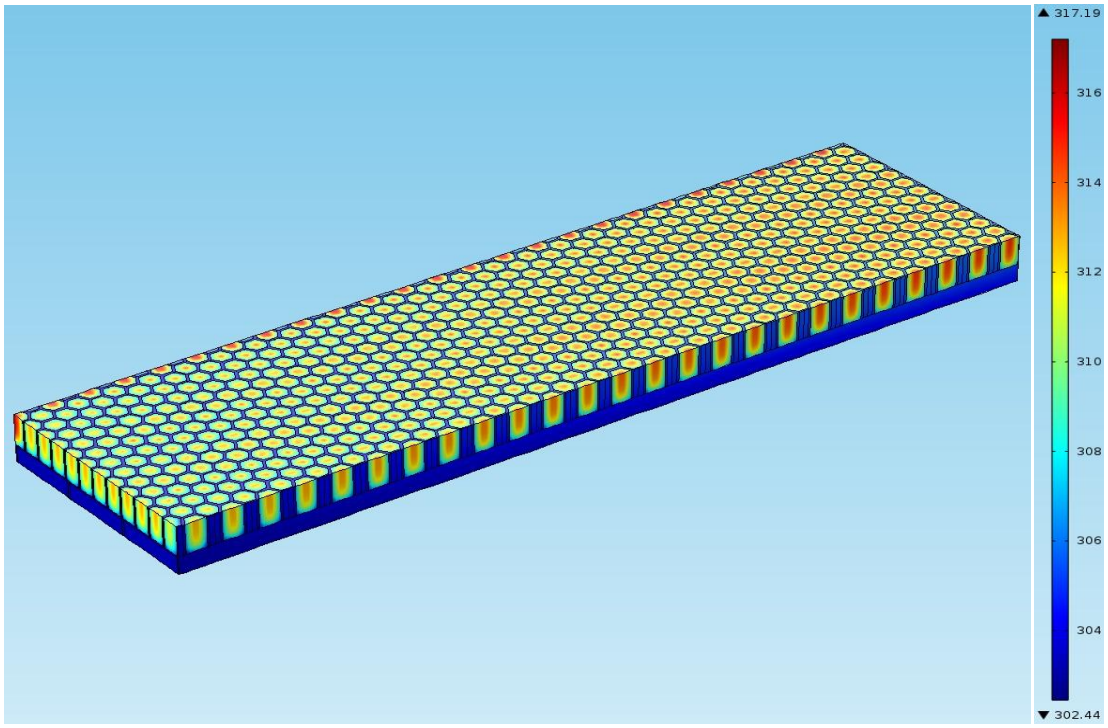

(b)

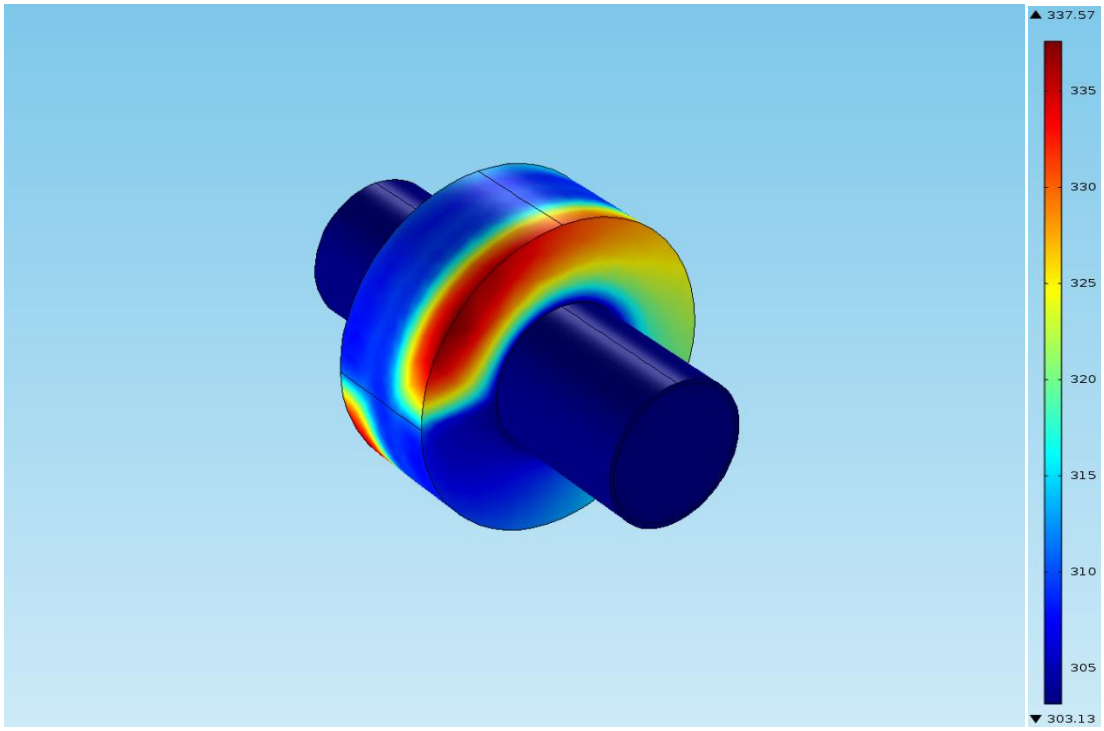

(c)

Figure 4-12 Temperature distribution of three adsorption bed designs at 600s: (a) rectangular finned tube adsorption bed; (b) honeycomb finned rectangular channel adsorption bed; (c) helix finned tube adsorption bed

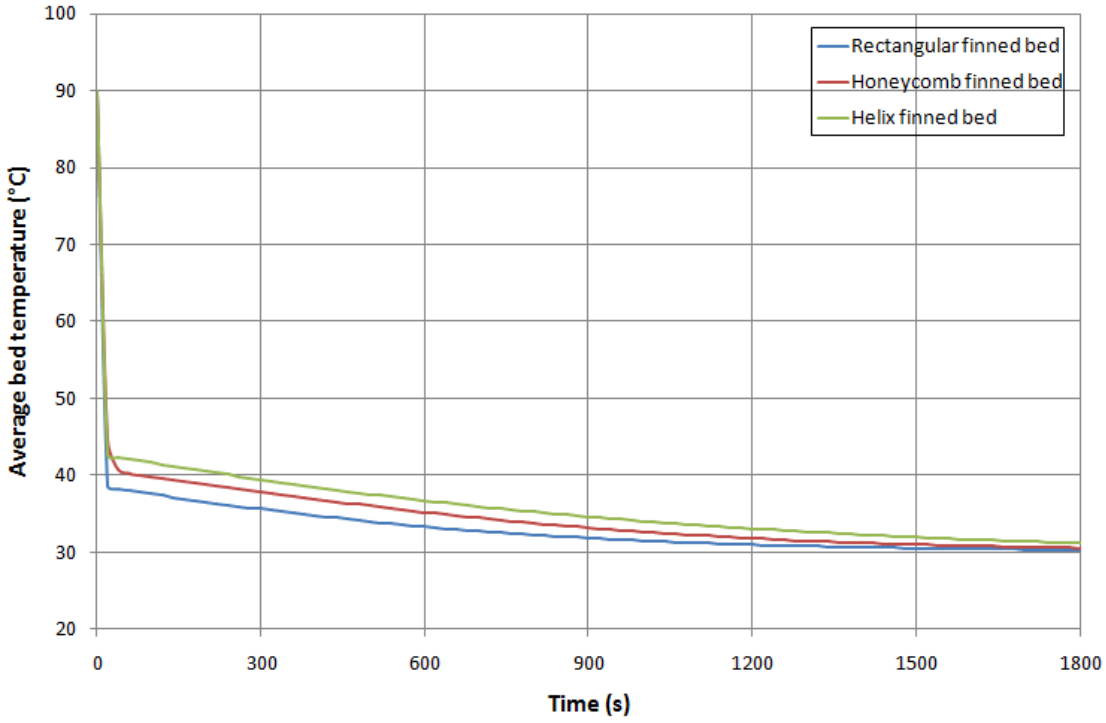

Figure 4-13 Comparison of average bed temperature for three adsorption bed designs

Apart from the water vapour uptake that affects the SCP of the adsorption air conditioning system, another parameter, the heat capacity ratio (HCR), is also used to measure the performance of the adsorption bed. The HCR is the ratio between the thermal capacities of the adsorbent to those of the adsorption bed's metal, as given in equation 4-15. A higher HCR means a higher amount of heat received by the adsorbent material compared with that received by the metal; which directly enhances the COP of the adsorption air conditioning system.

$$HCR = \frac{m_{ads} Cp_{ads}}{m_{metal} Cp_{metal}} \tag{4-15}$$

Table 4-5 shows the HCR values of the three adsorption bed designs. It shows that the HCR of the rectangular finned adsorption bed is much higher than that of the honeycomb finned bed and the helix finned bed by 120% and 76% respectively. Therefore the efficiency of energy utilisation of the rectangular finned adsorption bed is best; thus it can produce the highest COP.

Based on the results shown above, the rectangular finned tube adsorption bed offers potential in producing efficient adsorption system, compared with the honeycomb finned rectangular channel adsorption bed and the helix finned tube adsorption bed; due to its high rate of performance including water vapour uptake and HCR. This is in agreement with [151, 152] where various beds' geometry parameters were investigated; such as fin pitch, fin height, honeycomb fin height and honeycomb fin cell size using silica gel adsorbent. The conclusion is that the rectangular finned adsorption bed can achieve better performance than other designs.

Table 4-5 HCR values of three adsorption bed designs

Adsorption bed design	HCR
Rectangular finned adsorption bed	0.829
Honeycomb finned adsorption bed	0.377
Helix finned adsorption bed	0.471

Figures 4-14 and 4-15 present the desorption process with the initial bed temperature of 30 ℃, hot water temperature of 90 ℃ and initial water vapour uptake of 0.45. Similar to the adsorption process results shown in Figures 4-11 and 4-13, the desorption results indicate that the rectangular finned adsorption bed can achieve better performance than the honeycomb and the helix finned bed designs.

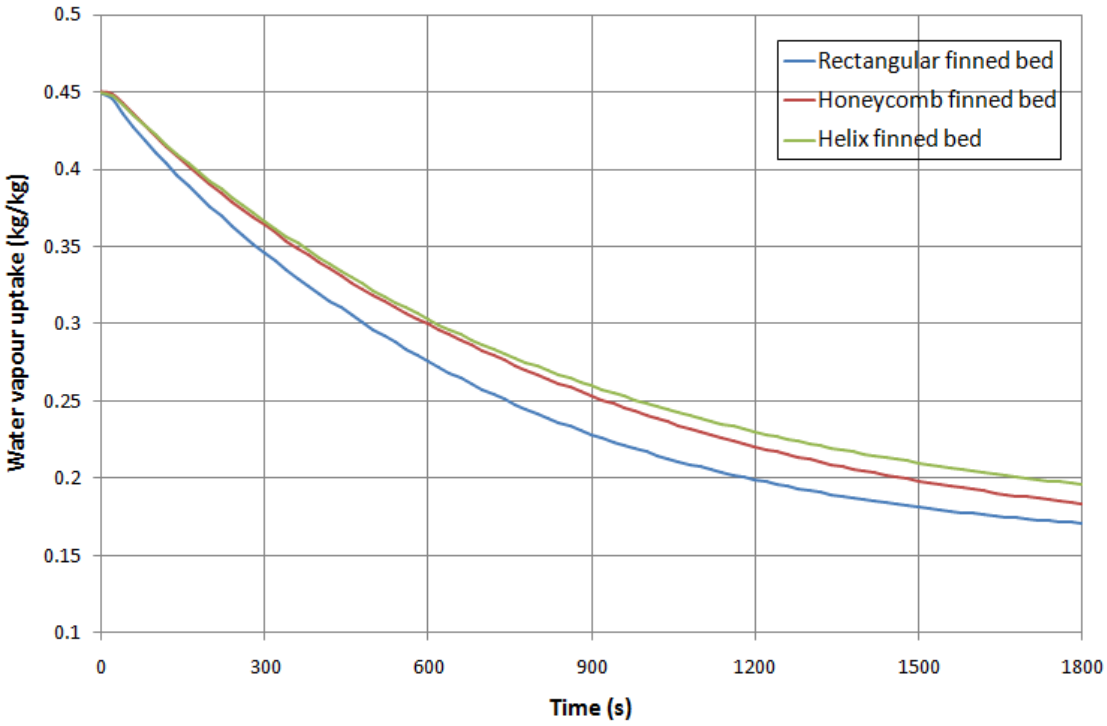

Figure 4-14 Water vapour uptake during desorption process for three adsorption bed designs' desorption

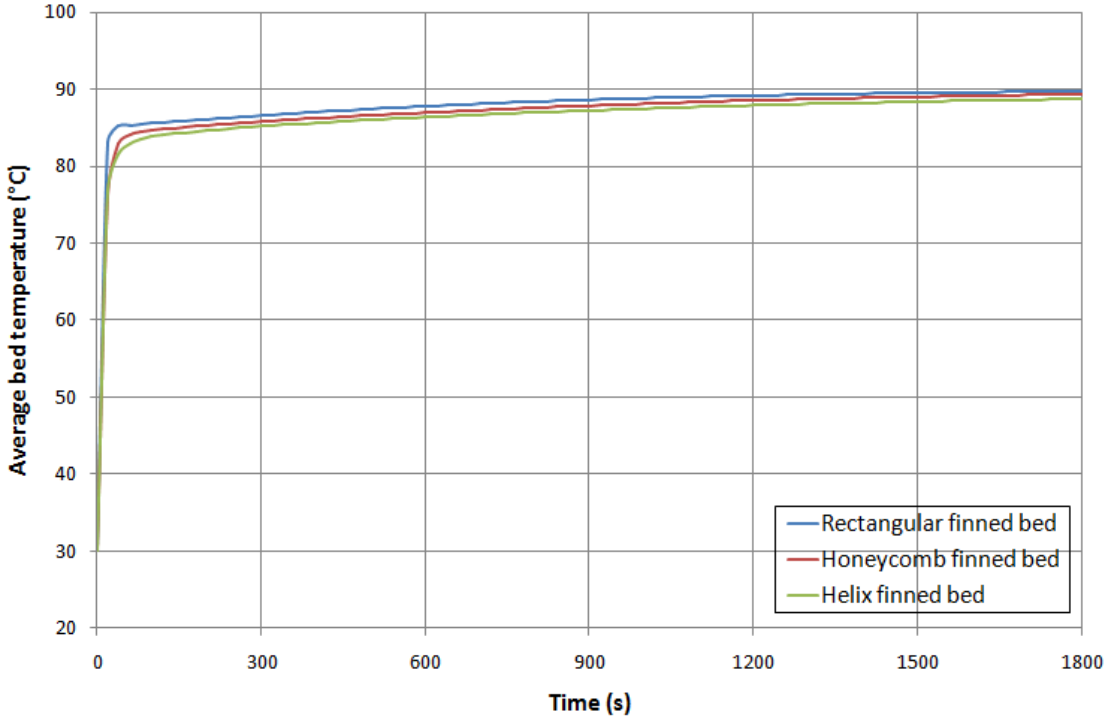

Figure 4-15 Average bed temperature during desorption process for three adsorption bed designs' desorption

4.5 Mesh sensitivity investigation of finite element modelling

A meshing process is necessary before computing the finite element modelling in COMSOL software. This section presents the investigation of mesh sensitivity of finite element modelling developed in this research. The model to simulate the adsorption process of the rectangular finned adsorption bed is computed three times using the operating conditions shown in Table 4-4 and different meshing procedures. The mesh number of each run is shown in Table 4-6. Figures 4-16 and 4-17 present the results of the water vapour uptake and average bed temperature respectively. The average deviations of the water vapour uptake and average bed temperature of these

three runs are 0.36% and 0.37% respectively; indicating that the different meshing densities have almost no influence on the finite element modelling prediction results.

Table 4-6 Mesh number of each meshing procedure

Runs	Mesh number
Run 1	9.87×10^5
Run 2	11.89×10^5
Run 3	13.77×10^5

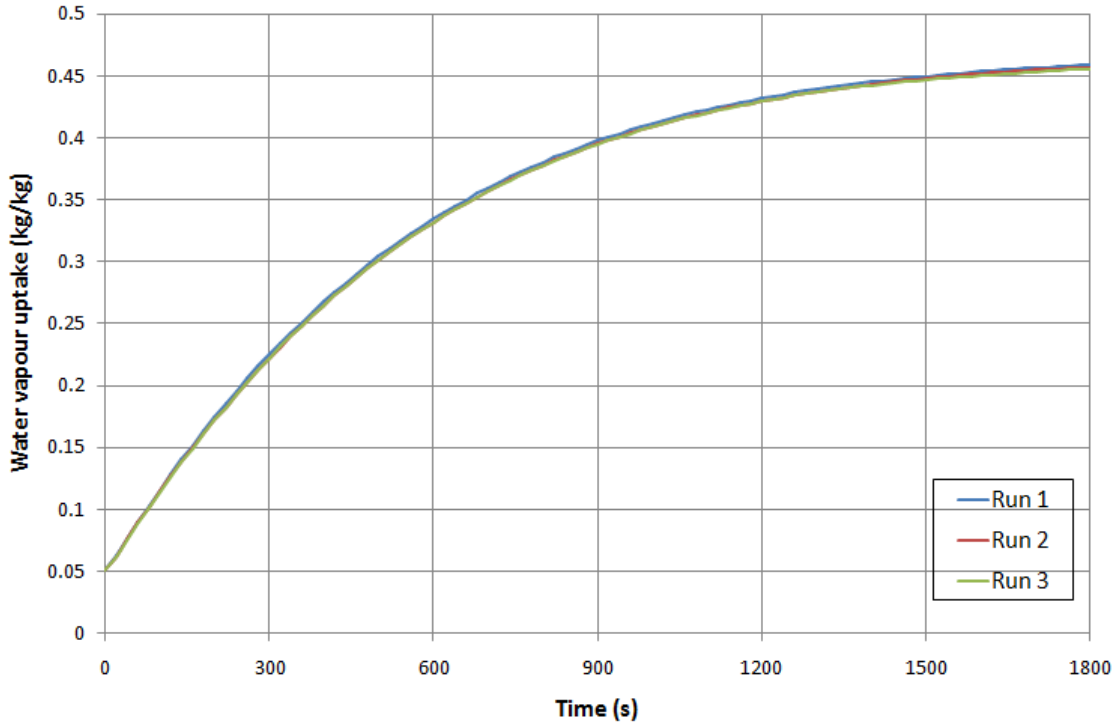

Figure 4-16 Water vapour uptake of three runs with different mesh numbers

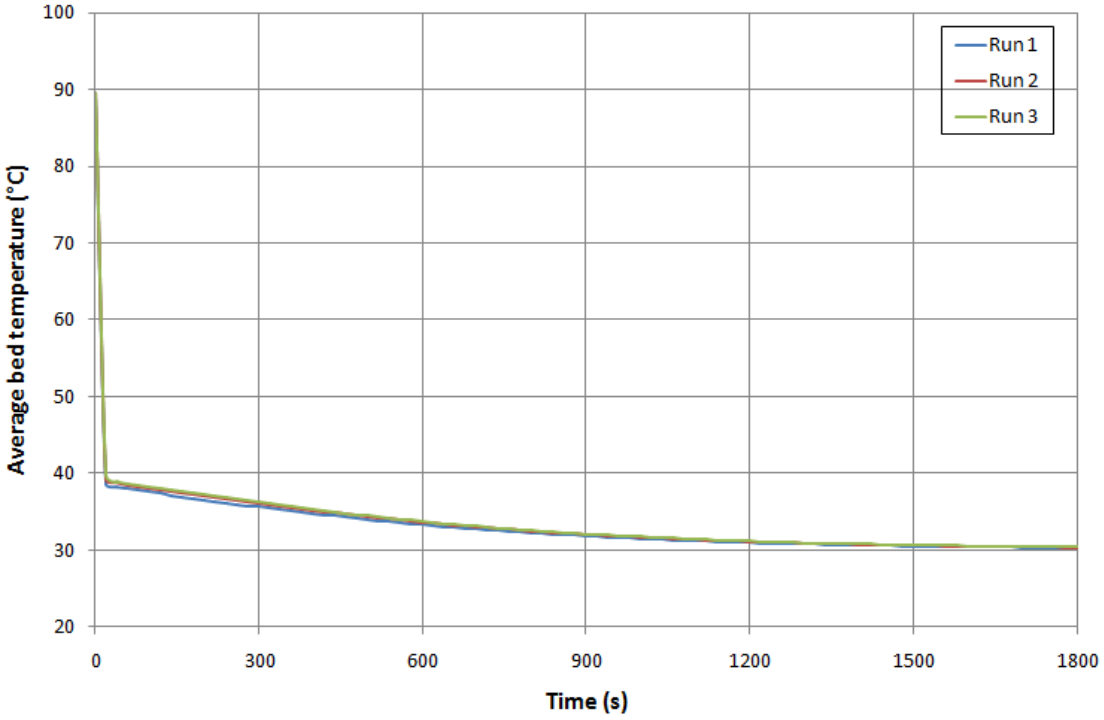

Figure 4-17 Average bed temperature of three runs with different mesh numbers

4.6 Summary

This chapter presented an investigation of three adsorption bed designs, including a rectangular finned tube adsorption bed, a honeycomb finned rectangular channel adsorption bed and a helix finned tube adsorption bed. A finite element modelling method is utilised in this research because of its advantages of high accuracy, as explained in section 2.10.2.2. Finite element models using COMSOL Multiphysics software were developed for these three adsorption bed designs packed with CPO-27Ni adsorbent material. The performances of three adsorption bed designs are compared based on the simulation results. It is concluded that the rectangular finned adsorption bed outperformed the honeycomb finned adsorption bed and the helix

finned adsorption bed; due to its very effective adsorption performance in terms of water vapour uptake and HCR.

CHAPTER 5 EXPERIMENTAL TEST FACILITY

5.1 Introduction

This chapter introduces the design, construction and commissioning of a test facility to evaluate the performance of rectangular finned tube adsorber beds packed with MOF material. To improve the performance of an adsorption air conditioning system, an efficient adsorption working pair and adsorption bed design should be investigated and tested. There are two methods used for investigating adsorption cooling systems as reported in the literature review, which are simulation and experimental methods. The simulation method utilises mathematical analysis to predict the performance of an adsorption refrigeration system based on solving all the governing equations. On the other hand, experimental work is required to prove the concepts and validate simulation work. Therefore, experimental investigation of performance including heat and mass transfer performance, cooling capacity and efficiency is important.

This test rig is flexible so adsorption beds with different structures and adsorption working pairs can be tested. Utilising this test facility, the performance of an adsorption system with CPO-27Ni/water and a rectangular finned tube adsorption bed design was investigated.

5.2 Test facility description

The test facility is based on a one-bed cycle which has the simplest adsorption system structure. Figure 5-1 shows a schematic diagram and Figure 5-2 is a pictorial presentation of the test rig. The test rig consists of an adsorber, evaporator/condenser, cooling water circulating system, chilled water circulating system and electrical heating system. The adsorber consists of a steel shell in which two finned tube heat exchangers packed with adsorbent material granules are fitted. Each of the finned heat exchangers consists of four copper tubes; with two tubes fitted with electrical heaters and two connected to the cooling water system. Electrical heaters were used to enable testing to be carried out at wide range of temperatures, representing both water heating and exhaust gas heating. The electrical heaters were used during the desorption process; while the cooling water was used during the adsorption process. There are three solenoid valves and two water pumps to control the water flow rate. In the adsorption process all pumps and valves are open; while in the desorption mode, valve 1, valve 2 and pump 1 are closed. In this test facility, evaporation and condensation are performed in one heat exchanger to make the system simpler. It works as an evaporator in the adsorption process and as a condenser in the desorption process. A heater-chiller is utilised in the test rig to provide the energy for the evaporation process and take heat out during the condensation process. Furthermore, three vacuum pumps are connected to the adsorber and evaporator/condenser tank respectively to suck air out and provide the required vacuum conditions. For measurements, probe thermocouples, pressure transducers and flow meters are installed in the test rig to measure temperature, pressure and water flow rate respectively.

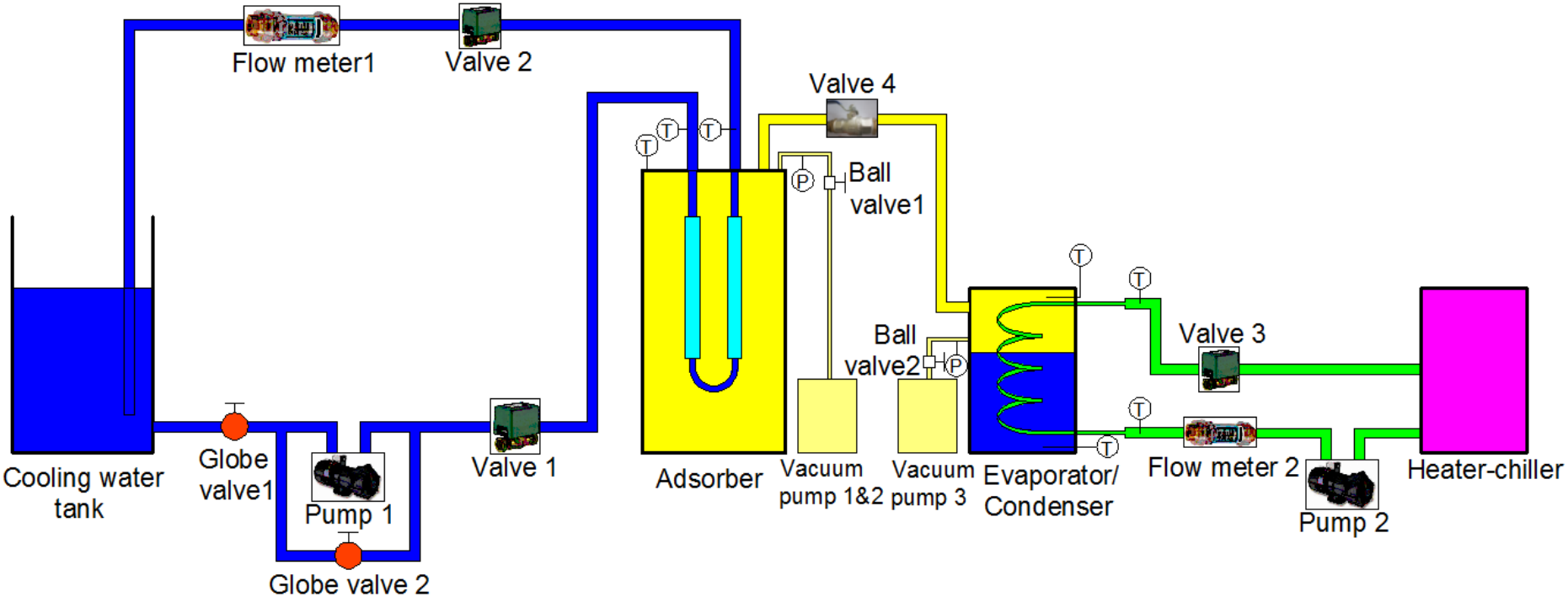

Figure 5-1 Schematic figure of the whole test facility

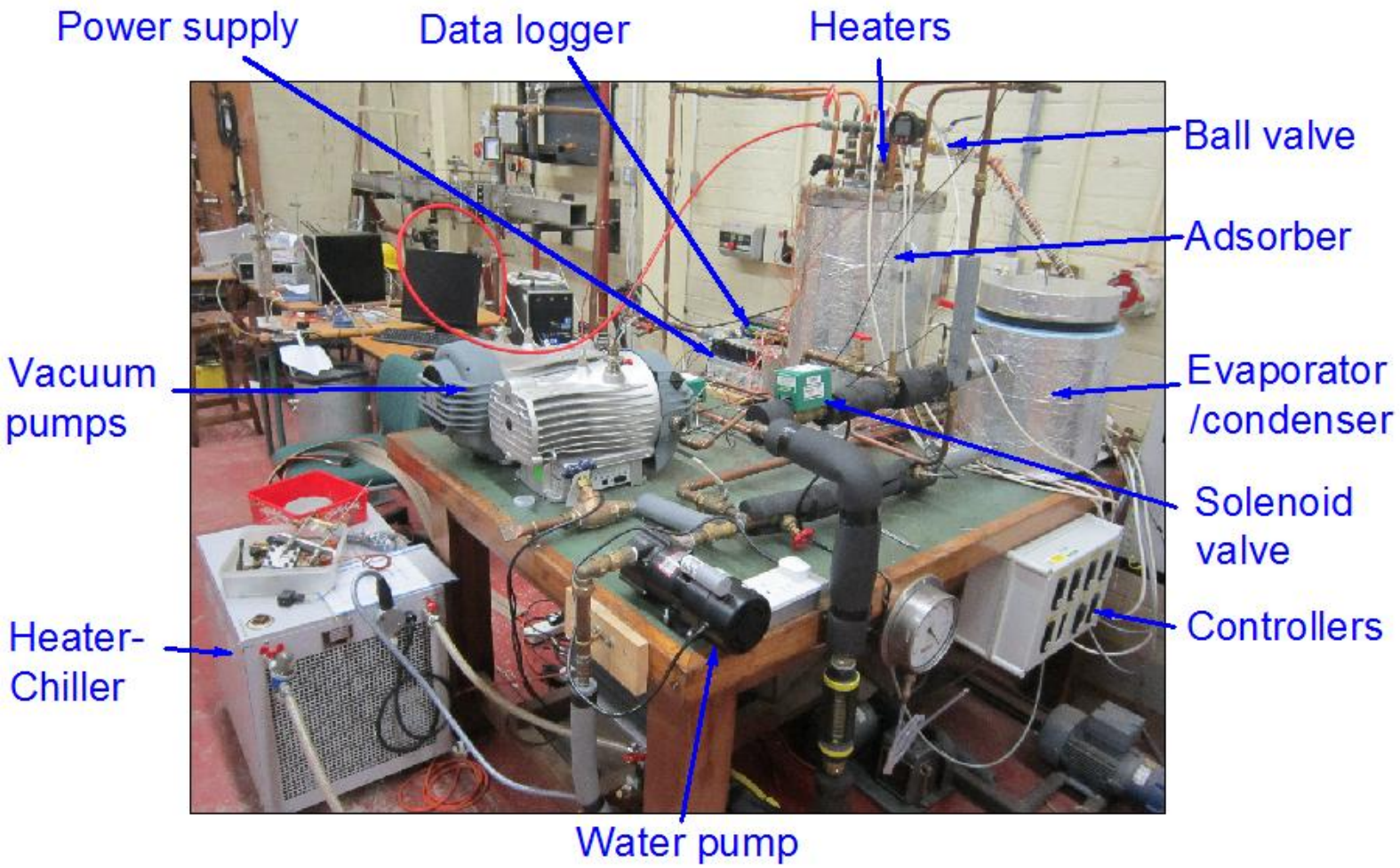

Figure 5-2 Pictorial figure of the whole test rig

Each component of the test facility is described in the following sections, including the adsorber, evaporator/condenser, heater-chiller, heaters and controllers, water pumps, valves, vacuum pumps and measuring instruments.

5.2.1 Adsorber

The adsorber is the most important part in the whole test facility. The adsorber consists of three parts: adsorption beds, shell and cover. The adsorption beds used in this test rig are rectangular finned tube heat exchangers made by the Weatherite Company. Each adsorption bed contains 270 aluminium fins and four copper tubes, as shown in Figure 5-3. Adsorbent granules are packed between the fins. Two helix electrical heaters are fitted in the two middle tubes respectively to heat the whole adsorption bed in the desorption process. In the adsorption process, cooling water flows through the remaining two tubes to cool down the adsorption bed; since the bed is hot after the desorption process. Two adsorption bed modules are installed in the adsorber shell and their tubes are connected by U-bends on one end. On the other side, tubes are extended to pass through the cover. All design parameters are shown in Table 5-1. The modules are covered by stainless steel mesh to contain the adsorbent granules and prevent them from falling out. Figure 5-4 shows photographs of the packed adsorption beds.

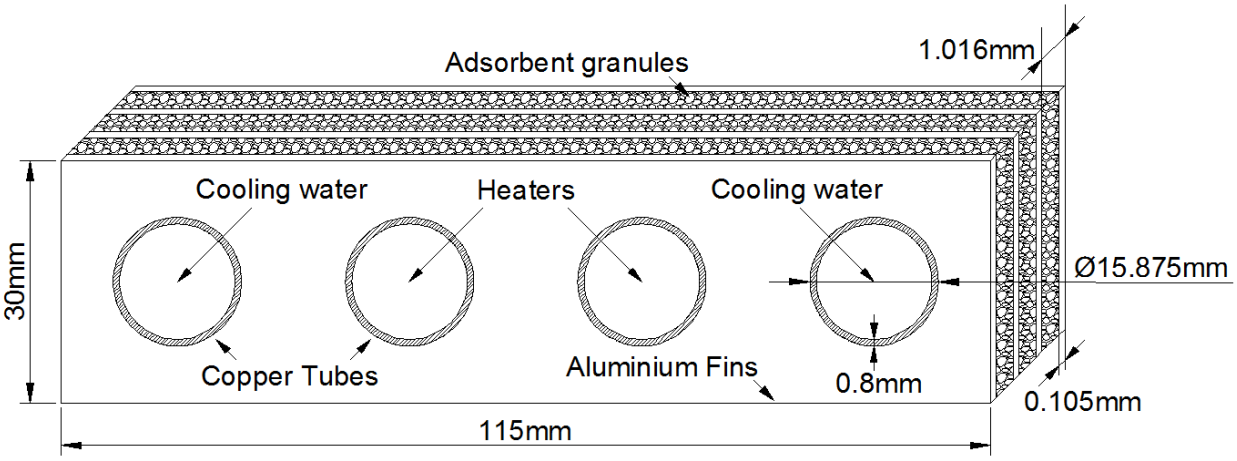

Figure 5-3 Schematic diagram of a rectangular finned tube adsorption bed

Table 5-1 Adsorption bed parameters

Parameters	Value
Bed length	275mm
Fin width	115mm
Fin height	30mm
Fin pitch	1.016mm
Fin thickness	0.105mm
Tube outer diameter	15.875mm
Tube thickness	0.8mm
Fin number in one adsorption bed	270

Figure 5-5 shows the adsorber steel shell with a height of 600mm, a diameter of 320mm and wall thickness of 6mm.

The finned tube heat exchangers are fitted to a metal plate. The metal plate is also used to seal the adsorber shell by being connected to a flange attached to the shell. To ensure effective sealing of the adsorber bed, an o-ring was fitted in a groove machined in the flange, as shown in Figure 5-6. The flange and the metal plate had 24 bolts to enable appropriate sealing of the adsorber, as shown in Figure 5-7.

Figure 5-4 Actual packed adsorption beds

Figure 5-5 Adsorber shell

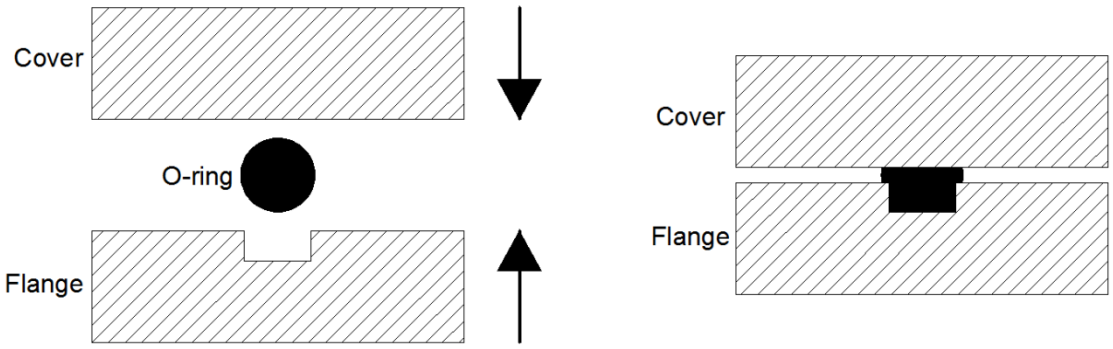

Figure 5-6 O-ring sealing for adsorber

Figure 5-7 shows a drawing and a photograph of the metal plate; it contains eight holes for fitting of the two adsorber bed modules; six holes for thermocouples; one hole for both vacuum pump and pressure transducer; and one hole for refrigerant vapour flow. The shell of the adsorber is covered with 20mm thick ROCKWOOL thermal insulation material, which has a thermal conductivity of 0.023W/(m·K), to reduce thermal losses to the environment.

5.2.2 Evaporator/condenser

In the test facility, there is one adsorber bed that works as an adsorber during the adsorption process and a desorber during the desorption process. That means that the adsorber will be connected to an evaporator during the adsorption mode and to a condenser during the desorption mode respectively. Therefore the evaporator and condenser can be integrated into one device.

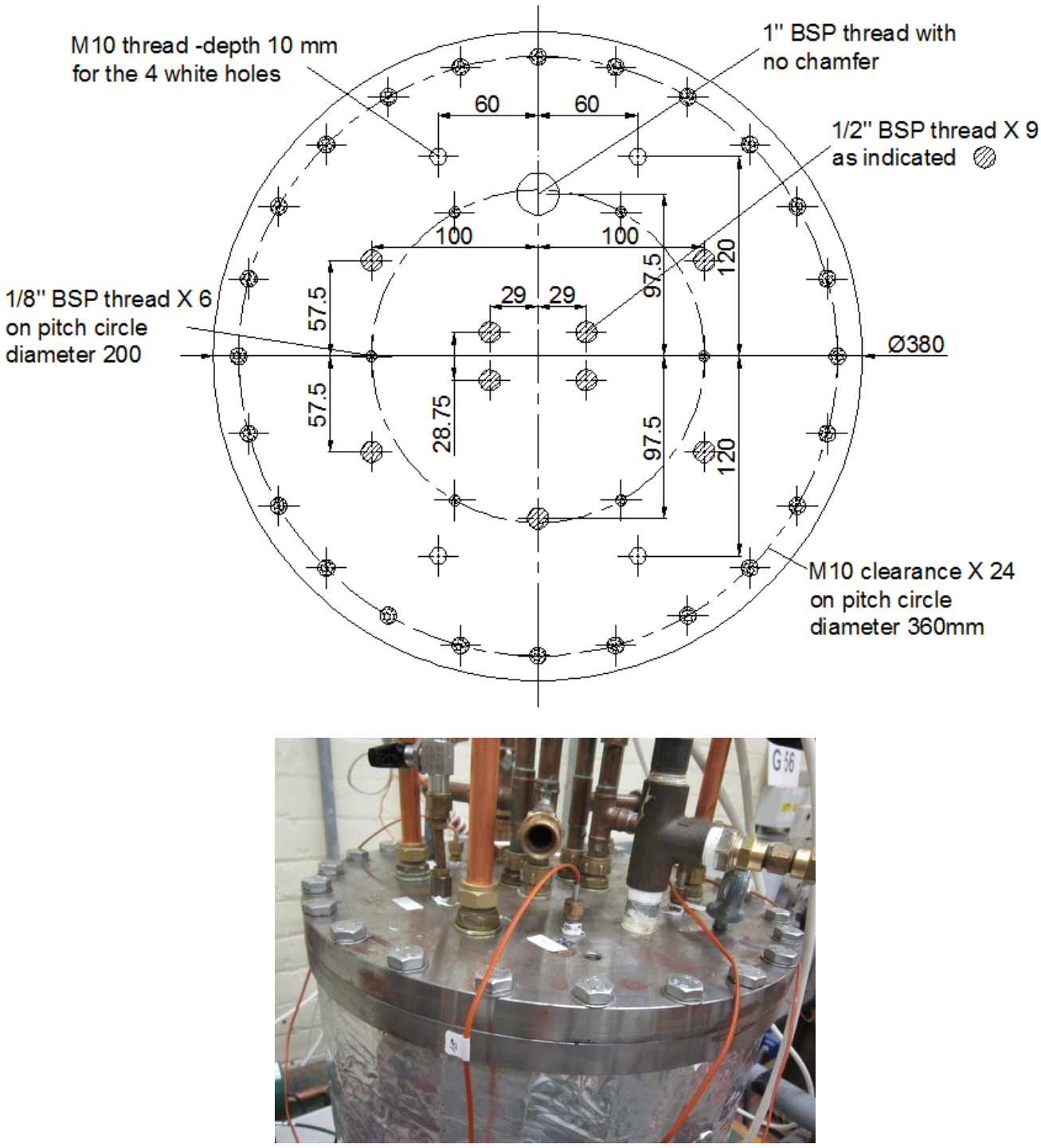

Figure 5-7 Cover of adsorber

The evaporator/condenser is a circular tank with a diameter of 320mm and a height of 340mm, as shown in Figure 5-8. The shell and base are made of steel with 3mm thickness. On the wall, there are two holes for cooling/heating fluid inlet and outlet;

two holes for thermocouples measuring the temperature of the refrigerant vapour and liquid respectively; one hole for both the pressure transducer and vacuum pump; and one hole for refrigerant vapour entering/leaving the shell.

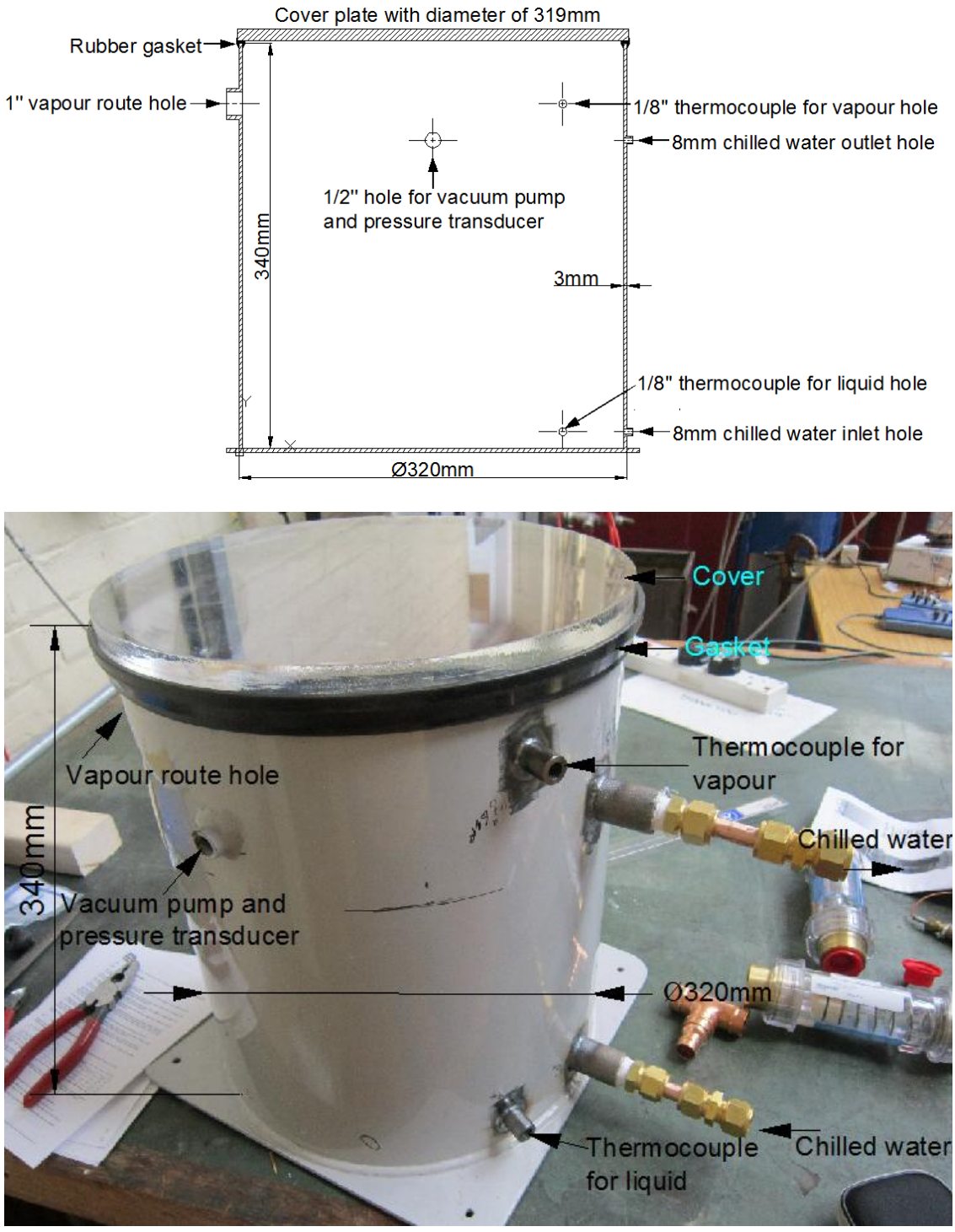

Figure 5-8 Evaporator/condenser

The cover is an acrylic plate; it seals the shell through a rubber gasket as shown in Figure 5-8. When the pressure inside the tank is smaller than that outside, the cover and shell will push onto the rubber gasket, as shown in Figure 5-9. The deformation makes the gasket contact the cover perfectly and prevent ambient air going inside. With this sealing method, a high vacuum level inside the evaporator/condenser tank was achieved. The results from the vacuuming test showed that the absorber and evaporator/condenser lost only 1mbar during 3 days.

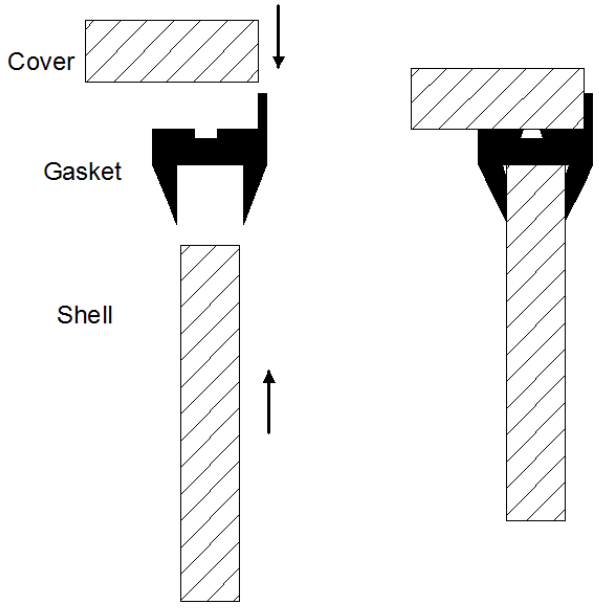

Figure 5-9 Sealing method of the evaporator/condenser

The cooling/heating fluid used to extract the heat of condensation or supply the heat of evaporation is water, which flows inside a tube coil. The coil is made of 8mm outside diameter tube and consists of two parts as shown in Figure 5-10. The first part is a coil made of a number of turns in the same plane and laid at the bottom of the shell. This coil is submerged in the liquid refrigerant and provides the heat required for evaporation. The second part is a helical coil with an outer diameter of 220mm

and eight turns. This part is submerged in the vapour and provides a surface for condensation.

During the adsorption process, chilled water flows inside the coil to provide heat to evaporate the refrigerant liquid. On the other hand, during the desorption process, cooling water flows inside the coil to condense the refrigerant vapour. The shell and cover are covered with thermal insulation materials to reduce heat flow to or from their surroundings.

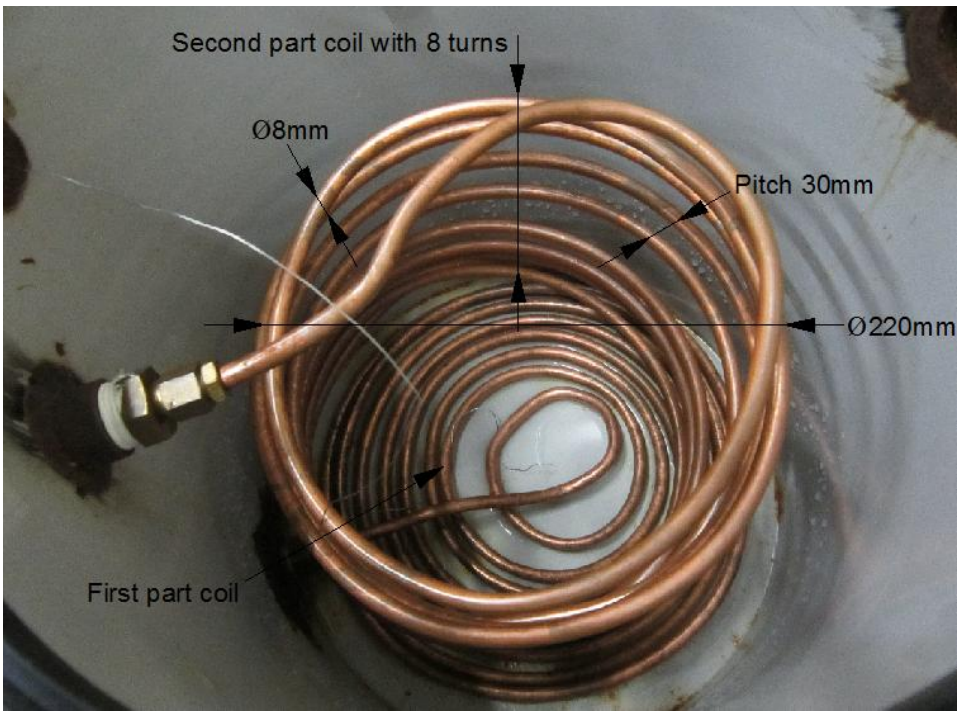

Figure 5-10 Coil inside evaporator/condenser

5.2.3 Heater-chiller

To investigate the performance of the adsorption cooling system at various operating conditions, the temperature of the evaporator and condenser needs to be controlled

during the experiment. To achieve this, a heater-chiller is used in this test facility to control the temperature of the heating/cooling fluid.

The heater-chiller system used is a CU-700 produced by the Betta-Tech company and Table 5-2 shows its specification. Figure 5-11 shows the front and back view of this heater-chiller, which has the following advantages: firstly, this heater-chiller can control temperature of fluid from -15 ℃ to 70 ℃, which is suitable for automotive air-conditioning application; secondly, this heater-chiller controls the temperature through a PID controller with an accuracy of 0.1 ℃; finally, this machine is compact and its operation is simple.

Table 5-2 Parameter of Betta-Tech CU 700 heater-chiller

Parameter	Value
Temperature range	-15 ℃ to 70 ℃
Cooling capacity at 15 ℃ water capacity	2500 kcal/h
Refrigeration	1 HP
Heating rating	2.5kW
Pump flow max zero pressure	0.05kPa
Tank capacity	3L
Dimensions	610mm ×450mm ×500mm
Weight	82kg
Electrical supply	230V

Figure 5-11 Front and back view of Betta-Tech CU 700 heater-chiller

5.2.4 Heaters and controllers

An electrical heating method for the desorption process is used in this test facility, in order to enable testing at a wide range of temperatures. Figure 5-12 shows the custom made heater bought from Under Control Instruments Ltd. It includes a heating element and connecting wires. Heating coils are inserted into the two middle tubes of each bed to heat the whole adsorption bed as mentioned in section 5.2.1; thus four heaters are used in total. There are also insulating materials on the surface of the heating coils to prevent electric conduction from the heaters to the whole rig. A J-type thermocouple is fixed in the inner ring of each heater's coils to monitor the heater temperature.

To control the temperature of the heaters, a N322 PID controller from Novus Company was used for each heater. It has a control range of 0 ℃ to 600 ℃ with an accuracy of 3 ℃ for the attached J-type thermocouple. The controllers use the

temperature sensed by the thermocouple fitted on the heater to switch on or off the heater's electrical power input. They work continuously so that the temperature of the heaters can be maintained at the setting value.

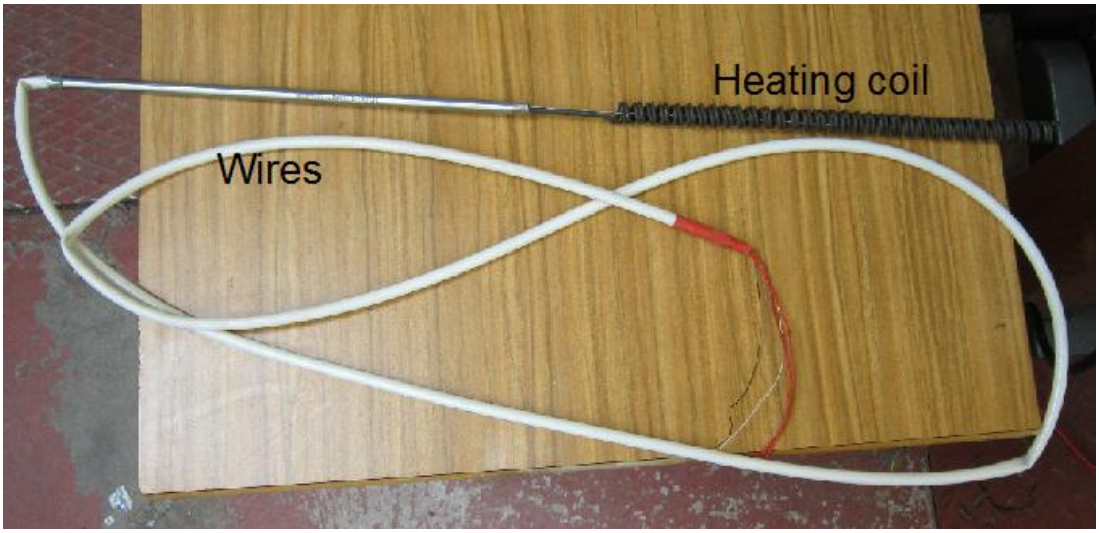

Figure 5-12 Heater

5.2.5 Water pumps

Two water pumps were used in the test facility. One was used to pump cooling water in the adsorber bed heat exchanger. The other one was used to pump water in the evaporator/condenser together with the pump inside the heater-chiller. An MSP-3 water pump from March May Ltd was chosen. The pumps are capable of circulating water at a flow rate ranging from 1 to 19.5L/min and producing a maximum pumping pressure of 3bar.

5.2.6 Valves

In this test facility, four valves were used at different positions, as shown in Figure 5-1. Valves 1 and 2 were used to control the flow of the adsorber cooling water; valve 3 was used to control the flow of the evaporator/condenser heating/cooling water and valve 4 was used to control the flow of refrigerant vapour between the adsorber and evaporator/condenser.

A motorised solenoid two port valve, type SMV2530 from the Inta Company was chosen for valves 1, 2 and 3. This valve type can handle the maximum temperature of 120 ℃ which is adequate for this research. Also, the opening time of this valve is only 10 seconds and the closing time is 4 seconds. Table 5-3 shows the operation mode of the valves and water pumps based on numbers shown in Figure 5-1.

Table 5-3 Operation of valves and water pumps

Mode	Valve 1	Valve 2	Valve 3	Valve 4	Pump 1	Pump 2
Adsorption	Open	Open	Open	Open	Open	Open
Desorption	Closed	Closed	Open	Open	Closed	Open

The control method for valves 1-3 is shown in Figure 5-13. An NI 6008 control board was used to control these three valves. There were two voltage outputs from the control board, one for opening and closing valves 1 and 2 simultaneously and the other one controlled valve 3. The output voltage signal from the ports of the control board can only be 0 or 5V to close or open the valve respectively. Since the valve can only be powered by 230V voltage, relays (one for each output signal) are needed to enhance the 5V output voltage signal to the 230V required by the valve. The NI

control board was connected to a computer and controlled using LabVIEW software. The operating interface in LabVIEW is shown in Figure 5-14.

For valve 4, a ball valve operated by hand was used to control the flow of refrigerant vapour between the adsorber and evaporator/condenser.

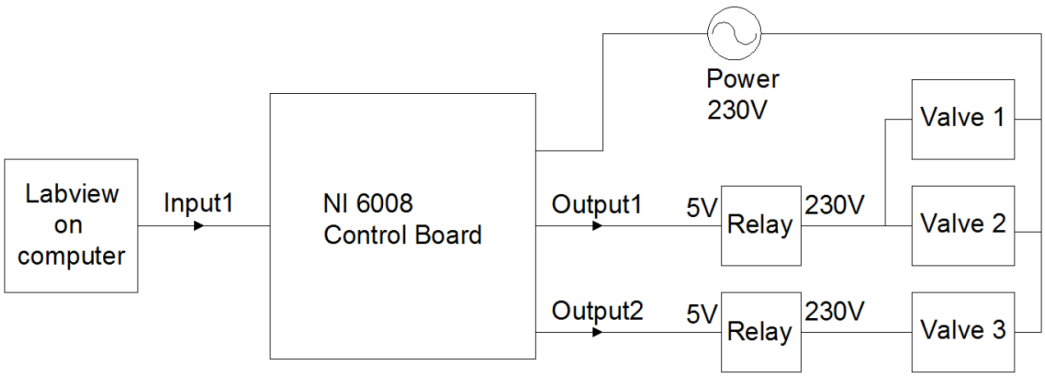

Figure 5-13 Control method for valve 1-3

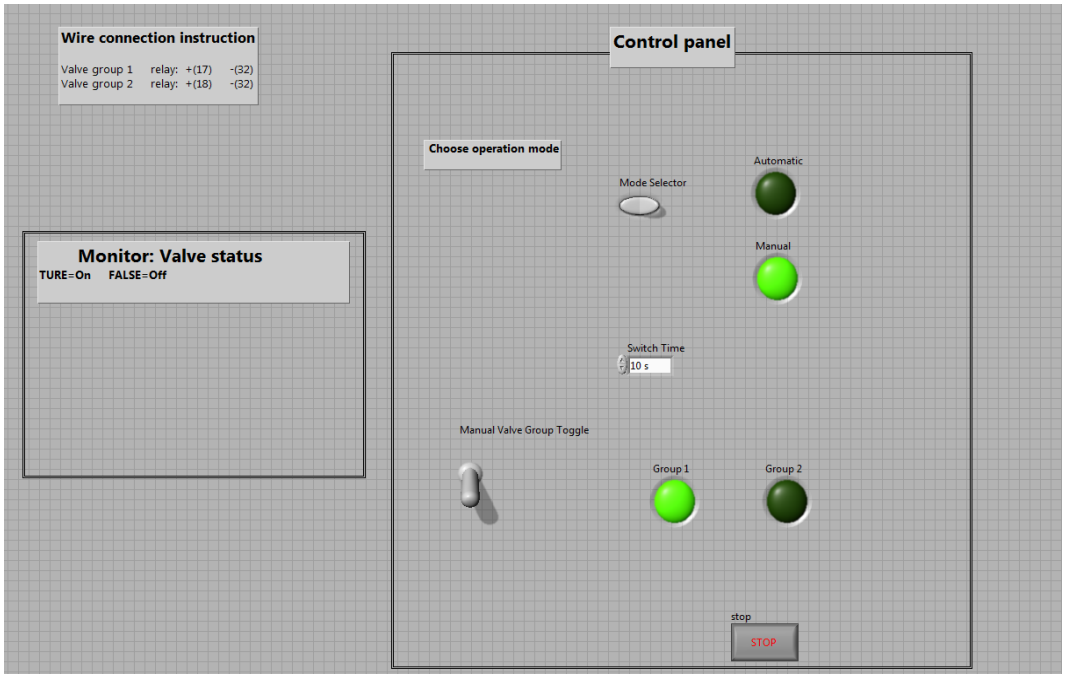

Figure 5-14 Operating interface in the LabVIEW software

5.2.7 Vacuum pumps

Vacuum pumps are needed to achieve the low pressure conditions required for using water as a refrigerant. An Edwards nXDS15i dry vacuum pump was used as shown in Figure 5-15. It has a maximum vapour pumping rate of 280g/h and can achieve minimum pressure of 0.5Pa. This pump is an oil free pump thus eliminating the need to change the oil when contaminated with condensate liquid water. In the test facility, two vacuum pumps were connected to the adsorber to accelerate the adsorbent granules' drying process. One other pump, ECVP425, was connected to the evaporator/condenser to evacuate the shell before the experiment. Ball valves (one for each vacuum pump) were used to control the connection between the pumps and the adsorber or evaporator/condenser tanks.

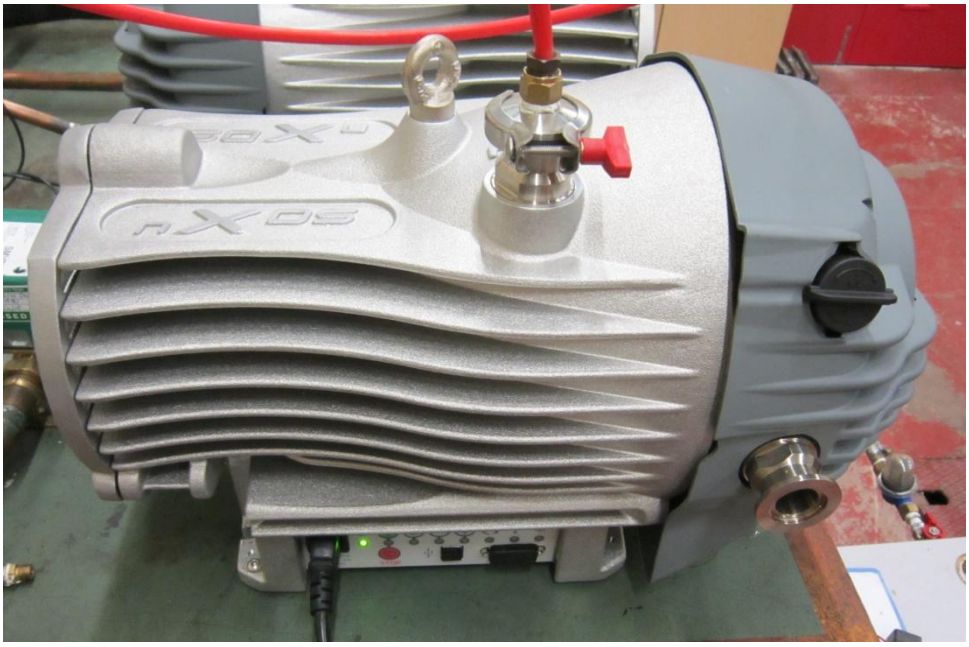

Figure 5-15 nXDS15i dry vacuum pump

5.2.8 Measuring instruments

A computerised measuring system was used in the test facility to monitor and record temperatures and pressures. This section describes the various measuring instruments used.

5.2.8.1 Temperature measurement

Thermocouples were installed at different positions in the test facility to measure the temperatures of the adsorption beds, heating/cooling fluid flowing through the adsorber and evaporator/ condenser at the inlet and outlet, liquid and vapour in the evaporator/condenser shell and adsorber space.

The thermocouples used for measuring the temperature of the adsorption beds and adsorber space were T-type compact transition joint probes from Omega Engineering Ltd., as shown in Figure 5-16. The transition joint has an outside diameter of 4.5mm and a length of 30mm which is made of stainless steel. The thermocouple sheath has a diameter of 1.5mm and different lengths were used at different positions. This type of thermocouple can measure temperature up to 260 ℃ according to the manufacturer's instructions.

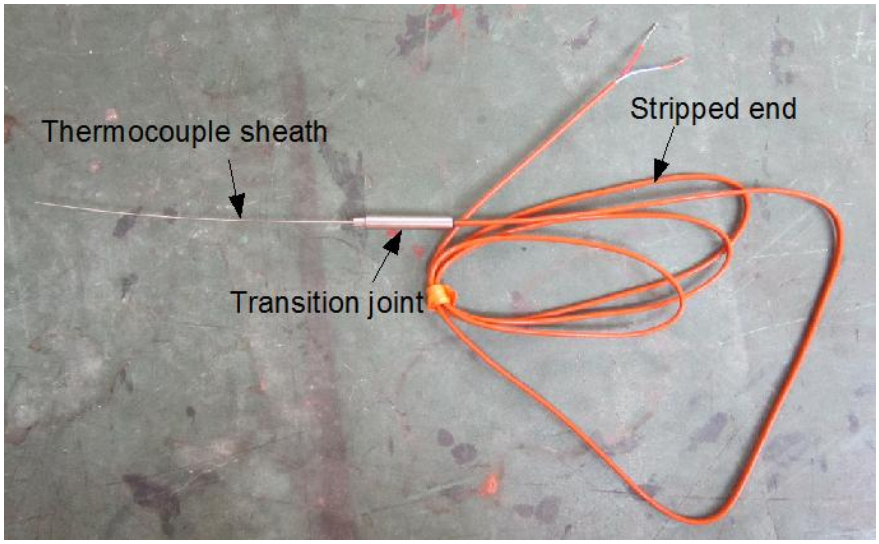

Figure 5-16 TJC100-CPSS thermocouple

All TJC100-CPSS thermocouples were sealed and fixed on the cover of the adsorber and the shell of the evaporator/condenser using compression fittings, as shown in Figure 5-17. The fitting was fixed at the transition joint of the thermocouple and it included a compression nut, compression ring and compression seat.

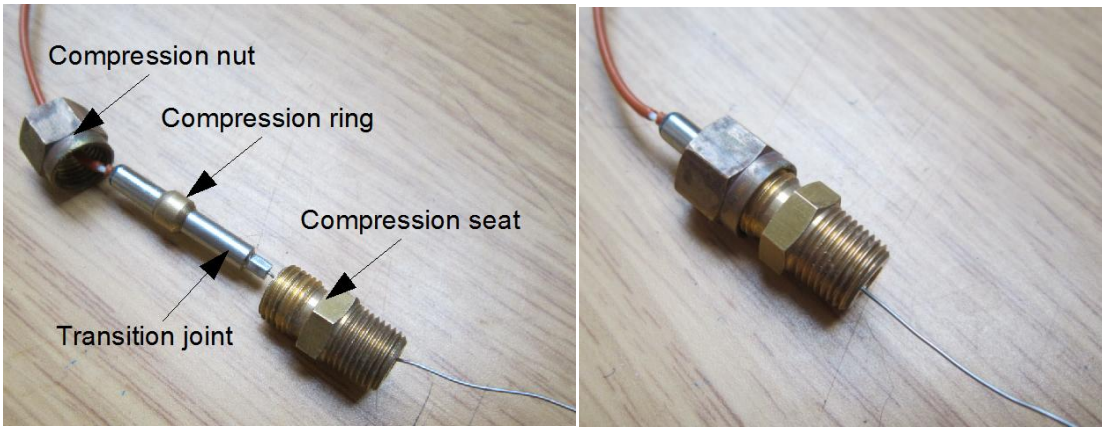

Figure 5-17 Thermocouple assembly

There were two thermocouples fixed similarly at each adsorption bed; one at the middle of the length and the other at the bottom, as shown in Figure 5-18. All these

thermocouples were probed through the metal mesh and immersed into the adsorbent granules. The thermocouples were fixed using aluminium tape to ensure firm contact with the surface. To monitor the temperature of refrigerant vapour in the adsorber space, one thermocouple was fixed such that the probe was suspended in the adsorber volume. In the evaporator/condenser, two thermocouples were fixed in the shell; the upper one to measure the temperature of the refrigerant vapour and the bottom one to measure the temperature of the refrigerant liquid.

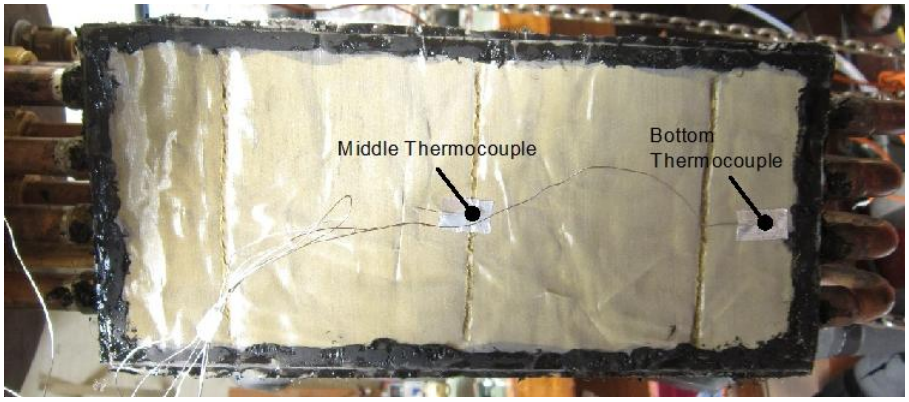

Figure 5-18 Adsorption bed temperature measurement

To measure the heating/cooling water temperature at the inlet and outlet of the adsorber and evaporator/condenser, Platinum RTD sensors were used owing to their high degree of accuracy of measurement, as shown in Figure 5-19. They have a sheath of 100mm in length and the tip was fixed at the centre of the flow of water inside the tube. The RTD thermocouples at the inlet and outlet of the evaporator measures the chilled water temperature ranging from 8.799 ℃ to 15.093 ℃, with the accuracy of ±0.025 ℃. While the T-type thermocouples fixed in the adsorption bed have the measuring range from 20.57 ℃ to 107.712 ℃, with the accuracy of ±0.1 ℃. Then the uncertainties of the chilled water temperature and the bed temperature, which are

measured by RTD thermocouples and T-type thermocouples respectively can be determined. They are 0.6-0.7% and 0.5-0.9%.

Figure 5-19 RTD thermocouple and the fitting

The voltage signal of all the thermocouples were logged using DataTaker-DT85 and the temperature values were displayed on the computer. Therefore, the temperature could be monitored and recorded during the experiment.

5.2.8.2 Pressure measurement

Two pressure transducers were used in the test facility to measure the pressure in the adsorber and evaporator/condenser respectively. The pressure transducers utilized were from Impress Sensors & Systems Ltd which can measure pressure from 0 to 10kPa. The measurement accuracy is ±0.01kPa with the output signal of the transducer being electrical current ranging from 4 to 20mA. The relationship between pressure and current is linear, as shown in Figure 5-20 [153]; thus the current signal can be converted to a voltage signal through 100ohms resistance connected to the data

logger terminal board. The electrical wiring of the pressure transducer with the data logger and power supply is illustrated in Figure 5-21.

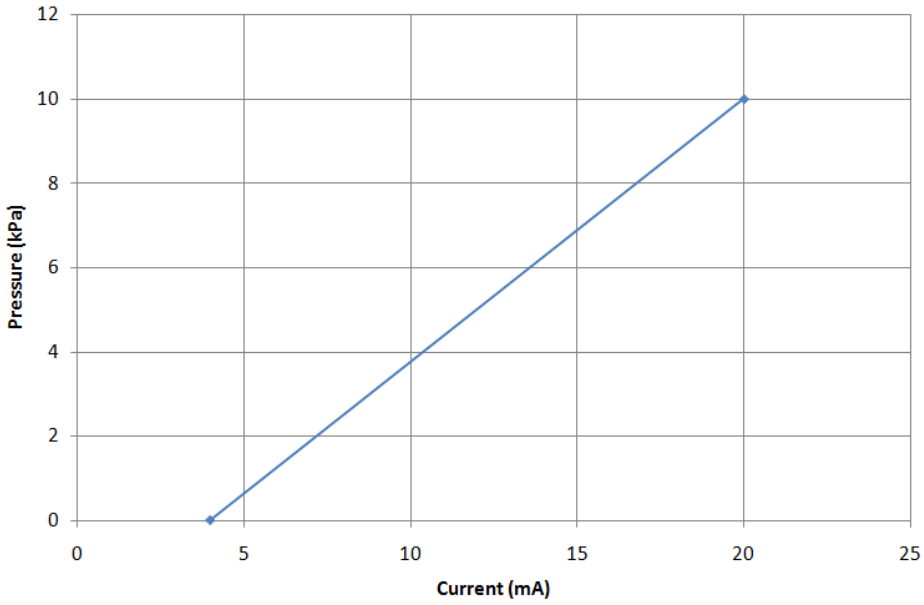

Figure 5-20 Relationship between pressure and current [153]

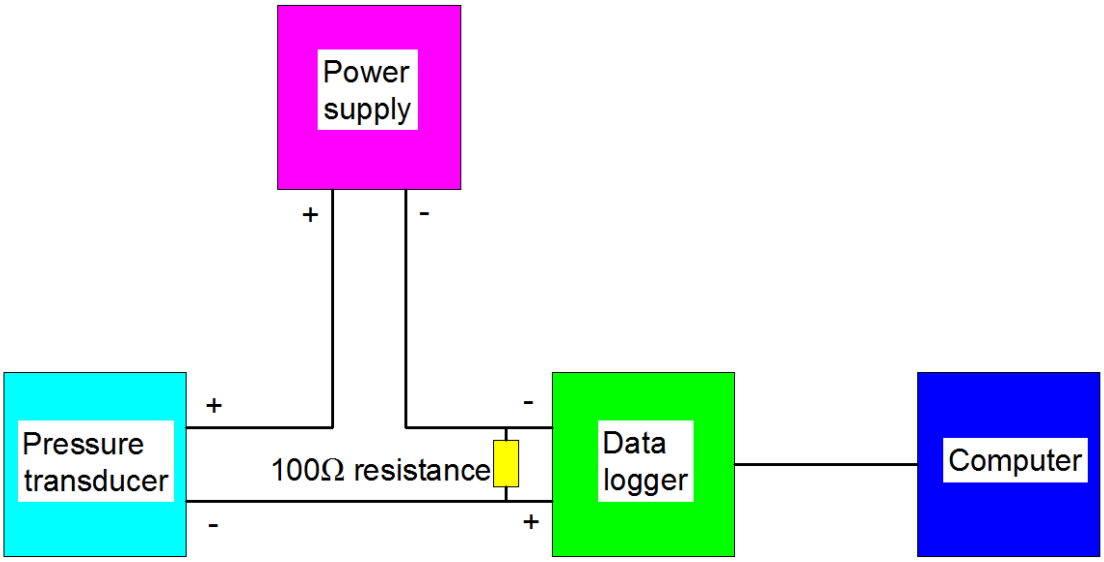

Figure 5-21 Electrical wiring diagram of pressure transducers

5.2.8.3 Flow rate measurement

The flow rate of the heating/cooling fluids through the adsorber and evaporator/condenser were measured respectively using two flow meters. The flow meters utilised in the test facility are FLC-H14 from Omega with the range of 0-57 L/min, as shown in Figure 5-22, with an accuracy of ±1L/min and a maximum operating temperature of 121 ℃. The flow meters are tubular with all internal wetted parts sealed within the body casing. Running through the centre of the body casing is a tapered centre shaft which is centred in the bore. Encircling the shaft is a sharp-edged, floating metering poppet. The metering poppet is held in the 'no flow' position by the biased return spring. As the flow moves through the meter it creates a pressure differential across the floating orifice disk, forcing the disk and transfer magnet against the return spring. As flow increases, the pressure differential across the metering poppet increases, forcing poppet to move along the tapered centre shaft. As flow decreases, the biased return spring forces the poppet down the tapered centre shaft, returning to the 'no flow' position [154]. The flow rate was measured manually and during the experiment, several readings were taken and their average was calculated. In the experiment, the flow meter was used to measure the water flow rate ranging of 8-14L/min. The uncertainty of the flow meter is between 7.1% and 12.5%.

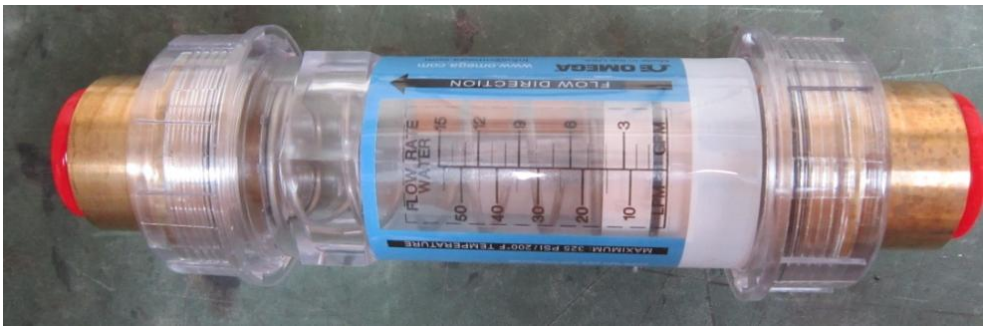

Figure 5-22 FLC-H14 flow meter

5.3 Test rig commissioning

The adsorber consisting of the adsorber shell, adsorber cover and adsorption bed was integrated with the evaporator/condenser, chiller and cooling water tank as shown schematically in Figure 5-1. The system was commissioned and initial testing for the various aspects of the investigation was carried out.

Firstly, the adsorber and evaporator/condenser were vacuumed to as low a pressure as possible at 3mbar and then left while the pressure was monitored to check whether there was any leak into the system. As a result, it was ensured that the pressure in the adsorber and evaporator/condenser would only increase by 1mbar during the 3 days, through eliminating any source of leakage. With this small pressure change, the adsorber and evaporator/condenser were capable of holding the vacuum. Besides, each dry vacuum pump can achieve the minimum pressure of 0.005mbar which indicates that the vacuum level of the test facility is high. This test is important because the refrigerant liquid can evaporate only when the pressure in the evaporator/condenser is at/below the saturation pressure corresponding to the operating temperature. If the adsorber and evaporator/condenser cannot hold the vacuum, the pressure in the evaporator/condenser will increase quickly to higher than the saturation pressure of the refrigerant in the adsorption process; which stops the evaporation process, as well as reduces the refrigerant uptake amount and cooling capacity. Besides, the air flowing into the system can affect the mass transfer and heat transfer performance of the adsorber beds and evaporator/condenser.

Secondly, the leakage of all pipes was inspected by opening all the water pumps and valves after the pipes were connected.

Thirdly, the heater's performance was tested. With all four heaters opening and the controllers of the heaters being set at 250 ℃, the adsorption beds could reach an average temperature of around 90 ℃ after 3 hours; which was adequate for regenerating the adsorber beds.

5.4 Testing procedure

The following steps describe the testing procedure in detail, including preparation and regeneration, adsorption, desorption and cycling.

A. Preparation and regeneration

1- Fill the evaporator/condenser with 2.5L water and fill the water tank with cooling water.

2- Vacuum the adsorber using the two dry vacuum pumps. In the vacuum process, valve 4 is closed to isolate the adsorber from the evaporator/condenser tank. At the same time, adsorption beds are heated using all four heaters. The controllers of the heaters are all set at 250 ℃. The data of the temperature and pressure is monitored and recorded simultaneously using a data logger and computer. The power consumed by the heater is also recorded using a plug-in power monitor.

3- Half an hour before the end of the predefined heating time, the heater-chiller is switched on and set at the required evaporation temperature. The refrigerant water inside the evaporator/condenser is cooled to the evaporation temperature by heat transfer with the chilled water going through the coils. At the same time water pump 2 and valve 3 are open to allow a large water flow rate to go

through the evaporator/condenser to reach a stable temperature in as short a time as possible. Simultaneously, the vacuum pump is used to vacuum the evaporator/condenser until the pressure inside reaches the saturation pressure corresponding to the evaporation temperature.

B. Adsorption

4- When the predefined heating time is reached, the adsorber and evaporator/ condenser are isolated from the vacuum pumps and the heaters are switched off. The set temperature of the heater-chiller stays at the evaporation temperature. Water pump 1 is turned on and valves 1 and 2 are opened to allow the cooling water flow through the adsorption beds. The required flow rate is controlled by the flow control valve and a bypass valve (see Figure 5-1). The flow rate is recorded for both the water flowing through the adsorber and the evaporator.

5- When the flow rate becomes stable, valve 4 is opened. The evaporator is connected to the adsorber to start the adsorption process for a specified length of time.

C. Desorption

6- After the adsorption process for a predefined adsorption time, water pump 1 is turned off and valves 1 and 2 are closed. Cooling water flowing through the adsorption beds is stopped.

7- Heaters are switched on to heat the adsorption beds. The set temperature of the heater-chiller is changed to the condensation temperature. In this process, the refrigerant vapour is desorbed from the adsorbent granules and condensed in

the condenser as valve 4 is open. The power consumed in the heating process and the flow rate of water flowing through the condenser, are recorded.

D. Cycling

8- After the desorption period, steps 4 to 7 are repeated to test the cycling performance of the adsorption system.

E. End

9- When the predefined times of the cycle are finished, the data of temperature and pressure recorded by the data logger is uploaded. All instruments are switched off.

10- Use the temperature and pressure data to evaluate the performance of the adsorption system. Two main results are calculated: the average bed temperature and the water vapour uptake during the adsorption process. The average bed temperature is the average value of the four temperature values measured by thermocouples fixed on the adsorber beds. The variation of the water vapour uptake $w(t)$ during the adsorption process is calculated using equation 5-1.

$$m_{ads} h_{fg} w(t) = \frac{1}{t} \sum_{n=1}^{n=t/\Delta t} (T_{chw,in} - T_{chw,out}) \dot{m}_{chw} Cp_{chw} \Delta t \qquad (5\text{-}1)$$

where m_{ads} is the dry adsorbent mass, h_{fg} is the water latent heat of evaporation, Δt is the time interval of data recording of the data logger, $T_{chw,in}$ and $T_{chw,out}$ are the temperatures of the chilled water at the inlet and outlet of the evaporator respectively recorded during the adsorption process, $\dot{m}_{chw}$ is the chilled water's mass flow rate and Cp_{chw} is the chilled water's specific heat capacity. The uncertainty of the average bed temperature is the same with the uncertainty of T-type thermocouples which is 0.5%-0.9% described in the

section 5.2.8.1. The uncertainty of the water uptake can be calculated using the following equation,

$$U_w = \sqrt{\left(\frac{f_w}{T_{chw,in}} U_{T_{chw,in}}\right)^2 + \left(\frac{f_w}{T_{chw,out}} U_{T_{chw,out}}\right)^2 + \left(\frac{f_w}{\dot{m}_{chw}} U_{\dot{m}_{chw}}\right)^2} \quad (5\text{-}2)$$

Where f_w is the funtion to calculate the water vapour uptake shown in euqation 5-1; U_w, $U_{T_{chw,in}}$, $U_{T_{chw,out}}$ and $U_{\dot{m}_{chw}}$ are uncertainties of water vapour uptake, temperatures of chilled water at inlet and outlet, and flow rate of the chilled water respectively. The calculated uncertainty of the water uptake is ranging from 5.2% to 10.1%.

5.5 Repeatability test

All instruments of the test facility were examined through a repeatability test. Three independent tests have been conducted at the same operating conditions, shown in Table 5-4. The time difference between the three tests is more than 12 hours to make sure the temperature of the system is the same as the ambient temperature at the beginning of each test. The results of liquid temperature, vapour temperature, heating/ cooling water temperature at the inlet and outlet of the evaporator in the adsorption process, pressure of adsorber and evaporator, average bed temperature are shown in Figures 5-23 to 5-26.

Table 5-4 Operating conditions of repeatability test

Operating condition	Value
Regeneration set temperature of heaters	250 ℃
Regeneration time	180mins
Evaporation temperature	15 ℃
Condensation temperature	15 ℃
Adsorption time	30mins
Water flow rate through adsorption beds	8L/min

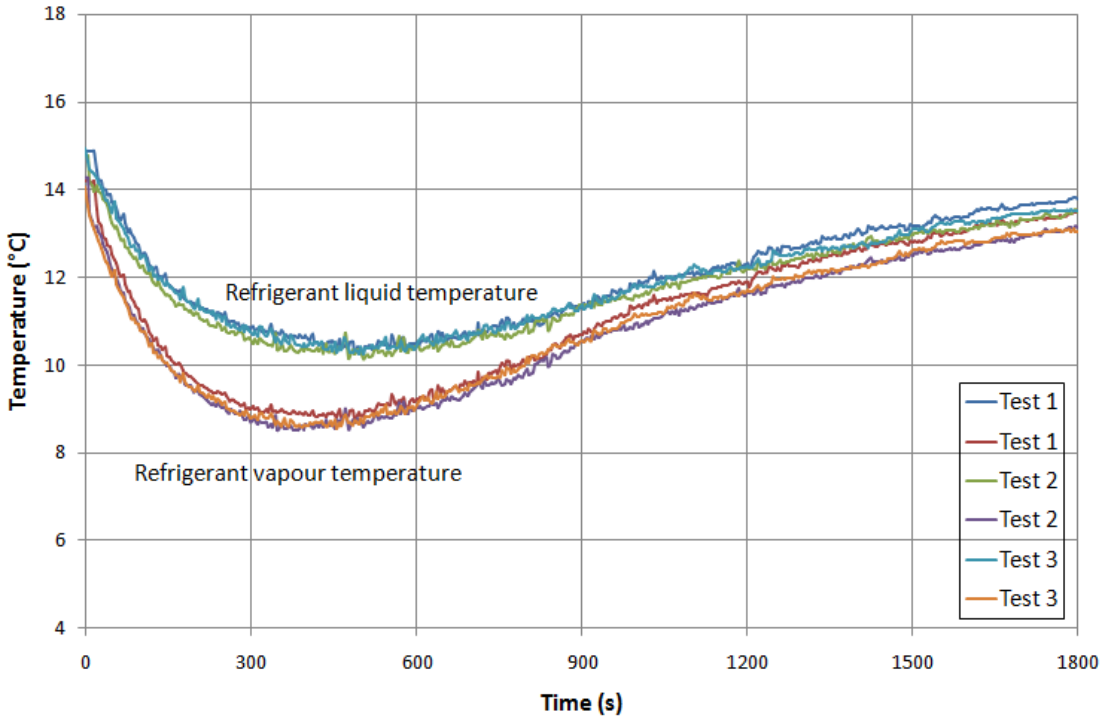

Figure 5-23 Refrigerant liquid and vapour temperature of the evaporator during the adsorption process

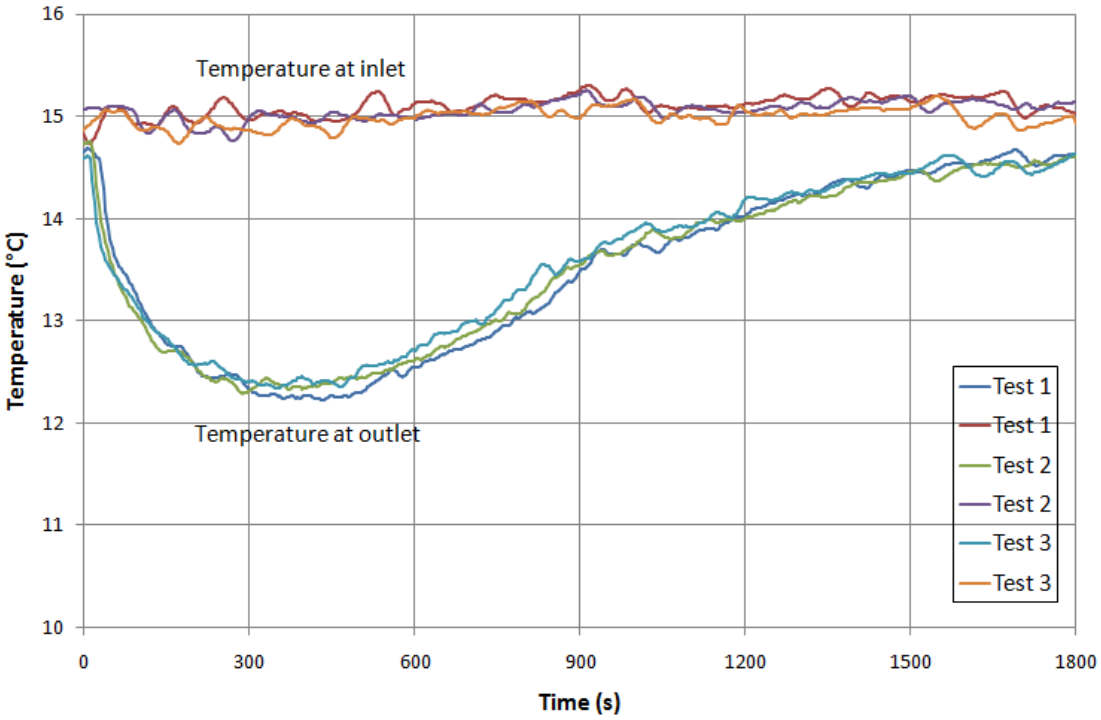

Figure 5-24 Second fluid's water temperature at the inlet and outlet of the evaporator during the adsorption process

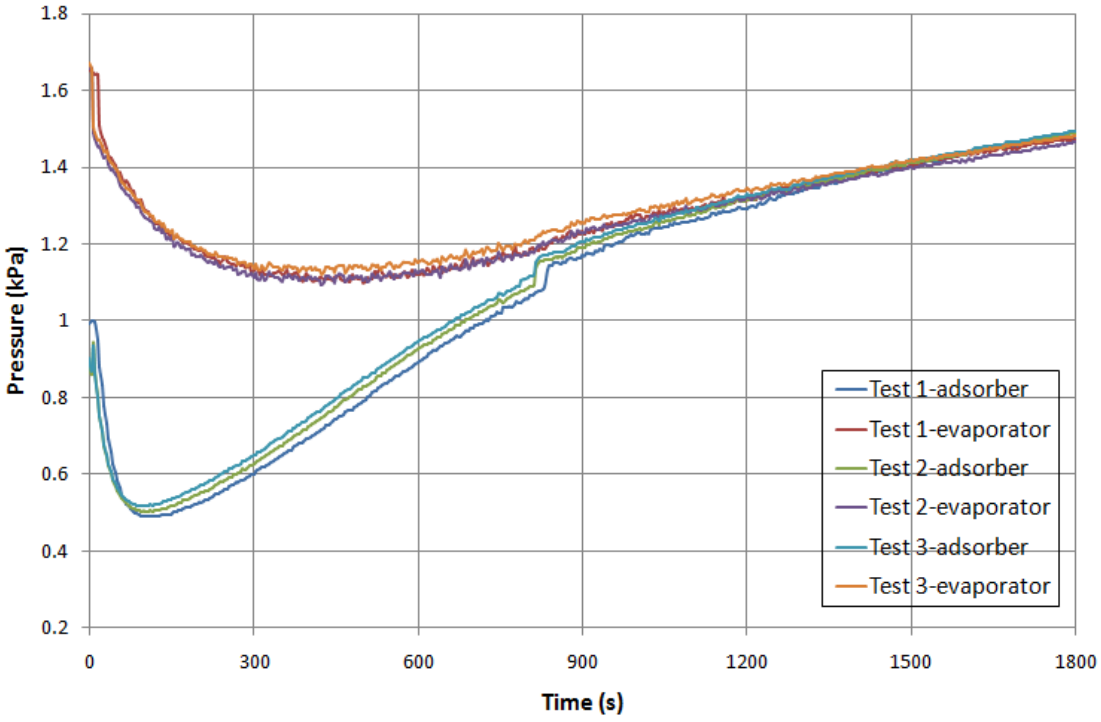

Figure 5-25 Pressure during the adsorption process

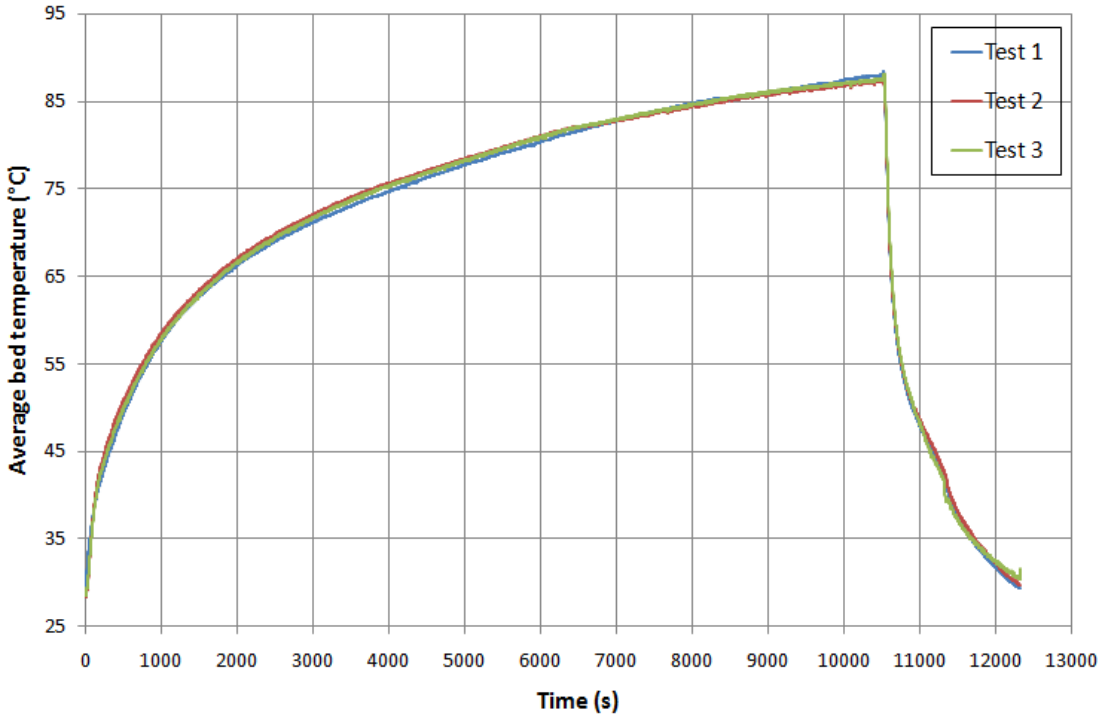

Figure 5-26 Average bed temperature of repeatability test

Table 5-5 shows the average deviations of the measured parameters for the three repeated tests. The results show that the average deviations are all within 1.33%, indicating the consistency of the instruments used.

Table 5-5 Deviations of results for repeatability test

Result parameter	Average deviation
Average bed temperature	0.43%
Evaporator liquid temperature	0.82%
Evaporator vapour temperature	1.15%
Evaporator inlet temperature	0.37%
Evaporator outlet temperature	0.41%
Adsorber pressure	1.33%
Evaporator pressure	0.78%

5.6 Validation of the finite element simulation model

Chapter 4 presented the development of the finite element modelling of the adsorption beds and described all governing equations. In this section, the finite element simulation model is validated using the experimental results.

5.6.1 CPO-27Ni/water working pair

Figures 5-27 to 5-29 compare the finite element predicted water vapour uptake, average bed temperature and cooling water outlet temperature in the adsorption process of the first, second and third cycles to the experimental results of the CPO-27Ni adsorbent; with the same cooling water inlet temperature and flow rate, initial bed temperature and refrigerant vapour pressure in the adsorber. Table 5-6 presents the average percentage deviation (APD, equation 5-3) and absolute average percent deviation ($ABS-PD$, equation 5-4) for water uptake, average bed temperature and cooling water outlet temperature in the adsorption process of all the first, second and third cycles. The results show that the maximum average percentage deviation is 5.5% and maximum absolute average percent deviation is 5.7%. Figures 5-27 to 5-29 and Table 5-6 clearly indicate the good agreement between the finite element model and the experimental results.

$$APD = \frac{1}{N_{data}} \sum_{0}^{N_{data}} \frac{Predicted\ value - experiment\ vale}{experiment\ valur} \times 100 \qquad (5\text{-}3)$$

$$ABS - PD = \frac{1}{N_{data}} \sum_{0}^{N_{data}} \frac{|Predicted\ value - experiment\ vale|}{experiment\ valur} \times 100 \qquad (5\text{-}4)$$

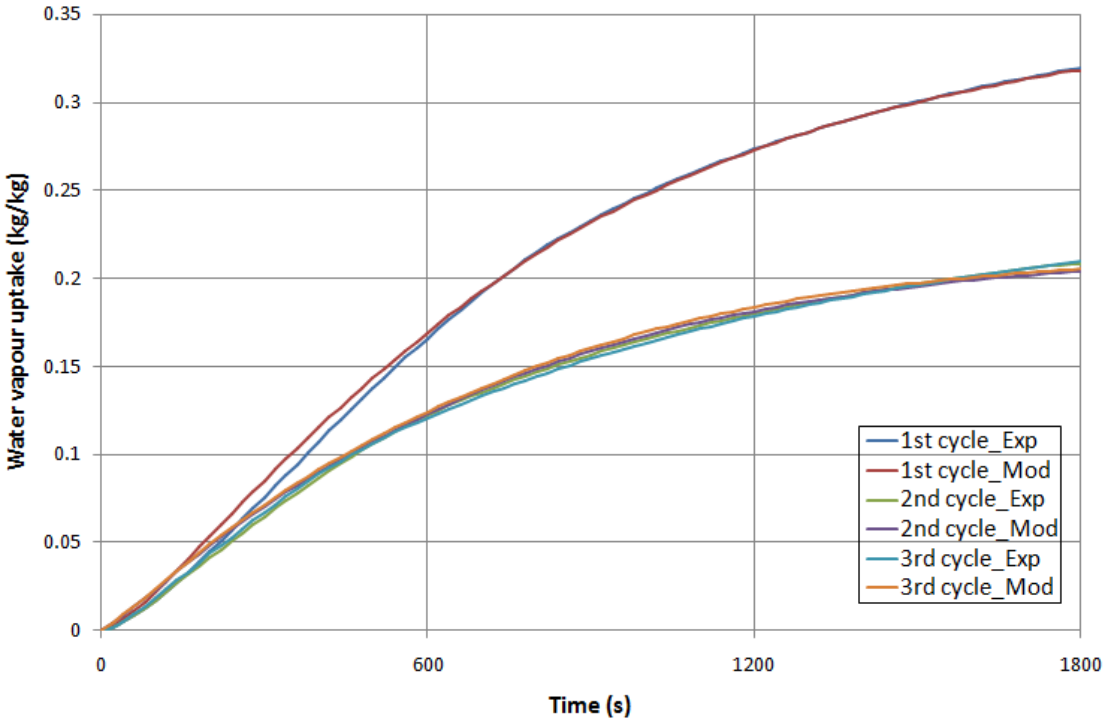

Figure 5-27 Comparison of water vapour uptake between predicted data and actual data for CPO-27Ni/water working pair

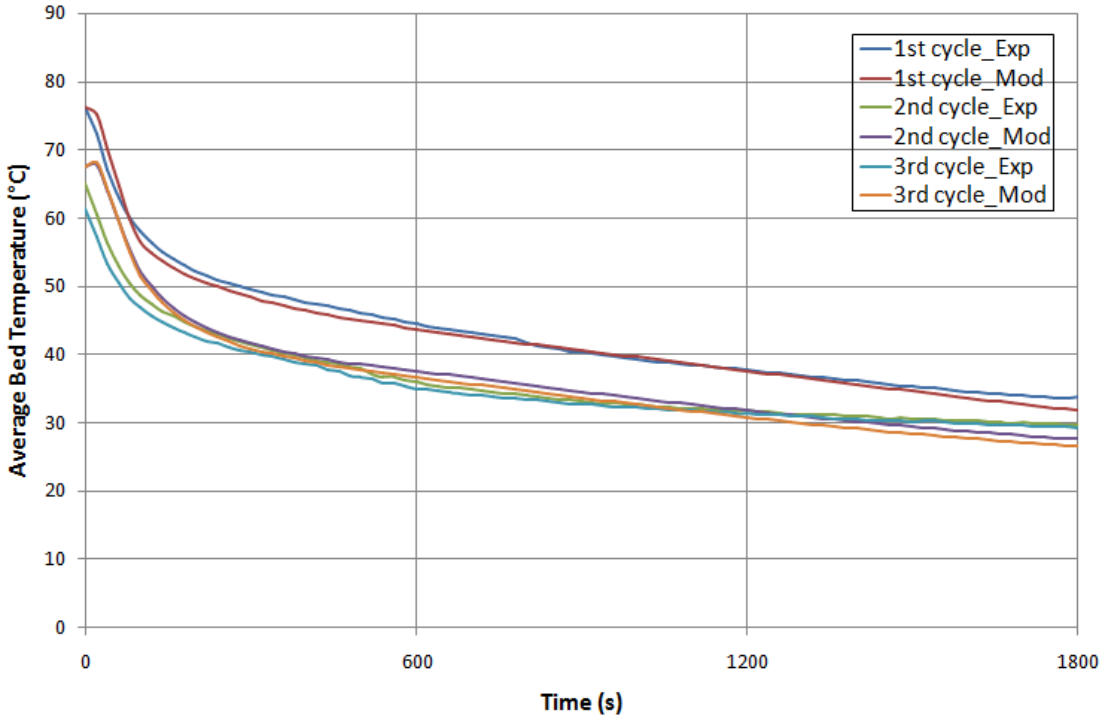

Figure 5-28 Comparison of average bed temperature between predicted data and actual data for CPO-27Ni/water working pair

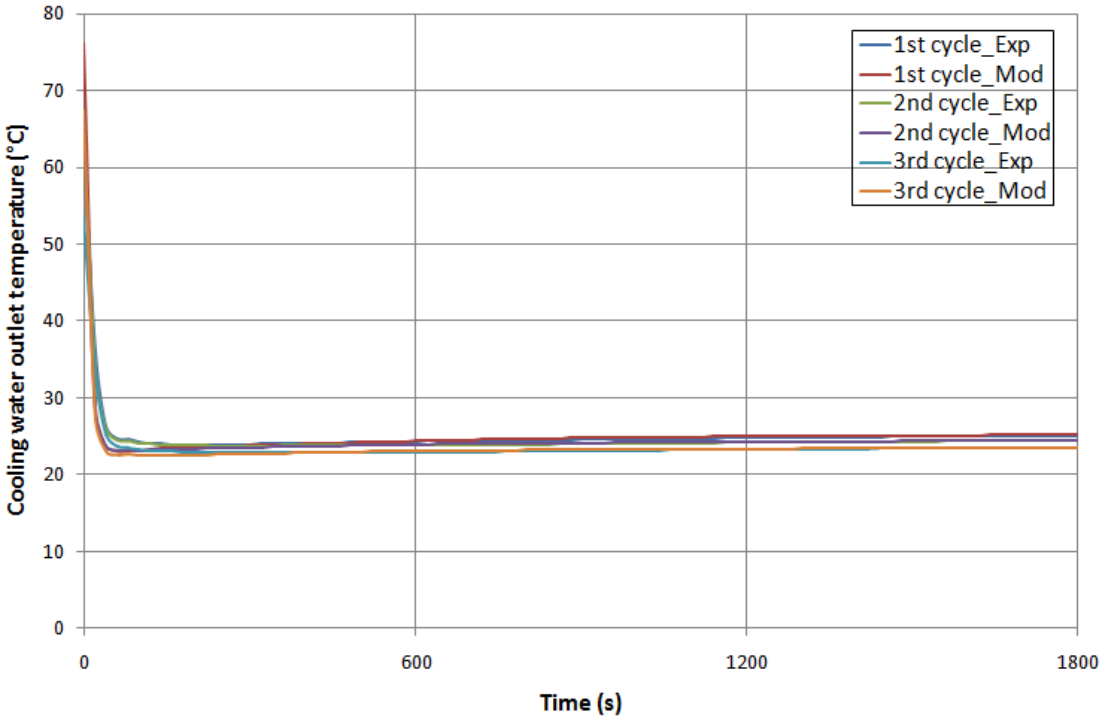

Figure 5-29 Comparison of cooling water outlet temperature between predicted data and actual data for CPO-27Ni/water working pair

Table 5-6 Finite element simulation model deviation analysis of CPO-27Ni/water

Term	First cycle		Second cycle		Third cycle	
	APD	ABS-PD	APD	ABS-PD	APD	ABS-PD
Water vapour uptake	4.6%	4.8%	5%	5.5%	5.5%	5.7%
Average bed temperature	-1.5%	1.8%	0.9%	3.5%	0.3%	4.4%
Cooling water outlet temperature	-0.1%	0.9%	-0.3%	0.8%	-0.1%	0.7%

5.6.2 SAPO-34/water working pair

Figures 5-30 to 5-32 compare the predicted and experimental results for water uptake, average bed temperature and cooling water outlet temperature for an adsorption cooling system using a SAPO-34/water working pair. Table 5-7 gives the values of

APD and $ABS - PD$ and therefore shows the good agreement between the finite element model and the experiments.

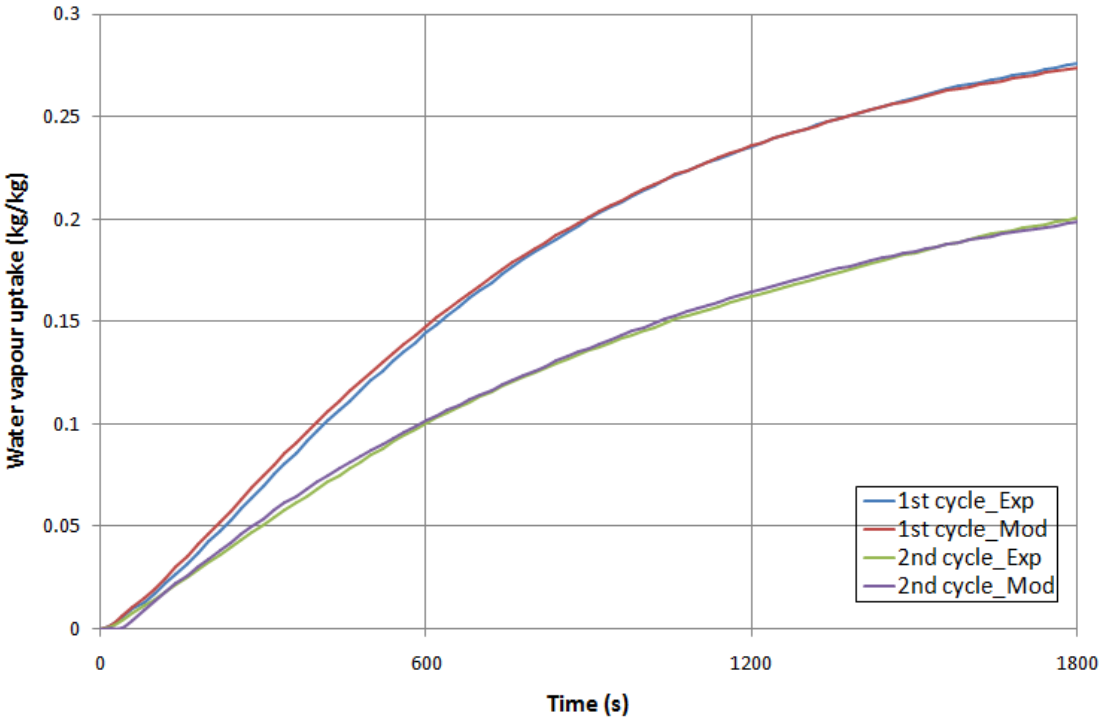

Figure 5-30 Comparison of water vapour uptake between predicted data and actual data for SAPO-34/water working pair

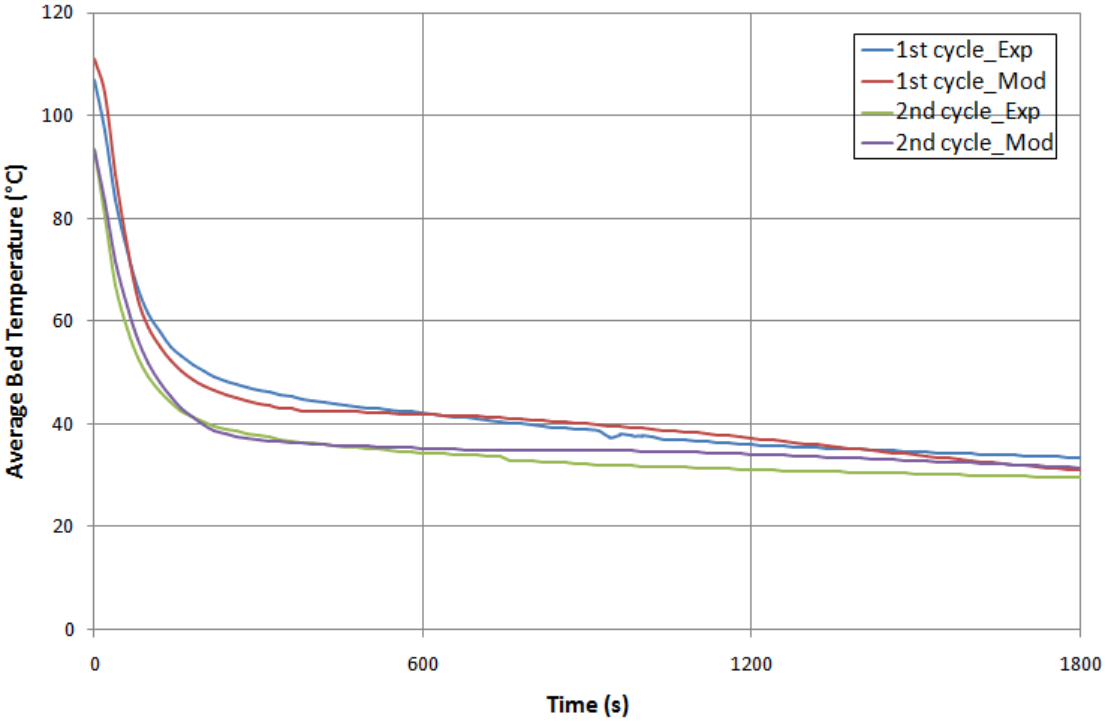

Figure 5-31 Comparison of average bed temperature between predicted data and actual data for SAPO-34/water working pair

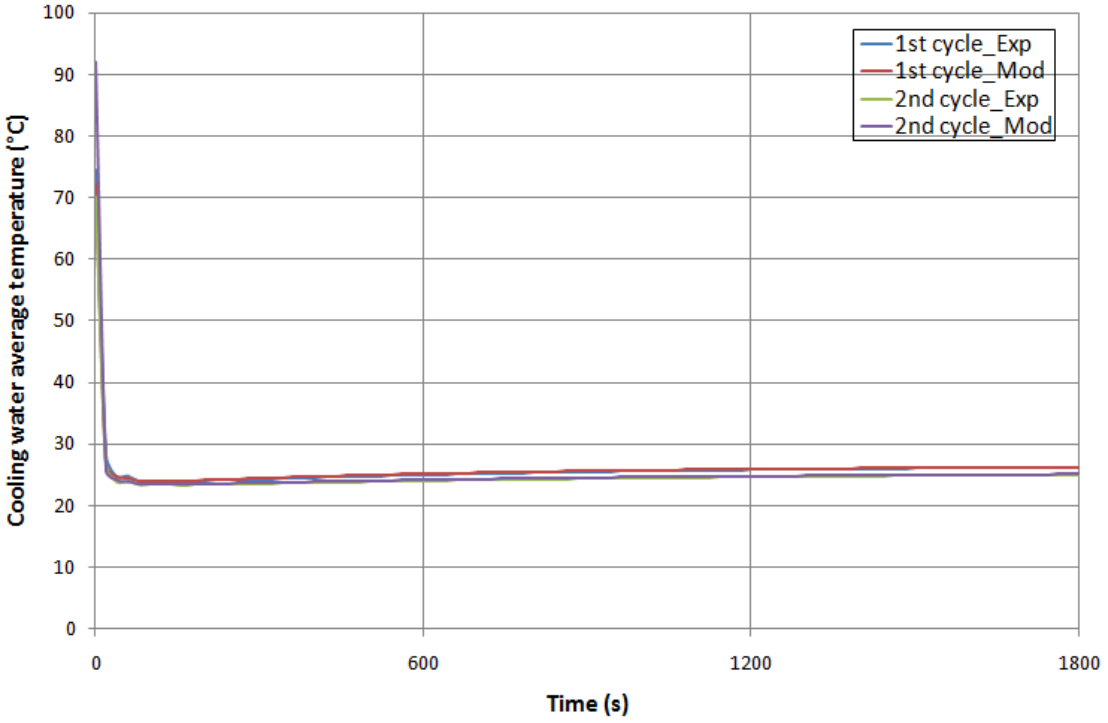

Figure 5-32 Comparison of cooling water outlet temperature between predicted data and actual data for SAPO-34/water working pair

Table 5-7 Finite element simulation model deviation analysis of SAPO-34/water

Term	First cycle		Second cycle	
	APD	ABS-PD	APD	ABS-PD
Water vapour uptake	2.3%	2.6%	-1.3%	4.6%
Average bed temperature	-0.7%	5.5%	5.5%	5.9%
Cooling water outlet temperature	0.4%	0.5%	0.5%	0.5%

5.7 Summary

A test facility built for investigating the performance of an adsorption air-conditioning system was introduced in this chapter. This test facility is flexible as it can be used to test different adsorption beds with different structures and adsorption working pairs. All components of the test facility are described in detail including the adsorber, evaporator/condenser, heater-chiller, heaters and controllers, water pumps, valves, vacuum pumps and measuring instruments. The test facility is based on a one-bed adsorption system. The evaporator and condenser are integrated in one tank and its operating temperature is controlled using the heater-chiller. The test rig's commissioning and test procedure are also explained. The repeatability test of the whole test facility has been conducted and the results show that average deviations of all measured parameters are small enough to prove the consistency of the test facility. Finally, the finite element model with all the equations described in Chapters 3 and 4 was validated using the experimental results.

CHAPTER 6 EFFECT OF OPERATING CONDITIONS ON ADSORPTION COOLING PERFORMANCE

6.1 Introduction

In this chapter, the effects of operating conditions on the performance of an adsorption cooling system packed with CPO-27Ni granules will be experimentally investigated; including heating time in the first cycle and steady operation, cooling water flow rate, adsorption time, desorption time and evaporation and condensation temperature. The operating conditions affect the adsorption cooling system's performance; therefore they can be optimised to obtain the maximum performance. Heating time in the first cycle is one of the operating parameters that affects the adsorption cooling system's performance, especially in the first cycle. The flow rate of the cooling water also affects the performance, as it controls the heat transfer rate from the adsorber [4, 31, 34, 35, 50, 113, 155]. The time required for the adsorption and desorption processes has an effect on the adsorption air-conditioning system's performance [37, 86, 143, 156-158] as well. Furthermore, evaporation and condensation temperatures affect the cooling capacity and efficiency of the adsorption cooling system [29, 36, 142]. Therefore, investigation of the operating conditions' effect on the performance of the adsorption refrigeration system is important to improve the cooling capacity of the system and determine the optimum operating conditions.

The experiment with the operating conditions shown in Table 6-1 is used as the baseline for comparison.

Table 6-1 Reference operating conditions

Operating condition	Value
Heater set temperature	250 ℃
Regeneration time	3h
Evaporation temperature	15 ℃
Condensation temperature	15 ℃
Adsorption time	1800s
Desorption time	3600s
Water flow rate through adsorption beds	8L/min

To compare the performance of the adsorption beds, two parameters are used as criteria. The first parameter is the specific cooling capacity (SCP) defined as the cooling capacity per unit mass of adsorbent material, equation 6-1. The second parameter is the coefficient of performance (COP) defined as the ratio of cooling capacity to the rate of heat used, equation 6-2. All calculations in this research exclude the consideration of dynamic losses for the casing to the ambience which is difficult to be defined and usually has a small proportion to the total amount of heat consumed.

$$SCP = \frac{\int_0^{t_{cycle}} \dot{m}_{chw} Cp_{chw} \left(T_{chw,in} - T_{chw,out} \right) dt}{t_{cycle}} \cdot \frac{1}{m_{ads}} \tag{6-1}$$

$$COP = \frac{\int_0^{t_{cycle}} \dot{m}_{chw} Cp_{chw} \left(T_{chw,in} - T_{chw,out} \right) dt}{t_{cycle}} \cdot \frac{1}{Q_{heat}} \tag{6-2}$$

Where $\dot{m}_{chw}$, Cp_{chw}, $T_{chw,in}$ and $T_{chw,out}$ are flow rate, heat capacity and temperatures at the inlet and outlet of the chilled water, respectively; m_{ads} is the mass of adsorbents and Q_{heat} is the rate of heat input during one cycle time.

6.2 Effect of heating time in the first cycle and steady operation

The heating time in the first cycle is different from the desorption time in the following cycles. During the heating process in the first cycle, the adsorber is isolated from the condenser and the water vapour desorbed from the adsorbent material will be sucked out by vacuum pumps. While in the following desorption process, the adsorber is connected to the condenser and isolated from the vacuum pumps thus the water vapour desorbed will be condensed in the condenser. Therefore the heating time in the first cycle and the desorption time in following cycles are different. Figure 6-1 compares the water uptake variation with time, of the first cycle with 1h, 3h and 5h heating times. As heating time increases the water vapour uptake increases by up to 61.9%. However, the rate of increase of water uptake decreases with the increase of heating time. Increasing the heating time from 1 hour to 3 hours increased the water uptake by 0.11; while increasing the heating time from 3 hours to 5 hours increased the uptake by only 0.01. On the other hand, the refrigerant vapour pressures in the adsorber after the heating process are 21.6mbar, 9.4mbar and 4.5mbar with heating times of 1h, 3h and 5h respectively; which shows that the adsorbent granules are dryer with a longer heating time.

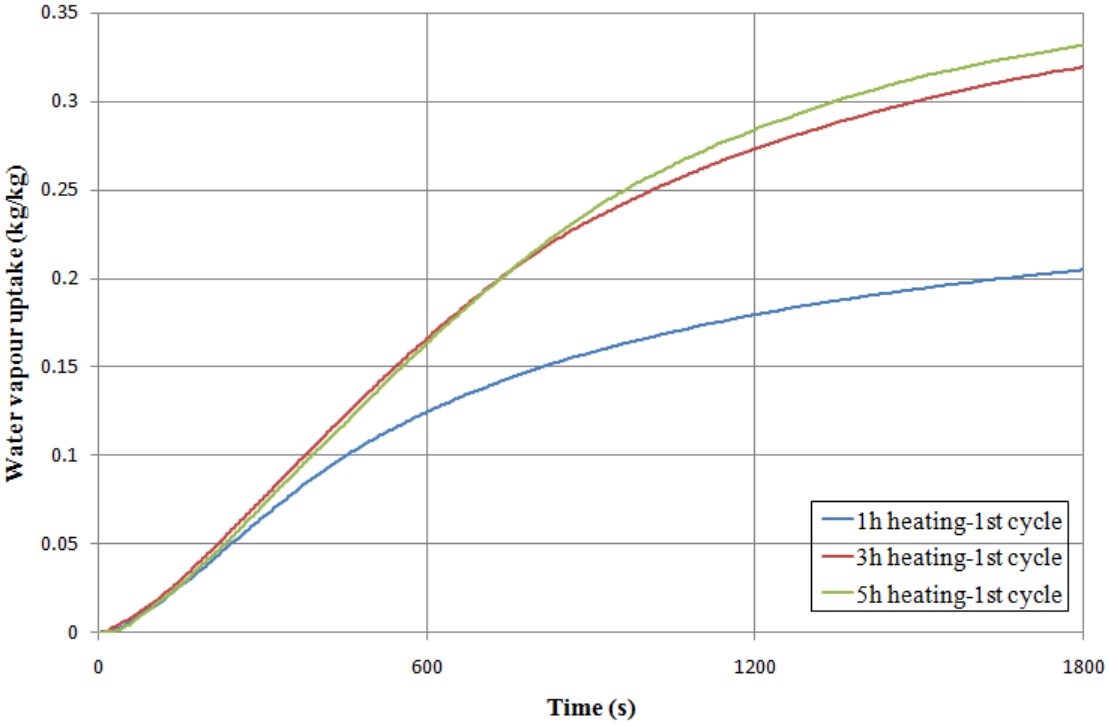

Figure 6-1 Comparison of water vapour uptake of the first cycle for 1h, 3h and 5h heating time for dry adsorbent preparation using CPO-27Ni

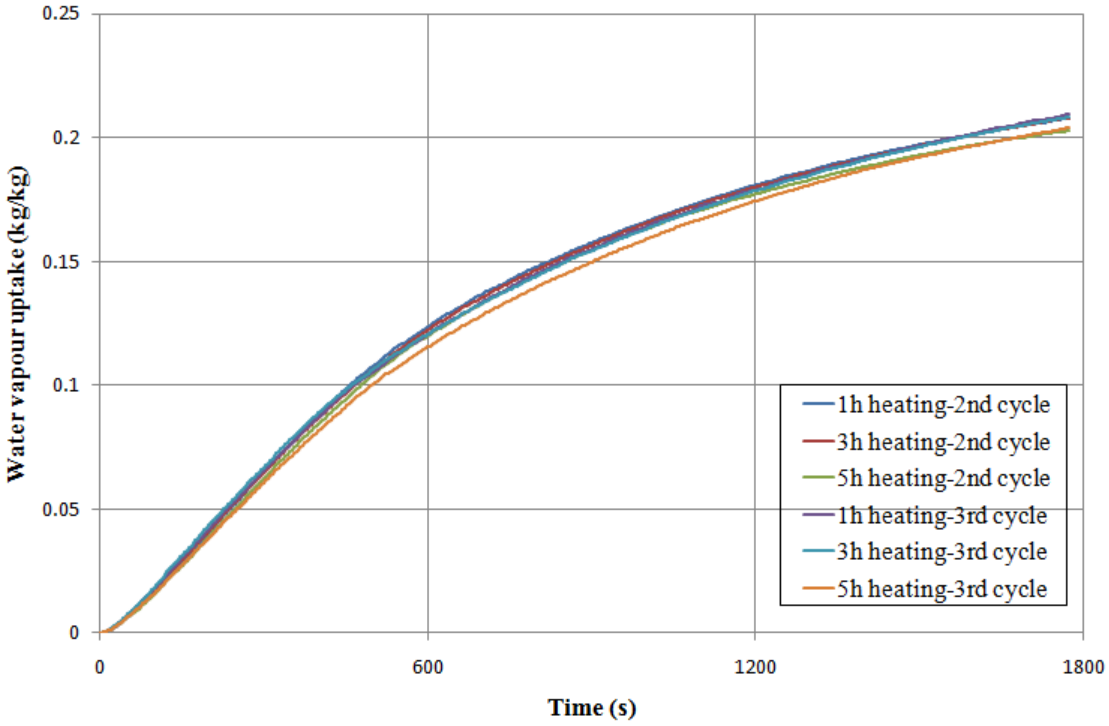

Figure 6-2 Comparison of water vapour uptake of second and third cycles for 1h, 3h and 5h heating time for dry adsorbent preparation using CPO-27Ni

Figure 6-2 compares the water vapour uptake of the second and third cycles for 1h, 3h and 5h heating time at the start of the experiments. There is no significant difference among the different groups. It can be concluded that different heating times of the adsorbent preparation only affects the performance of the adsorption bed in the first cycle and has no effect on the following cycles.

Figure 6-3 compares the average bed temperature variation with heating time used in the first cycle adsorption process. The results show that the average bed temperature with 1 hour heating time is much lower than that of 3 hours and 5 hours heating time in the adsorption process of the first cycle and the desorption process of the second cycle; this is due to the small amount of refrigerant adsorbed and the associated adsorption heat produced during the adsorption process. However, there is no significant difference between the average bed temperature with 3 hours and 5 hours of heating time. Also as concluded from Figure 6-2, Figure 6-3 shows that the average bed temperature during the 3rd cycle is not affected by the heating time used in the first cycle.

Figures 6-2 and 6-3 also indicate that there is no difference of water vapour uptake and average bed temperature between the second cycle and third cycle in all experiments. Therefore, it can be concluded that the adsorption cooling system in the test facility becomes stable from the second cycle. Therefore, only the performance of the first adsorption cycle and second adsorption cycle are investigated in the following sections.

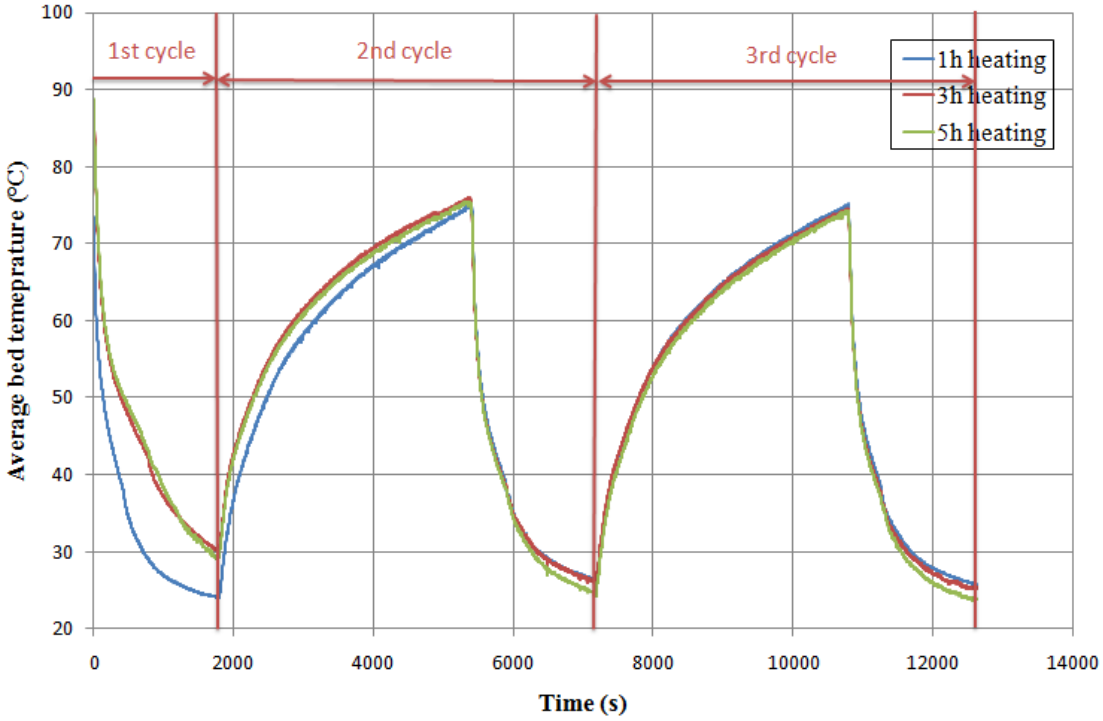

Figure 6-3 Comparison of average bed temperature for 1h, 3h and 5h heating time for dry adsorption preparation using CPO-27Ni

6.3 Effect of cooling water flow rate

Cooling water flow rate significantly affects the adsorption cooling system's performance. Increasing the cooling water flow rate increases the heat transfer between the adsorption beds and the cooling water; thus increasing the adsorption rate. Therefore, the refrigerant water uptake is increased in the adsorber and the cooling capacity is enhanced.

This section experimentally investigated the effect of the adsorber bed's cooling water flow rate variation from 8L/min to 14L/min on the performance of the adsorption cooling system using CPO-27Ni adsorbent with 3h of heating in the first cycle. Figure 6-4 compares the water vapour uptake with experiments of 8L/min, 11L/min and

14L/min cooling water flow rate respectively. It shows that water vapour uptake increases by up to 3.2% with the increase of the cooling water flow rate in both the first and second cycles. However, when the cooling water flow rate is higher than 11L/min, the effect of its variation on the adsorption cooling system's performance is very small, less than 0.6%. The measuring error of water flow rate and the water vapour uptake are 7.1%-12.5% and 5.2%-10.1% respectively as explained in the sections 5.2.8.3 and 5.4.

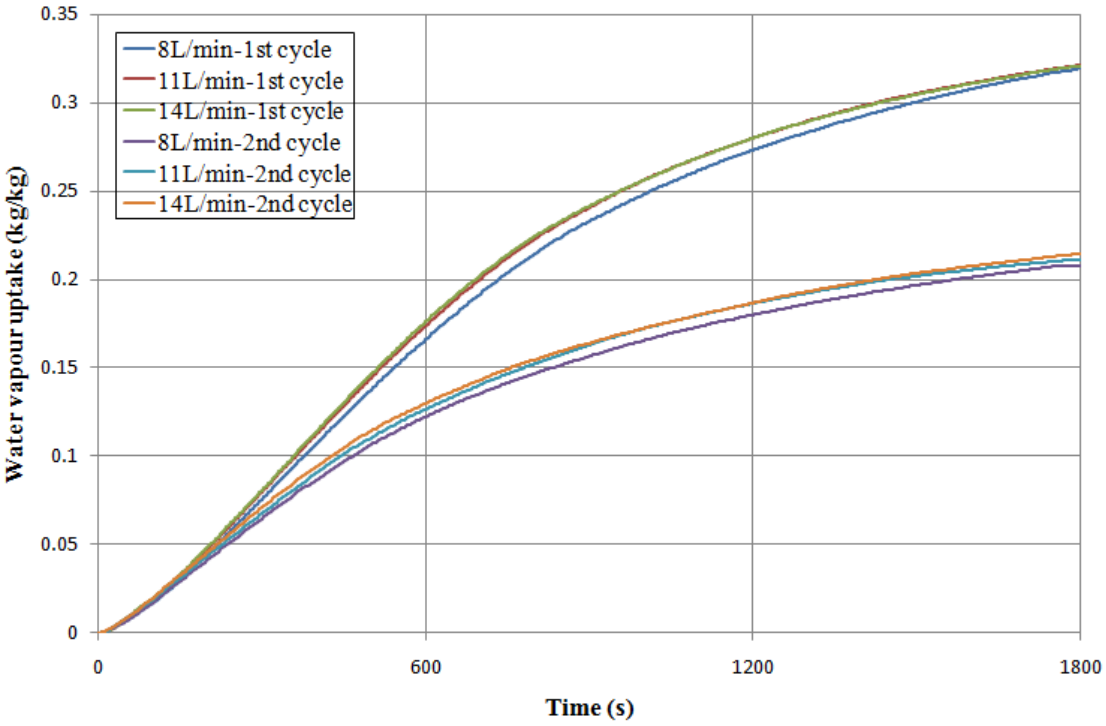

Figure 6-4 Comparison of water vapour uptake for 8L/min, 11L/min and 14L/min cooling water flow rate using CPO-27Ni

Figure 6-5 compares the average bed temperature using 8L/min, 11L/min and 14L/min adsorbent bed cooling water flow rate. It can be seen that average bed temperature decreases with increasing the cooling water flow rate, due to the higher heat transfer coefficient produced by the increase in the cooling water flow rate. The

bed temperature is relatively high after the desorption process and adsorption heat is produced in the adsorption process. A high bed temperature slows down the rate of the adsorption process. Therefore, when cooling water flow rate increases more heat is taken by the cooling water and the average bed temperature decreases; which results in increasing the water vapour uptake thus producing a higher cooling effect.

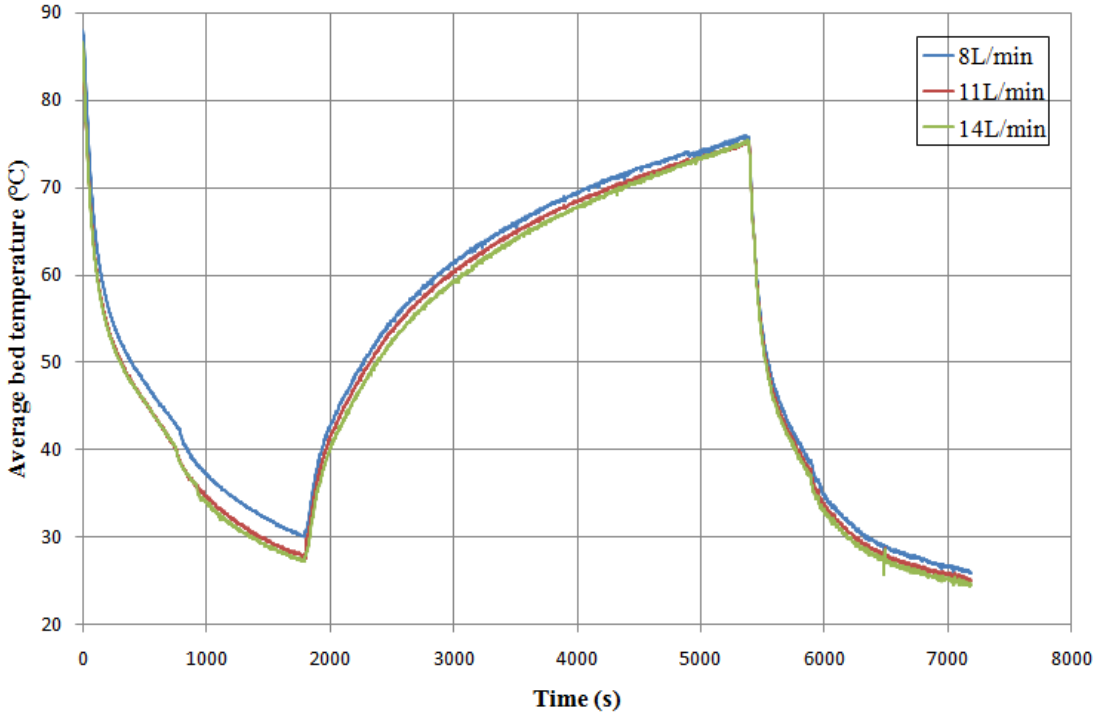

Figure 6-5 Comparison of average bed temperature for 8L/min, 11L/min and 14L/min cooling water flow rate using CPO-27Ni

Table 6-2 shows all SCP and COP values for both the first and second cycles at the three flow rates tested. The SCP of the second cycle is higher than that of the first cycle due to its shorter cycle time. The SCP slightly increased by up to 3.2% with the increase of the cooling water flow rate. However, the COP did not change with variation of cooling water flow rate. In the first cycle, the COP is lower than that of the second cycle because of its longer heating time and larger energy input.

Table 6-2 SCP and COP values for variation of cooling water flow rate

Cycle	8L/min		11L/min		14L/min	
	SCP (W/kg)	COP	SCP (W/kg)	COP	SCP (W/kg)	COP
1st	67.1	0.09	67.4	0.09	67.5	0.09
2nd	101.9	0.26	103.6	0.26	105.2	0.26

6.4 Effect of adsorption time

During the adsorption process, adsorbent granules adsorb the refrigerant vapour from the evaporator to develop a cooling effect through the evaporation process. In the adsorption process, heat is generated which should be removed together with the heat input during the desorption process by cooling water, to sustain the adsorption process and obtain a cooling effect. However, during the adsorption period the rate of adsorption decreases with the increasing amount of refrigerant vapour adsorbed by the adsorption bed, until the adsorbents become saturated with refrigerant. Therefore, the cooling effect produced decreases with time.

This section experimentally investigated the effect of the adsorption time on the performance of the adsorption bed fitted in the test facility presented in Chapter 5. The experiments were conducted with adsorption times of 600s, 1800s and 3000s respectively, with the same heating time used for desorption of 3600s. Figure 6-6 compares the water uptake in both the first and second cycles. It clearly shows that with the increase of adsorption time the water uptake increased from 0.167 to 0.374 for the first cycle and from 0.128 to 0.239 for the second cycle. Also, the results show that the rate of adsorption decreases with time of the adsorption process. In the first cycle, the water uptake increased by 92% with adsorption time increasing from 600s

to 1800s; while it increased by only 17% when adsorption time increased from 1800s to 3000s. In the second cycle, these values are 63% and 15% respectively.

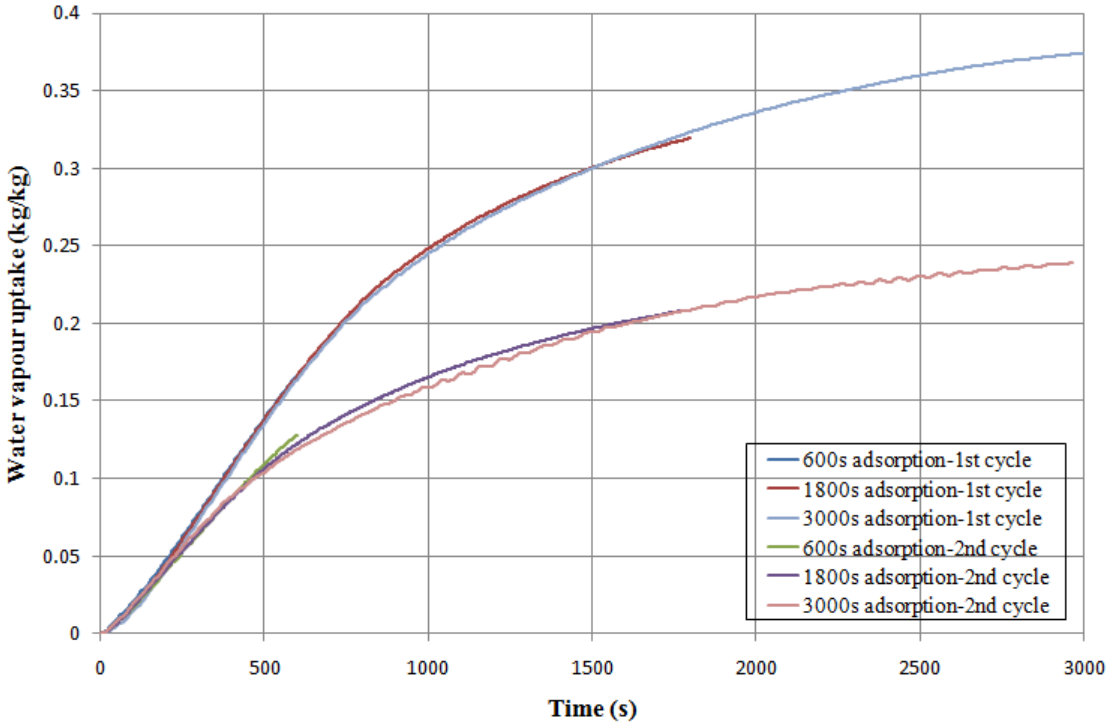

Figure 6-6 Comparison of water vapour uptake for 600s, 1800s and 3000s adsorption time using CPO-27Ni

The adsorption process is much slower than that of measurement by DVS analyser shown in Figure 3-3. It is mainly due to following two reasons. The first one is that in the desorption process, the adsorbent material is heated to 150 ℃ during the DVS test process. Thus after the desorption process the adsorbent material is totally dry and has a very large adsorption capacity in the following adsorption process which makes the adsorption process very quick. While in the experiment using the lab-scale test facility described in Chapter 5, the adsorbent granules are only heated up to around 100 ℃ by 3 hours which is not enough to make adsorbent totally dry. Therefore, at the beginning of adsorption process, the adsorption capacity of adsorbent material is

lower than that of during the DVS test which makes the adsorption process much slower. The second reason is that the adsorption beds packed 676g CPO-27Ni granules in the experimental test facility while the DVS analyser only conducts the measurement with 10mg CPO-27Ni granules. The large amount adsorbent granules packed reduces the heat and mass transfer performance of the adsorption beds dramatically and thus decreases the adsorption kinetics. Due to these two reasons, the adsorption rate shown in Figure 6-6 is not as large as that of the measurement results of DVS test.

Figure 6-7 compares the average bed temperature with an adsorption time of 600s, 1800s and 3000s. With longer adsorption time, the adsorption bed can reach a lower temperature after the adsorption process, leading to a larger refrigerant uptake and cooling effect.

Table 6-3 shows the SCP and COP values due to the variation of adsorption time for the CPO-27Ni adsorption system. For the first cycle SCP increased with a longer adsorption process due to the increase in the amount of refrigerant adsorbed. In the second cycle, SCP also increased with an adsorption time increase from 600s to 1800s. However, it decreased with an adsorption time increase from 1800s to 3000s, due to the small increase in the refrigerant uptake. Therefore, with longer time the specific cooling power decreases. On the other hand, a long adsorption process can increase COP by enhancing the cooling capacity with the same energy input.

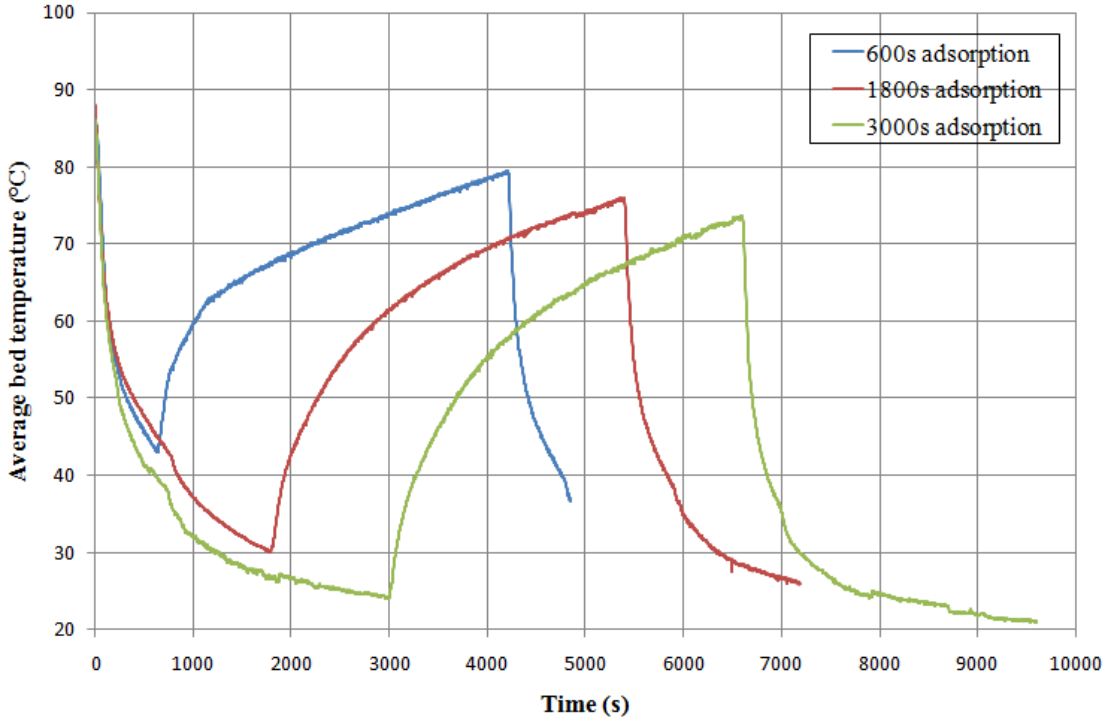

Figure 6-7 Comparison of average bed temperature for 600s, 1800s and 3000s adsorption time using CPO-27Ni

Table 6-3 SCP and COP values for a variation of adsorption times

Cycle	600s		1800s		3000s	
	SCP (W/kg)	COP	SCP (W/kg)	COP	SCP (W/kg)	COP
1st	38.6	0.05	67.1	0.09	71.8	0.1
2nd	80.6	0.16	101.9	0.26	95.9	0.3

6.5 Effect of desorption time

During the desorption process, the adsorption bed is heated to desorb the refrigerant vapour which is then condensed in the condenser to repeat the cycle. As the desorption time increases, more refrigerant is released from the adsorbent material; thus increasing the adsorption bed's capacity to adsorb refrigerant in the adsorption process and obtain higher cooling effect. This section experimentally investigates the effect of the desorption time ranging from 1800s to 5400s on the performance of the

adsorption bed fitted in the test facility, with the same heating time in the first cycle of 3h and the same adsorption time of 1800s. Figures 6-8 and 6-9 present the variation of water vapour uptake and average bed temperature in both the first and second cycles with time at different desorption times. The performance in the first cycle is the same because of the same operating conditions. In the second cycle, the water vapour uptake increased by up to 75.8% with the increase in the desorption time; due to dryer adsorbents in the adsorption beds. Figure 6-9 also shows that the average bed temperatures are higher at the end of the desorption process with a longer desorption time, which results in more refrigerant being desorbed. The adsorber pressure reached 1.98kPa, 1.89kPa and 1.83kPa with the increase of desorption time to 1800s, 3600s and 5400s, respectively; thus a lower amount of rerigerant remained in the adsorption bed. This is due to the refrigerant desorption rate in the adsorber being higher than the refrigerant condensation rate in the condenser at the beginning of the desorption process and becoming lower as time progresses.

Table 6-4 shows the values of the SCP and COP with variations of desorption time. In the second cycle, the SCP increased by 5.3% with the increasing of the desorption time from 1800s to 3600s, but decreased by 16.5% with the increasing of the desorption time from 3600s to 5400s. This is due to the increase in water vapour uptake, when desorption time increased from 1800s to 3600s being larger than that obtained with increasing the desorption time from 3600s to 5400s. Therefore, the SCP for a desorption time of 5400s became smaller than that with 3600s desorption; this was mainly due to the longer cycle time. However, the second cycle COP increased with the decreasing of the desorption time because of the decrease in the amount of heat input.

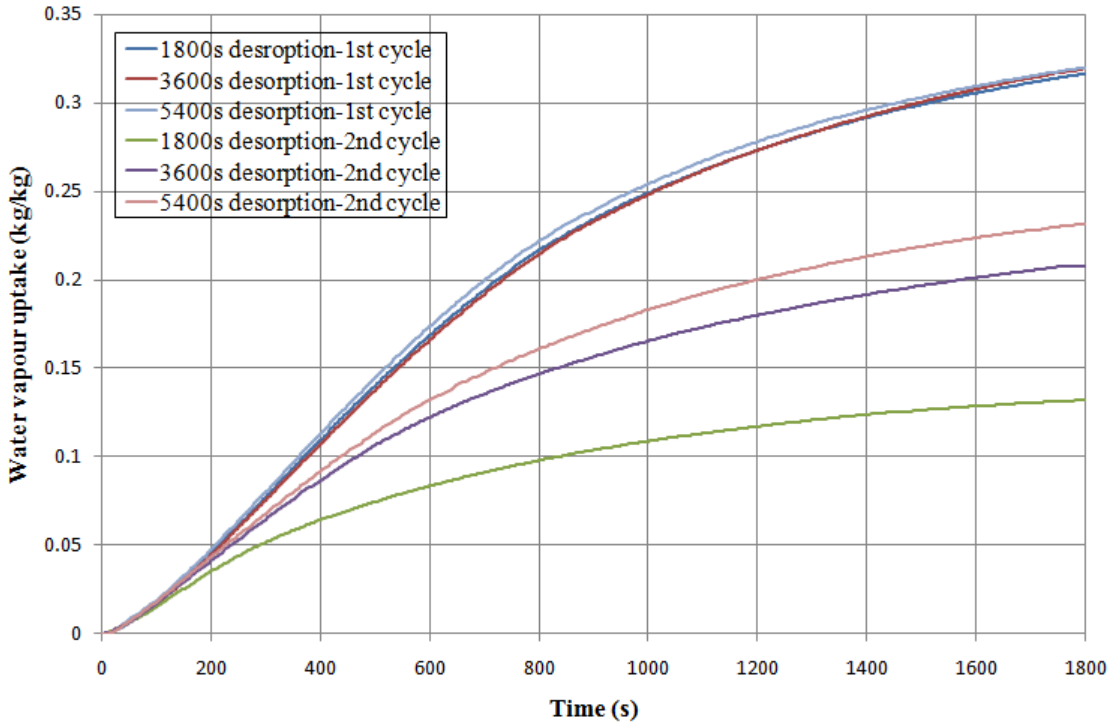

Figure 6-8 Comparison of water vapour uptake for 1800s, 3600s and 5400s desorption time using CPO-27Ni

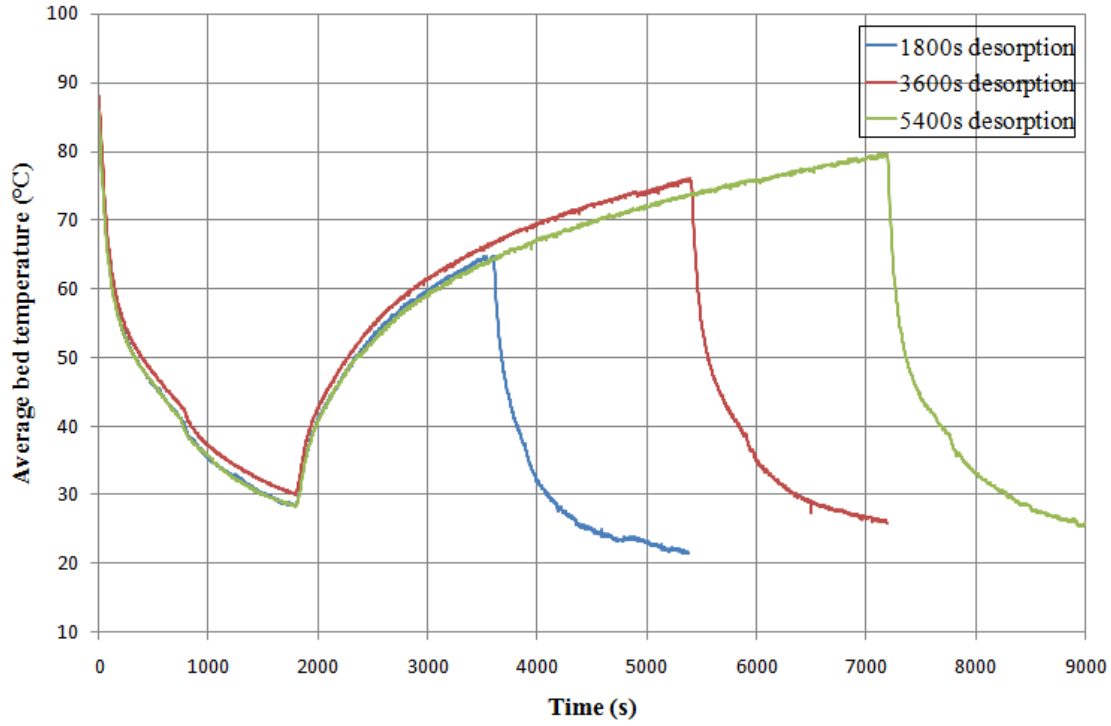

Figure 6-9 Comparison of average bed temperature for 1800s, 3600s and 5400s desorption time using CPO-27Ni

Table 6-4 SCP and COP values for a variation of desorption times

Cycle	1800s		3600s		5400s	
	SCP (W/kg)	COP	SCP (W/kg)	COP	SCP (W/kg)	COP
1st	67.1	0.09	67.1	0.09	67.1	0.09
2nd	96.8	0.31	101.9	0.26	85.1	0.22

6.6 Effect of evaporation and condensation temperature

Evaporation and condensation temperature affects the adsorption cooling system's performance. During the adsorption process, increasing evaporation temperature can increase the mass transfer performance of the adsorption bed and thus increase the refrigerant uptake rate [4, 35, 36, 52, 155]. On the other hand, decreasing the condensation temperature can help condensing the refrigerant vapour which is desorbed from the adsorption bed. In this way, adsorbents desorb more refrigerant in the desorption process and obtain a larger capacity to adsorb refrigerant in the adsorption process leading to a higher cooling effect [29, 142].

This section experimentally investigates the effect of the evaporation and condensation temperature on the performance of the adsorption cooling system. Since there was only one tank used as both the evaporator and condenser in the test facility, experiments were conducted with the same evaporation and condensation temperature in each test. Figures 6-10 and 6-11 compare the variation of water vapour uptake and average bed temperature respectively with time while both evaporation and condensation temperatures varying from 15 ℃, 20 ℃ and 25 ℃. In the first cycle, the water vapour uptake increased by up to 8.2% by increasing the evaporation temperature from 15 ℃ to 25 ℃ with the heating time held constant. Thus the

adsorption cooling system can achieve a larger cooling capacity with a higher evaporation temperature. However, in the second cycle increasing both evaporation and condensation temperatures resulted in decreasing the water uptake by up to 18.4%. These results show that the performance of the adsorption bed is more sensitive to the variation of condensation temperature. It can be concluded that the variation of condensation temperature has a larger effect on the adsorption cooling system's performance than the variation of evaporation temperature; similar conclusion was also made by [29]. Therefore, optimising condensation temperature is important to enhance the adsorption cooling system's performance. To obtain a larger cooling power, a lower condensation temperature is needed.

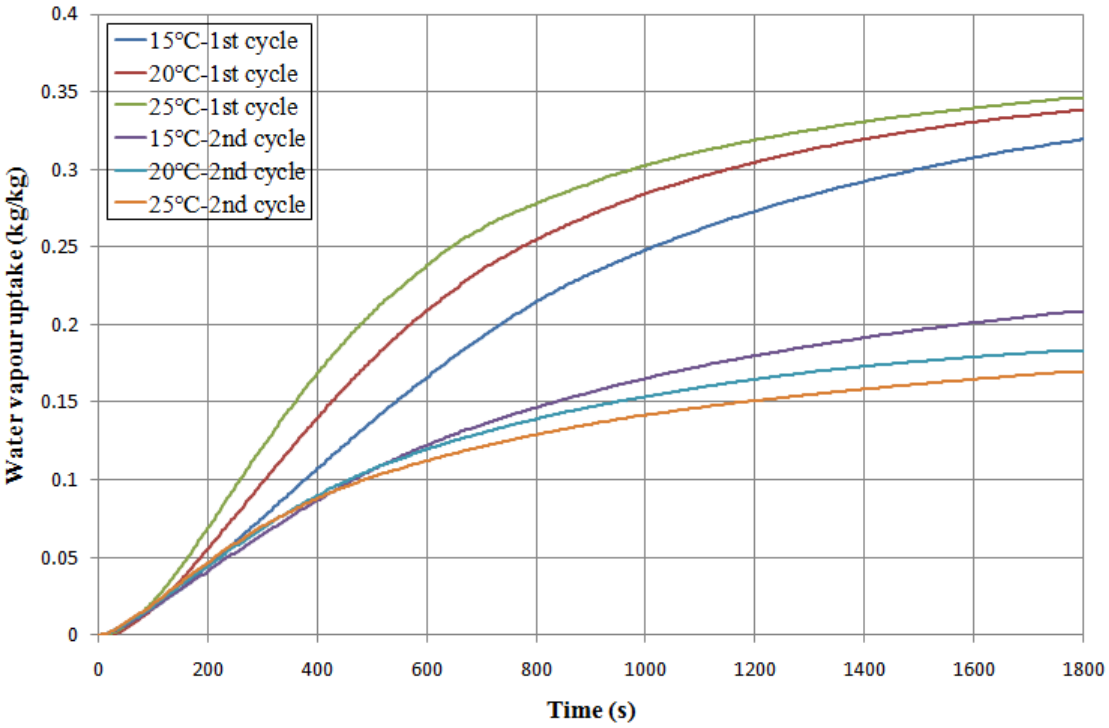

Figure 6-10 Comparison of water vapour uptake for 15 ℃, 20 ℃ and 25 ℃ for both evaporation and condensation temperature using CPO-27Ni

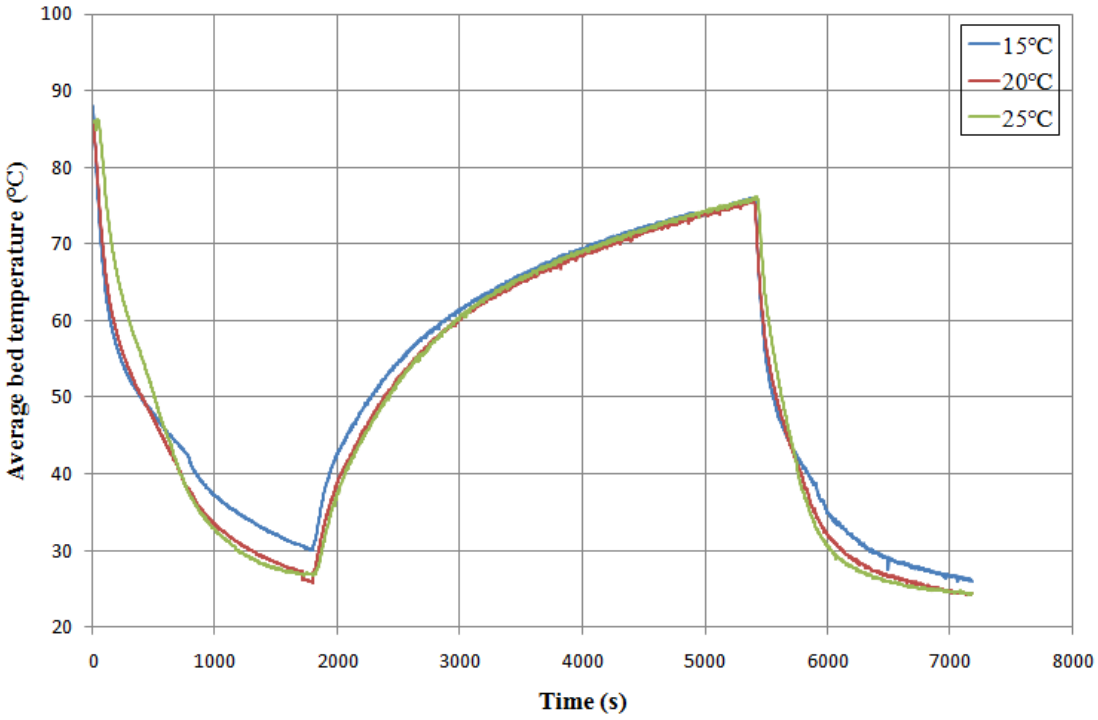

Figure 6-11 Comparison of average bed temperature for 15 ℃, 20 ℃ and 25 ℃ for both evaporation and condensation temperature using CPO-27Ni

Table 6-5 presents the SCP and COP values with a variation of evaporation and condensation temperature. During the first cycle, the SCP and COP increased by 8.2% and 11.1% respectively with the increasing of the evaporation/condensation temperature, due to the increase of the water vapour uptake and cooling capacity. Conversely, in the second cycle the values of the SCP and COP decreased by 18.4% and 19.2% with the increase of both the evaporation and condensation temperature, resulting from the decrease of water vapour uptake.

Table 6-5 SCP and COP values for a variation of evaporation and condensation temperatures

Cycle	15 ℃		20 ℃		25 ℃	
	SCP (W/kg)	COP	SCP (W/kg)	COP	SCP (W/kg)	COP
1st	67.1	0.09	71	0.09	72.6	0.1
2nd	101.9	0.26	89.7	0.23	83.1	0.21

6.7 Summary

The effects of various operating conditions have been experimentally investigated using the test facility introduced in Chapter 5 with an adsorber bed packed with CPO-27Ni granules; including heating time in the first cycle and steady operation; cooling water flow rate; adsorption time; desorption time and evaporation and condensation temperatures.

It has been concluded that the increasing of the adsorbent heating time in the first cycle can improve the cooling capacity of the first cycle but has no effect on the performance of the following cycles. The water uptake performance can be enhanced as the cooling water flow rate increases before it reaches 11L/min and after that, the effect of the cooling water flow rate becomes negligible. It is observed that water vapour uptake is higher with longer adsorption and desorption time. However, the specific cooling power of the adsorption cooling system increased gradually and subsequently reduced with the increasing of the adsorption time or desorption time. Raising evaporation temperature and reducing condensation temperature can increase the refrigerant uptake. However, the control of the condensation temperature is more important than that of the evaporation temperature.

CHAPTER 7 PERFORMANCE OF A TWO-BED SYSTEM FOR AUTOMOTIVE APPLICATION

7.1 Introduction

This chapter investigates the performance of an adsorption air-conditioning system for automotive application with a two-bed refrigeration cycle; using the same bed design described in section 5.2.1 packed with CPO-27Ni as the adsorbent material. In Chapter 6 an experimental investigation on the effect of operating conditions on the performance of an adsorption cooling system, based on CPO-27Ni MOF adsorbent material packed in the adsorber of the test facility, which was described in Chapter 5, was presented. The test facility was constructed based on a single bed refrigeration cycle, containing only one adsorber and one heat exchanger used as both an evaporator and condenser. However, the single bed cycle cannot provide a continuous cooling effect because the adsorber can only work on either the adsorption process or desorption process at any one time. An adsorption air-conditioning system for automotive application should provide a continuous cooling effect in the car cabin, which means that a refrigeration cycle with two or more adsorption beds is needed. Based on the literature review of adsorption cooling systems for automotive application presented in section 2.10, two-bed refrigeration cycles are mostly utilised by researchers to obtain good performance while maintaining as low as possible overall weight.

This system includes two adsorbers, one evaporator and one condenser as shown in Figure 7-1. As for the investigation method, the lumped-parameter mathematical simulation technique described in section 2.10.2.1 was chosen in this work due to its simplicity and high level of accuracy. The development of a lumped-parameter mathematical model using MATLAB Simulink software for the whole automotive adsorption air-conditioning system is presented in the following sections. To simplify the mathematical model and save computational time, the temperature is assumed to be uniform along the adsorption bed, evaporator and condenser.

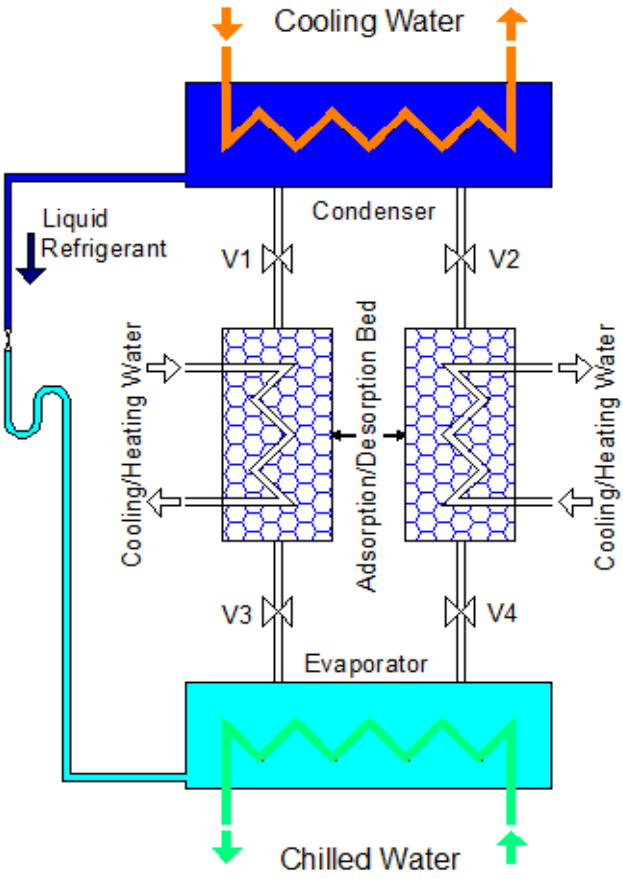

Figure 7-1 Adsorption air conditioning system investigated

7.2 Governing equations of the mathematical model

This section explains all the governing equations of the mathematical modelling process. They include adsorption isotherms and kinetics equations, energy equations of the adsorber, evaporator and condenser, and the mass balance equation. The adsorption isotherms and kinetics equations of the CPO-27Ni/water working pair have been presented in section 3.4, which are equations 3-16 to 3-18.

7.2.1 Energy equation for adsorption beds

Energy equations are used to describe the heat transfer in adsorption beds. In the lump-parameter mathematical technique, the adsorbent material, refrigerant and metal in one adsorber are assumed to have the same temperature momentarily. Also the adsorption cooling system is assumed to be perfectly insulated, which means there is no heat or mass transfer to the surroundings. Utilising these assumptions, the energy balance of the adsorption beds can be written as equation 7-1.

$$\begin{aligned}&\left(m_{Cubed}Cp_{Cu}+m_{Al}Cp_{Al}+m_{ads}Cp_{ads}+m_{ads}wCp_{ref}\right)\frac{dT_{bed}}{dt}\\&=m_{ads}\Delta H_{ads}\frac{dw}{dt}+\dot{m}_{bed}Cp_{bedw}\left(T_{bed,in}-T_{bed,out}\right)\end{aligned} \tag{7-1}$$

Where T_{bed} is the adsorption bed's temperature; $\dot{m}_{bed}$ is the mass flow rate of the heating/cooling fluid flowing through the adsorption bed; $T_{bed,in}$ and $T_{bed,out}$ are temperatures of the heating/cooling fluid at the inlet and outlet.

The terms on the left side of equation 7-1 are the rate of heat required to heat or cool the copper tubes, aluminium fins, adsorbent material and refrigerant remaining in the pores of the adsorbent material, respectively. The terms on the right side of equation

7-1 present the rate of adsorption heat generated or extracted during the adsorption process or desorption process, respectively and the rate of heat added or removed by the heating/cooling fluid.

The outlet temperature of the heating/cooling fluid $T_{bed,out}$ is calculated by equation 7-2.

$$T_{bed,out} = T_{bed} + \left(T_{bed,in} - T_{bed}\right)\exp\left(-\frac{UA_{bed}}{\dot{m}_{bed}Cp_{bedo}}\right) \tag{7-2}$$

Where UA_{bed} is the overall heat transfer conductance of the whole adsorption bed, which is calculated using the sum of all thermal resistances as described below.

The components of the heat transfer resistances for the adsorber bed are shown in Figure 7-2. Figure 7-2(a) presents all the heat transfer resistances in one element of the adsorption bed; where R1 is the convection thermal resistance from the heating/cooling fluid to the tube wall; R2 is the thermal resistance in the copper tube wall; R3 and R4 are contact thermal resistances between adsorbent granules and the tube surface and fin surface respectively; R5 and R6 are thermal resistances through the adsorbent granules in radial and axial directions respectively. To simplify the process of simulation, rectangular fins are transformed to circular fins with the same fin surface area as shown in Figure 7-2(b). Figure 7-2(c) shows the thermal resistance electrical analogy.

R1 is calculated by equations 7-3 to 7-6, and equations 7-7 to 7-11 are used for calculating R2-R6 [1].

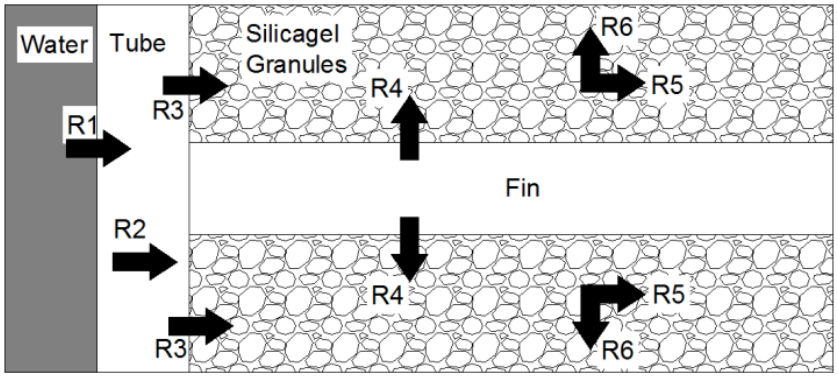

(a)

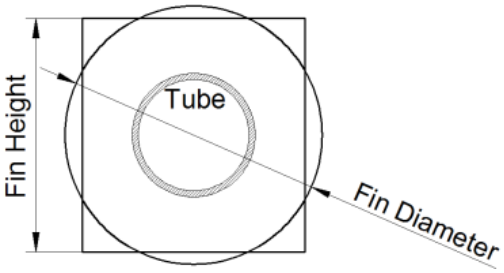

(b)

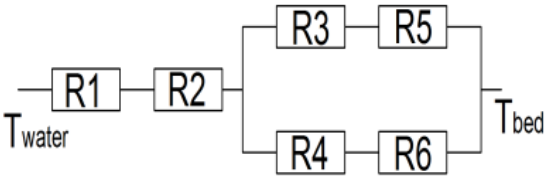

(c)

Figure 7-2 Heat transfer resistance of the adsorption bed

$$R1 = \frac{d_i}{Nuk_c} \cdot \frac{1}{S_i} \tag{7-3}$$

$$\text{where } Nu = 4.36 \text{ for } Re < 2300 \tag{7-4}$$

$$Nu = \frac{\left(\frac{f_c}{8}\right)(Re_c - 1000)Pr_c}{1+12.7\left(\frac{f_c}{8}\right)^{\frac{1}{2}}\left(Pr_c^{\frac{2}{3}}-1\right)} \text{ for } Re > 2300 \tag{7-5}$$

$$\frac{1}{\sqrt{f_c}} = -1.8\log\left[\frac{6.9}{Re_c} + (\varepsilon_0/3.6d_i)^{1.11}\right] \tag{7-6}$$

$$R2 = \frac{\ln(d_o/d_i)}{2\pi k_t \delta_p} \tag{7-7}$$

$$R3 = \frac{R_{cont}}{2\pi d_o \delta_s} \tag{7-8}$$

$$R4 = \frac{R_{cont}}{2S_{fin,side}} \tag{7-9}$$

$$R5 = \frac{\ln(d_p/d_o)}{4\pi k_{ads} \delta_s} \tag{7-10}$$

$$R6 = \frac{\delta_s}{2S_{fin,side}k_{ads}} \tag{7-11}$$

Finally, UA_{bed} is calculated by equation 7-12.

$$UA_{bed} = \frac{1}{R1 + R2 + \frac{(R3 + R5)(R4 + R6)}{R3 + R4 + R5 + R6}} \tag{7-12}$$

Where d_i, d_o and d_p are the inner, outer and fin diameters of the tubes respectively; k_c, k_t and k_{ads} are the thermal conductively of the heating/cooling fluid, tube and adsorbent material respectively; Nu, Re and Pr are the Nusselt number, Reynolds number and Prandtl number respectively; f_c and ε_0 are the friction factor and the tube internal wall roughness; S_i and $S_{fin,side}$ are the surface area of the tube's internal wall and fins; δ_p is half of the thickness of the adsorbent material between two of the fins; R_{cont} is the thermal contact resistance between the adsorbent material and the metal. R_{cont} was calculated using equation 4-12 given in Chapter 4.

7.2.2 Energy equation for the evaporator

The energy equation for the evaporator presents the heat transfer between the refrigerant, finned tubes and the chilled water in the evaporator. Assuming that the refrigerant and metal in the evaporator are at the same temperature momentarily, the energy balance of the evaporator can be expressed as equation 7-13.

$$\begin{aligned} &\left(m_{Cuevap}Cp_{Cu} + m_{refevap}Cp_{refevap}\right)\frac{dT_{evap}}{dt} = \\ &\dot{m}_{chw}Cp_{chw}\left(T_{chw,in} - T_{chw,out}\right) - m_{ads}h_{fg}\frac{dw_{ads}}{dt} - m_{ads}\frac{dw_{des}}{dt}h_{condw} \end{aligned} \tag{7-13}$$

Where m_{Cuevap} and $m_{refevap}$ are the mass of the copper tubes and liquid refrigerant in the evaporator respectively and m_{ads} is the mass of the adsorbent material packed in the adsorber beds; $T_{evap}, T_{chw,in}$ and $T_{chw,out}$ are the temperatures of the evaporator and the chilled water at the inlet and outlet respectively; h_{fg} is the water's latent heat of evaporation and h_{condw} is the enthalpy of the water in the condenser; w_{ads} is a positive value presenting the adsorption rate of the adsorption bed in the adsorption process; while w_{des} is a negative value presenting the desorption rate of the adsorption bed in the desorption process.

Terms on the left hand side of equation 7-13 present the rate of heat transfer to the metal and the refrigerant maintained in the evaporator respectively. Terms on the right hand side are the rate of heat transferred from the chilled water, heat loss by evaporation of refrigerant adsorbed by the adsorption bed during the adsorption process; and energy added by liquid refrigerant coming from the condenser and entering the evaporator.

7.2.3 Energy equation for the condenser

The energy equation for the condenser presents the heat transfer between the refrigerant, tubes and cooling water passing through the tubes of the condenser. Here it is assumed that the refrigerant and the metal in the condenser are at the same temperature momentarily. The energy balance of the condenser can be explained as equation 7-14.

$$\left(m_{Cucond}Cp_{Cu}+m_{refcond}Cp_{refcond}\right)\frac{dT_{cond}}{dt}= \\ \dot{m}_{condw}Cp_{condw}\left(T_{condw,in}-T_{condw,out}\right)-m_{ads}h_{fg}\frac{dw_{des}}{dt} \tag{7-14}$$

Where m_{Cucond} and $m_{refcond}$ are the mass of the copper tubes and liquid refrigerant in the condenser respectively and m_{ads} is the mass of the adsorbent material packed in the adsorber beds; T_{cond} , $T_{condw,in}$ and $T_{condw,out}$ are the temperatures of the condenser and the cooling water flowing through condenser at the inlet and outlet, respectively.

Terms on the left hand side of equation 7-14 present the rate of heat transfer to the metal and refrigerant maintained in the condenser respectively. Terms on the right hand side are the rate of heat added by the cooling water and heat added by the condensation energy of the refrigerant desorbed from the adsorption bed during the desorption process.

7.2.4 Mass balance equation

The evaporator/condenser's mass balance can be determined by equation 7-15 with the assumption that there is no liquid receiver in this automotive adsorption air conditioning system.

$$\frac{dm_{refevap}}{dt}=-m_{ads}\frac{dw_{ads}}{dt}-m_{ads}\frac{dw_{des}}{dt} \tag{7-15}$$

7.2.5 Modelling using MATLAB/Simulink

A mathematical simulation model of a two-bed adsorption air-conditioning system for automotive application is set up and all the governing equations presented above are solved by MATLAB Simulink software. Simulink is integrated with MATLAB, providing an interactive graphical environment and a customizable set of block libraries used to design, simulate, implement and test various time-varying systems [159]. Users can build models simply by dragging and dropping blocks from the library browser on to the graphical editor and connecting them with lines that establish mathematical relationships between the blocks. It can update the state of each block of the model at each time step during the time span of the calculation process [159]. Figure 7-3 presents the flow chart of the model; and the model built in Simulink for the two-bed adsorption air-conditioning system packed with CPO-27Ni is shown in Figure 7-4.

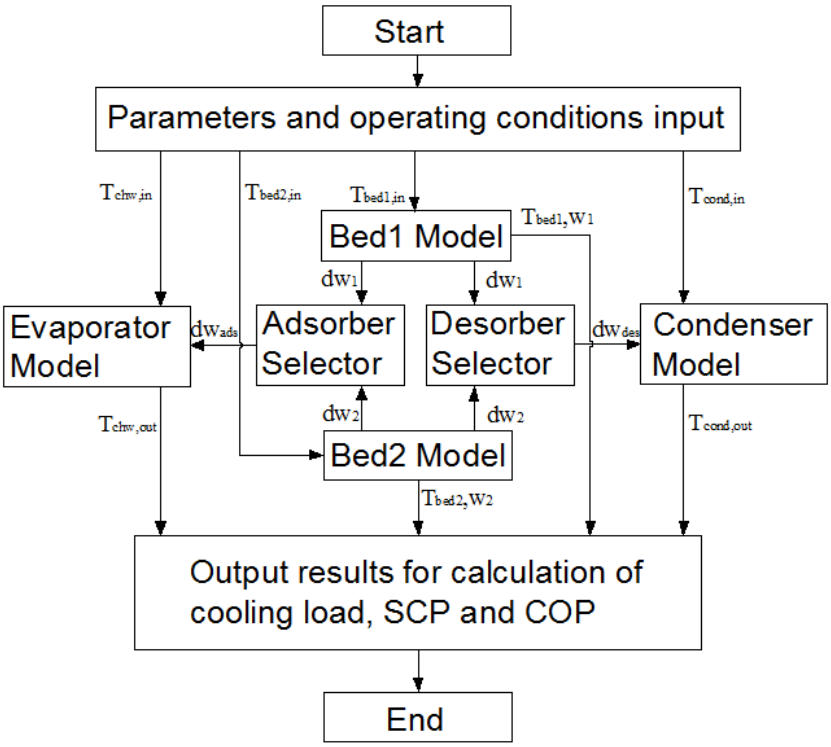

Figure 7-3 The flow chart of the model

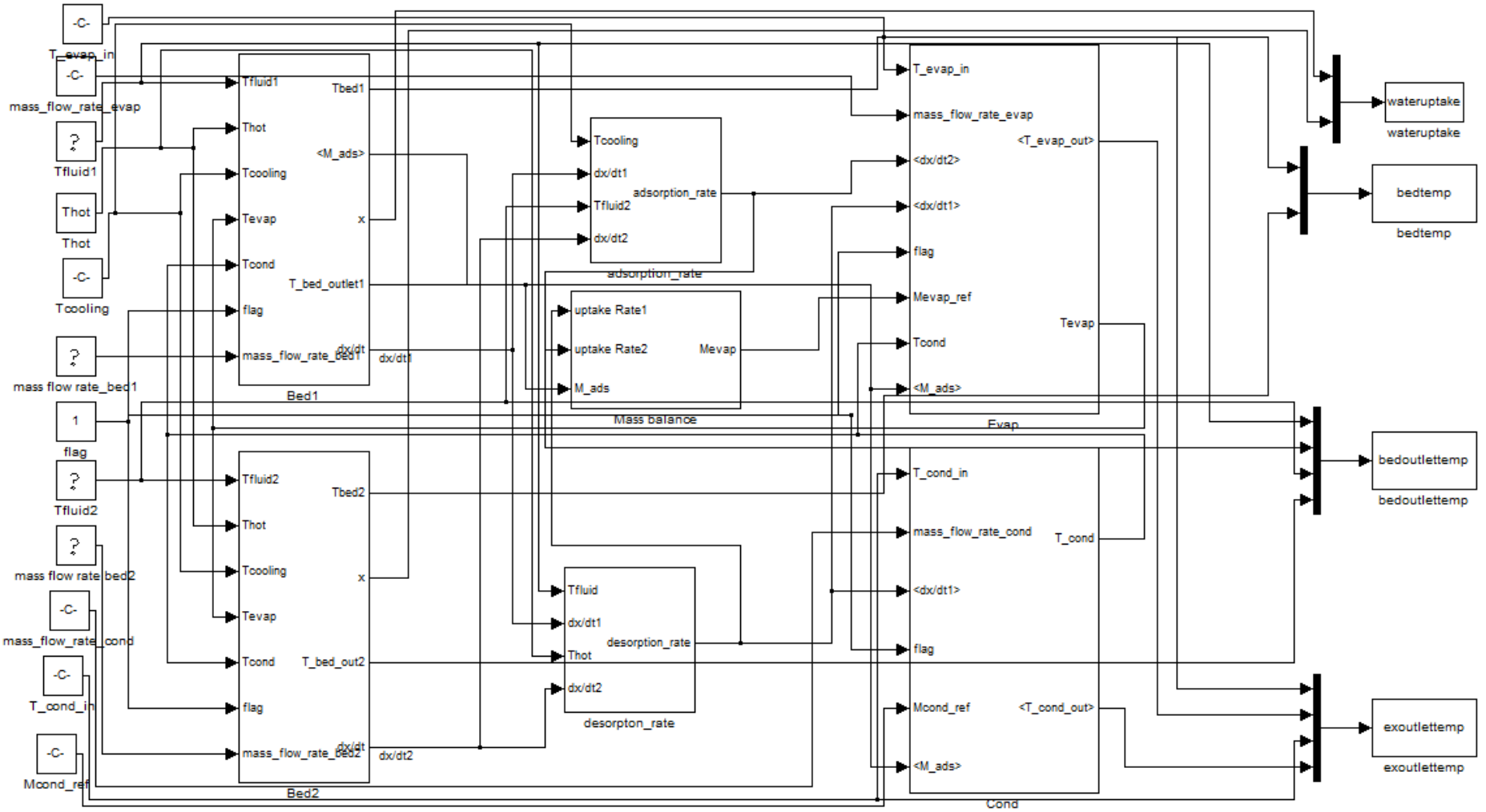

Figure 7-4 Model built in Simulink for the two-bed adsorption cooling system

7.3 Validation of Simulink mathematical model

In this section the mathematical model presented above was validated using the experimental results described in Chapter 6. The lumped-parameter mathematical model using MATLAB Simulink software was run based on a single bed cycle and using the same dimensions as the adsorption cooling system used in the test facility. Figures 7-5 to 7-7 compare the predicted water vapour uptake, cooling water outlet temperature and chilled water outlet temperature in the adsorption process with their actual analogous values obtained experimentally using the test facility with the same cooling water inlet temperature, initial bed temperature, chilled water inlet temperature and flow rate of both cooling water and chilled water.

Table 7-1 presents the average percentage deviation and absolute average percentage deviation for water uptake, cooling water outlet temperature and chilled water outlet temperature in the adsorption process. The results show that the maximum average percentage deviation and maximum absolute average percentage deviation are both 8.1%. Figures 7-5 to 7-7 and Table 7-1 show clearly the good agreement between the mathematical model and the experimental results.

Table 7-1 Mathematical simulation model deviation analysis

Terms	APD	ABS-PD
Water vapour uptake	8.1%	8.1%
Cooling water outlet temperature	-1.4%	1.5%
Chilled water outlet temperature	-0.3%	1.3%

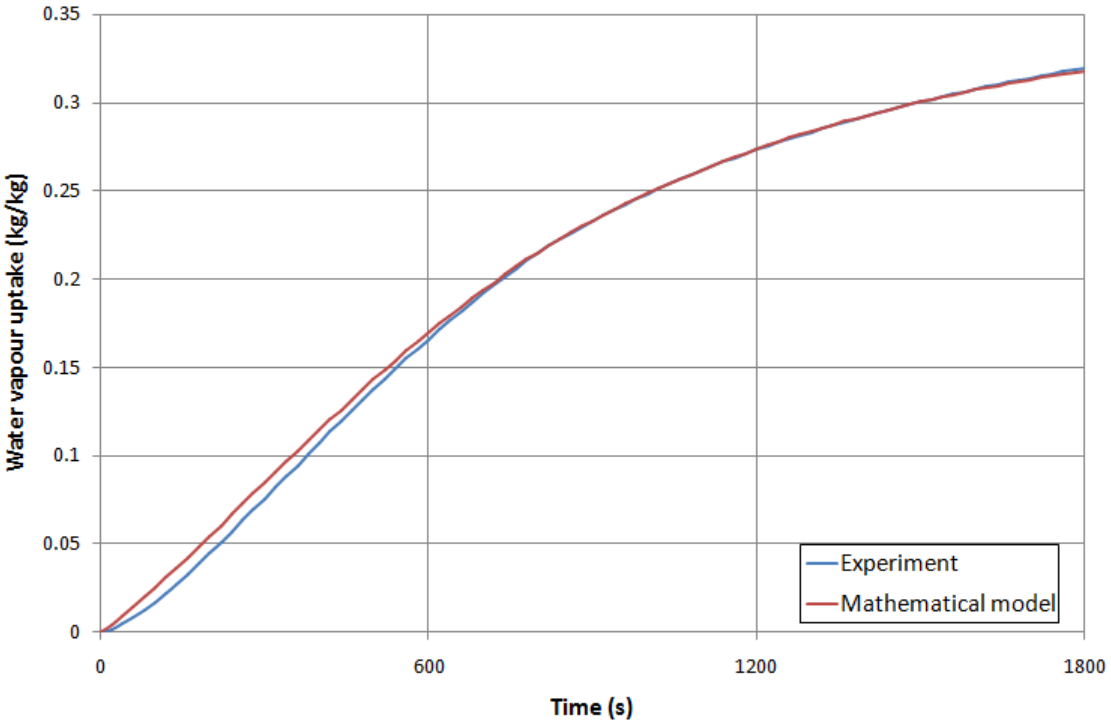

Figure 7-5 Comparison of water vapour uptake between predicted data and actual data

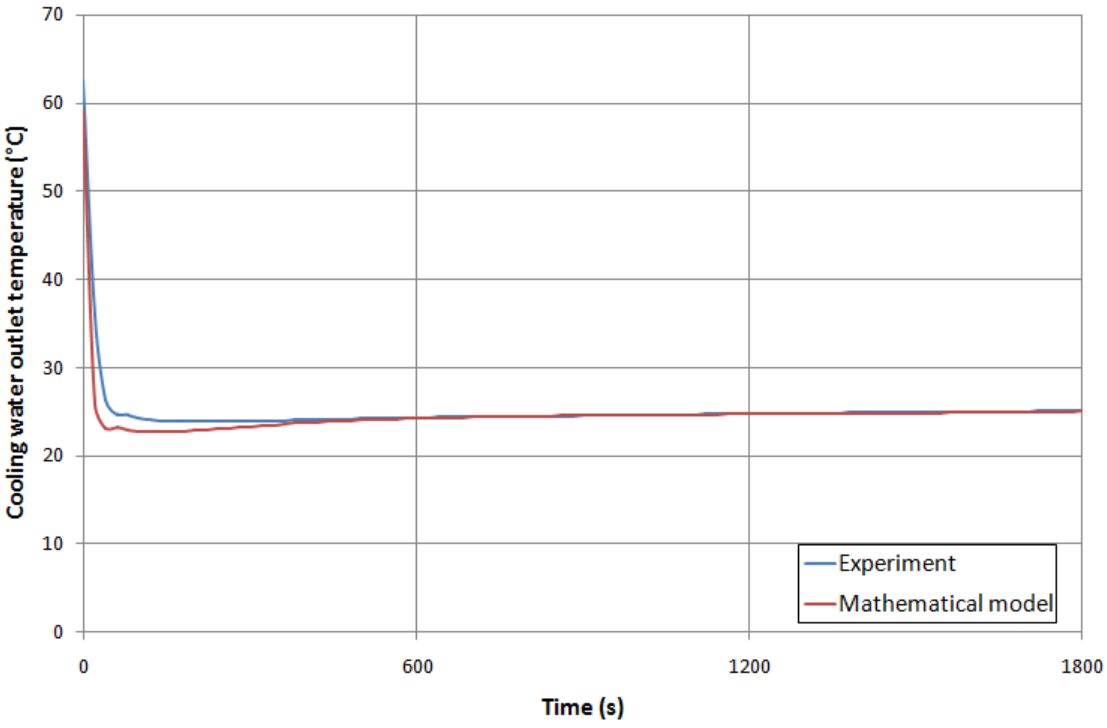

Figure 7-6 Comparison of cooling water outlet temperature between predicted data and actual data

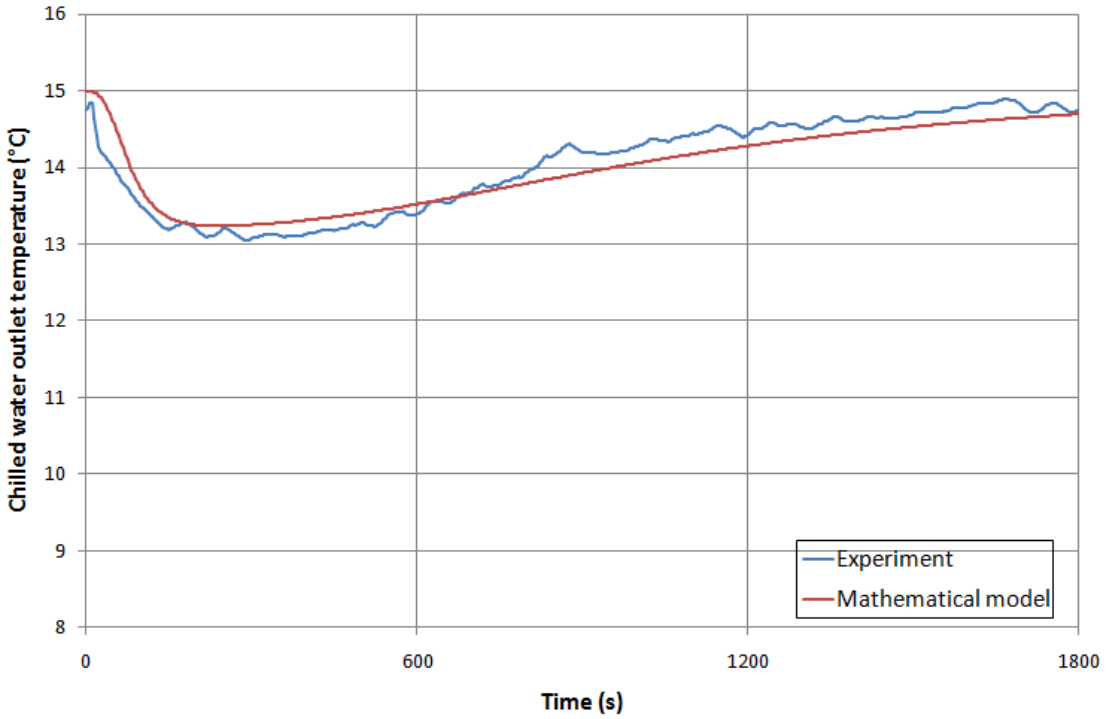

Figure 7-7 Comparison of chilled water outlet temperature between predicted data and actual data

7.4 The automotive adsorption air-conditioning system

The automotive adsorption air-conditioning system contains two adsorbers, one evaporator, one condenser and several valves. Each adsorber includes eight adsorption bed modules with the same structure as described in section 5.2.1. All adsorbers are generated by hot secondary fluid in the desorption process; while the desorbed refrigerant vapour is condensed in the condenser. Thermal oil is utilised for heating the adsorber beds to enable a performance prediction of CPO-27Ni at a wide range of temperatures. The generated energy can be obtained from exhaust gas or engine coolant water from the automotive engine. In the adsorption process, cooling fluid flows through the tubes of the adsorption beds to cool down the adsorbent material. Refrigerant is evaporated in the evaporator to produce a cooling effect. The operation

principle has been described in detail in section 2.6.2. The evaporator and condenser are both shell and tube heat exchangers. The refrigerant flows on the shell side and the heating/cooling water flows inside the tubes. The evaporator is constructed from externally enhanced high efficiency finned copper tubes; while the condenser is constructed from plain copper tubes. Some specific dimensions of adsorption beds, an evaporator and condenser are shown in Table 7-2.

Table 7-2 Simulated physical data for adsorption beds, evaporator and condenser

Adsorption beds	
Bed length	275mm
Fin width	115mm
Fin height	30mm
Fin pitch	1.016mm (25fins/inch)
Fin thickness	0.105mm
Tube outer diameter	15.875mm
Tube thickness	0.8mm
Fin number in one adsorption bed	270
Number of adsorption bed in one adsorber	8
Total adsorbent mass	5.422kg
Evaporator	
Tube outer diameter	15.875mm
Tube thickness	0.8mm
Fin diameter	17.875mm
Fin pitch	0.5mm
Fin height	1mm
Fin thickness	0.2mm
Tube length	5500mm
Tube number	4
Condenser	
Tube outside diameter	15.875mm
Tube thickness	0.8mm
Tube length	5500mm
Tube number	4

7.5 Investigation of the performance of a two-bed adsorption system

The validated mathematical model was then used to simulate the working process and investigate the performance of a two-bed adsorption cooling system for automotive application. This section presents the performance of the system and the effects of cycle time, heating fluid temperature and flow rate, fin height and fin number on the system's performance. The operating conditions shown in Table 7-3, which are normally used in the research of automotive adsorption air conditioning systems [34, 36, 37, 85] are used as the baseline for comparison.

Table 7-3 Reference operating conditions

Operating condition	Value
Heating fluid inlet temperature	90 ℃
Cooling oil inlet temperature	30 ℃
Chilled water inlet temperature	15 ℃
Condensation second fluid water inlet temperature	20 ℃
Hot water flow rate	15L/min
Cooling water flow rate	15L/min
Chilled water flow rate	15L/min
Condensation second fluid water flow rate	15L/min
Initial refrigerant liquid mass in evaporator	15kg
Initial refrigerant liquid mass in condenser	15kg
Cycle time	900s

To compare the performance of the adsorption air-conditioning system the cooling load, COP and SCP are used as criteria; as described in section 6.1. The cooling load is the cooling effect produced during the adsorption and evaporation process, which is equal to the SCP multiplied by the adsorbent's mass. All calculations in this research exclude the consideration of dynamic losses for the casing to the ambience which is

difficult to be defined and usually has a small proportion to the total amount of heat consumed.

7.5.1 Effect of temperature and flow rate of the heating fluid

This section investigates the effect of temperature and flow rate of the heating fluid on the performance of the adsorption air-conditioning system. Normally, increasing the temperature and flow rate of the heating fluid can improve the amount and rate of refrigerant desorption in the desorption process; which increases the refrigerant adsorption capacity of the adsorbents in the following adsorption process. In this way, the cooling load and SCP can be enhanced. However, the energy input increases with the increase in temperature and flow rate of the heating fluid. The variation of cooling load, SCP and COP are shown in Figures 7-8 to 7-10.

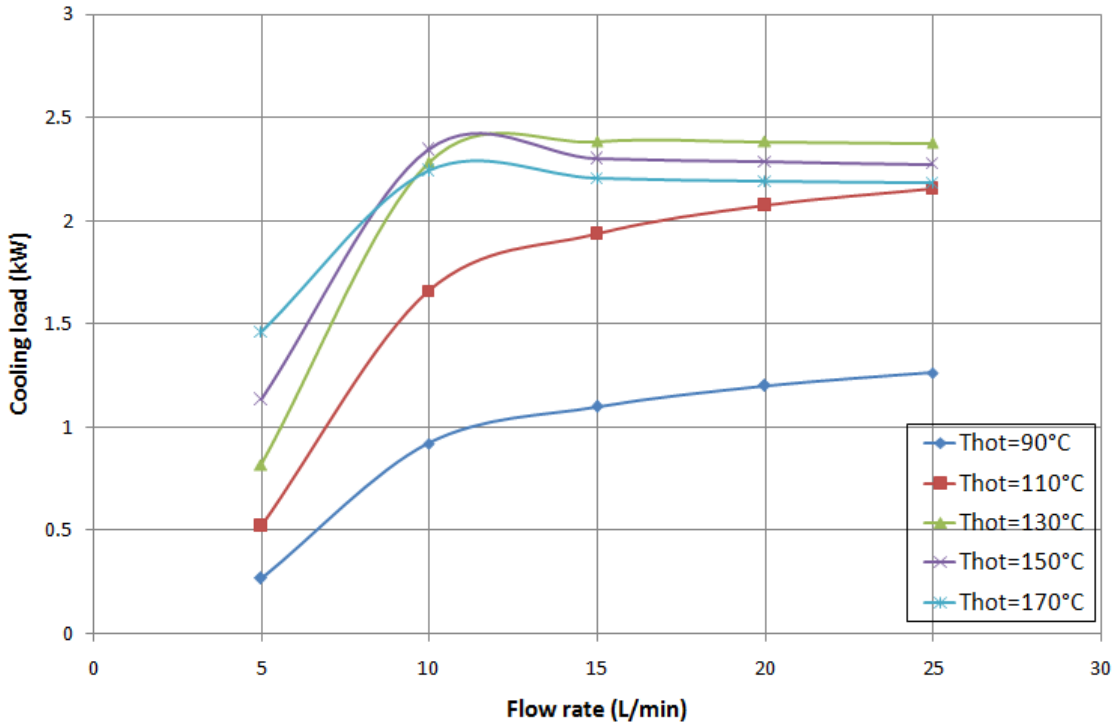

Figure 7-8 Variation of cooling load with different temperatures and flow rates of hot oil

Figures 7-8 and 7-9 present the variation of the cooling load and SCP with temperatures ranging from 90 ℃ to 170 ℃ and flow rates ranging from 5L/min to 25L/min of the heating fluid respectively. It is shown that the cooling load and SCP increased with the increase of the heating fluid's flow rate when the temperature was lower than 130 ℃. When the temperature was higher than 130 ℃, the SCP and cooling load increased dramatically with the increase of the hot oil's flow rate below 10L/min; while the flow rate has no significant effect on the performance at values higher than 10L/min. The cooling load and SCP increased by up to 2.45 times with increasing the flow rate from 5L/min to 15L/min. Therefore a flow rate of up to 15L/min is adequate to produce high cooling load and SCP values.

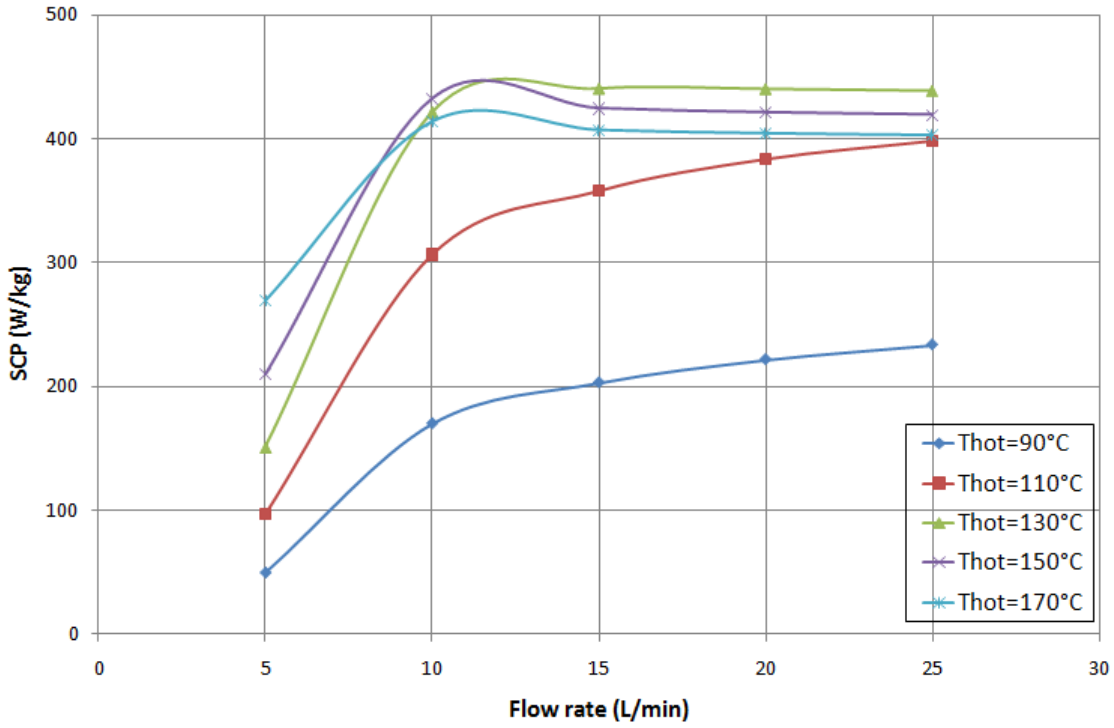

Figure 7-9 Variation of SCP with different temperatures and flow rates of the heating fluid

On the other hand, increasing the hot oil temperature from 90 ℃ to 170 ℃, the cooling load and SCP increased by 4.46 times at a hot oil flow rate of 5L/min. It can be concluded that a hot oil temperature of 130 ℃ and flow rate of 15L/min can produce the maximum cooling load of 2.39kW and SCP of 440W/kg; which proves the potential of the developed system for automotive air-conditioning.

Figure 7-10 shows the variation of the COP with different heating fluid temperatures and flow rates. The results show that increasing the hot oil flow rate above 10L/min has no significant impact on the coefficient of performance. With the increase of the hot oil flow rate from 5L/min to 10L/min, the COP increased when the hot oil temperature was lower than around 150 ℃ but decreased when the hot oil temperature was higher than 150 ℃.

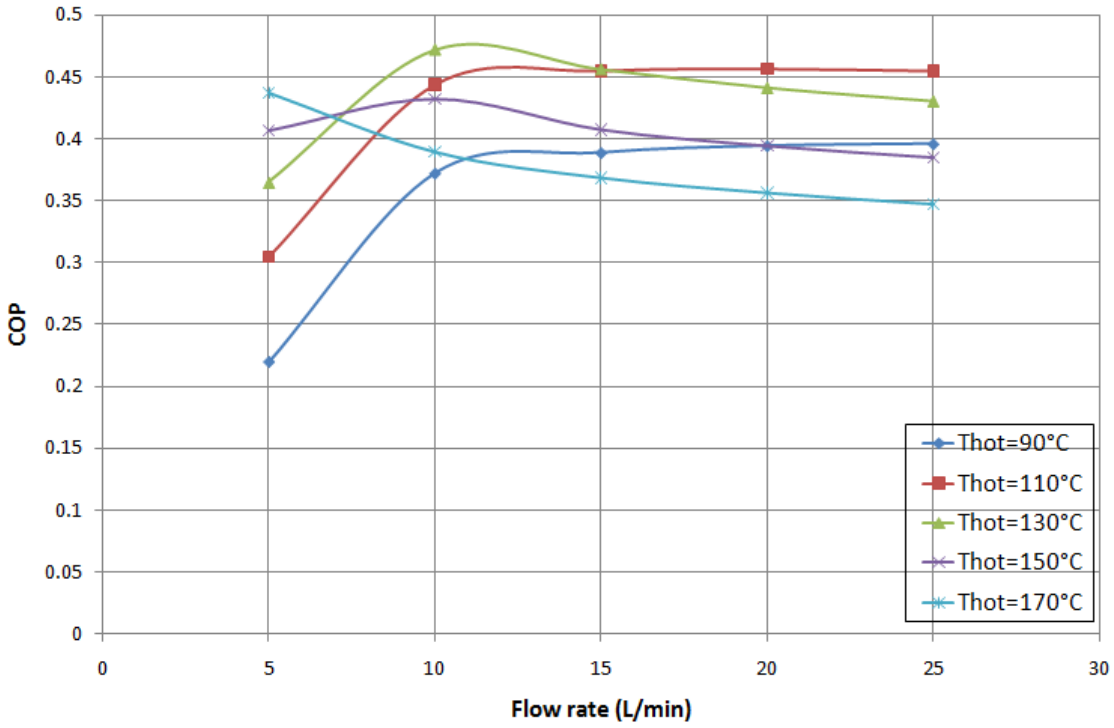

Figure 7-10 Variation of the COP with different temperatures and flow rates of the heating fluid

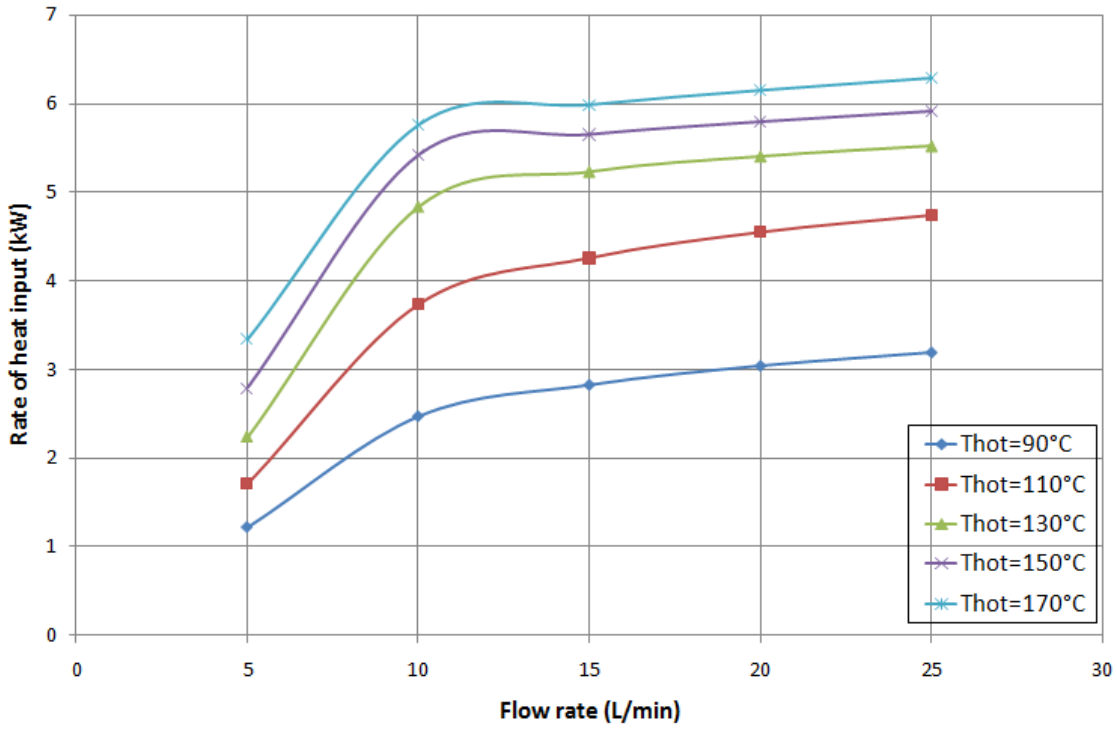

Figure 7-11 Variation of rate of heat input with different temperatures and flow rates of the heating fluid

As for the effect of the heating fluid's temperature, the COP increased by 99% when the hot oil flow rate was 5L/min by increasing the temperature from 90 ℃ to 170 ℃. With a flow rate of higher than 5L/min, as the hot oil temperature increased, the COP increased at first and then decreased. In conclusion, a maximum COP value of 0.471 was achieved with a hot oil temperature and flow rate of 130 ℃ and 10L/min respectively.

Figure 7-11 presents the variation of heat input rate with different temperatures and flow rates of the heating fluid. The results show that the rate of heat input increased with the increase of temperature and/or flow rate of the heating fluid. The heat power input increased significantly with the increase of the hot oil's temperature from 90 ℃ to 130 ℃ and flow rate from 5L/min to 10L/min; while the increase becomes

relatively slower with the increase of the hot oil's temperature to higher than 130 ℃ and flow rate to higher than 10L/min.

Finally, as a conclusion, the CPO-27Ni MOF adsorption air-conditioning system developed in this work can achieve the required cooling load of 2.39kW with a specific cooling capacity of 440W/kg and COP of 0.456 with a hot oil temperature of 130 ℃ and flow rate of 15L/min. A hot oil temperature of 130 ℃ can be achieved since the exhaust gas, with a temperature of around 200 ℃ from the automotive engine, can be used to provide the required heat for the desorption process.

Since the system with a hot oil temperature of 130 ℃ can achieve the best performance, the following investigations were carried out using this hot oil temperature as the baseline.

7.5.2 Effect of cycle time

Normally, in the operation process of a two-bed refrigeration cycle the adsorption time is the same as the desorption time. The cycle time has a significant effect on the performance of an adsorption air-conditioning system, as described in sections 6.4 and 6.5. In this section, the effects of cycle time on cooling load, SCP and COP are investigated, as shown in Figures 7-12 and 7-14.

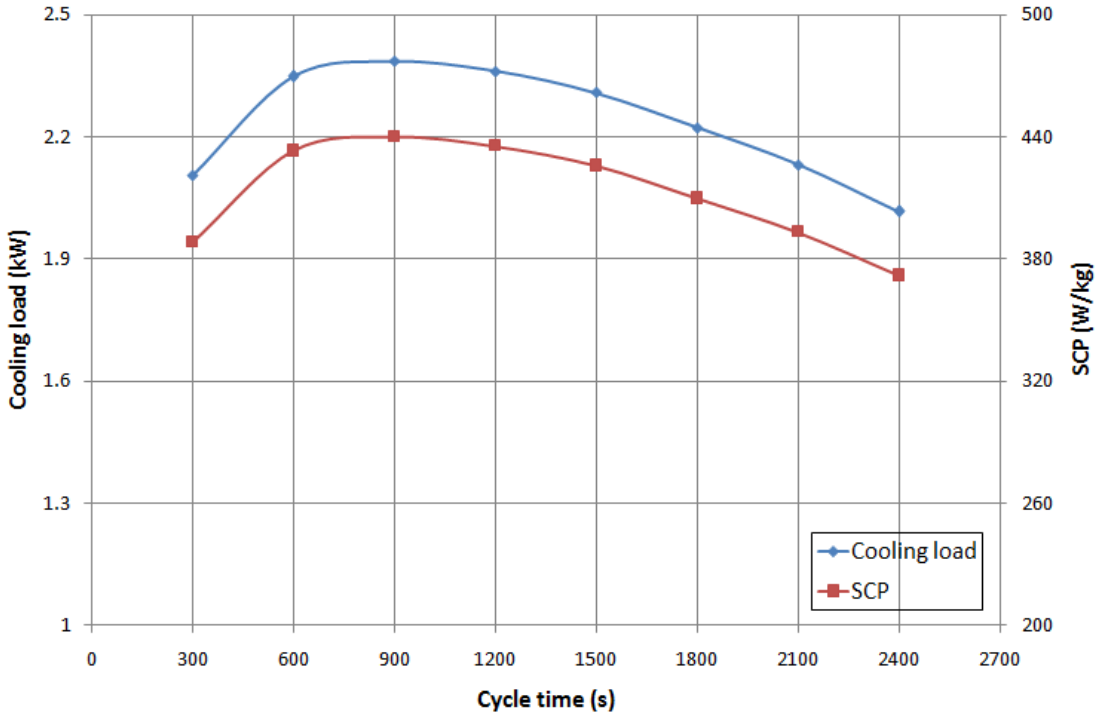

Figure 7-12 Variation of cooling load and SCP with different cycle times

Figure 7-12 shows the variation of cooling load and SCP with different cycle times. The cooling load and SCP both increased with the increase of the cycle time from 300s to 900s; and then decreased when the cycle time was longer than 900s. Each run was carried out at the same operating conditions and adsorbent mass but with a varying cycle time; thus the cooling load and SCP had the same trend. Since the refrigerant adsorption rate is high at the beginning of the adsorption process and then it becomes slower with time, the cooling load is enhanced by increasing the cycle time from 300s to 900s. When the cycle time is longer than 900s, the increase in the cooling effect with the increase of cycle time becomes smaller, resulting in a lower cooling effect. As a conclusion, the cycle time of 900s produced the highest cooling load of 2.39kW and SCP of 440W/kg.

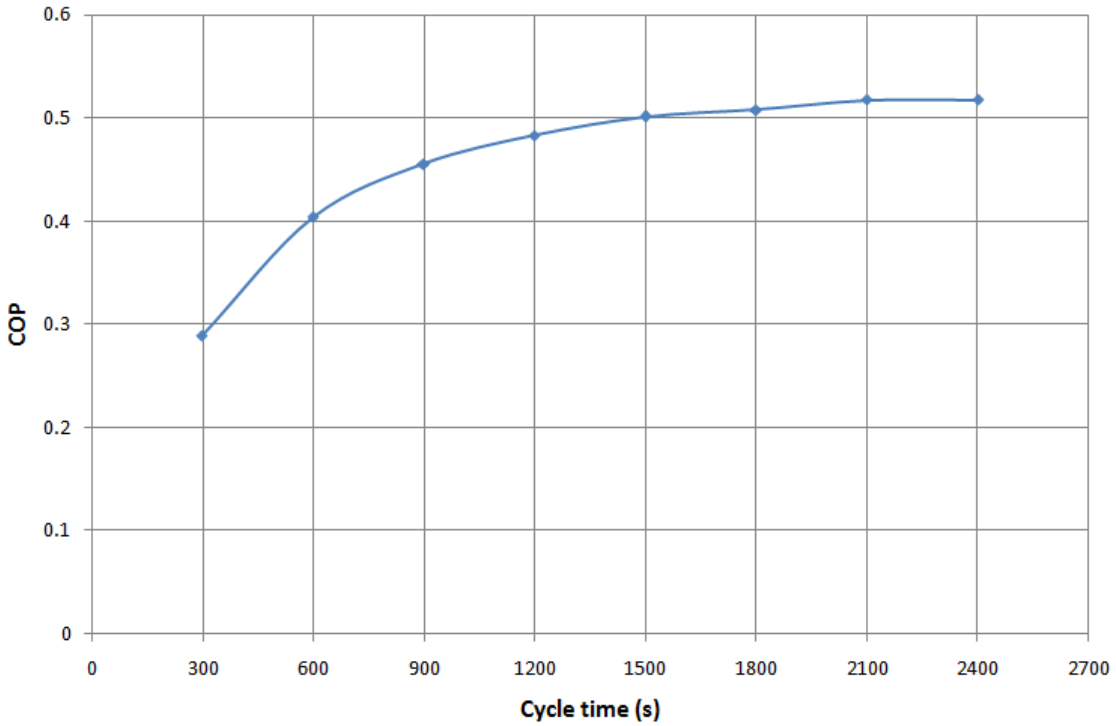

Figure 7-13 Variation of the COP with different cycle times

Figure 7-13 presents the variation of the COP with different cycle times. The results show that the COP increased by 80% with the increase of cycle time from 300s to 2400s. It means that this system can achieve the larger energy utilisation efficiency with a longer operating cycle time. Furthermore, the COP increased significantly by 58% with the increase of cycle time from 300s to 900s; while the increase becomes relatively slower at 14%, with the increase of cycle time from 900s to 2400s. Figure 7-14 presents the variation of heat input with different cycle times. The results show that the rate of heat input decreases by 47% with the increase of the cycle time from 300s to 2400s; thus increasing the COP with the increase of the cycle time, as shown in Figure 7-14. However, significant reduction in the rate of heat input by increasing the cycle time from 300s to 900s while lower reduction occurred with increasing the cycle time above 900s.

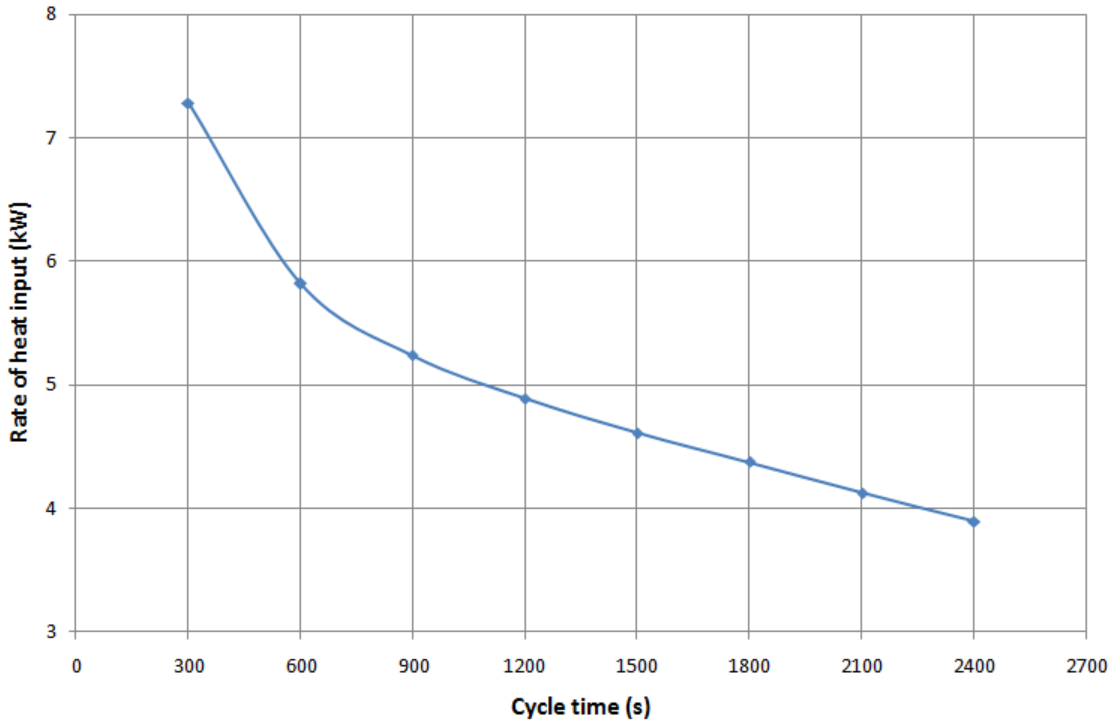

Figure 7-14 Variation of rate of heat input with different cycle times

7.5.3 Effect of fin height and fin number of the adsorption beds

Apart from operating conditions, adsorption bed physical parameters also affect the performance of an adsorption cooling system. This section presents a study of the effect of fin height and fin number of the rectangular finned tube adsorption beds on the performance of the whole system.

Figures 7-15 and 7-16 present the variation of cooling load and SCP with fin height ranging from 20mm to 50mm and fin number ranging from 15 fins/inch to 35 fins/inch respectively. Figure 7-15 shows that the cooling load increased with fin height. It is because adsorption beds with large fin height can be packed with more adsorbents to adsorb more refrigerant vapour and produce higher cooling effect. As for SCP, it increased when the fin height is smaller than 30mm and then decreased

when the fin height is larger than 30mm as shown in Figure 7-16. On the other hand, variation of fin number produced no significant effect on the cooling load as shown in Figure 7-15. However, with the fin height higher than 30mm the SCP increased by up to 12% with increasing fin number from 15 fins/inch to 35 fins/inch due to the higher heat and mass transfer performance achieved with smaller fin number. With fin height of 20mm, SCP decreased by 8.5% with the increase of fin number. In conclusion, the results described above show that the adsorption bed with fin number of 25fins/inch and fin height of 30mm can achieve the highest SCP.

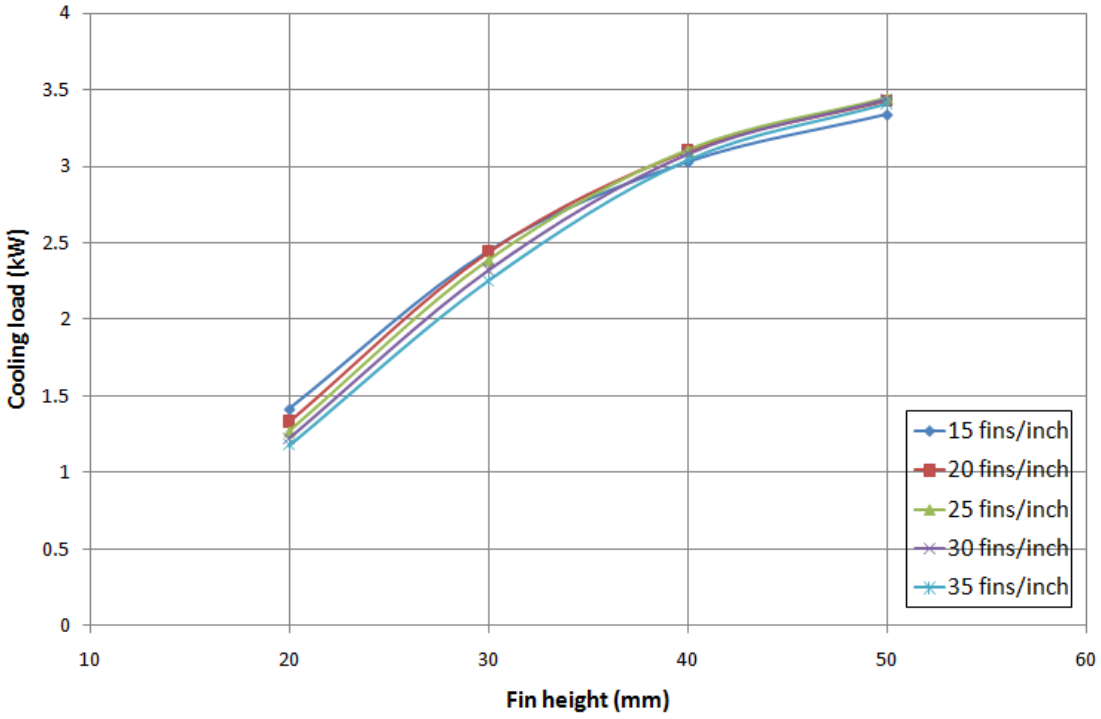

Figure 7-15 Variation of the cooling load with different fin height and fin numbers

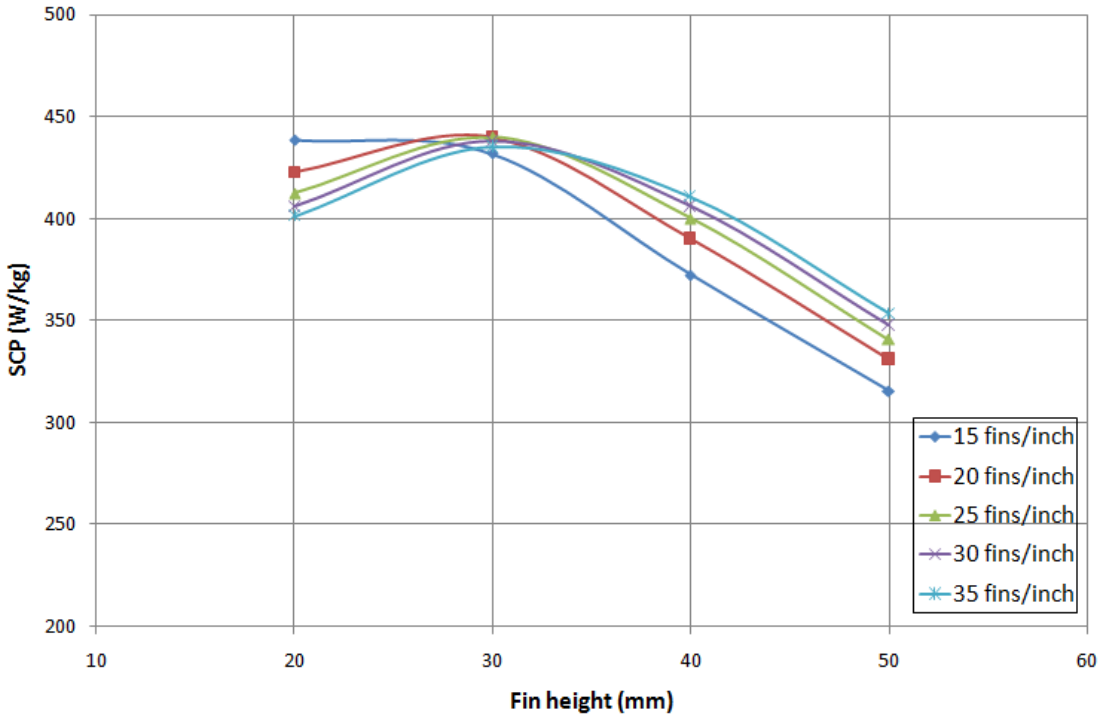

Figure 7-16 Variation of the SCP with different fin height and fin numbers

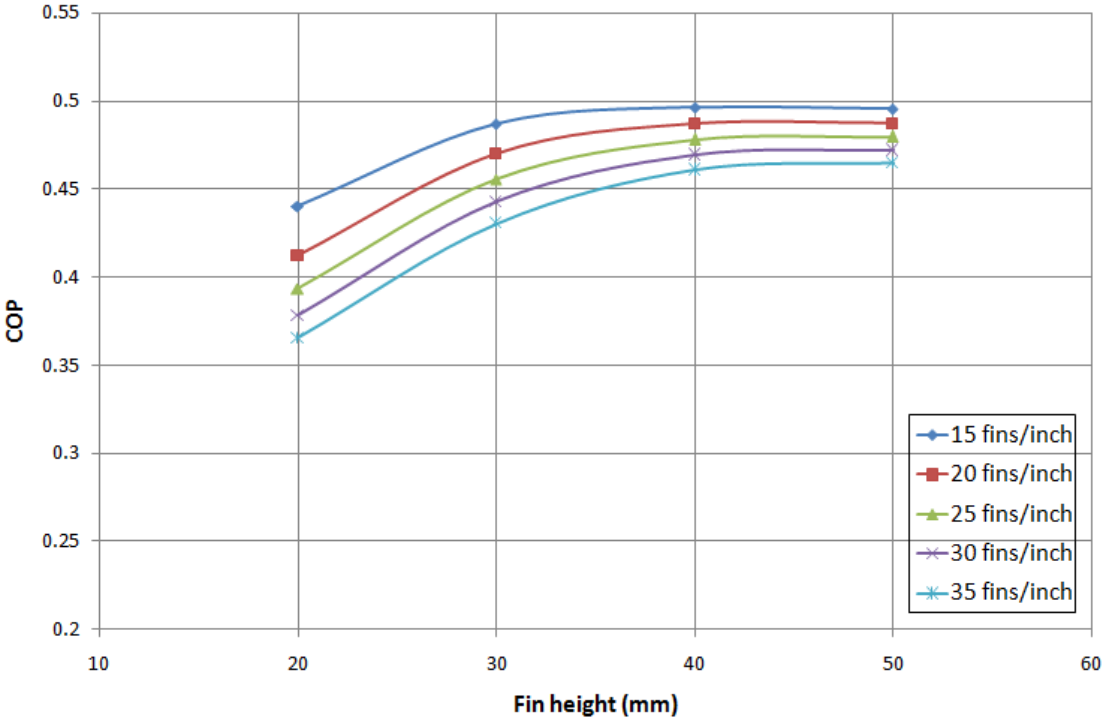

Figure 7-17 Variation of the COP with different fin height and fin numbers

Figure 7-17 shows the variation of the COP with different fin height and fin numbers. The results show that the COP decreased by 17% with the increase of the fin number from 15 fins/inch to 35 fins/inch and increased by 27.1% with the increase of the fin height from 20mm to 50mm.

7.5.4 Performance of system with the optimum operating conditions

Based on the investigations presented in sections 7.5.1, 7.5.2 and 7.5.3, optimum operating conditions can be concluded as shown in Table 7-4. Using these operating conditions, the water vapour uptake, inlet and outlet temperatures of the adsorber bed, evaporator and condenser are shown in Figures 7-18 to 7-20 when the performance of the refrigeration cycles are stable.

Figure 7-18, shows the water uptake performance of the two adsorbers. The results show that the water uptake increases from around 0.07 to 0.25 during the 450s long adsorption process and in the next desorption process of 450s the uptake reduces back to 0.07. The difference of water vapour uptake among the first and second cycles is smaller than 0.0001, which indicates that the cycling process is steady during the cycles.

Table 7-4 Optimum operating conditions

Operating condition	Value
Heating fluid inlet temperature	130 ℃
Cooling oil inlet temperature	30 ℃
Chilled water inlet temperature	15 ℃
Condensation second fluid water inlet temperature	20 ℃
Hot water flow rate	15L/min
Cooling water flow rate	15L/min
Chilled water flow rate	15L/min
Condensation second fluid water flow rate	15L/min
Initial refrigerant liquid mass in the evaporator	15kg
Initial refrigerant liquid mass in the condenser	15kg
Cycle time	900s

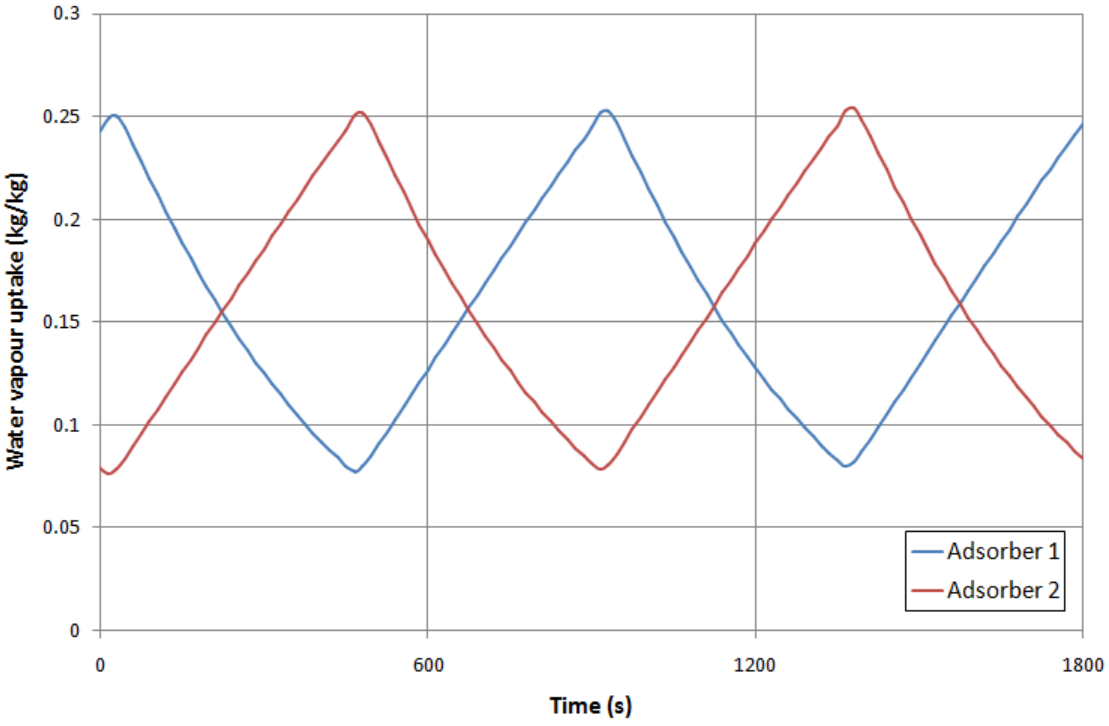

Figure 7-18 Water vapour uptake of cyclic operation

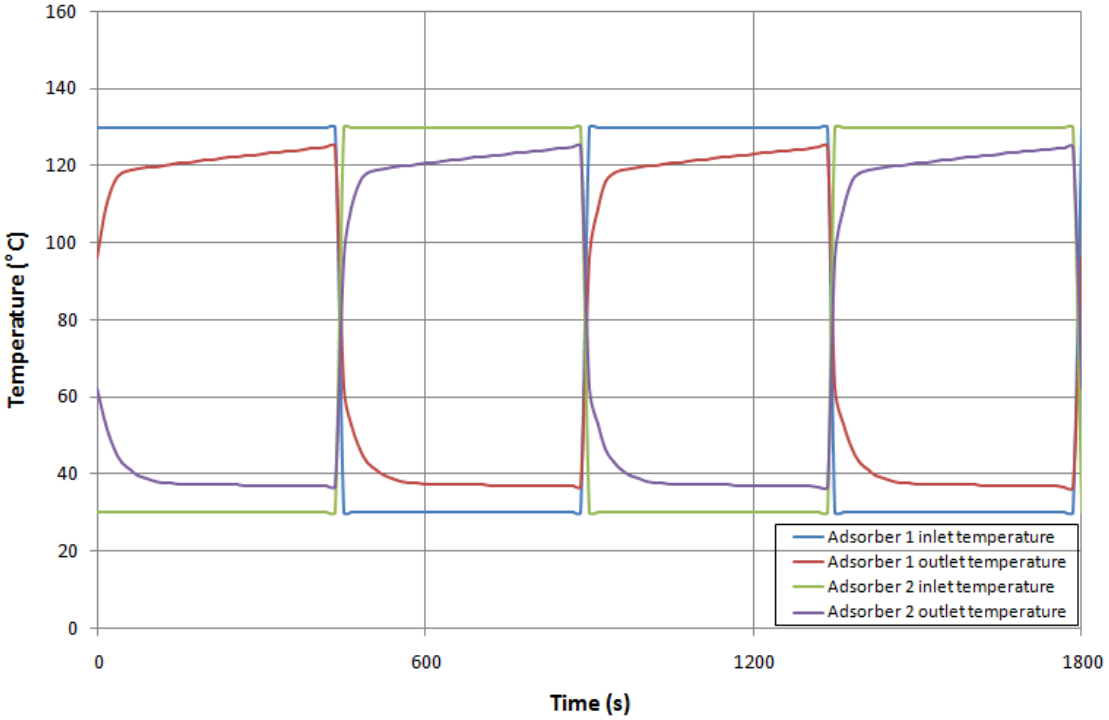

Figure 7-19 Temperatures of heating/cooling fluid through adsorbers at the inlet and outlet of cyclic operation

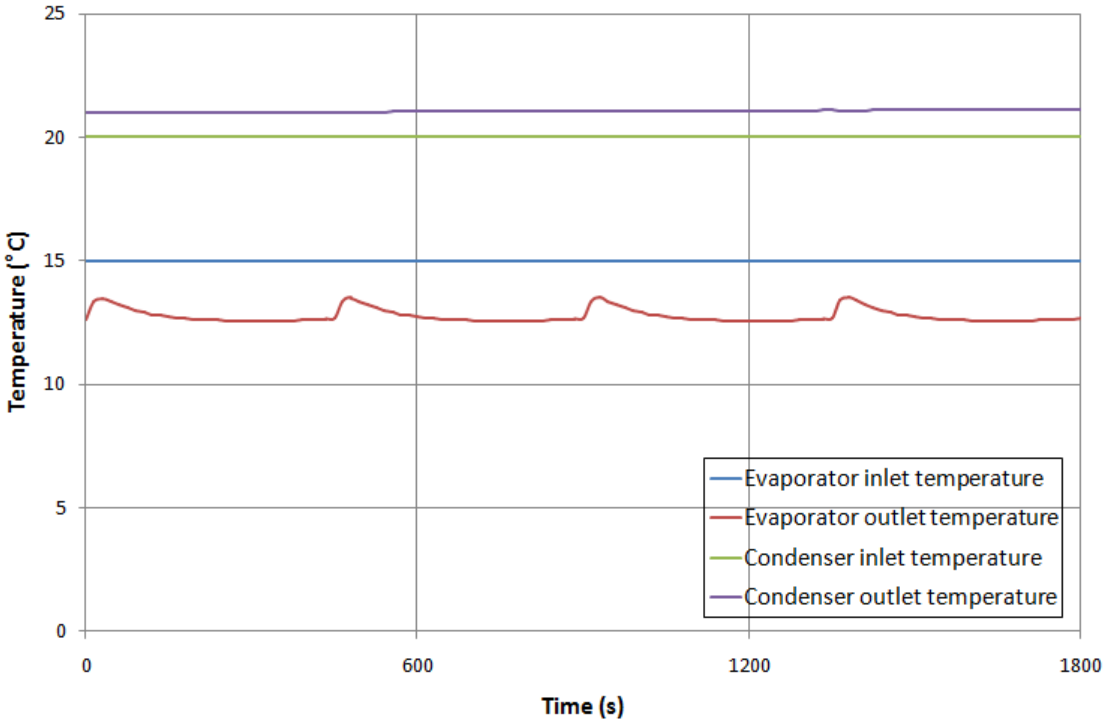

Figure 7-20 Temperatures of second fluid water through the evaporator and condenser at the inlet and outlet of cyclic operation

Figures 7-19 and 7-20 present the heating/cooling fluid temperatures during the adsorption/desorption cycles. The working process of both adsorber beds were stable since the temperatures of the heating/cooling fluid through the adsorbers at the inlet and outlet achieve repeatable values, as shown in Figure 7-19. The condenser outlet temperature is almost the same during the working process since the condensation rate of the refrigerant desorbed does not change in the desorption process, as shown in Figure 7-20. As for the evaporator outlet temperature, it decreases at first due to the high adsorption at the beginning of the adsorption process leading to a high evaporation rate and cooling effect. Then the evaporator outlet temperature increases slowly as heat is transferred from the water passing through the evaporator tubes to the refrigerant liquid in the evaporator shell.

Based on the simulation results, the SCP of the adsorption air conditioning system with the basic operating conditions can achieve 440W/kg. This value is larger than that of all the adsorption cooling systems for automotive application using water as a refrigerant and packed with adsorbents like silica gel, SAPO-34 or zeolite, which were reviewed in the literature presented in section 2.10. Based on the literature, the system using water as a refrigerant achieved a maximum SCP of around 334W/kg [36]. The automotive adsorption air-conditioning system developed in this work can improve the SCP by 31.7%, which means that it saves around 1/3 of the adsorbent mass to provide the same cooling load. With the consideration of the error produced by the deviation during the validation process of the mathematical model using experimental results, the increase of SCP by this automotive adsorption air-conditioning system developed is between 21% and 42.4%, which also indicates a dramatic improvement. Besides, the cooling load with the basic operating conditions

can achieve 2.39kW, which is adequate for the cooling requirements of a car's cabin. The COP can reach 0.456 which is also higher than most of the adsorption air-conditioning systems for automotive application based on the literature review presented in Chapter 2.

7.5.5 Comparison of CPO-27Ni/water and SAPO-34/water

This section compares the performance of an adsorption cooling system with CPO-27Ni and SAPO-34 respectively. Table 7-5 compares the cooling load, SCP and COP of these two adsorbents at the optimum operating conditions shown in Table 7-4.

Table 7-5 Comparison of cooling load, SCP and COP between CPO-27Ni/water and SAPO-34/water

Terms	CPO-27Ni/water	SAPO-34/water
Cooling load (kW)	2.39	1.79
SCP (W/kg)	440	311
COP	0.456	0.422

The results show that with the same operating conditions the cooling load of an adsorption cooling system packed with CPO-27Ni is larger than that of a system packed with SAPO-34, by around 0.6kW. The SCP of CPO-27Ni/water is higher than that of SAPO-34/water by 41.5%; while the COP of the adsorption cooling system using CPO-27Ni/water is higher than that of SAPO-34/water, by around 8%. With the consideration of the error produced by the deviation during the validation process of the mathematical model using experimental results, the improvement of SCP by the automotive adsorption air-conditioning system using CPO-27Ni is between 30% and

53% compared to that using SAPO-34, which also indicates a dramatic increase. In conclusion, the CPO-27Ni/water working pair can produce a higher cooling load per unit of adsorbent mass and can utilise energy more efficiently than the SAPO-34/water pair.

7.6 Summary

In this chapter a lumped-parameter mathematical simulation model using MATLAB Simulink software was developed and used to investigate the performance of an adsorption air-conditioning system for automotive application, with a two-bed refrigeration cycle and the same bed structure shown in section 5.2.1 packed with CPO-27Ni as the adsorbent material. This model was validated using the experimental results. Then the performance of the adsorption cooling system was investigated at varying cycle times, varying heating fluid temperatures and flow rates and different adsorption bed fin numbers and fin heights using this validated mathematical model. The results show that this adsorption air-conditioning system can work steady and be generated by hot oil with a temperature of 130℃ heated by the engine's exhaust gas to produce a cooling power of 2.39kW, which is adequate for the cooling of a normal car's cabin. The SCP of this adsorption air-conditioning system can reach up to 440W/kg, which is higher than all the systems reported in the literature review in Chapter 2 using water as a refrigerant. An adsorber bed with a fin number of 25 fins/inch and a fin height of 30mm produced the highest SCP value. Comparing CPO-27Ni to SAPO-34 showed that the MOF material can achieve a 41.5% higher SCP value.

CHAPTER 8 CONCLUSIONS AND FUTURE WORK

8.1 Introduction

Adsorption air conditioning systems have received significant interest during the last few decades as an alternative technique for traditional vapour compression refrigeration systems to satisfy the market demand for cooling systems and cope with current environmental issues. The present study developed an MOF based adsorption air conditioning system for automotive application. The system performance was theoretically and experimentally investigated at various operating conditions and physical parameters in terms of the cooling load and the coefficient of performance.

8.2 Conclusions

This PhD project was set out to develop and investigate an MOF based adsorption air conditioning system for automotive application; to improve the performance, including specific cooling power and coefficient of performance. To achieve this, utilising a working pair with high refrigerant adsorption capacity and an adsorption bed design with good heat and mass transfer performance are two selected methods. Therefore, the adsorption characteristics of three water based adsorbents: silica gel RD-2060, SAPO-34 and CPO-27Ni, were experimentally tested using a DVS analyser and their adsorption characteristics were compared. In addition, a finite element

model was developed to evaluate and compare the adsorption performance of three different adsorption bed designs: a rectangular finned tube adsorption bed, a honeycomb finned rectangular channel adsorption bed and a helix finned tube adsorption bed. Then an MOF based adsorption air conditioning system for automotive application was developed. The CPO-27Ni/water combination was selected as the adsorption working pair and the rectangular finned tube adsorption bed was utilised.

A lab-scale test facility, based on a single bed refrigeration cycle containing one adsorber and one heat exchanger used as both the evaporator and condenser, was constructed. The effect of various operating conditions on the system's performance, including dry adsorbent desorption time, cooling water flow rate, adsorption time, desorption time and temperatures of evaporation and condensation was experimentally investigated using this test facility. Finally, a lumped-parameter mathematical simulation technique was developed to simulate the working process of a two-bed automotive adsorption air conditioning system. The performance of the adsorption cooling system was investigated at varying cycle times, varying heating fluid temperatures and flow rates and with different adsorber bed fin number and fin height using this mathematical model. The main findings could be summarized:

- CPO-27Ni has the best water adsorption characteristics among several MOF adsorbent materials tested particularly at the relative pressure range suitable for automotive air conditioning. The adsorption characteristics of three water based adsorbents: silica gel RD-2060, SAPO-34 and CPO-27Ni were experimentally tested. For relative pressure values ranging form 0 to 0.4, the water vapour uptake of CPO-27Ni is much higher than that of SAPO-34 and

silica gel RD-2060; indicating that the CPO-27Ni is the most promising among these three adsorbent materials.

- A finite element model was developed to simulate the adsorption process of an adsorption bed which was validated using the experimental results with good accuracy ±5.7%. The rectangular finned adsorption bed is the most promising design compared to the honeycomb finned adsorption bed and the helix finned adsorption bed; this is due to its outstanding adsorption performance including water vapour uptake and HCR.
- Operating conditions such as dry adsorbent desorption time, cooling water flow rate, adsorption time, desorption time and evaporation and condensation temperatures affect the adsorption air conditioning system's performance. Increasing the dry adsorbent desorption time can improve the cooling capacity of the first cycle by up to 61.9% but has no effect on the performance of the following cycles. The water uptake performance can be enhanced by up to 3.2% as the cooling water flow rate increases before it reaches 11L/min and after that the effect of the cooling water flow rate becomes negligible. The water vapour uptake is higher with a longer adsorption and desorption time; and raising the evaporation temperature and reducing the condensation temperature can increase the refrigerant uptake. It is concluded that it is preferable to optimise the cooling water flow rate, adsorption time, desorption time and condensation temperature to obtain higher cooling capacity.
- A lumped-parameter mathematical model was developed to simulate the working process of the whole adsorption air conditioning system with a two-bed refrigeration cycle and rectangular finned tube adsorption beds packed with CPO-27Ni as the adsorbent material. The model was validated using the

experimental results with a good accuracy of ±8.1%. The system's performance was investigated at varying cycle times, varying heating fluid temperatures and flow rates and with different adsorption bed fin number and fin height. The results show that this adsorption air conditioning system can produce the required cooling power of 2.39kW with SCP of 440W/kg and COP of 0.456, generated by hot oil with a temperature of 130 ℃ heated by the engine's exhaust gas. This SCP value is higher than all adsorption air conditioning systems for automotive application reported in the literature using water as a refrigerant.

- Based on the results by Johnson, the average value of waste heat for a representative vehicle Ford Taurus, using a 3.0L engine to output maximum 115kW engine power, is 23kW over the Federal Test Procedure [160]. The MOF based adsorption air conditioning system investigated in this research with the optimum operating conditions can produce the cooling load of 2.39kW which is sufficient to provide the required cooling effect to the vehicle's cabin, with the heat power input of 5.2kW which is only 22% of the waste heat available.

8.3 Future work

This thesis described the experimental and theoretical work for developing an MOF based adsorption air conditioning system for automotive application and it can be considered as a strong foundation for further work. It is suggested that more research is needed in the following points:

- This research presented the finite element modelling technique to simulate the adsorption process of the adsorber bed. Future research is needed to develop the finite element model to simulate the cycling process for the whole adsorption air conditioning system to predict a more accurate performance.
- This thesis presented the construction of a test facility based on a single bed refrigeration cycle containing one adsorber and one heat exchanger. Most of adsorption air conditioning systems use two-bed refrigeration cycles. Therefore, a test rig based on a two-bed cycle containing two adsorbers, one evaporator and one condenser is needed to be developed to achieve better performance. Also, using electrical heating in the desorption process is not practical in the automotive adsorption air conditioning system. The hot fluid (water or oil) heating method should be utilised in the future test rig.
- This thesis concluded that the developed adsorption air conditioning system can achieve the best performance when generated by hot oil with a temperature of 130 ℃ heated by the engine's exhaust gas. More experimental research is needed to realize the hot oil heated by the engine's exhaust gas to 130 ℃ in order to ensure enough energy is provided to the automotive adsorption air conditioning system.
- In this research, CPO-27Ni adsorbent material was experimentally tested with the highest generating temperature of around 100 ℃. It is desirable to test the cycling performance of CPO-27Ni with all temperatures up to 200 ℃ to investigate its stability with water vapour at both low and high temperatures.

REFERENCES

[1] Rezk, A. Theoretical and experimental investigation of silica gel/water adsorption refrigeration systems. (Doctor of Philosophy),2011, University of Birmingham.

[2] Sharafian, A., Bahrami, M. Assessment of adsorber bed designs in waste-heat driven adsorption cooling systems for vehicle air conditioning and refrigeration. *Renewable & Sustainable Energy Reviews.* 2014;30:440-451.

[3] Buzelin, L. O. S., Amico, S. C., Vargas, J. V. C., Parise, J. A. R. Experimental development of an intelligent refrigeration system. *International Journal of Refrigeration.* 2005;28(2):165-175.

[4] Critoph, R. E., Metcalf, S. J., Tamainot-Telto, Z. Proof of Concept Car Adsorption Air Conditioning System Using a Compact Sorption Reactor. *Heat Transfer Engineering.* 2010;31(11):950-956.

[5] Zhang, L. Z. Design and testing of an automobile waste heat adsorption cooling system. *Applied Thermal Engineering.* 2000;20(1):103-114.

[6] Zhong, Y. Size Reduction of an Engine Waste-Heat Driven Air- Conditioner for Passenger Cars and Light-Duty Trucks. *Energy Procedia.* 2012;14(0):351-357.

[7] Pang, S. C., Masjuki, H. H., Kalam, M. A., Hazrat, M. A. Liquid absorption and solid adsorption system for household, industrial and automobile applications: A review. *Renewable and Sustainable Energy Reviews.* 2013;28(0):836-847.

[8] Abdullah, M. O., Tan, I. A. W., Lim, L. S. Automobile adsorption air-conditioning system using oil palm biomass-based activated carbon: A review. *Renewable and Sustainable Energy Reviews.* 2011;15(4):2061-2072.

[9] Küsgens, P., Rose, M., Senkovska, I., Fröde, H., Henschel, A., Siegle, S., Kaskel, S. Characterization of metal-organic frameworks by water adsorption. *Microporous and Mesoporous Materials.* 2009;120(3):325-330.

[10] Karra, J. R., Grabicka, B. E., Huang, Y. G., Walton, K. S. Adsorption study of CO2, CH4, N-2, and H2O on an interwoven copper carboxylate metal-organic framework (MOF-14). *Journal of Colloid and Interface Science.* 2013;392:331-336.

[11] Lincke, J., Lassig, D., Moellmer, J., Reichenbach, C., Puls, A., Moeller, A., Glaser, R., Kalies, G., Staudt, R., Krautscheid, H. A novel copper-based MOF material: Synthesis, characterization and adsorption studies. *Microporous and Mesoporous Materials.* 2011;142(1):62-69.

[12] Rezk, A., AL-Dadah, R., Mahmoud, S., Elsayed, A. Investigation of Ethanol/metal organic frameworks for low temperature adsorption cooling applications. *Applied Energy.* 2013;112:1025-1031.

[13] Rezk, A., Al-Dadah, R., Mahmoud, S., Elsayed, A. Experimental investigation of metal organic frameworks characteristics for water adsorption chillers. *Proceedings of the Institution of Mechanical Engineers, Part C: Journal of Mechanical Engineering Science.* 2012.

[14] Ehrenmann, J., Henninger, S. K., Janiak, C. Water Adsorption Characteristics of MIL-101 for Heat-Transformation Applications of MOFs. *European Journal of Inorganic Chemistry.* 2011.

[15] Srivastava, N. C., Eames, I. W. A review of adsorbents and adsorbates in solid–vapour adsorption heat pump systems. *Applied Thermal Engineering.* 1998;18(9–10):707-714.
[16] Sumathy, K., Yeung, K. H., Yong, L. Technology development in the solar adsorption refrigeration systems. *Progress in Energy and Combustion Science.* 2003;29(4):301-327.
[17] Dieng, A. O., Wang, R. Z. Literature review on solar adsorption technologies for ice-making and air-conditioning purposes and recent developments in solar technology. *Renewable and Sustainable Energy Reviews.* 2001;5(4):313-342.
[18] Wang, L. W., Wang, R. Z., Oliveira, R. G. A review on adsorption working pairs for refrigeration. *Renewable and Sustainable Energy Reviews.* 2009;13(3):518-534.
[19] Dąbrowski, A. Adsorption — from theory to practice. *Advances in Colloid and Interface Science.* 2001;93(1–3):135-224.
[20] Critoph, R. E. Evaluation of alternative refrigerant—adsorbent pairs for refrigeration cycles. *Applied Thermal Engineering.* 1996;16(11):891-900.
[21] Kühn, A. Thermally driven heat pumps for heating and cooling. 2013.
[22] Wang, D. C., Li, Y. H., Li, D., Xia, Y. Z., Zhang, J. P. A review on adsorption refrigeration technology and adsorption deterioration in physical adsorption systems. *Renewable and Sustainable Energy Reviews.* 2010;14(1):344-353.
[23] Ullah, K. R., Saidur, R., Ping, H. W., Akikur, R. K., Shuvo, N. H. A review of solar thermal refrigeration and cooling methods. *Renewable and Sustainable Energy Reviews.* 2013;24(0):499-513.
[24] Wang, W., Wang, R. Z., Xu, Y. X., Wu, J. Y., Gui. Investigation on adsorption refrigeration with a single adsorbent bed. *International Journal of Energy Research.* 1998;22(13):1157–1163.
[25] Tamainot-Telto, Z., Critoph, R. E. Adsorption refrigerator using monolithic carbon-ammonia pair. *International Journal of Refrigeration.* 1997;20(2):146-155.
[26] Critoph, R. E. Rapid cycling solar/biomass powered adsorption refrigeration system. *Renewable Energy.* 1999;16(1–4):673-678.
[27] Oertel, K., Fischer, M. Adsorption cooling system for cold storage using methanol/silicagel. *Applied Thermal Engineering.* 1998;18(9–10):773-786.
[28] Restuccia, G., Freni, A., Vasta, S., Aristov, Y. Selective water sorbent for solid sorption chiller: experimental results and modelling. *International Journal Of Refrigeration-Revue Internationale Du Froid.* 2004;27(3):284-293.
[29] Restuccia, G., Freni, A., Russo, F., Vasta, S. Experimental investigation of a solid adsorption chiller based on a heat exchanger coated with hydrophobic zeolite. *Applied Thermal Engineering.* 2005;25(10):1419-1428.
[30] Freni, A., Russo, F., Vasta, S., Tokarev, M., Aristov, Y. I., Restuccia, G. An advanced solid sorption chiller using SWS-1Ll. *Applied Thermal Engineering.* 2007;27(13):2200-2204.
[31] Wang, R. Z. Adsorption refrigeration research in Shanghai Jiao Tong University. *Renewable & Sustainable Energy Reviews.* 2001;5(1):1-37.
[32] Wang, D. C., Wu, J. Y. Influence of intermittent heat source on adsorption ice maker using waste heat. *Energy Conversion and Management.* 2005;46(6):985-998.
[33] Nunez, T., Mittelbach, W., Henning, H. M. Development of an adsorption chiller and heat pump for domestic heating and air-conditioning applications. *Applied Thermal Engineering.* 2007;27(13):2205-2212.

[34] Tamainot-Telto, Z., Metcalf, S. J., Critoph, R. E. Novel compact sorption generators for car air conditioning. *International Journal of Refrigeration.* 2009;32(4):727-733.
[35] de Boer, R., Smeding, S. F. Thermally operated mobile air-conditioning system. Development and test of a laboratory prototype. *Paper presented at the International Sorption Heat Pump Conference, Seoul, Korea*. 2008.
[36] de Boer, R., Smeding, S. F., Mola, S. Silicagel-water adsorption cooling prototype system for mobile air conditioning. *Paper presented at the Heat Powered Cycles Conference, Berlin*. 2009.
[37] Vasta, S., Freni, A., Sapienza, A., Costa, F., Restuccia, G. Development and lab-test of a mobile adsorption air-conditioner. *International Journal of Refrigeration.* 2012;35(3):701-708.
[38] Wang, R. Z. Performance improvement of adsorption cooling by heat and mass recovery operation. *International Journal Of Refrigeration-Revue Internationale Du Froid.* 2001;24(7):602-611.
[39] Akahira, A., Alam, K. C. A., Hamamoto, Y., Akisawa, A., Kashiwagi, T. Experimental investigation of mass recovery adsorption refrigeration cycle. *International Journal of Refrigeration.* 2005;28(4):565-572.
[40] Saha, B. B., Koyama, S., Lee, J. B., Kuwahara, K., Alam, K. C. A., Hamamoto, Y., Akisawa, A., Kashiwagi, T. Performance evaluation of a low-temperature waste heat driven multi-bed adsorption chiller. *International Journal of Multiphase Flow.* 2003;29(8):1249-1263.
[41] Khan, M. Z. I., Saha, B. B., Alam, K. C. A., Akisawa, A., Kashiwagi, T. Study on solar/waste heat driven multi-bed adsorption chiller with mass recovery. *Renewable Energy.* 2007;32(3):365-381.
[42] Sapienza, A., Santamaria, S., Frazzica, A., Freni, A. Influence of the management strategy and operating conditions on the performance of an adsorption chiller. *Energy.* 2011;36(9):5532-5538.
[43] Farid, S. K., Billah, M. M., Khan, M. Z. I., Rahman, M. M., Sharif, U. M. A numerical analysis of cooling water temperature of two-stage adsorption chiller along with different mass ratios. *International Communications in Heat and Mass Transfer.* 2011;38(8):1086-1092.
[44] Wang, X. L., Chua, H. T., Ng, K. C. Experimental investigation of silica gel-water adsorption chillers with and without a passive heat recovery scheme. *International Journal Of Refrigeration-Revue Internationale Du Froid.* 2005;28(5):756-765.
[45] Alam, K. C. A., Khan, M. Z. I., Uyun, A. S., Hamamoto, Y., Akisawa, A., Kashiwagi, T. Experimental study of a low temperature heat driven re-heat two-stage adsorption chiller. *Applied Thermal Engineering.* 2007;27(10):1686-1692.
[46] Oliveira, R. G., Silveira, V., Wang, R. Z. Experimental study of mass recovery adsorption cycles for ice making at low generation temperature. *Applied Thermal Engineering.* 2006;26(2-3):303-311.
[47] Akahira, A., Alam, K. C. A., Hamamoto, Y., Akisawa, A., Kashiwagi, T. Mass recovery four-bed adsorption refrigeration cycle with energy cascading. *Applied Thermal Engineering.* 2005;25(11-12):1764-1778.
[48] Hamamoto, Y., Alam, K. C. A., Akisawa, A., Kashiwagi, T. Performance evaluation of a two-stage adsorption refrigeration cycle with different mass ratio. *International Journal Of Refrigeration-Revue Internationale Du Froid.* 2005;28(3):344-352.

[49] Saha, B. B., Akisawa, A., Kashiwagi, T. Solar/waste heat driven two-stage adsorption chiller: the prototype. *Renewable Energy.* 2001;23(1):93-101.
[50] Saha, B. B., Boelman, E. C., Kashiwagi, T. Computational Analysis of an Advanced Adsorption Refrigeration Cycle. *Energy.* 1995;20(10):983-994.
[51] Khan, M. Z. I., Alam, K. C. A., Saha, B. B., Akisawa, A., Kashiwagi, T. Performance evaluation of multi-stage, multi-bed adsorption chiller employing re-heat scheme. *Renewable Energy.* 2008;33(1):88-98.
[52] Saha, B. B., Koyama, S., Ng, K. C., Hamamoto, Y., Akisawa, A., Kashiwagi, T. Study on a dual-mode, multi-stage, multi-bed regenerative adsorption chiller. *Renewable Energy.* 2006;31(13):2076-2090.
[53] Saha, B. B., Koyama, S., Kashiwagi, T., Akisawa, A., Ng, K. C., Chua, H. T. Waste heat driven dual-mode, multi-stage, multi-bed regenerative adsorption system. *International Journal Of Refrigeration-Revue Internationale Du Froid.* 2003;26(7):749-757.
[54] Anyanwu, E. E. Review of solid adsorption solar refrigeration II: An overview of the principles and theory. *Energy Conversion and Management.* 2004;45(7-8):1279-1295.
[55] Saha, B. B., Habib, K., El-Sharkawy, I. I., Koyama, S. Adsorption characteristics and heat of adsorption measurements of R-134a on activated carbon. *International Journal of Refrigeration.* 2009;32(7):1563-1569.
[56] Habib, K., Saha, B. B., Rahman, K. A., Chakraborty, A., Koyama, S., Ng, K. C. Experimental study on adsorption kinetics of activated carbon/R134a and activated carbon/R507A pairs. *International Journal of Refrigeration.* 2010;33(4):706-713.
[57] Askalany, A. A., Saha, B. B., Ahmed, M. S., Ismail, I. M. Adsorption cooling system employing granular activated carbon–R134a pair for renewable energy applications. *International Journal of Refrigeration.* 2013;36(3):1037-1044.
[58] Jin, Z., Tian, B., Wang, L., Wang, R. Comparison on Thermal Conductivity and Permeability of Granular and Consolidated Activated Carbon for Refrigeration. *Chinese Journal of Chemical Engineering.* 2013;21(6):676-682.
[59] Dawoud, B., Sohel, M. I., Freni, A., Vasta, S., Restuccia, G. On the effective thermal conductivity of wetted zeolite under the working conditions of an adsorption chiller. *Applied Thermal Engineering.* 2011;31(14–15):2241-2246.
[60] Zhang, L. Z., Wang, L. Effects of coupled heat and mass transfers in adsorbent on the performance of a waste heat adsorption cooling unit. *Applied Thermal Engineering.* 1999;19(2):195-215.
[61] Aristov, Y. I. Challenging offers of material science for adsorption heat transformation: A review. *Applied Thermal Engineering.* 2013;50(2):1610-1618.
[62] Henninger, S. K., Jeremias, F., Kummer, H., Schossig, P., Henning, H.-M. Novel Sorption Materials for Solar Heating and Cooling. *Energy Procedia.* 2012;30(0):279-288.
[63] Mahzoon, S., Fatemi, S., Hashemi, S. J. Modeling based investigation of ultrafine sapo-34 core-shell adsorbent in cyclic adsorption process for purification of natural gas from CO_2. *International Journal of Theoretical and Applied Nanotechnology.* 2012;1(1):90-98.
[64] Bonaccorsi, L., Calabrese, L., Proverbio, E., Frazzica, A., Freni, A., Restuccia, G., Piperopoulos, E., Milone, C. Synthesis of SAPO-34/graphite composites for low temperature heat adsorption pumps. *Journal of Energy Chemistry.* 2013;22(2):245-250.

[65] Chen, H. J., Cui, Q., Li, Q. G., Zheng, K., Yao, H. Q. Adsorption-desorption characteristics of water on silico-alumino-phosphate-34 molecular sieve for cooling and air conditioning. *Journal of Renewable and Sustainable Energy.* 2013;5(5):-.
[66] Henninger, S. K., Schmidt, F. P., Henning, H. M. Water adsorption characteristics of novel materials for heat transformation applications. *Applied Thermal Engineering.* 2010;30(13):1692-1702.
[67] Ng, E. P., Mintova, S. Nanoporous materials with enhanced hydrophilicity and high water sorption capacity. *Microporous and Mesoporous Materials.* 2008;114(1-3):1-26.
[68] Jänchen, J., Stach, H. Adsorption properties of porous materials for solar thermal energy storage and heat pump applications. *Energy Procedia.* 2012;30(0):289-293.
[69] Qiu, S. L., Zhu, G. S. Molecular engineering for synthesizing novel structures of metal-organic frameworks with multifunctional properties. *Coordination Chemistry Reviews.* 2009;253(23-24):2891-2911.
[70] Kondo, A., Daimaru, T., Noguchi, H., Ohba, T., Kaneko, K., Kanob, H. Adsorption of water on three-dimensional pillared-layer metal organic frameworks. *Journal of Colloid and Interface Science.* 2007;314(2):422-426.
[71] Calleja, G., Botas, J. A., Sánchez-Sánchez, M., Orcajo, M. G. Hydrogen adsorption over Zeolite-like MOF materials modified by ion exchange. *International Journal of Hydrogen Energy.* 2010;35(18):9916-9923.
[72] Aristov, Y. I. Novel Materials for Adsorptive Heat Pumping and Storage: Screening and Nanotailoring of Sorption Properties. *Journal of Chemical Engineering of Japan.* 2007;40(13):1242-1251.
[73] Castillo, J. M., Vlugt, T. J. H., Calero, S. Understanding Water Adsorption in Cu−BTC Metal−Organic Frameworks. *The Journal of Physical Chemistry C.* 2008;112(41):15934-15939.
[74] Gul-E-Noor, F., Jee, B., Poppl, A., Hartmann, M., Himsl, D., Bertmer, M. Effects of varying water adsorption on a Cu3(BTC)2 metal-organic framework (MOF) as studied by 1H and 13C solid-state NMR spectroscopy. *Physical Chemistry Chemical Physics.* 2011;13(17):7783-7788.
[75] Gul-E-Noor, F., Michel, D., Krautscheid, H., Haase, J., Bertmer, M. Time dependent water uptake in Cu3(btc)2 MOF: Identification of different water adsorption states by 1H MAS NMR. *Microporous and Mesoporous Materials.* 2013;180(0):8-13.
[76] Min Wang, Q., Shen, D., Bülow, M., Ling Lau, M., Deng, S., Fitch, F. R., Lemcoff, N. O., Semanscin, J. Metallo-organic molecular sieve for gas separation and purification. *Microporous and Mesoporous Materials.* 2002;55(2):217-230.
[77] Dietzel, P. D. C., Johnsen, R. E., Blom, R., Fjellvåg, H. Structural Changes and Coordinatively Unsaturated Metal Atoms on Dehydration of Honeycomb Analogous Microporous Metal–Organic Frameworks. *Chemistry – A European Journal.* 2008;14(8):2389-2397.
[78] Caskey, S. R., Wong-Foy, A. G., Matzger, A. J. Dramatic Tuning of Carbon Dioxide Uptake via Metal Substitution in a Coordination Polymer with Cylindrical Pores. *Journal of the American Chemical Society.* 2008;130(33):10870-10871.
[79] Dietzel, P. D. C., Panella, B., Hirscher, M., Blom, R., Fjellvag, H. Hydrogen adsorption in a nickel based coordination polymer with open metal sites in the

cylindrical cavities of the desolvated framework. *Chemical Communications.* 2006(9):959-961.
[80] Grant Glover, T., Peterson, G. W., Schindler, B. J., Britt, D., Yaghi, O. MOF-74 building unit has a direct impact on toxic gas adsorption. *Chemical Engineering Science.* 2011;66(2):163-170.
[81] Henninger, S. K., Habib, H. A., Janiak, C. MOFs as Adsorbents for Low Temperature Heating and Cooling Applications. *Journal of the American Chemical Society.* 2009;131(8):2776-2777.
[82] Saha, D., Deng, S. Ammonia adsorption and its effects on framework stability of MOF-5 and MOF-177. *Journal of Colloid and Interface Science.* 2010;348(2):615-620.
[83] Furukawa, H., Gándara, F., Zhang, Y.-B., Jiang, J., Queen, W. L., Hudson, M. R., Yaghi, O. M. Water Adsorption in Porous Metal–Organic Frameworks and Related Materials. *Journal of the American Chemical Society.* 2014;136(11):4369-4381.
[84] Cui, Q., Tao, G., Chen, H., Guo, X., Yao, H. Environmentally benign working pairs for adsorption refrigeration. *Energy.* 2005;30(2–4):261-271.
[85] Verde, M., Cortés, L., Corberán, J. M., Sapienza, A., Vasta, S., Restuccia, G. Modelling of an adsorption system driven by engine waste heat for truck cabin A/C. Performance estimation for a standard driving cycle. *Applied Thermal Engineering.* 2010;30(13):1511-1522.
[86] Zhong, Y., Fang, T., Wert, K. L. An adsorption air conditioning system to integrate with the recent development of emission control for heavy-duty vehicles. *Energy.* 2011;36(7):4125-4135.
[87] Lambert, M. A., Jones, B. J. Automotive adsorption air conditioner powered by exhaust heat. Part 1: conceptual and embodiment design. *Proceedings of the Institution of Mechanical Engineers, Part D: Journal of Automobile Engineering.* 2006;220:959-972.
[88] Lambert, M. A., Jones, B. J. Automotive Adsorption Air Conditioner Powered by Exhaust Heat. Part 2: Detailed Design and Analysis. *Proceedings of the Institution of Mechanical Engineers, Part D: Journal of Automobile Engineering.* 2006;220:973-989.
[89] Suzuki, M. Application of adsorption cooling systems to automobiles. *Heat Recovery Systems and CHP.* 1993;13(4):335-340.
[90] Inoue, S., Inoue, S., Kobayashi, N. A Study on Adsorption Refrigerators for Automobiles Utilizing the Temperature Dependency of Adsorbents. *Journal of Chemical Engineering of Japan.* 2007;40:1313-1318.
[91] Verde, M., Corberan1, J. M., de Boer, R., Smeding, S. F. Modelling of a waste heat driven silica gel/water adsorption cooling system comparison with experimental results. *Paper presented at the International Sorption Heat Pump Conference, Padua, Italy*. 2011.
[92] Wu, W.-D., Zhang, H., Men, C.-l. Performance of a modified zeolite 13X-water adsorptive cooling module powered by exhaust waste heat. *International Journal of Thermal Sciences.* 2011;50(10):2042-2049.
[93] Jiangzhou, S., Wang, R. Z., Lu, Y. Z., Xu, Y. X., Wu, J. Y. Experimental investigations on adsorption air-conditioner used in internal-combustion locomotive driver-cabin. *Applied Thermal Engineering.* 2002;22(10):1153-1162.

[94] Jiangzhou, S., Wang, R. Z., Lu, Y. Z., Xu, Y. X., Wu, J. Y., Li, Z. H. Locomotive driver cabin adsorption air-conditioner. *Renewable Energy.* 2003;28(11):1659-1670.
[95] Lu, Y. Z., Wang, R. Z., Jianzhou, S., Xu, Y. X., Wu, J. Y. Practical experiments on an adsorption air conditioner powered by exhausted heat from a diesel locomotive. *Applied Thermal Engineering.* 2004;24(7):1051-1059.
[96] Jiangzhou, S., Wang, R. Z., Lu, Y. Z., Xu, Y. X., Wu, J. Y. Experimental study on locomotive driver cabin adsorption air conditioning prototype machine. *Energy Conversion and Management.* 2005;46(9–10):1655-1665.
[97] Ramji, H. R., Leo, S. L., Abdullah, M. O. Parametric study and simulation of a heat-driven adsorber for air conditioning system employing activated carbon–methanol working pair. *Applied Energy.* 2014;113(0):324-333.
[98] Cacciola, G., Restuccia, G. Reversible Adsorption Heat-Pump - a Thermodynamic Model. *International Journal Of Refrigeration-Revue Internationale Du Froid.* 1995;18(2):100-106.
[99] Sami, S. M., Tribes, C. An improved model for predicting the dynamic behaviour of adsorption systems. *Applied Thermal Engineering.* 1996;16(2):149-161.
[100] Critoph, R. E. Performance Limitations of Adsorption Cycles for Solar Cooling. *Solar Energy.* 1988;41(1):21-31.
[101] Lima, P. M., Goncalves, C. V., Cavalcante, C. L., Cardoso, D. Sorption kinetics of linear paraffins in zeolite BEA nanocrystals. *Microporous and Mesoporous Materials.* 2008;116(1-3):352-357.
[102] Tamainot-Telto, Z., Metcalf, S. J., Critoph, R. E., Zhong, Y., Thorpe, R. Carbon-ammonia pairs for adsorption refrigeration applications: ice making, air conditioning and heat pumping. *International Journal Of Refrigeration-Revue Internationale Du Froid.* 2009;32(6):1212-1229.
[103] Wu, J. W., Biggs, M. J., Hu, E. J. Thermodynamic analysis of an adsorption-based desalination cycle. *Chemical Engineering Research and Design.* 2010;88(12):1541-1547.
[104] Sakoda, A., Suzuki, M. Fundamental-Study on Solar Powered Adsorption Cooling System. *Journal of Chemical Engineering of Japan.* 1984;17(1):52-57.
[105] Chua, H. T., Ng, K. C., Malek, A., Kashiwagi, T., Akisawa, A., Saha, B. B. Modeling the performance of two-bed, silica gel-water adsorption chillers. *International Journal Of Refrigeration-Revue Internationale Du Froid.* 1999;22(3):194-204.
[106] Chua, H. T., Ng, K. C., Malek, A., Kashiwagi, T., Akisawa, A., Saha, B. B. Multi-bed regenerative adsorption chiller - improving the utilization of waste heat and reducing the chilled water outlet temperature fluctuation. *International Journal Of Refrigeration-Revue Internationale Du Froid.* 2001;24(2):124-136.
[107] Zhang, X. J., Wang, R. Z. Design and performance simulation of a new solar continuous solid adsorption refrigeration and heating hybrid system. *Renewable Energy.* 2002;27(3):401-415.
[108] Akahira, A., Alam, K. C. A., Hamamoto, Y., Akisawa, A., Kashiwagi, T. Mass recovery adsorption refrigeration cycle-improving cooling capacity. *International Journal Of Refrigeration-Revue Internationale Du Froid.* 2004;27(3):225-234.
[109] Wang, D. C., Xia, Z. Z., Wu, J. Y., Wang, R. Z., Zhai, H., Dou, W. D. Study of a novel silica gel-water adsorption chiller. Part I. Design and performance

prediction. *International Journal Of Refrigeration-Revue Internationale Du Froid.* 2005;28(7):1073-1083.
[110] Liu, Y., Leong, K. C. Numerical study of a novel cascading adsorption cycle. *International Journal Of Refrigeration-Revue Internationale Du Froid.* 2006;29(2):250-259.
[111] Wang, X. L., Chua, H. T. Two bed silica gel-water adsorption chillers: An effectual lumped parameter model. *International Journal Of Refrigeration-Revue Internationale Du Froid.* 2007;30(8):1417-1426.
[112] Khan, M. Z. I., Alam, K. C. A., Saha, B. B., Akisawa, A., Kashiwagi, T. Study on a re-heat two-stage adsorption chiller - The influence of thermal capacitance ratio, overall thermal conductance ratio and adsorbent mass on system performance. *Applied Thermal Engineering.* 2007;27(10):1677-1685.
[113] Miyazaki, T., Akisawa, A. The influence of heat exchanger parameters on the optimum cycle time of adsorption chillers. *Applied Thermal Engineering.* 2009;29(13):2708-2717.
[114] Schicktanz, M., Nunez, T. Modelling of an adsorption chiller for dynamic system simulation. *International Journal Of Refrigeration-Revue Internationale Du Froid.* 2009;32(4):588-595.
[115] Uyun, A. S., Akisawa, A., Miyazaki, T., Ueda, Y., Kashiwagi, T. Numerical analysis of an advanced three-bed mass recovery adsorption refrigeration cycle. *Applied Thermal Engineering.* 2009;29(14-15):2876-2884.
[116] AL-Dadah, R., Rezk, A. R. M. Empirical simulation model of silica gel/water adsorption chiller. *Paper presented at the Conference on Thermal and Environmental Issues in Energy Systems, Sorrento, Italy*. 2010.
[117] Rezk, A. R. M., Al-Dadah, R. K. Physical and operating conditions effects on silica gel/water adsorption chiller performance. *Applied Energy.* 2012;89(1):142-149.
[118] Miyazaki, T., Akisawa, A., Saha, B. B., El-Sharkawy, I. I., Chakraborty, A. A new cycle time allocation for enhancing the performance of two-bed adsorption chillers. *International Journal Of Refrigeration-Revue Internationale Du Froid.* 2009;32(5):846-853.
[119] Cho, S. H., Kim, J. N. Modeling of a Silica-Gel Water-Adsorption Cooling System. *Energy.* 1992;17(9):829-839.
[120] Chua, H. T., Ng, K. C., Wang, W., Yap, C., Wang, X. L. Transient modeling of a two-bed silica gel-water adsorption chiller. *International Journal of Heat and Mass Transfer.* 2004;47(4):659-669.
[121] Voyiatzis, E., Palyvos, J. A., Markatos, N. C. Heat-exchanger design and switching-frequency effects on the performance of a continuous type solar adsorption chiller. *Applied Energy.* 2008;85(12):1237-1250.
[122] San, J. Y., Lin, W. M. Comparison among three adsorption pairs for using as the working substances in a multi-bed adsorption heat pump. *Applied Thermal Engineering.* 2008;28(8-9):988-997.
[123] Freni, A., Bonaccorsi, L., Proverbio, E., Maggio, G., Restuccia, G. Zeolite synthesised on copper foam for adsorption chillers: A mathematical model. *Microporous and Mesoporous Materials.* 2009;120(3):402-409.
[124] Saha, B. B., Chakraborty, A., Koyama, S., Aristov, Y. I. A new generation cooling device employing CaCl2-in-silica gel-water system. *International Journal of Heat and Mass Transfer.* 2009;52(1-2):516-524.
[125] Zhang, L. Z., Wang, L. Momentum and heat transfer in the adsorbent of a waste-heat adsorption cooling system. *Energy.* 1999;24(7):605-624.

[126] Zhang, L. Z. A three-dimensional non-equilibrium model for an intermittent adsorption cooling system. *Solar Energy.* 2000;69(1):27-35.
[127] Saha, B. B., EI-Sharkawy, I. I., Chakraborty, A., Koyama, S. Study on an activated carbon fiber-ethanol adsorption chiller: Part I - system description and modelling. *International Journal Of Refrigeration-Revue Internationale Du Froid.* 2007;30(1):86-95.
[128] Jribi, S., Saha, B. B., Koyama, S., Bentaher, H. Modeling and simulation of an activated carbon-CO2 four bed based adsorption cooling system. *Energy Conversion and Management.* 2014;78:985-991.
[129] Luo, L., Tondeur, D. Transient thermal study of an adsorption refrigerating machine. *Adsorption-Journal of the International Adsorption Society.* 2000;6(1):93-104.
[130] Zhao, Y. L., Hu, E., Blazewicz, A. A non-uniform pressure and transient boundary condition based dynamic modeling of the adsorption process of an adsorption refrigeration tube. *Applied Energy.* 2012;90(1):280-287.
[131] Zhao, Y. L., Hu, E., Blazewicz, A. Dynamic modelling of an activated carbon-methanol adsorption refrigeration tube with considerations of interfacial convection and transient pressure process. *Applied Energy.* 2012;95:276-284.
[132] Cacciola, G., Restuccia, G., van Benthem, G. H. W. Influence of the adsorber heat exchanger design on the performance of the heat pump system. *Applied Thermal Engineering.* 1999;19(3):255-269.
[133] Critoph, R. E. Simulation of a continuous multiple-bed regenerative adsorption cycle. *International Journal Of Refrigeration-Revue Internationale Du Froid.* 2001;24(5):428-437.
[134] El-Sharkawy, I. I., Saha, B. B., Koyama, S., He, J., Ng, K. C., Yap, C. Experimental investigation on activated carbon-ethanol pair for solar powered adsorption cooling applications. *International Journal Of Refrigeration-Revue Internationale Du Froid.* 2008;31(8):1407-1413.
[135] Loh, W. S., El-Sharkawy, I. I., Ng, K. C., Saha, B. B. Adsorption cooling cycles for alternative adsorbent/adsorbate pairs working at partial vacuum and pressurized conditions. *Applied Thermal Engineering.* 2009;29(4):793-798.
[136] Freni, A., Maggio, G., Cipiti, F., Aristov, Y. I. Simulation of water sorption dynamics in adsorption chillers: One, two and four layers of loose silica grains. *Applied Thermal Engineering.* 2012;44:69-77.
[137] Xu, S. Simulation on a New Adsorption Bed about Adsorption Refrigeration Driven by Solar Energy. *Procedia Engineering.* 2011;15(0):3865-3869.
[138] Ambaw, A., Delele, M. A., Defraeye, T., Ho, Q. T., Opara, L. U., Nicolai, B. M., Verboven, P. The use of CFD to characterize and design post-harvest storage facilities: Past, present and future. *Computers and Electronics in Agriculture.* 2013;93:184-194.
[139] Jafari, A., Zamankhan, P., Mousavi, S. M., Pietarinen, K. Modeling and CFD simulation of flow behavior and dispersivity through randomly packed bed reactors. *Chemical Engineering Journal.* 2008;144(3):476-482.
[140] Rahimi, M., Mohseni, M. CFD modeling of the effect of absorbent size on absorption performance of a packed bed column. *Korean Journal of Chemical Engineering.* 2008;25(3):395-401.
[141] Dixon, A. G., Nijemeisland, M. CFD as a design tool for fixed-bed reactors. *Industrial & Engineering Chemistry Research.* 2001;40(23):5246-5254.

[142] Zhang, L. Z., Wang, L. Performance estimation of an adsorption cooling system for automobile waste heat recovery. *Applied Thermal Engineering.* 1997;17(12):1127-1139.
[143] Hu, P., Yao, J.-J., Chen, Z.-S. Analysis for composite zeolite/foam aluminum–water mass recovery adsorption refrigeration system driven by engine exhaust heat. *Energy Conversion and Management.* 2009;50(2):255-261.
[144] Jribi, S., Saha, B. B., Koyama, S., Chakraborty, A., Ng, K. C. Study on activated carbon/HFO-1234ze(E) based adsorption cooling cycle. *Applied Thermal Engineering.* 2013;50(2):1570-1575.
[145] Surface Measurement Systems Company, DVS Advantage-Operating Manual.
[146] Ilić, M., Budak, I., Vučinić Vasić, M., Nagode, A., Kozmidis-Luburić, U., Hodolič, J., Puškar, T. Size and shape particle analysis by applying image analysis and laser diffraction – Inhalable dust in a dental laboratory. *Measurement.* 2015;66(0):109-117.
[147] Lee Black, D., McQuay, M. Q., Bonin, M. P. Laser-based techniques for particle-size measurement: A review of sizing methods and their industrial applications. *Progress in Energy and Combustion Science.* 1996;22(3):267-306.
[148] Eddie Setekleiv, A., Svendsen, H. F. Comparison of piezo electric particle monitor with laser diffraction technique. *Measurement.* 2014;55(0):133-141.
[149] Fuldner, G., Schnabel, L. Non-Isothermal Kinetics of Water Adsorption in Compact Adsorbent Layers on a Metal Support. *Paper presented at the COMSOL Conference, Hannover*. 2008.
[150] Freni, A., Dawoud, B., Cipiti, F., Chmielewski, S., Maggio, G., Restuccia, G. Finite element-based simulation of the heat and mass transfer process through an adsorbent bed in an adsorption heat pump/chiller. *Paper presented at the Conference on Thermal and Environmental Issues in Energy Systems, Sorrento, Italy*. 2010.
[151] Shi, B., AL-Dadah, R. K., Mahmoud, S., Elsayed, A., Rezk, A. Mathematical and CFD modelling for a rectangular finned tube adsorption bed for automotive cooling system. *Paper presented at the International Conference on Applied Energy, Pretoria, South Africa*. 2013.
[152] Shi, B., Elsayed, A., AL-Dadah, R., Mahmoud, S. CFD Simulation of Honeycomb Adsorption Bed for Automotive Cooling System. *Paper presented at the International Conference on Heat Transfer and Fluid Flow, Prague, Czech Republic*. 2014.
[153] Impress Sensors and System Company, Low Range Industrial Pressure Transmitter User's Guide.
[154] Omega Company, FLC Series Clear In-Line Flowmeters User's Guide.
[155] Chang, W. S., Wang, C. C., Shieh, C. C. Experimental study of a solid adsorption cooling system using flat-tube heat exchangers as adsorption bed. *Applied Thermal Engineering.* 2007;27(13):2195-2199.
[156] Critoph, R. E., Metcalf, S. J. Specific cooling power intensification limits in ammonia–carbon adsorption refrigeration systems. *Applied Thermal Engineering.* 2004;24(5–6):661-678.
[157] Wang, D. C., Wu, J. Y., Xia, Z. Z., Zhai, H., Wang, R. Z., Dou, W. D. Study of a novel silica gel–water adsorption chiller. Part II. Experimental study. *International Journal of Refrigeration.* 2005;28(7):1084-1091.

[158] Saha, B. B., El-Sharkawy, I. I., Chakraborty, A., Koyama, S. Study on an activated carbon fiber–ethanol adsorption chiller: Part II – performance evaluation. *International Journal of Refrigeration.* 2007;30(1):96-102.
[159] Badiali, S., Colombo, S. Dynamic modelling of mechanical heat pumps for comfort heating. (MSc),2009, Kungliga Tekniska högskola.
[160] Johnson, V. H. Heat-generated cooling opportunities in vehicles. *Washington D.C., U.S.A.: SAE Technical Papers.* 2002:2002-2001-1969.